Roles of protein phosphorylation during effector-triggered immunity

Sophie Louise Johnson

A thesis submitted to the University of East Anglia for the degree of Doctor of Philosophy

The Sainsbury Laboratory

March 2023

Registration number: 100239799

Abstract

Plants have intracellular nucleotide-binding leucine-rich repeat (NLR) immune receptors. NLRs recognize pathogen-derived effectors and activate effector-triggered immunity (ETI). This work aimed to investigate protein phosphorylation events that occur during the early activation of ETI using Arabidopsis lines carrying estradiol-inducible AvrRps4. We used a quantitative phospho-proteomics approach and generated a comprehensive phospho-peptide library from the nuclear fraction. We used parallel reaction monitoring (PRM) to target and quantify several hundred phospho-peptides. We identified proteins with differential phosphorylation upon ETI activation, some of which are known transcriptional regulators, suggesting a role of phosphorylation in activating ETI-induced transcriptional changes. To understand the biological significance of phosphorylation changes in these proteins, we assessed the impact of amino-acid substitutions at the phosphorylated residues on transcriptional regulation and protein interactions.

The signalling pathways downstream of helper NLR activation remain elusive. Therefore, we used proximity labelling and identified novel protein interactors of SARD1, TPR1 and EDS1. We identified an overlap between proteins phosphorylated during ETI and those interacting with SARD1, suggesting these proteins may be involved in ETI signal transduction. We also revealed a WRKY18 EAR domain is important for TPR1 nuclear puncta co-localisation. This study provides an important protein interaction database for which further work can utilise to enhance our understanding of protein complex formation to regulate transcriptional changes.

Previous work has revealed that PTI and ETI are required for NRG1 oligomerisation. In the third section of this study, we aimed to identify phosphorylation changes of NRG1 during PTI and ETI activation using Phos-tag gels and IP-MS. We revealed two residues of NRG1 important for HR activation in *N. benthamiana*. Further investigations could reveal if these phosphorylation sites are required for NRG1 oligomerisation, enhancing our understanding of helper NLR signalling mechanisms.

Table of contents

List of tables

List of figures

List of appendices

List of supplementary tables

Acknowledgements

I would like to express my huge thanks to my two supervisors Jonathan Jones and Frank Menke for giving me the opportunity to conduct my PhD research and providing continued support and guidance over the last 4.5 years.

Thank you to Pingtao Ding for being a great mentor and supervisory team member, who contributed to many experimental ideas for my PhD and gave me great support and advice. Thank you to members of the JJ Arabidopsis team for great scientific discussions, feedback, and advice particularly Hee-Kyung Ahn, Hailong Guo and Jianhua Huang.

A huge thanks to the Proteomics team Paul Derbyshire and Jan Sklenar for all the work they contributed towards my project.

Thank you to Joanna Feehan and Bruno Ngou who's work I largely built upon.

Thank you to all the TSL students for being such a friendly group.

Thank you to the TSL support staff, in particular the media kitchen for sieving many thousands of my seeds and Aleksandra Wawryk from the transformation team for all the Arabidopsis transformation lines she generated for me.

Thank you to the wider TSL community for being such an amazing place to do science.

Thank you to the NRP horticultural services, in particular Timothy Wells, for taking care of my plants. Also thanks to Sara Perkins and Justine Smith.

Thank you to my family for their support and encouragement.
Thank you to all my amazing friends for their continued love and emotional support.

Chapter 1

Introduction

1. Introduction

Research into plant disease resistance is essential for ensuring future food security. Plants face threats from bacterial, fungal, viral and oomycete pathogens, as well as nematodes and herbivores. Thirty percent of rice and twenty percent of wheat, maize and soybean are lost annually to plant pathogens and pests (Savary et al., 2019). Introducing resistance genes into crop species to create resilient plants ensures farmers do not receive such huge losses in income. Research into plant immunity allows us to identify these important resistance genes and introduce them into crops either through traditional breeding or using genetic modification or gene editing technologies. Arabidopsis provides a model system with a well annotated genome and quick generation time to understand the fundamental mechanisms of plant immune signalling pathways.

1.1 Pattern-triggered-immunity

A plant's cuticle and cell wall act as natural barriers to pathogens, yet some fungal pathogens can penetrate the cuticle and bacterial pathogens can enter through wounds and natural openings such as stomata. Plants have evolved mechanisms to detect the presence of pathogens and activate an immune response, thereby restricting pathogen growth and preventing further damage to the plant.

Plants have two interlinked layers of immune activation. The first layer is focused at the plasma membrane where plants perceive the pathogens via transmembrane pattern recognition receptors (PRRs). These PRRs detect elicitors such as chitin from fungal cell walls or conserved peptides from pathogens referred to as pathogen-associated molecular patterns (PAMPs). PAMPs bind to PRRs and activate pattern-triggered immunity (PTI). Receptor-like proteins and receptor kinases both function as PRRs, which can be subdivided into those containing leucine-rich-repeats (LRR), lysine motifs (LysM) or lectin-type, recognising flagellin, chitin or bacterial lipopolysaccharides respectively (Couto & Zipfel, 2016). PTI is often studied using flg22, a 22 amino-acid peptide from the N-terminus of flagellin (Felix et al., 1999). flg22 induces PTI activation through recognition by the receptor-like-kinase FLAGELLIN-SENSITIVE 2 (FLS2) (Gomez-Gomez et al., 1999, Gomez-Gomez & Boller, 2000). PRRs can also detect plant derived peptides known as damage-associated-molecular-patterns (DAMPs). DAMPs e.g. oligogalacturonides (oligomers of alpha-1,4-linked galacturonosyl residues), derived from a plant cell-wall, are signatures of cellular damage and indicate pathogen infection (De Lorenzo & Cervone, 2022). PRRs form complexes with different co-receptor kinases depending on their ectodomain. For example, the LRR domain- containing FLAGELLIN-SENSITIVE 2 (FLS2) recruits BRI1-ASSOCIATED RECEPTOR

KINASE (BAK1), and LysM-domain containing receptor-like kinase 5 (LYK5) recruits CHITIN ELICITOR RECEPTOR KINASE 1 (CERK1) (Couto & Zipfel, 2016).

Receptor-like cytoplasmic kinases (RLCKs) also play an important role in PTI signal transduction (Sun & Zhang, 2020). Upon perception of flg22, FLS2 and its co-receptor BAK1 phosphorylate the RLCK BOTRYTIS-INDUCED KINASE1 (BIK1) (Lu et al., 2010) (Figure 1.1). This triggers BIK1 to disassociate from the PRR complex and phosphorylate RBOHD, thus activating the production of reactive oxygen species (ROS) (Lu et al., 2010, Kadota et al., 2014, Li et al., 2014b) (Figure 1.1). There is also transphosphorylation of FLS2 and BAK1 by BIK1 to further enhance PTI signalling (Lu et al., 2010). Elf18 is an acetylated 18-amino acid peptide from the bacterial translation protein Elongation Factor Thermo Unstable (EF-Tu) (Kunze et al., 2004). Elf18 is recognised by the LRR-receptor kinase EF-Tu Receptor (EFR) (Zipfel et al., 2006). Perception of Elf18 also induces BIK1 phosphorylation, suggesting BIK1 has a conserved role in PTI signal transduction upon detection of multiple PAMPs (Lu et al., 2010). Flg22 perception also induces the phosphorylation of another RLCK AVRPPHB SUSCEPTIBLE-LIKE 1 (PBL1), triggering dissociation of PBL1 from FLS2 and activating downstream PTI responses (Zhang et al., 2010a).

PTI involves multiple cellular signals and physiological responses. Between 30 seconds and two minutes after PAMP perception there is an influx of Ca^{2+} into the cytosol and after ten minutes a burst of ROS follows (Jeworutzki et al., 2010) (Figure 1.1). Ca^{2+} acts as an intracellular secondary messenger, amplifying the PTI signal. An influx of Ca^{2+} activates the opening of K^+, Cl^- and H^+ membrane channels, leading to changes in polarisation of the cell membrane (Jeworutzki et al., 2010). Calcium-dependent protein kinases (CDPKs) and RLCKs phosphorylate RESPIRATORY BURST OXIDASE HOMOOG D (RBOHD) and increase ROS production (Lu et al., 2010, Kadota et al., 2014, Li et al., 2014b, Bigeard et al., 2015) (Figure 1.1). In addition to CDPKs, MITOGEN-ACTIVATED PROTEIN KINASEs (MAPKs) are activated within two minutes of flg22 treatment and play a role in PTI signal transduction: MITOGEN-ACTIVATED PROTEIN KINASE KINASE 4/5 (MKK4/5) phosphorylates MPK3/6 and MKK1/2 phosphorylates MPK4 (Asai et al., 2002) (Figure 1.1). MAPKs then induce transcription of defence genes, e.g. via phosphorylation of the transcription factor WRKY DNA-BINDING PROTEIN 33 (WRKY33) (Mao et al., 2011).

Upon pathogen infection, systemic acquired resistance (SAR) refers to enchanced resistance in uninfected distant leaves. Two pathways involving salicylic acid (SA) and pipecolic acid promote the activation of SAR (Vlot et al., 2021). FMO1 is an important component of SAR, catalysing pipecolic acid

to N-hydroxypipecolic acid (NHP) (Hartmann et al., 2018). NHP then accumulates in distal leaves to activate SAR (Hartmann et al., 2018).

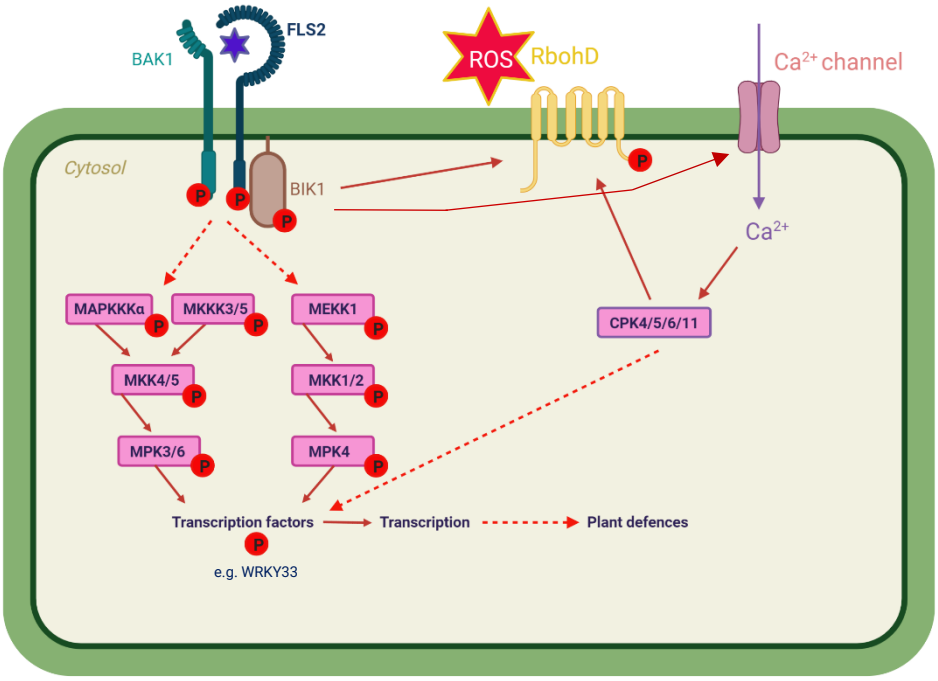

Figure 1.1. Signalling mechanisms induced during pattern-triggered immunity. Perception of flg22 by FLS2 and BAK1 induces BIK1 phosphorylation, $Ca2^{+}$ influx and a ROS burst. This then leads to activation of a MAPK cascade and phosphorylation of transcription factors to activate downstream defence responses.

1.2 Effector-triggered-immunity

Pathogens have evolved virulence factors called effectors, some of which interfere with PTI, allowing colonisation of the host plant. This inhibition of PTI signalling is referred to as effector triggered susceptibility (ETS). The *Pseudomonas syringae* effector AvrPphB, a cysteine protease, cleaves BIK1 and PBL1, and likely additional RLCKs, thus disrupting PTI signalling, leading to ETS (Zhang et al., 2010a). Additionally, another *P. syringae* effector HopAI1 inhibits MAPKs (e.g. MPK3 and MPK6) through its phosphothreonine lyase activity, inhibiting transcriptional activation of defence genes (Zhang et al., 2007). The second layer of plant immunity involves intracellular nucleotide-binding leucine-rich-repeat receptors (NLRs) which detect these effectors and activate effector triggered immunity (ETI). The connection between PTI, ETS and ETI is known as the zig-zag-zig model (Jones & Dangl, 2006). NLR proteins can be divided into several groups, but the two best studied groups are: those with a Toll/interleukin-1 receptor domain (TIR), or those with a coiled-coil domain (CC).

Recognition of pathogen effectors occurs through direct or indirect perception (Figure 1.2). The TIR-NLR Recognition of XopQ 1 (ROQ1) recognises the Xanthomonas effector XopQ through direct binding, leading to ROQ1 oligomerisation (Schultink et al., 2017, Martin et al., 2020). Indirect perception of effectors includes detection by NLR proteins of effector manipulation of guarded host proteins, decoys or integrated decoy domains within the NLR (van der Hoorn & Kamoun, 2008, Cesari et al., 2014a) (Figure 1.2). These decoys mimic virulence targets of effectors (van der Hoorn & Kamoun, 2008). The effector AvrAC from *Xanthomonas campestris* pv.*campestris* uridylylates the protein kinase PBL2, acting as a decoy for the true AvrAC target BIK1 (Wang et al., 2015). HOPZ-ACTIVATED RESISTANCE 1 (ZAR1), together with the pseudokinase RESISTANCE RELATED KINASE 1 (RKS1) interacts with the modified PBL2, leading to a conformational change in ZAR1 (Wang et al., 2019b). Indirect recognition of effectors may have evolved to allow recognition of multiple effectors by one decoy or guardee (Cesari, 2018). The NLR pair RESISTANT TO P. SYRINGAE 4 (RPS4) and RESISTANT TO RALSTONIA SOLANACEARUM 1 (RRS1)-R allele in Arabidopsis *thaliana* ecotype Ws-2 can recognise two bacterial pathogen effectors and an unknown effector from *Colletotrichum higginsianum* (Gassmann et al., 1999, Hinsch & Staskawicz, 1996, Deslandes et al., 2003, Narusaka et al., 2009).

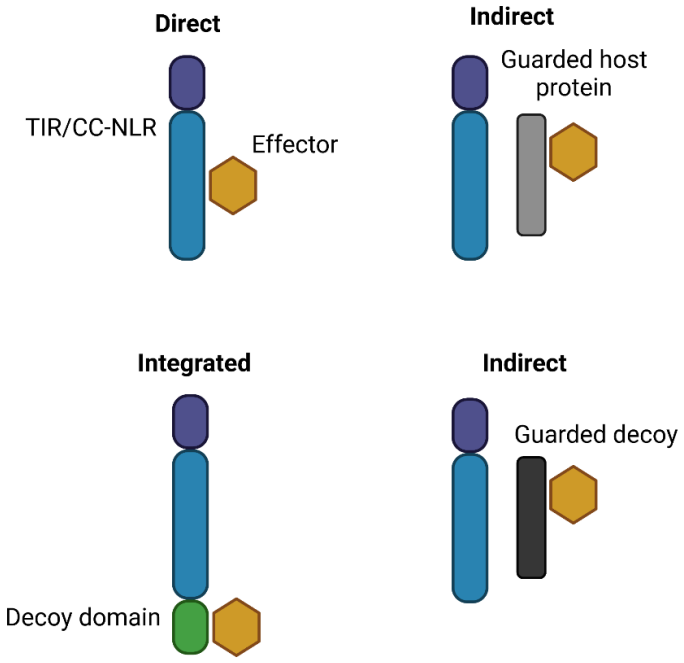

Figure 1.2. Recognition of pathogen effectors occurs through direct or indirect perception by NLRs. Effectors can bind NLRs directly or bind to integrated decoy domains within the NLR. Effectors can also bind to guarded host proteins or decoy proteins which mimic host proteins, leading to indirect effector recognition.

Some NLRs function on their own for effector recognition and defence signalling, known as singleton NLRs (Figure 1.3). Examples of a singleton NLR include RPS2 and RPM1 which recognise the effectors AvrRpt2 and AvrRpm1 respectively (Kunkel et al., 1993, Boyes et al., 1998). Some NLRs function in pairs, with one member carrying an integrated decoy domain for effector recognition, and the other member required for activating downstream defence responses (Adachi et al., 2019b, Feehan et al., 2020) (Figure 1.3). NLR pairs include the TIR-NLRs RRS1/RPS4 mentioned previously. The CC-NLR pair in rice RGA4/RGA5 contain a Heavy Metal Associated (HMA) decoy domain in RGA5 which recognises the effector AVR-Pia from *Magnaporthe oryzae* (Cesari et al., 2013, Cesari et al., 2014b). Some singleton and paired NLRs also require helper NLRs e.g. ACTIVATED DISEASE RESISTANCE 1 (ADR1) and N REQUIREMENT GENE 1 (NRG1) in Arabidopsis and NLR-Required for Cell death (NRCs) in *Solanaceae* plants (Adachi et al., 2019b, Feehan et al., 2020) (Figure 1.3). Helper NLRs are CC-NLRs with a RESISTANCE TO POWDERY MILDEW 8-like (RPW8-like) CC domain (Peart et al., 2005, Bonardi et al., 2011, Collier et al., 2011). Therefore, NLRs can form networks to connect effector recognition to the activation of downstream defence responses. The role of helper NLRs is discussed below in sections 1.2.2.1 and 1.2.3.

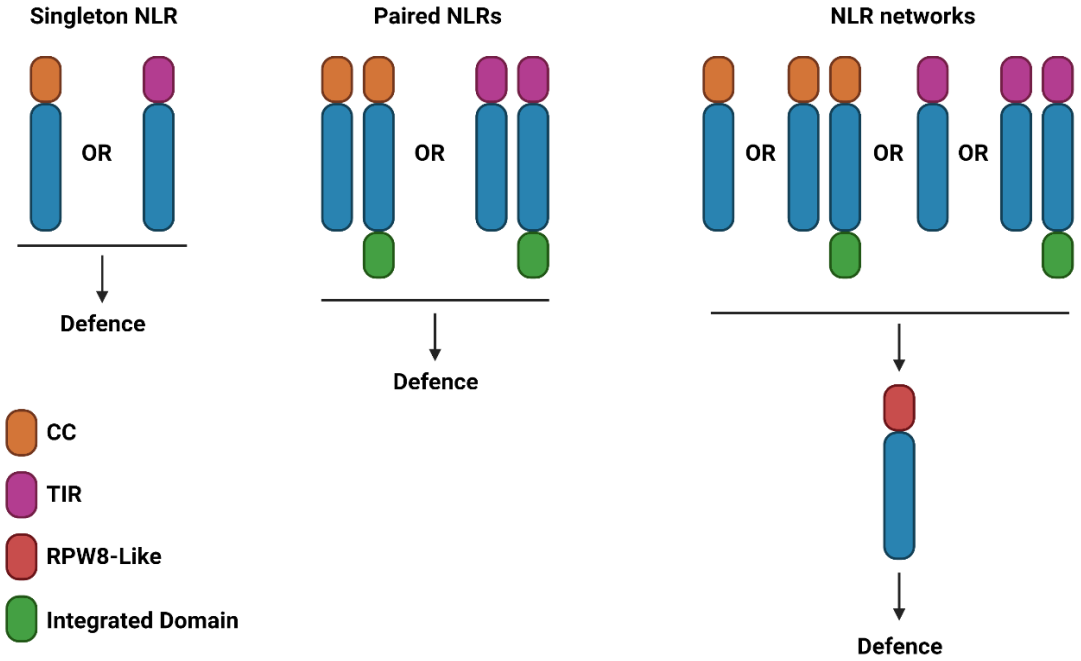

Figure 1.3. Intracellular NLRS signal on their own, in pairs or in NLR networks to activate defence. Singleton CC or TIR-NLRs recognise an effector and activate downstream signalling. Paired NLRs contained an integrated decoy domain in one member of the pair to recognise an effector and activate defence. Some singleton or paired NLRs also require downstream RPW8-Like helper NLRs to activate downstream defence responses. Redrawn from Feehan et al.,(2020) *Current Opinion in Plant Biology*.

Even with such diversification in effector detection by NLRs, the ETI downstream response is surprisingly conserved. ETI shares some of the same signalling components as PTI, such as MAPK activation, production of ROS, phytohormone signalling, influx of Ca^{2+} and transcriptional changes (Navarro et al., 2004, Tsuda & Katagiri, 2010, Hamdoun et al., 2013, Tsuda et al., 2013). However, ETI initiates a stronger and prolonged activation of defence, compared to PTI alone (Ngou et al., 2021, Yuan et al., 2021). Callose deposition is stronger and PTI-responsive genes *FLG22-INDUCED RECEPTOR-LIKE KINASE 1 (FRK1)*, *NDR1/HIN1-LIKE 10 (NHL10)* and *FAD-LINKED OXIDOREDUCTASE 1 (FOX1)* express to a higher level in PTI + ETI treatment, compared to PTI or ETI alone (Ngou et al., 2021). ETI also removes negative regulators of immunity; repression of gene expression of negative regulators DEFENSE NO DEATH 1 (DND1) and DND2 is induced by detection of the bacterial effector AvrRps4 (Zhu et al., 2010). Additionally, ETI activation often leads to a hypersensitive response (HR) in the infected cell (Jones & Dangl, 2006). PTI is required for activation of HR during ETI, as macroscopic HR is absent after estradiol-inducible *AvrRps4* expression (ETI alone) (Ngou et al., 2021). PTI and ETI treatment leads to a stronger accumulation and prolonged phosphorylation of PTI components MPK3, BIK1 and RBOHD compared to PTI alone (Ngou et al., 2020a, Yuan et al., 2020). The stronger phosphorylation is caused by the potentiation of PTI by ETI, as ETI alone does not lead to the phosphorylation of MAPKs or RBOHD and only a weak phosphorylation of RBOHD is seen in dexamethasone-inducible AvrRpt2 (Kadota et al., 2019, Ngou et al., 2021, Yuan et al., 2021). ETI-induced prolonged MPK3/6 activation requires the ETI signalling protein ENHANCED DISEASE SUSCEPTIBILITY 1 (EDS1) (Lang et al., 2022). However, EDS1 is not required for PTI-induced transient MPK3/6 phosphorylation (Lang et al., 2022). Furthermore, ETI and PTI are linked, with PRRs required for NLR-induced resistance and helper NLRs required for PTI signalling (Ngou et al., 2021, Pruitt et al., 2021, Yuan et al., 2021, Tian et al., 2021). The *bak1-5/bkk1-1* double mutant shows similar levels of susceptibility to *Pseudomonas syringae pv. Tomato* (*Pst)* DC3000 AvrRps4, as the *rps4-21/rps4b-1* double mutant (Ngou et al., 2021). A triple mutant plant deficient in the three main PRRs (*fls2/efr/cerk1*) and therefore unable to activate PTI, was also unable to activate ETI in response to *Pst* DC3000 AvrRpt2 (Yuan et al., 2021). TIR signalling enhances PTI immunity, as flg22 treatment of *eds1-24/pad4-1/adr1* triple mutant plants resulted in reduced accumulation of SA compared to wildtype (WT) plants (Tian et al., 2021). Therefore, there is mutual potentiation between PTI and ETI (Ngou et al., 2021). There are slight differences in immune responses activated by TIR-NLRs or CC-NLRs during ETI alone. CC-NLR activation in the absence of PTI leads to RBOHD phosphorylation, MAPK activation and ROS production and a calcium influx (Kadota et al., 2019, Bi et al., 2021, Ngou et al., 2021, Yuan et al., 2021). However, these defence outputs do not occur upon TIR-NLR activation without PTI (Ngou et al., 2021, Ngou et al., 2020). Therefore, there are differences in the signalling pathways and outputs activated between CC- and TIR-NLRs. However,

both CC-NLR and TIR-NLR-activated ETI acts to potentiate defence responses induced by PTI, by increasing the abundance of PTI signalling components through transcriptional and post-transcriptional changes (Ngou et al., 2021, Yuan et al., 2021).

ETI is characterised by the activation of HR and the restriction of pathogen growth. However, ETI does not require HR for full resistance to be induced (Heidrich et al., 2011). Mis-localisation of the effector AvrRps4 to the nucleus results in a failure to activate cell death but induces full bacterial resistance (Heidrich et al., 2011). Furthermore, nuclear export of AvrRps4 compromises resistance, indicating that cytosolic AvrRps4 is needed to activate cell death and nuclear AvrRps4 is required to restrict bacterial growth (Heidrich et al., 2011). This suggests two immunity branches are activated during AvrRps4-triggered ETI, by effector recognition in different subcellular compartments. Further evidence for an uncoupling of cell death and immune resistance is shown by the effector HopZ5, which activates defence in both Arabidopsis accessions Col-0 and Ct-1, despite only activating HR in Ct-1 (Jayaraman et al., 2017). Whether additional effectors activate different immunity pathways in different subcellular localisations should be further explored.

There is extensive transcriptional regulation during PTI and ETI signalling (Ding et al., 2020, Ding et al., 2021, Bjornson et al., 2021, Li et al., 2016). Rapid transcriptional changes occur within 30 minutes of PAMP treatment (Bjornson et al., 2021). These changes are conserved in response to different PAMPs e.g. elf18, flg22, Pep1, OGs and nlp20 (Bjornson et al., 2021). There is also extensive overlap in transcriptional changes that occur during PTI or PTI + ETI (Ding et al., 2021). However, PTI + ETI induces stronger expression of SA biosynthesis genes e.g. *ICS1*, *EDS5* and *PBS3* than PTI alone (Ding et al., 2020). There is also considerably less transcriptional changes during ETI alone (1584 upregulated genes in ETI, compared to 5000 in PTI + ETI), emphasising the mutual potentiation between PTI and ETI activation (Ding et al., 2021). Transcriptional regulation upon PTI + TIR-NLR-ETI or PTI + CC-NLR-ETI treatment is more similar to each other than during PTI alone, suggesting different NLRs activate a similar core set of defence genes (Ding et al., 2020).

1.2.1 RRS1/RPS4 are a pair of nuclear-localised TIR-NLRs in Arabidopsis

Changes in defence gene expression during immune activation are mediated by transcription factors including the WRKY family (Wani et al., 2021). WRKY transcription factors are targeted by some pathogen effectors, thus blocking DNA binding and inhibiting PTI transcriptional changes (Le Roux et al., 2015, Sarris et al., 2015). RRS1 and RPS4 are a pair of nuclear-localised TIR-NLRs in Arabidopsis *thaliana*. An integrated WRKY decoy domain in the RRS1 C-terminus protein can detect two

structurally different effectors, and with RPS4, activate defence (Zhang et al., 2017, Mukhi et al., 2021).

RRS1-R/RPS4 function together to recognise PopP2 from *Ralstonia solanacearum* and AvrRps4 from *Pseudomonas syringae pv pisi* (Gassmann et al., 1999, Hinsch & Staskawicz, 1996, Deslandes et al., 2003, Narusaka et al., 2009). The RRS1-R/RPS4 immune receptor also recognises an unknown effector from *Colletotrichum higginsianum* (Narusaka et al., 2009). There are two major alleles of RRS1; RRS1-R, found in Arabidopsis accession Ws-2 and RRS1-S in Col-0 (Deslandes et al., 2002). Both alleles can interact with PopP2, but interaction in RRS1-S does not lead to activated defence, due to the absence of 83 amino-acid C-terminal extension present in RRS1-R (Sarris et al., 2015). RRS1B and RPS4B, another pair with 60% similarity to RRS1 and RPS4, were found to confer resistance to AvrRps4 but not to PopP2 (Saucet et al., 2015). No difference in defence gene activation was found between the two pairs, suggesting they share downstream signalling components (Saucet et al., 2015). Incorrect pairing of RRS1 and RPS4B results in the absence of HR to AvrRps4, confirming specificity within each pair (Saucet et al., 2015).

Phosphorylation and acetylation of RRS1-R-WRKY domain show antagonistic roles in RRS1-R activation (Guo et al., 2020). Phosphorylation of RRS1-R at T1214 maintains RRS1-R in an inactive state (Guo et al., 2020). Phospho-dead mutants of RRS1-R (RRS1-R^{T1214A}) show constitutive defence responses and phospho-mimics (RRS1-R^{T1214D}) lose PopP2 responsiveness (Guo et al., 2020). RRS1-R^{T1214D} is still able to recognise AvrRps4, suggesting phosphorylation-induced maintenance of inactive RRS1-R is specific for PopP2 recognition (Guo et al., 2020). Surprisingly, the equivalent phospho-dead mutant in RRS1-S (RRS1-S^{T1212A}) is not auto active, suggesting the phospho-dead-induced auto-activity requires the 83-amino acid extension in RRS1-R (Guo et al., 2020). Acetylation of RRS1-R by PopP2 was enhanced in RRS1-R^{T1214A} and reduced in RRS1-R^{T1214D}, suggesting phosphorylation at T1214 inhibits the acetylation of lysines in the WRKY domain of RRS1-R (Guo et al., 2020). Furthermore, PopP2 was found to acetylate T1214, directly inhibiting T1214 capability of being phosphorylated (Guo et al., 2020). Phosphorylation of RRS1 D56-R, at different sites to T1214, is required for PopP2 but not AvrRps4-induced proximity of RRS1-R TIR and the C-terminal domain (Guo et al., 2020). AvrRps4 and PopP2 enhance the proximity of the TIR domain of RRS1 to its C terminus, leading to derepression of RRS1 and releasing the inhibition of RPS4 TIR domain by RRS1 TIR domain (Ma et al., 2018, Guo et al., 2020). Therefore, PopP2 acetylation of RRS1-R leads to enhanced proximity of the RRS1-TIR domain to its C terminus, activating RPS4 (Guo et al., 2020).

The recognition of AvrRps4 by RRS1/RPS4 is distinct from the recognition mechanisms of PopP2. The C-terminal domain of AvrRps4 directly binds the RRS1-WRKY domain (Mukhi et al., 2021). RRS1-WRKY domain is a WRKY transcription factor decoy and AvrRps4 binds WRKY41 with similar binding affinities as to RRS1-WRKY (Mukhi et al., 2021). Mutations of AvrRps4 at the RRS1-WRKY binding interface disrupt binding with both RRS1-WRKY and WRKY41, suggesting the same binding interface is involved in binding to multiple WRKYs (Mukhi et al., 2021). Mutations at the AvrRps4 binding interface inhibit HR activation and abolished bacterial resistance (Mukhi et al., 2021). The same AvrRps4 residues are also required for binding to the RRS1B WRKY domain (Mukhi et al., 2021). However, AvrRps4-RRS1B-WRKY binding affinity is much weaker than RRS1-WRKY (Mukhi et al., 2021). How AvrRps4 binding to RRS1-WRKY leads to RRS1/RPS4 activation needs to be further explored. These papers give further insight into how the RRS1/RPS4 complex has different mechanisms for activation, upon recognition of structurally different pathogen effectors.

1.2.2 ADR1 and NRG1 are helper NLRs in Arabidopsis

NRG1 was first described in *N. benthamiana* as required for resistance, mediated by the TIR-NLR N, against Tobacco mosaic virus (TMV) (Peart et al., 2005). Helper NLRs NRG1 and ADR1 work together with upstream sensor NLRs to activate downstream signalling events. Arabidopsis carries three gene copies of NRG1: NRG1.1 (NRG1A), NRG1.2 (NRG1B) and NRG1.3 (NRG1C) (Castel et al., 2019). NRG1.1 and NRG1.2 are functionally redundant and NRG1.3 acts antagonistically to NRG1.1 and NRG1.2 (Castel et al., 2019, Wu et al., 2019, Wu et al., 2022). The ADR1 family in Arabidopsis consists of three members: ADR1, ADR1-L1 and ADR1-L2 (Bonardi et al., 2011). ADR1 is required for the function of CC- and TIR-NLRs, whereas NRG1 functions downstream of only TIR-NLRs (Qi et al., 2018, Castel et al., 2019). Some NLRs signal through both ADR1 and NRG1, whereas some signal through one helper NLR (Castel et al., 2019).

After *Pst* DC3000 AvrRps4 infection, *nrg1.1/ nrg1.2* have similar resistance to WT plants (Saile et al., 2020). NRG1 has a role in induction of cell death but in the presence of ADR1, NRG1 isn't required for bacterial resistance, defence gene activation or an increase in salicylic acid levels in response to *Pst* (Castel et al., 2019). However, *adr1* triple mutants are more susceptible than WT and RRS1/RPS4-mediated resistance was completely abolished in a *helperless* pentuple mutant (*nrg1.1/nrg1.2* double combined with an *adr1* triple mutant) and are phenotypically indistinguishable from an *eds1* mutant. (Saile et al., 2020). This suggests an unequal genetic redundancy between NRG1s and ADR1s during AvrRps4-triggered ETI (Saile et al., 2020).

Conversely, NRG1 and ADR1 are equally redundant in WRR4A-mediated resistance, as Col-0, *adr1* triple and *nrg1.1/nrg1.2* mutants are resistant to Ac2V, but the *helperless* plants are as susceptible as *eds1-12* plants (Saile et al., 2020). Therefore, NRG1 may have an additional role in oomycete resistance, not required in response to the bacterial effector AvrRps4, perhaps due to the contribution of localised cell death in resistance to haustorial pathogens (Castel et al., 2019). Additionally, the manner of redundancy is dependent on the TIR-NLR activated (Saile et al., 2020). The role of RNLs in regulating gene expression during PTI is small (Saile et al., 2020). However, they are fully required for transcriptional reprogramming during TIR-NLR-mediated immunity, as 86% of genes induced after 4 hours of AvrRps4 recognition, are not induced in the *helperless* mutant (Saile et al., 2020).

1.2.2.1 Helper NLRs form heterotrimers with EDS1-PAD4 or EDS1-SAG101

EDS1, PHYTOALEXIN DEFICIENT 4 (PAD4) and SENESCENCE-ASSOCIATED GENE 101 (SAG101) are lipase-like proteins involved in downstream ETI signalling (Falk et al., 1999, Jirage et al., 1999, Feys et al., 2005). EDS1 is an important positive regulator of plant immunity (Parker et al., 1996). Loss of EDS1 in Arabidopsis abolishes TIR-NLR mediated, but not CC-NLR mediated immunity (Parker et al., 1996, Falk et al., 1999). PAD4, EDS1 and SAG101 share a novel C-terminal domain named EDS1 and PAD4-defined (EP) (Feys et al., 2001). SAG101 and PAD4 both interact with EDS1 at the same interface, forming mutually exclusive heterodimers (Feys et al., 2001, Feys et al., 2005, Wagner et al., 2013, Sun et al., 2021). Both the lipase-like and EP domains are important for heterodimer formation (Wagner et al., 2013). EDS1-PAD4 and EDS1-SAG101 form distinct heterotrimers with ADR1 and NRG1 respectively (Lapin et al., 2019, Sun et al., 2021) (Figure 1.4). Conserved residues in the EP domains of PAD4 and SAG101 are required for these associations with ADR1 or NRG1 (Dongus et al., 2022). Effector recognition alone induces formation of NRG1-EDS1-SAG101 heterotrimers (Feehan et al., 2023). SAG101 has stronger binding to NRG1.1 compared to NRG1.2 (Dongus et al., 2022), suggesting there may be different roles between NRG1.1 and NRG1.2 in Arabidopsis that are not yet understood.

In Arabidopsis, NRG1 and EDS1-SAG101 are vital for inducing cell death but are not required for restricting bacterial growth (Lapin et al., 2019). EDS1-PAD4 and ADR1 proteins are essential for bacterial resistance but not required for activating cell death (Lapin et al., 2019). EDS1 is required for both cell death induction and bacterial resistance branches of immunity (Lapin et al., 2019). SAG101 and NRG1 work downstream of TIR-NLRs to activate cell death but are not required for CC-NLR-mediated ETI (Sun et al., 2021). SAG101 and NRG1 are also not required for basal resistance to *Pst* (Sun et al., 2021). However, in the absence of the PAD4-ADR1 pathway, SAG101-NRG1 act to restrict

bacterial growth (Sun et al., 2021). Additionally, in the absence of SAG101-NRG1 pathway and SA signalling, PAD4-ADR1 functions to restore cell death (Sun et al., 2021).

The truncated allele of NRG1.3 has induced expression upon AvrRps4 recognition (Wu et al., 2022). Over-expression of NRG1.3 inhibits HR activation, resembling the *nrg1.1/nrg1.2* phenotype (Wu et al., 2022). NRG1.3 forms a complex with EDS1-SAG101 to inhibit formation of the NRG1.1/EDS1/SAG101 heterotrimer (Wu et al., 2022). Therefore, NRG1.3 acts as negative regulator of immunity by inhibiting heterotrimer formation and consequently inhibition of downstream defence activation (Wu et al., 2022).

1.2.2.2 There are evolutionary differences in the requirement of EDS1/PAD4/SAG101/NRG1 proteins

The *N. benthamiana* mutant in EDS1a, PAD4, SAG101a and SAG101b (*Nb_epss*) cannot activate HR (Lapin et al., 2019). Transient expression of *At*EDS1-*At*SAG101 in *Nb_epss* cannot activate bacterial growth restriction or mediate XopQ-triggered cell death (Lapin et al., 2019). Therefore, *At*EDS1-*At*SAG101 are unable to signal together with *Nb*NRG1, and there is a molecular incompatibility between signalling components from different species (Lapin et al., 2019). XopQ-mediated HR can be restored in *Nb_epss* when Arabidopsis alleles of NRG1, SAG101 and EDS1 are co-expressed (Lapin et al., 2019).

Different signalling networks act downstream of TIR NLRs in Solanaceous species, compared to Brassicas. In *N. benthamiana* immunity, downstream of the NLR ROQ1, SAG101b, NRG1 and EDS1a are required for both cell death and restricting bacterial growth, with no role for PAD4 (Gantner et al., 2019, Lapin et al., 2019). This contrasts with the role of PAD4 in bacterial growth restriction in Arabidopsis, suggesting there are different roles for EDS1-SAG101-NRG1 and EDS1-PAD4-ADR1 heterotrimers in *Brassicaceae* and *Solanaceae* (Lapin et al., 2019). Both Arabidopsis and *N. benthamiana* require SAG101 and NRG1 to activate cell death. However, in beet (*Beta vulgaris),* the Roq1 TIR-NLR can function and activate cell death, in the absence of SAG101 and NRG1, suggesting other proteins are involved in activating cell death in this plant species (Schultink et al., 2017). This indicates that immunity pathways and protein interactions identified in model species such as Arabidopsis and *N. benthamiana* may be absent downstream of the same NLR proteins in other plant species.

EDS1 and PAD4 are found in almost all angiosperm species but had been independently lost at least five times (Baggs et al., 2020). TIR-NLRs and SAG101 are absent from monocots (Baggs et al., 2020). *Ta*EDS1 *Triticum aestivum* can complement the *A. thaliana eds1*-2 mutant, suggesting EDS1 from evolutionary divergent species retain similar immunity functions (Baggs et al., 2020). However, this contradicts the incompatibility seen between Arabidopsis and *N. benthamiana* alleles of NRG1, EDS1 and SAG101 (Lapin et al., 2019). The five angiosperm species identified that lack EDS1/PAD4 have also lost RPW8-like helper NLR genes, suggesting these species have evolved to signal via a pathway independent of helper-NLRs and lipase-like proteins (Baggs et al., 2020). Additionally, the SA pathway is conserved in species that have lost EDS1, PAD4, SAG101, NDR1 and helper NLR genes, suggesting SA defence may be activated by another unknown pathway in these species (Baggs et al., 2020).

1.2.3 NLR oligomerisation and TIR-NLR signalling

1.2.3.1 NLR proteins oligomerise to activate downstream signalling

Animal NLRs oligomerise to form inflammasomes and activate downstream signalling pathways (Burdett et al., 2019). However, only recently was oligomerisation and formation of a NLR resistosome shown for plant NLRs. This was first shown for the Arabidopsis NLR ZAR1 (Wang et al., 2019a, Wang et al., 2019b). The AvrAC effector from *Xanthomonas campestris* pv. *campestris* uridylylates the protein kinase PBL2 (Wang et al., 2015). ZAR1 in Arabidopsis, together with RKS1, interact with the two uridylyl moieties of PBL2, leading to a conformation change in ZAR1. This initiates the release of ADP, switching ZAR1 from an inactive to a monomeric intermediate state (Wang et al., 2019b). Upon release of ADP, dATP or ATP can bind, leading to the formation of a $PBL2^{UMP}$-ZAR1-RKS1 oligomeric complex (Wang et al., 2019a). The pentameric ZAR1 resistosome contains a ZAR1 α-helical funnel-like structure formed by the ZAR1 CC-domains (Wang et al., 2019a). Later work showed that these α-helical funnels create pores in the plasma membrane and activated ZAR1 forms calcium channels (Bi et al., 2021). These ZAR1 Ca^{2+} channels trigger cell death (Bi et al., 2021). The same ZAR1 residues and α -helices required for AvrAC-induced ZAR1 oligomerisation, are also required for HopZ1a-induced ZAR1 oligomerisation (Hu et al., 2020). Therefore, there is conservation in ZAR1 activation and oligomerisation by two distinct pathogen effectors. The monocot CC-NLR Sr25 oligomerises upon direct recognition of the wheat stem rust *Puccinia graminis f. sp. tritici* effector AvrSr35 to form a Sr35 resistosome (Forderer et al., 2022, Zhao et al., 2022). Like ZAR1, the Sr35 resistosome forms calcium channels (Forderer et al., 2022). Therefore, activation mechanisms between CC-NLR resistosomes from dicot and monocot species are conserved.

In addition to CC-NLRs, the TIR-NLRs ROQ1 and RPP1 also oligomerise upon effector recognition (Ma et al., 2020a, Martin et al., 2020). The ZAR1 pentamer resistosome forms through indirect recognition of the effector AvrAC (Wang et al., 2019a, Wang et al., 2019b). However, the ROQ1 and RPP1 tetramer resistosomes are activated by direct effector recognition (Ma et al., 2020a, Martin et al., 2020). The structure of the NB-ARC domain of ROQ1 is similar to ZAR1, suggesting they share similar activation mechanisms (Martin et al., 2020). Mutations in the P-loop of ROQ1 inhibit oligomerisation, suggesting that ATP binding is required for ROQ1 oligomerisation (Martin et al., 2020). However, ADP, instead of ATP, binds to the P-loop of RPP1 in its active state (Ma et al., 2020a), suggesting there are differences in the activation mechanisms of TIR-NLR oligomerisation.

Oligomerisation has also been shown for helper NLRs NRG1 and NLR-Required for Cell death (NRCs) (Jacob et al., 2021, Contreras et al., 2022, Ahn et al., 2023, Feehan et al., 2023, Wang et al., 2023). NRCs are a class of helper NLRs in *Solanaceae* plants. A conserved motif found in the N-terminus of NRCs and in 20% of CC-NLRs including ZAR1, named the MADA motif, is required for cell death (Adachi et al., 2019a). This motif is within the α1 helix of ZAR1, which forms the calcium channel pore during resistosome formation (Adachi et al., 2019a, Wang et al., 2019a). Upon recognition of the effector Rpi-amr3 from *Phytophthora infestans* by AVRamr3 in *Solanum americanum*, NRC2 forms oligomers (Ahn et al., 2023). Additionally, multiple distinct sensor NLRs induce NRC2 oligomerisation (Contreras et al., 2022, Ahn et al., 2023). These NRC2 oligomers do not contain the sensor NLRs, suggesting the NRC2 oligomer is distinct from the AVRamr3-Rpi-amr3 complex (Ahn et al., 2023). NRC2 re-localises to the plasma membrane upon oligomerisation (Contreras et al., 2022, Ahn et al., 2023). Mutations within the P-loop of NRC2, required for ATP binding in ZAR1, abolish HR and NRC2 oligomerisation (Ahn et al., 2023). This suggests that ATP binding may be required for NRC2 oligomerisation (Ahn et al., 2023). Rpi-amr3 lacks the MADA motif, aligning with the observation that the sensor NLR Rpi-amr3 does not form oligomers (Ahn et al., 2023). Another helper NLR NRC4 mutated within the MADA motif can still form puncta at the plasma membrane (Duggan et al., 2021). This observation suggests that the MADA motif is not required for oligomerisation and may only be required to create Ca^{2+} channel activity that can promote cell death (Duggan et al., 2021). This work suggests a new mechanism whereby in some instances the helper NLR, instead of the sensor NLR, forms oligomers, localises to the plasma membrane and forms Ca^{2+} channels to activate cell death.

The helper NLR NRG1 oligomerises upon effector recognition to form puncta at the plasma membrane (Jacob et al., 2021, Feehan et al., 2023, Wang et al., 2023). Both cell-surface receptor activation (PTI) and intracellular NLR activation (ETI) are required for NRG1 oligomerisation (Feehan et al., 2023). NRG1 self-association is paralog specific with no association found between NRG1.1-V5 and NRG1.2-FLAG (Feehan et al., 2023). In addition to the NRG1 oligomer, the formation of an EDS1-SAG101-NRG1

resistosome upon PTI + ETI activation was proposed (Feehan et al., 2023). However, a paper from a different lab has suggested that EDS1 and SAG101 are not present within the NRG1 oligomer (Wang et al., 2023). Wang et al., (2023) propose that EDS1-SAG101 disassociate from the EDS1-SAG101-NRG1 heterotrimer prior to NRG1 oligomerisation. Wang et al., (2023) experiments were done with total protein lysate, instead of immune-precipitated NRG1 as used in Feehan et al., (2023), where only a small proportion of EDS1/SAG101/NRG1 protein was detected within a resistosome. Additionally, the EDS1-SAG101-NRG1 resistosome was detected 8 hours after PTI + ETI activation in Arabidopsis (Feehan et al., 2023), whereas Wang et al., (2023) investigated complex formation 42 hours after transient expression in *N. benthamiana*. Therefore, the EDS1-SAG101-NRG1 resistosome may have been present but below the levels of detection due to the methods used by Wang et al., (2023).

P-loop mutants prevent NRG1 oligomerisation and cell death activation, suggesting ATP binding may be a conserved mechanism of activation (Jacob et al., 2021, Sun et al., 2021). Mutations in NRG1, in similar structural positions to those in the ZAR1 α1-helix, are unable to activate cell death but still heterodimerise with EDS1-SAG101 (Sun et al., 2021). Like ZAR1, NRG1 and ADR1 form Ca^{2+} influx channels at the plasma membrane (Jacob et al., 2021). Despite the localisation of NRG1 to the plasma membrane, a cytoplasmic pool of SAG101 and EDS1 is also required for cell death activation (Wang et al., 2023). Additionally, effector-dependent NRG1-SAG101-EDS1 associations were recently found in the nucleus, indicating that these associations are found in multiple subcellular locations (Feehan et al., 2023). The crystal structure of the NRG1 N-terminal signalling domain resembles the animal cell death pore-forming MLKL cation channel and ZAR1 which also form a calcium channel (Jubic et al., 2019, Bi et al., 2021, Jacob et al., 2021). The first 16 amino acids of NRG1 are essential for Ca^{2+} influx and induction of cell death but are not required for oligomerisation or plasma membrane localisation (Jacob et al., 2021). The auto-active NRG1-driven Ca^{2+} influx was also blocked by Ca^{2+} channel blockers (Jacob et al., 2021). These results suggest active NRG1 forms ion channels at the plasma membrane that mediate Ca^{2+} influx (Jacob et al., 2021). Therefore, there is a structurally conserved mechanism for oligomerisation, membrane localisation and the creation of Ca^{2+} channels in the plasma membrane between both singleton CC-NLRs and helper NLRs.

1.2.3.2 TIR-NLRs catalyse the production of small molecules which activate heterotrimer formation of downstream signalling partners

TIR-NLRs activate downstream signalling components by producing TIR-catalysed small molecules (Huang et al., 2022). TIR-NLRs have NADase activity and catalyse the production of small molecules (Horsefield et al., 2019, Wan et al., 2019, Huang et al., 2022, Jia et al., 2022). Formation of a TIR-

resistosome is required for NADase activity (Ma et al., 2020a). EDS1-PAD4-ADR1-L1 interaction is dependent on RPP1 resistosome formation and NADase activity (Huang et al., 2022). Therefore, TIR-catalysed products induce EDS1-PAD4-ADR1-L1 associations (Huang et al., 2022). pRIB-ADP/AMP interact with a pocket formed by the C-terminal EP domains of EDS1 and PAD4 (Huang et al., 2022). Binding of pRIB-ADP/AMP results in a conformational change in PAD4, promoting EDS1-PAD4 interaction with ADR1-L1 (Huang et al., 2022) (Figure 1.4). The TIR-catalysed molecules are also weakly bound by EDS1-SAG101, promoting NRG1.1 interaction, suggesting a preference for EDS1-PAD4 (Huang et al., 2022). TIR proteins also catalyse the production of ADPr-ATP and di-ADPR (Jia et al., 2022). These are preferentially bound by EDS1-SAG101, triggering a conformational change in SAG101 and promoting associations with NRG1.1 (Jia et al., 2022) (Figure 1.4). TIR domain NADase activity has also been shown to be required for EDS1-SAG101-NRG1 association *in vivo* (Feehan et al., 2023). The SAG101 residues which interact with ADPr-ATP are not well conserved in PAD4, providing a structural mechanism for the binding specificity (Jia et al., 2022). This work provides a mechanism whereby two signalling pathways are activated by two distinct TIR-catalysed products (Huang et al., 2022, Jia et al., 2022). EDS1^{R493A}, a mutation in the EP domain, maintains PAD4 interaction but has increased disease susceptibility, delayed transcriptional responses and abolished HR (Bhandari et al., 2019, Lapin et al., 2019). As TIR-catalysed products bind the EDS1 EP domain, this suggests a link between binding of pRIB-ADP/AMP and activation of defence pathways (Bhandari et al., 2019).

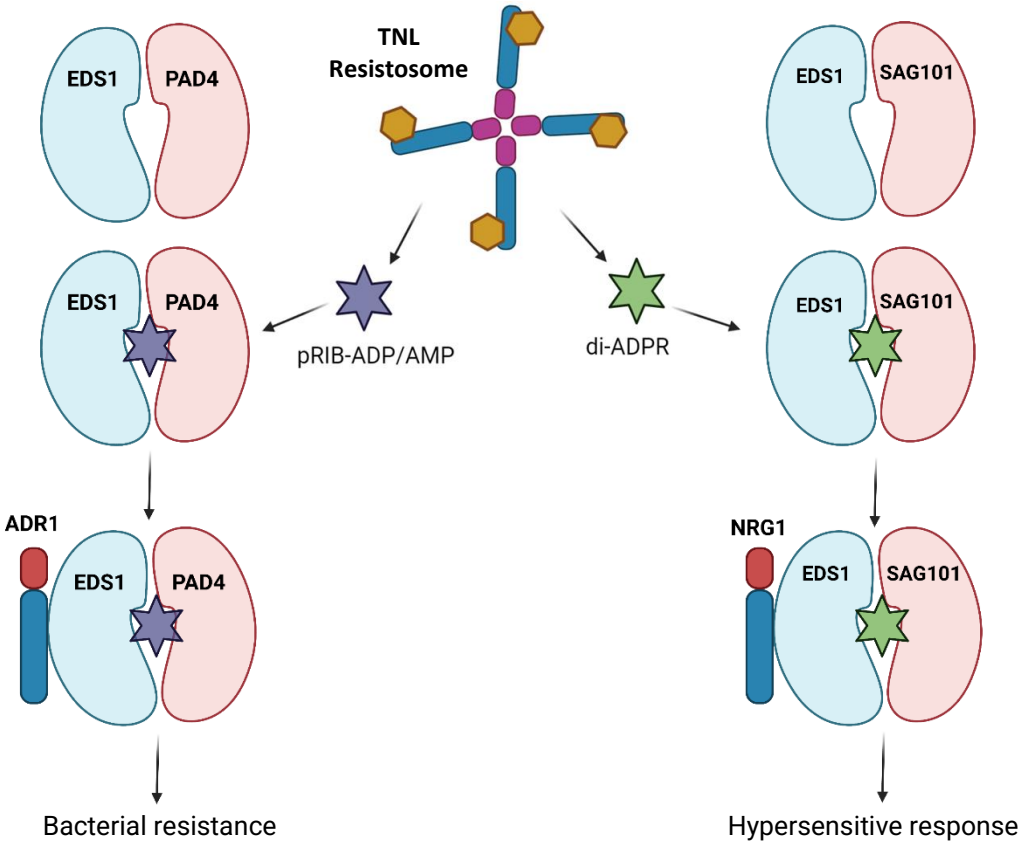

Figure 1.4. TIR-NLR oligomerisation and NADase activity triggers EDS1-SAG101-NRG1 and EDS1-PAD4-ADR1 heterotrimer formation. Upon effector recognition TIR-NLRs oligomerise and catalyse the production of small molecules e.g. pRIB-ADP/AMP, ADPr-ATP and di-ADPR. Binding of these small molecules to a pocket formed by the EP-domains of EDS1-PAD4 or EDS1-SAG101 promotes interaction with ADR1 or NRG1 respectively. Adapted from Sun et al., (2021) *Nature Communications.*

1.4 Phosphorylation has an important role in defence signalling pathways

Phosphorylation is one of the most abundant post-translational modifications (PTMs), with 47% of the proteome containing phosphorylation sites (Mergner et al., 2020). Phosphorylation regulates cell signalling by altering protein activity and mediating protein interactions. Levels of protein phosphorylation vary between proteins (Mergner et al., 2020). The Late Embryogenesis Abundant (LEA) protein family shows high phosphorylation levels throughout the protein at nearly all their serine, threonine and tyrosine residues (Mergner et al., 2020). However, other proteins were found to only be phosphorylated at a few sites in a specific protein region e.g. regulatory domains (Mergner et al., 2020). Additionally, all detected phosphorylation sites may not have a functional consequence.

Proteins involved in PTI signal transduction from flg22 detection to transcriptional activation are already present in the cell, but become activated by complex formation, conformational change or PTMs (Bigeard et al., 2015, Couto & Zipfel, 2016). Protein phosphorylation and phospho-relay is one of the key changes that are responsible for PTI signal transduction (Bigeard et al., 2015). Perception of flg22 facilitates trans-phosphorylation and autophosphorylation of the kinase domains of FLS2 and its co-receptor BAK1 (Lu et al., 2010). This leads to BAK1 trans-phosphorylation of BIK1, allowing BIK1 to disassociate from the PRR complex and phosphorylate RBOHD (Lu et al., 2010, Kadota et al., 2014, Li et al., 2014b, Lin et al., 2014). PRR phosphorylation also leads to downstream MAPK signalling cascades (Asai et al., 2002). PRRs activate MAPKKKs, which phosphorylate MAPKKs, which activate downstream MAPKs (Rasmussen et al., 2012). CDPKs are activated within 30 minutes of flg22 treatment by a Ca^{2+} influx into the cell (Boudsocq et al., 2010). CPK4/5/6/11 are involved in activating the ROS burst, transcriptional reprogramming and bacterial resistance (Boudsocq et al., 2010). For example, CPK5 phosphorylates RBOHD upon PAMP treatment (Dubiella et al., 2013). In addition to protein kinases, protein phosphatases also negatively regulate PTI activation. The protein phosphatase 2A (PP2A) associates with and negatively regulates BAK1 phosphorylation (Segonzac et al., 2014). Many of the phosphorylation sites involved in PTI signal transduction have been identified by quantitative phospho-proteomics (Benschop et al., 2007, Nühse et al., 2007, Mithoe et al., 2012, Rayapuram et al., 2014).

The role of phosphorylation during ETI is not as well studied as PTI. Dexamethasone-inducible AvrRpt2-triggered ETI induces phosphorylation sites in RBOHD which overlap with sites phosphorylated during PTI (Kadota et al., 2019). However, the ETI-induced phospho-sites in RBOHD are BIK1 independent, suggesting they may be phosphorylated in a pathway separate from that activated during PTI (Kadota et al., 2019). The calcium ATPase ACA8 forms a complex with FLS2 and regulates Ca^{2+} levels during flg22 induced PTI (Frei dit Frey et al., 2012). Overlapping phospho-sites between ETI and PTI were also found in ACA8 (Kadota et al., 2019). Novel ETI phosphorylation sites were found in proteins such as PLASMA MEMBRANE INTRINSIC PROTEIN (PIP) aquaporins (Kadota et al., 2019). The phosphorylation sites mentioned are induced upon CC-NLR-mediated ETI. Phosphorylation sites induced upon TIR-NLR-mediated ETI remain unknown. Additionally, phosphorylation induced during PTI + ETI may be more extensive than that identified during ETI alone, due to the mutual potentiation between PTI and ETI (Ngou et al., 2021, Yuan et al., 2021). However, quantitative phospho-proteomics has not been performed comparing PTI, ETI and PTI + ETI conditions.

1.4.1 Quantitative proteomic methods to identify phosphorylation changes

1.4.1.1 Parallel reaction monitoring (PRM)

Mass spectrometry can identify protein phosphorylation as a mass shift of +79.99 Da, due to the addition of HPO_3 on a serine, threonine, or tyrosine residue. Different quantitative phospho-proteomic methods can be utilised depending on the specificity, accuracy and biological insight required. Discovery phospho-proteomics using a data dependent acquisition (DDA) mass-spectrometry method provides information on what phospho-peptides are present in a sample (Elmore et al., 2021). A phospho-peptide library generated by DDA can then be used to create a peptide target list for quantification by parallel reaction monitoring (PRM). During PRM, target peptides termed precursor ions are selected using a quadrupole mass filter and fragmented into fragment ions. These fragment ions are measured in the Orbitrap mass analyser. Using Skyline software, chromatograms are created overlaying the intensity of each fragment ion for each peptide. The peak areas of the fragment ions are then used for peptide quantification. Quantification by PRM of the MS2 spectra is very sensitive and accurate due to multiple observations of a fragment ion. Fragment ions can also be used to narrow down the exact phosphorylation site within a peptide. PRM was successfully used to quantify phosphorylation sites within the TIR-NLR RRS1 (Guo et al., 2020).

1.4.1.2 MS1 quantification

MS1 quantification is a different method of quantification which quantifies the precursor MS1 and relies on matching MS2 spectra to identify the correct MS1 precursor peaks (Wang et al., 2019c, Elmore et al., 2021). MS1 can be less accurate, as it may be difficult to differentiate between different precursors with the same mass and tends to work better for precursors with a high frequency. However, MS1 can quantify low abundant peptides across all biological samples, even if only detected in a few samples by MS2, removing any issues associated with missing data (Wang et al., 2019c). In addition to quantifying MS1 precursors in Skyline, MS1 quantification using MaxQuant software is frequently used for protein quantification, as well as phosphorylation (Mergner et al., 2020)

1.5 Study aims and objectives

This study aimed to use quantitative proteomic approaches to identify phosphorylation changes during ETI signalling. Phosphorylation events during PTI have been extensively studied. However, the phosphorylation changes during ETI are less well defined. Additionally, previously studies have not focused on phosphorylation of nuclear-localised proteins upon TIR-NLR ETI-activation. Therefore, the

first part of this study aimed to fill the knowledge gap in this area. We aimed to use estradiol-inducible AvrRps4 lines to identify ETI-induced phosphorylation sites in nuclear proteins. Functional characterisation of phospho-sites can reveal the biological function of phosphorylation changes that were identified in large-scale quantitative proteomic studies. We aimed to investigate the function of phosphorylation changes in SARD1 during its role as a transcriptional activator of defence genes. Dual-luciferase constructs were transiently expressed in Arabidopsis protoplasts to measure differences in the ability of SARD1 phospho-variants to bind to the EDS5 promoter.

Targeted proteomic methods are used to quantify phosphorylation changes of a protein of interest. We used targeted proteomic methods to investigate phosphorylation changes of the helper NLR NRG1, whose phosphorylation was not identified by global phosphorylation methods. Previous research has reported that both PTI and ETI are required for NRG1 oligomerisation (Feehan et al., 2023). This study aimed to investigate if phosphorylation is required for NRG1 signalling. Phos-tag gels identified phosphorylated NRG1 bands during Pf0-1 treatment. Mass spectrometry analysis identified two phosphorylation sites in NRG1. Further assays revealed that one of these phospho-sites is required for HR activation in *N. benthamiana*.

TurboID proximity labelling labels proteins in close proximity to a protein of interest. Therefore, TurboID can be used to provide leads to novel protein interactors of key ETI signalling components, revealing new ETI signalling pathways and protein complex formations. Proximity labelling may also reveal kinases/phosphatases responsible for the phosphorylation changes during ETI activation identified by quantitative proteomics. This studied aimed to use proximity labelling to identify protein interactors of SARD1, TPR1 and EDS1 during both PTI, ETI and PTI + ETI signalling. Protein interactors identified by proximity labelling were confirmed by Co-immunoprecipitation and the biological relevance of their interaction further investigated.

This study provides excellent proteomic datasets from which further studies can build upon to expand our understanding of ETI signalling pathways. Additionally, this work gives insight into helper NLR signalling mechanisms and will guide future investigations into NRG1 oligomerisation activation.

Chapter 2

Materials and Methods

2 Materials and Methods

Chemicals and reagents were purchased from Merck (Sigma Aldrich), Melford Laboratories, Thermo Fisher Scientific and Sartorius.

2.1 Bacterial methods

2.1.1 Media for bacterial growth

2.1.1.1 Lysogeny broth media

Lysogeny broth (LB) of 1% (w/v) tryptone, 0.5% (w/v) yeast extract, and 1% (w/v) sodium chloride at pH of 7.0 was made in de-ionised water before autoclaving. To make selection plates, 1.5% (w/v) agar was included prior to autoclaving. Molten LB agar was cooled to 65 °C before addition of antibiotics and poured into 90 mm Petri dishes. LB liquid media and LB agar plates were used to culture *E. coli* and *Agrobacterium* strains.

2.1.1.2 King's B medium

King's B medium (KB) was made with 2% (w/v) proteose peptone, 0.1% (v/v) glycerol, and 0.15% (w/v) potassium phosphate dibasic at pH of 7.0 in de-ionised water before autoclaving. To prevent precipitation, magnesium sulphate was adjusted to 1.5% (w/v) after autoclaving. For KB selection plates, 1.5% (w/v) agar was added before autoclaving. Molten KB agar was cooled to 65 °C before addition of antibiotics and poured into 90 mm Petri dishes. KB media was used to culture *Pseudomonas fluorescence* (Pf0-1) and *Pseudomonas syringae pv tomato* (DC3000) strains.

2.1.1.3 Antibiotics

Stock and working concentrations of antibiotics used are listed in Table 2.1. Solutions were filter sterilised with a 0.3 µM Minisart® filter. Stock solutions were stored at – 20 °C, except Rifampicin which was stored at 4 °C.

Table 2.1. Stock and working concentrations of antibiotics used to grow bacteria on media selection plates or in liquid cultures.

Antibiotic	Stock (mg/mL)	Working (µg/mL)			
		E.coli	*A. tumefaciens*	Pf0-1	DC3000
Carbenicillin	100 in H_20	100	100	-	-
Chloramphenicol	10 in Ethanol	-	-	30	-
Gentamicin	10 in H_20	-	20	100	-
Kanamycin	50 in H_20	50	50	100	50
Rifampicin	10 in Methanol	-	50	-	50
Spectinomycin	100 in H_20	50	50	-	-

2.1.2 Bacterial strains

2.1.2.1 *Agrobacterium tumefaciens*

Agrobacterium strain used in this study was GV3101. GV3101 was grown for 48 hours at 28 °C on LB media with rifampicin, gentamycin and a third plasmid-carried selectable marker. GV3101 was used for transient transformation of *Nicotiana benthamiana* and stable transformation of Arabidopsis.

2.1.2.2 *E.coli*

Electrocompetent *Escherichia coli* strain DH10B was used for Golden Gate molecular biology. One Shot™ TOP10 Chemically Competent *E. coli* (Thermo: C404010) were used for USER cloning. DH10B or TOP10 were grown on LB media supplemented with the antibiotic corresponding to the plasmid-carried selectable marker at 37 °C for 15 hours.

2.1.2.3 Pf0-1

A non-pathogenic strain of *Pseudomonas fluorescence* (Pf0-1) has been engineered with a type III secretion system to deliver an effector (Thomas et al., 2009). Pf0-1 was used in this study for pathogen assays in *Arabidopsis thaliana* and *Nicotiana benthamiana.* Pf0-1 was grown on KB media supplemented with chloramphenicol and gentamycin (Pf0-1_AvrRps4, Pf0-1_XopQ) or chloramphenicol and kanamycin (Pf0-1_AvrRps4^{EEAA} or Pf0-1_Empty vector) at 28 °C for 48 hours. Pf0-1 strains were inherited from other lab members.

2.1.2.4 *Pst* DC3000

Pseudomonas syringae pv tomato strain (*Pst*) DC3000 was used for bacterial growth assays in *Arabidopsis thaliana*. DC3000 was grown on KB media supplemented with rifampicin and kanamycin at 28 °C for 48 hours. DC3000 strains were expressing the effector AvrRps4 or an empty vector. DC3000 strains were inherited from other lab members.

2.1.3 Bacterial transformation

2.1.3.1 Transformation of *E.coli* DH10B and *A.tumefaciens* GV3101 cells

Plasmids were transformed into electrocompetent *E.coli* DH10B and *A.tumefaciens* GV3101 using electroporation. Electrocompetent cells were thawed on ice for 10 minutes before addition of isolated plasmid DNA or a ligation reaction. The bacteria-DNA mix was then added into a cold 0.1 cm electroporation cuvette and electroporation conducted using a MicroPulser (Bio-Rad). *E.coli* cells were pulsed once at 1.k kV with the "Ec1" pre-programmed settings and *A. tumefaciens* cells were pulsed once at 2.4 kV with the "Agr" pre-programmed settings. Cells were resuspended in 200 µL of LB media and incubated with shaking at 200 RPM for 1 hour at 37 °C for *E. coli* or 28 °C for *A. tumefaciens*. 50 µL of cells were spread on antibiotic selection LB plates and grown overnight at 37 °C for *E.coli* or 28 °C for *A. tumefaciens*. For blue/white selection, 10 µL of 1 M IPTG and 50 µL of 50 mg/mL 5-bromo-4-chloro-3-indolyl β-D-galactopyranoside (X-gal) were spread onto plates prior to plating of cells.

2.1.3.2 Glycerol stocks

A single colony from selection plates was placed in 5 mL of LB media with appropriate antibiotics and incubated overnight at 200 RPM at 37 °C for *E. coli* and 28 °C for *A. tumefaciens*, Pf0-1 or DC3000. 500 µL of the grown liquid culture was mixed with 250 µL of 60% glycerol, frozen in liquid nitrogen and stored at – 80 °C.

2.2 Plant Methods

2.2.1 Growth conditions

Arabidopsis seeds were sown onto compost and grown in a controlled environment room (CER) at 21 °C, with 8 hours of light, 16 hours of dark and 70% relative humidity. For seed collection, Arabidopsis plants were grown at 21 °C, with 16 hours of light, 8 hours of dark and 70% humidity.

Nicotiana benthamiana seeds were sown onto compost and grown in a controlled environment room (CER) at 21 °C, with 16 hours of light, 8 hours of dark and 70% humidity. 4-week-old plants were used for *A. tumefaciens*-mediated transient transformation of leaf tissue and cell death assays.

2.2.2 Plant growth on plates

2.2.2.1 Seed sterilisation

For sterilisation *Arabidopsis* seeds were placed in open Eppendorf 1.5 mL tubes, next to a 500 mL glass beaker containing 100 mL 10% sodium hypochlorite and 3 mL of hydrochloric acid, within a gas tight chamber, and left overnight within a fume hood. After vapour-phase sterilisation, seeds were sterilised with a 1% hypochlorite solution wash followed by five sterile water washes. After sterilisation, the seeds were kept at 4 °C in the dark for 24 hours before sowing on ½ MS media plates.

2.2.2.2 ½ Murashige and Skoog

½ Murashige and Skoog (MS) was made with 0.2% Murashige and Skoog medium and 1% sucrose. pH was adjusted to 5.8 with NaOH. For agar plates, 1.5% (w/v) agar was included before autoclaving.

2.2.2.3 Estradiol plates

Molten ½ MS agar was cooled to 65 °C before addition of 25 µM estradiol and poured into 90 mm square Petri dishes.

2.2.2.4 Basta plates

Molten ½ MS agar was cooled to 65 °C before addition of 10 µg/mL Phosphinotricin (PPT) (Melford Duchefa: P0159.0250) and poured into 120 mm square Petri dishes.

2.2.3 Creation of stable Arabidopsis lines

2.2.3.1 Arabidopsis transformation

Arabidopsis transformation was carried out by the transformation team at The Sainsbury Laboratory. Flowering plants were dipped in a solution of *A. tumefaciens* at OD_{600} =0.5 (2.5x108 cfu/mL) (Clough & Bent, 1998).

Col-0: *eds1-2* (Falk et al., 1999) and SETI (Ngou et al., 2020) were crossed by previous lab member Dr Pingtao Ding to create a SETI: *eds1-2* line.

2.2.3.2 Basta selection

Transformed seeds were sown on soil sprayed three times with basta by the horticultural services at JIC and survived plants bagged to collect seeds. T2 seeds were sterilised and plated on ½ MS media supplemented with 10 µg/mL Phosphinotricin (PPT) (Melford Duchefa: P0159.0250) (Figure 2.1). Lines segregating at 3(survived):1(died) after 2 weeks were then transferred to soil and T3 seeds collected. T3 seeds were sterilised and sown onto ½ MS supplemented with 10 µg/mL PPT to identify homozygous lines. 100 seeds were sown and evenly spaced out on each 120 mm plate to prevent false negatives.

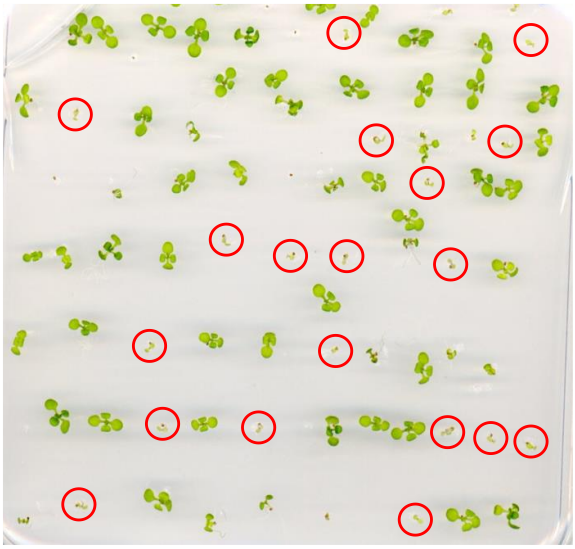

Figure 2.1. Segregating T2 seeds with basta resistance at 3:1 ratio. T2 seeds were grown on ½ MS media with 10 µg/mL Phosphinotricin (PPT) for 14 days. Surviving seeds are either homozygous or heterozygous for Basta resistance and EDS1-TurboID construct. The seedlings circled in red have died and are not transformed with basta resistance.

2.2.3.3 Fast-Red selection

FAST (fluorescence-accumulating seed technology) under a seed coat specific promoter, enables quick identification of transformed/homozygous seeds (Shimada et al., 2010). *Agrobacterium* transformed seeds were screened using Fast-Red selection using a Leica M165 fluorescent stereo microscope with DSR filter. Seeds with a red fluorescence were selected and sown on soil. T2 lines were selected which showed at 3 (Red): 1 (not red) ratio and grown to collect T3 seeds. T3 transformant lines were selected which were homozygous for Fast-Red fluorescence.

2.2.4 Plant infiltrations

2.2.4.1 flg22 treatment of seedlings

Arabidopsis seeds were sterilised as described in 2.2.2.1, sown onto a ½ MS plate and grown for 4 days. 10 seedlings were transferred into each well of a 6-well plate (Starlab UK: 08003866). 4 mL of ½ MS liquid media was added to each well and the lids sealed with 3M Micropore surgical tape. The plates were placed on a rotator at 40 RPM for 10 days and grown in conditions as described in 2.2.1. The media was then replaced with ½ MS media containing 100 nM flg22 or water. After 90 minutes seedlings were dried with a paper towel and frozen in liquid media.

2.2.4.2 Vacuum infiltration of Arabidopsis seedlings

Seedlings grown in 6-well plates in ½ MS liquid media for 14 days were transferred into 10 mL of fresh ½ MS media in a 50 mL beaker, containing 200 nM flg22 or mock (water). A smaller beaker was placed on top of the seedlings to fully submerge them in the liquid media. The seedlings were placed under a vacuum for 5 minutes and were harvested at 5, 10 and 30 minutes after flg22 treatment. Seedlings were dried with blue roll and frozen in liquid nitrogen.

2.2.4.3 Pf0-1 flooding of seedlings on plates

After surface sterilisation, seeds were stored at 4 °C for 24-48 hours. 10 seeds were sown on each petri dish containing ½ MS media with 0.3% Phytagel added before autoclaving. Seedlings were grown for two weeks as described in 2.2.1. 40 mL of bacterial suspension containing Pf0-1_AvrRps4 at OD_{600}: 0.2 and 0.025% Silwet L-77 in 10 mM $MgCl_2$ was added to the petri dish. A mock suspension with 0.025% Silwet L-77 and 10 mM $MgCl_2$ was added to mock samples. The plates were left to incubate for 4 minutes at room temperature. The bacterial suspension was decanted, and plates sealed with 3M Micropore surgical tape. After 4 hours the seedlings were patted dry, placed in a 2 mL Eppendorf tube with two 3MM Tungsten Carbide Beads (Qiagen) and frozen in liquid nitrogen. RNA was extracted as described in 2.3.9.

2.2.4.4 Pf0-1 infiltrations of leaves

Pf0-1 strains were streaked on to KB antibiotic selection plates from glycerols stored at – 80 °C. Pf0-1 was grown at 28 °C for 48 hours. Cells were resuspended in 10 mM $MgCl_2$ and OD_{600} measured by spectrophotometer. Cells were diluted to OD_{600} = 0.2 for Arabidopsis or OD_{600} =0.3 for *N. benthamiana* infiltrations. 5-week-old Arabidopsis rosette leaves or 4-week-old *N. benthamiana*

leaves were infiltrated with Pf0-1 using a blunt ended 1 mL syringe. Leaves for protein extraction were harvested, frozen in liquid nitrogen and stored at – 80 °C.

2.2.4.5 β-Estradiol infiltration of Arabidopsis leaves

5-week-old Arabidopsis leaves of stable lines carrying the XVE cassette and LexA promoter-driven AvrRps4 were infiltrated with 50 µM β-estradiol diluted in 10 mM MgCl2 with 0.01% Silwet® L-77. Mock leaves were infiltrated with the same volume of DMSO instead of β-estradiol.

2.2.4.6 *Nicotiana benthamiana* transient expression

Agrobacterium strains carrying required expression plasmids were streaked on to LB antibiotic selection plates from glycerols stored at – 80 °C. *Agrobacterium* was grown at 28 °C for two days. Cells were resuspended in infiltration buffer (10 mM $MgCl_2$, 10 mM MES, pH 5.6) and OD_{600} measured by spectrophotometer. Cells were diluted to OD_{600} = 0.5, unless otherwise stated. The abaxial leaf surface of 4-week-old *N. benthamiana* leaves were infiltrated with a blunt ended 1 mL syringe. For protein extraction, *N. benthamiana* leaves were harvested 2 days post inoculation using a leaf disc borer, avoiding the mid-vein. Leaf tissue was placed in a 2 mL Eppendorf tube with two 3MM Tungsten Carbide Beads (Qiagen), frozen in liquid nitrogen and stored at – 80 °C.

2.2.4.7 Biotin treatment

TurboID transgenic Arabidopsis 5-week-old leaves were co-infiltrated with 50 µM biotin and either Pf0-1 or 50 µM estradiol. 20 Arabidopsis plants, with 3 leaves per plant were infiltrated per treatment. After 4 hours, leaves were flash-frozen in liquid nitrogen.

N. benthamiana leaves were infiltrated 48-hours prior with *Agrobacterium* carrying 35S:TPR1-TurboID-V5 or 35S:NLS-TurboID-V5. The leaves were either co-infiltrated with 50 µM Biotin and Pf0-1 for 4 hours of labelling or infiltrated first with Pf0-1, then 2-hours later infiltrated with 50 µM Biotin for 2 hours labelling. Three *N. benthamiana* leaves were infiltrated per treatment.

2.2.4.8 Hypersensitive response (HR) infiltrations

Agrobacterium strains were streaked on antibiotic selection plates and grown for 48 hours at 28 °C. A mixed *Agrobacterium* suspension was prepared in 10 mM $MgCl_2$-MES infiltration buffer, containing 200 µg/mL acetosyringone and A*grobacterium* strains carrying 35S:NRG1.2-HF (or NRG1.2 phosphorylation variants), 35S:EDS1-V5, 35S:SAG101-Myc, p19 (inhibits RNA silencing, (Scholthof,

2006)) and either 35S:WRR4A-Flag and 35S:CCG28-Myc-E9 or Strep-XopQ or AvrRps4-V5. AvrRps4-V5, Strep-XopQ, P19 and NRG1-HF were infiltrated at OD_{600} = 0.2. 35S:WRR4A-Flag and 35S:CCG28-Myc-E9 were infiltrated at OD_{600} = 0.5. SAG101-Myc and EDS1-V5 were infiltrated at OD_{600} = 1 and 0.05 respectively. These OD_{600} concentrations of EDS1, SAG101 and NRG1 was optimised by Dr Joanna Feehan to induce hetero-complex associations in *N. benthamiana* upon effector recognition (Feehan et al., 2023). *N. benthamiana*^{epss}plants deficient in *Nb*EDS1, *Nb*PAD4, *Nb*SAG101a and *Nb*SAG101b were used for HR assays (Lapin et al., 2019). The fourth youngest leaf was infiltrated and up to 5 different sectors were infiltrated on one leaf. Photos were taken and HR was scored 6 days later using the following HR score scale: 0 = no HR, 1 = chlorosis, 2 = mild HR, 3 = moderate HR, 4 = severe HR, 5= very severe HR.

2.2.4.9. Confocal microscopy

N. benthamiana leaves were infiltrated with *Agrobacterium* carrying plasmids expressing proteins under a 35S promoter. After 48 hours, a leaf disc was cut and placed onto a glass slide. Water was pipetted onto the leaf disc and a coverslip placed on top. Confocal microscopy was performed with a Leica SP5 and a ×63/1.20 water-immersion objective. An Argon ion 488 nm laser was used for GFP fluorophore excitation and emission was collected for 495-550 nm wavelengths with PMT detector. mCherry fluorophores were excited with the Yellow DPSS 561 nm laser and emission was collected for 570-690 nm wavelengths with PMT detector. Scan resolution was 512 × 512 and a 2-frame average. Pinhole size was set at Airy 1. All other settings were set to default. Images were acquired using Leica LAS AF software. Images for mCherry and GFP fluorophores were collected separately and merged in ImageJ. Bright-field images were also collected to visualize cell membranes.

2.3.DNA methods

2.3.1 DNA Isolation for PCR genotyping

Leaf tissue was printed by mechanical pressing onto a Whatman® FTA® card. The card was stored at room temperature and air-dried for at least 30 minutes before DNA isolation. A 1.2 mm diameter disc was cut from the printed leaf with a Harris Uni-Core Punch. The disc was incubated for 30 minutes at room temperature with 50 µL FTA extraction buffer (10 mM TrisHCl, 0.01 %v/v Tween 20, 2 mM EDTA). The buffer was discarded and the disc washed with 200 µL of TE-1 solution (10 mM TrisHCl, 0.1 mM EDTA) before being used as a template for PCR. PCR with primers for gene of interest was carried out

to confirm homozygous lines of T-DNA insertions received from previous lab members or to confirm insertion of expression plasmid in stable Arabidopsis lines.

2.3.2 Plant DNA extraction

For cloning purposes Arabidopsis Col-0 plant tissue was ground to a powder using a Geno/Grinder® for 60 seconds at 1000 RPM. gDNA was extracted using Qiagen DNeasy Plant Mini Kit and following the manufacturer's instructions. Col-0 DNA was then used as a template for PCR amplification.

2.3.3 DNA Oligonucleotides

Oligonucleotides were synthesised by Merck or IDT at 0.025 nm scale and resuspended in ddH2O to a stock concentration of 100 µM and stored at – 20 °C. Oligos were diluted to a working concentration of 20 µM and stored at – 20 °C.

2.3.4 Polymerase Chain Reaction (PCR)

Polymerase chain reactions (PCRs) were performed to amplify regions of DNA for cloning purposes using high fidelity Phusion DNA polymerase (NEB) for Golden Gate cloning or KAPA uracil (Roche) for USER cloning. Reaction mixes were made as per the manufactures instructions and performed in a C1000 Touch thermocycler (Bio-Rad). Plasmid DNA or Arabidopsis gDNA were used as PCR templates. Elongation times and annealing temperatures were optimised for each set of primers and amplification fragment length.

2.3.5 Agarose gels

Agarose gels for DNA electrophoresis were made by heating 1% (w/v) agarose in TAE (40 mM Tris pH 7.6, 20 mM acetic acid, 1 mM EDTA). The agarose was cooled to 60 °C before 0.5 µg/mL ethidium bromide was added. The agarose was then poured into a gel mould, well-combs added and cooled at room temperature to polymerise. DNA samples were loaded into the gel wells next to a Quick-Load® Purple 1 kb DNA Ladder (NEB). TAE buffer was added to the gel tanks for electrophoresis, with an electric current of 110V for 20 minutes. Gels were imaged using an ultraviolet transilluminator (Bio-Rad). DNA bands for cloning purposes were cut using a razor and purified using a QIAquick DNA Gel extraction kit (QIAGEN) following the manufacturer's instructions.

2.3.6 User cloning

USER cloning was used to generate constructs for transient expression in *N. benthamiana* if gDNA sequences contained too many Bpi1 or Bsa1 sites, making domestication for Golden Gate cloning difficult. USER cloning uses an Uracil-specific excision reagent (USER) enzyme mix (NEB) and KAPA HiFi HotStart Uracil DNA Polymerase (Roche). The USER enzyme mix contains an Uracil DNA glycosylase and a DNA glycosylase-lyase Endonuclease which remove the uracil base and break the phosphodiester backbone, leaving a 3' overhang (Geu-Flores et al., 2007). Fragments with a 3' Uracil are amplified by PCR and assembled into a USER cassette, due to overlapping regions between the fragment and plasmid backbone. DNA fragments were amplified by PCR using primers listed in Appendix 4.

For linearisation of the USER cassette (2.5 µg) was mixed with 2.5 µL PacI (NEB) and 1x Cutsmart Buffer (NEB) and left overnight at room temperature. 0. 75 µL of PacI was then added and incubated at 37 °C for 1 hour, followed by addition of Nt. BbvCI (NEB) and incubated at 37 °C for another 2 hours. The USER cassette was then heated to – 80 °C for 20 minutes and finally excised from an agarose gel and extracted with a QIAquick DNA Gel extraction kit (QIAGEN).

For ligation 30 ng of PCR fragments, 30 ng of USER plasmid, 1x USER enzyme (NEB), 1x CutSmart buffer (NEB) were mixed and incubated at 37 °C for 30 minutes and room temperature for 1 hour 30 minutes. Ligation was added to One Shot™ TOP10 Chemically Competent *E. coli* (Thermo: C404010) and left on ice for 40 minutes. The cells were then heat shocked at 42 °C for 35 seconds and incubated at 37 °C for 1 hour in LB media before plating on LB antibiotic selection plates and grown overnight at 37 °C.

2.3.7 Golden Gate cloning

Golden Gate assembly allows assembly of multiple DNA fragments into a vector using type II endonucleases BsaI (Thermofisher) and BpiI (Bbsl-Thermofisher) and DNA ligase T4 (NEB) (Engler et al., 2009). BsaI and BpiI cleave outside of their recognition site to create 4 bp overhangs at the 5' and 3' end of each module. Unwanted BsaI and BpiI recognition sites within a gDNA sequence must be removed without changing the resulting protein sequence, known as domestication. DNA fragments were amplified from genomic DNA and domesticated by PCR using primers listed in Appendix 4. TSL Synbio has generated Golden Gate modules for easy assembly of transcriptional units (L1) and assembly of multi-gene constructs (L2).

Constructs were assembled in a single digestion and ligation reaction using the TSL Synbio protocols (Table 2.2) in a C1000 Touch thermocycler (Bio-Rad). Digestion/ligation reactions required 100-200 ng

of acceptor plasmid with a 2:1 molar ratio of inserts:acceptor, mixed with 1 µL BsaI (10U/µL Thermofisher) or 1 µL BpiI (10U/µL Thermofisher), 1 µL T4 DNA ligase (400 U/µL, NEB), 2 µL CutSmart® buffer (NEB), 2 µL 10 mM ATP and water to a final volume of 20 µL. 2 µL of ligation was used for transformation into electro-competent *E. coli*.

Table 2.2. Protocols for digestion/ligation reactions for Golden Gate cloning using BpiI or BsaI.

BsaI		BpiI	
10 min 40 °C 10 min 16 °C	x3	10min 37 °C 10min 16 °C	x3
10min 50 °C 20min 80 °C Hold 16 °C		10min 37 °C 20min 65 °C Hold 16 °C	

2.3.8 Plasmid isolation and sequencing

Single *E.coli* colonies grown on selection plates were inoculated into 5 mL of LB medium and grown overnight at 37 °C with shaking at 200 RPM. Cells were pelleted with centrifugation at 3800 x g (Thermo Heraeus X3R TX-1000 rotor) for 10 minutes and plasmid purified using QIAquick Spin Miniprep kit (QIAGEN) as per manufacturer's instruction. Each plasmid was eluted in 40 µL of ddH2O. DNA concentration was measured using a Nanodrop spectrophotometer. Purified plasmid DNA was stored at − 20°C. All plasmid sequences were verified by Genewiz Azenta Life Sciences Sanger Sequencing using primers listed in Appendix 4 and results analysed using Geneious Prime software. Constructs used for transient assays or transformed into Arabidopsis in this study are listed in Appendix 5.

2.3.9 RNA extraction

Plant tissue was ground to a powder using a Geno/Grinder® for 60 seconds at 1000 RPM. RNA was extracted with RNeasy Plant Mini Kit (Qiagen) and treated with RNase-free DNase I recombinant (Merck) to remove DNA contamination. RNA was eluted in 40 µL RNase-free water, concentration quantified with Nanodrop and diluted to 500 ng/µL. Reverse transcriptase was performed with 1 µg of RNA using SuperScript IV Reverse Transcriptase (Invitrogen) as per manufactures instructions and

stored at – 80 °C. qPCR was performed with KAPA SYBR® FAST (Merck) and CFX96 Touch™ Real-Time PCR Detection System (Biorad). Primers used for qPCR are listed in Table 2.3.

Table 2.3. Primers used for qPCR

Primers	**Sequence**
EF1A Fw	CAGGCTGATTGTGCTGTTCTTA
EF1A Rv	GTTGTATCCGACCTTCTTCAGG
ICS1 Fw	CAATTGGCAGGGAGACTTACG
ICS1 Rv	GAGCTGATCTGATCCCGACTG
AvrRps4 Fw	AATGACTCGAATTTCAACCAGTTCAG
AvrRps4 Rv	CGAACCTTGGTTGATTCTGCGGTCTT
FRK1 Fw	GCCAACGGAGACATTAGAG
FRK1 Rv	CCATAACGACCTGACTCATC
WRKY15 Fw	GGAGCTCATGACTCGGAATTAC
WRKY15 Rv	CGGAAGAAGAAGATGGCTGATC
PEN3 Fw	GGTCAGATCGTGTACCAAGG
PEN3 Rv	CTACTGGCAAACTCTGAAACCG
MYB31 Fw	CAGAACTGGACAAGCTCATC
MYB31 Rv	CTATGTCTGGCTTGCTCTCAC
SARD1 Fw	CCGATATGCGAAGTTATGAAAGC
SARD1 Rv	AGTGGCTCGCAGCATATTGTT
WRKY18 Fw	GTTACGAGAGGAGCTAAACAGAG
WRKY18 Rv	CATTAACCAGATCCAAAGTCACTG
WRKY40 Fw	AGCTTACGGGAACTTCCACA
WRKY40 Rv	AGGGCTGATTTGATCCCTCT

2.4 Protein methods

2.4.1 Protein homolog alignment

*At*NRG1, *At*SARD1, *At*WRKY18 and *At*TPR1 protein sequences were searched in NCBI BLAST. The top protein identity hits from across the plant kingdom were selected and protein sequences downloaded from NCBI. Multiple protein sequence alignment was performed using T-Coffee and imported into Geneious Prime.

2.4.2 Protein extractions

2.4.2.1 Total protein extraction

Total protein was extracted for testing protein expression in transgenic Arabidopsis lines. Frozen plant tissue was ground to a fine powder either with a Geno/Grinder® for 60 seconds at 1000 RPM or in liquid nitrogen with a pre-cooled pestle and mortar. 500 µL of extraction buffer (150 mM Tris-HCl, pH 7.5, 150 mM NaCl, 1 mM EDTA, 10 % v/v glycerol, 10 mM DTT, 1% Nodinet-40 (NP40), anti-protease tablet (cOmplete™ EDTA-free Sigma Aldrich), 2% (w/v) PVPP (Polyvinylpolypyrrolidone), 1% Triton X-100 and 0.5% SDS) was added to the powder and incubated at 4 °C on a rotor for 20 minutes. Cell debris was pelleted with centrifugation at 4100 x g for 25 minutes at 4 °C and the supernatant collected. 100 µL of supernatant was boiled in 50 µL of 3x SDS-PAGE loading buffer (187.5 mM Tris-HCl, pH 6.8, 30 mM dithiothreitol (DTT), 8% (w/v) SDS, 0.1 % bromophenol blue, 40 % glycerol) at 95 °C for 5 minutes.

2.4.2.2 Nuclear protein extraction and co-immunoprecipitation

4-week-old wildtype *N. benthamiana* leaves were infiltrated with *Agrobacterium* carrying 35S promoter driven GFP, *At*WRKY18-GFP, *At*WRKY18$^{DLN\text{-}AAA}$-GFP, or *At*WRKY^{EAR}-GFP and co-infiltrated with 35S promoter driven *At*SARD1-6xHIS-3xFLAG (SARD1-HF) or *At*TPR1-6xHIS-3xFLAG (TPR1-HF). After 48 hours, Pf0-1_XopQ was infiltrated into the same leaves and harvested after 4 hours. Leaf discs were taken, placed in a 2 mL Eppendorf tube with two Tungsten beads and frozen in liquid nitrogen. Nuclear protein extraction protocol was adapted from (Xu & Copeland, 2012). Tissue was ground with a Geno/Grinder®. 2 mL of lysis buffer (20 mM Tris-HCl (pH 7.4), 25% glycerol, 20 mM KCl, 2 mM EDTA, 2.5 mM $MgCl_2$, 250 mM sucrose, 1 mM DTT, 2 mM NaF, 2 mM Na_3VO_4, 2 mM B-glycero-phosphate) was added and immediately vortexed and placed on ice. The homogenate was filtered through a 75 µM filter and centrifuged at 4 °C for 10 minutes. The nuclear pellets were then resuspended in nuclear resuspension buffer with Triton-X (NRBT) (20 mM Tris-HCl (pH 7.4), 25% glycerol, 2.5 mM $MgCl_2$, 0.2%

Triton X-100, 2 mM NaF, 2 mM Na_3VO_4, 2 mM B-glycero-phosphate) and incubated on ice for 10 minutes. Centrifugation and re-suspension of pellets in NRBT was repeated twice more. To remove Triton-X, the pellets were then resuspended in nuclear resuspension buffer (20 mM Tris-HCl (pH 7.4), 25% Glycerol, 2.5 mM $MgCl_2$), centrifuged at 4 °C for 10 minutes and the pellets resuspended in RIPA buffer (1xPBS; 1% NP-40; 0.5% sodium deoxycholate; 0.1% SDS) with 50U/100µL Benzonase (Merck) and incubated at 4 °C for 30 minutes. Samples were then given 12x two-second pulses of sonication in an ice bath and finally centrifuged at 18,000 x g for 10 minutes. 30 µL of anti-FLAG® M2 affinity gel beads (Merck: A2220) slurry was added to each sample and incubated for 2 hours. The beads were then washed four times with wash buffer (1xPBS; 1% NP-40; 0.5% sodium deoxycholate; 0.1% SDS, 2 mM NaF, 2 mM Na_3VO_4, 2 mM B-glycero-phosphate). After centrifugation at 800 x g for 5 minutes, the beads were boiled in 100 µL of 1x SDS buffer for western blot analysis.

2.4.2.3 Proximity labelling protein extraction

Plant tissue was ground to a powder with a pestle and mortar. 1x V/V of extraction buffer (150 mM Tris-HCl pH 7.5, 150 mM NaCl, 1 mM EDTA, 10% glycerol, 10 mM DTT, 0.4% Nonidet P-40, 2% polyvinylpolypyrrolidone (PVPP), 0.5% deoxycholic acid, cOmplete EDTA-free protease inhibitor cocktail tablet) was added and incubated at 4 °C for 20 minutes. Samples were centrifuged twice for 20 minutes at 4575 x g (Sorvall SH-3000) at 4 °C and the supernatant filtered through two layers of Miracloth (Merck 475855) into to a fresh pre-chilled 15 mL corning tube on ice. Zeba™ Spin Desalting Columns 7K MWCO (ThermoFisher 89894) were centrifuged at 3,800 x g (Thermo Heraeus X3R TX-1000 rotor) for 1 minute, equilibrated with GTEN buffer (150 mM Tris-HCl pH 7.5, 150 mM NaCl, 1 mM EDTA, 10% glycerol) and centrifuge repeated. The protein lysate was then added to the desalting columns and centrifuged at 3,800 x g for 1-2 minutes, until the protein lysate had passed through the columns into the 50 mL collection tube. 30 µL of Pierce™ High-Capacity Streptavidin agarose beads (ThermoFisher: 20361) were added to each sample and incubated at 4 °C for three hours. Beads were precipitated by centrifugation at 4 °C at 4575 x g for 5 minutes and washed three times in GTEN buffer (150 mM Tris-HCl pH 7.5, 150 mM NaCl, 1 mM EDTA, 10% glycerol). The beads were sequentially washed once with 1 mL 2% SDS at room temperature and the following at 4 °C: once with buffer 2 [GTEN, 0.1% deoxycholic acid (w/v), 1% Triton X-100], and once with buffer 3 [10 mM Tris-HCl, pH 7.4, 250 mM LiCl, 1 mM EDTA, 0.1% deoxycholic acid (w/v), 1% NP40 (v/v)]. To remove detergent, the beads were then washed twice in 50 mM Tris-HCl, pH 7.5 and six times in 50 mM ammonium bicarbonate, pH 8.0 and finally resuspended in 1 mL of 50 mM ammonium bicarbonate and kept at –80 °C.

2.4.2.4 NRG1 protein extraction from Arabidopsis

The method was optimised by a previous lab member Dr Joanna Feehan. 5g of infiltrated transgenic NRG1.2-HF or NRG1.1-V5 Arabidopsis leaf tissue was ground to a powder in liquid nitrogen with a pestle and mortar. Lysis buffer (100 mM Hepes pH 7.5, 10% glycerol, 500 mM Nacl, 5 mM $MgCl_2$, 1% NIDP40, cOmplete™ EDTA-free Protease Inhibitor Cocktail, 2% PVPP, Halt™ Phosphatase Inhibitor Single-Use Cocktail (Thermo Scientific), 10 mM DTT) was added at a V:V ratio 1:1 and incubated at 4 °C for 20 minutes. The protein sample was centrifuged for 35 minutes at 4,000 x g (Thermo Heraeus X3R TX-1000 rotor) and the supernatant filtered through miracloth. NRG1.2-HF or NRG1.1-V5 were immunoprecipitated with 100 µL of anti-FLAG® M2 affinity gel beads (Merck: A2220) or anti-V5 affinity agarose beads for 2 hours at 4 °C. Beads were washed 6 times with wash buffer (100 mM Hepes pH 7.5, 10% glycerol, 500 mM NaCl, 5 mM $MgCl_2$, 1% NIDP40)), 5-minute incubation at 4 °C and centrifuged at 800 x g for 5 minutes. Proteins were eluted with 750 ng/µL 3xFLAG peptide with incubation at 4 °C for 2.5 hrs with shaking at 750 RPM for 5 minutes, every 25 minutes. Eluate was filtered through a chilled spin column (Sigmaprep SC1000-1KT) at 8200 x g at 4 °C for 1 minute and stored at 4 °C overnight.

Protein eluates were diluted with buffer (10 mM HEPES pH 7.5, 150 mM NaCl, 5 mM $MgCl_2$, 5 % Glycerol, 1 mM DTT) and concentrated from 1 mL to 60 µL using 0.5 mL Vivaspin 500 concentrator membranes (Sartorious). To prepare Vivaspin columns, the day before use the concentrators were washed once with dH_2O and centrifuged at 12,000 x g. The concentrators were then left in dH_2O overnight. The next day, the dH_2O was poured out and washed once more with fresh dH_2O. After concentration, the protein sample was transferred to a low-bind Eppendorf tube with Fisherbrand™ Gel-Loading Tips (1-200µL, Fisher Scientific). A 10 µL aliquot was made up to a total of 40 µL with buffer (10 mM HEPES pH 7.5, 150 mM NaCl, 5 mM $MgCl_2$, 5 % Glycerol, 1 mM DTT) and used for phosphatase treatment as described in 2.4.1.6. The remaining sample was submitted for mass-spectrometry analysis.

2.4.2.5 NRG1.2^{EEAA}-HF protein extraction from *N. benthamiana^{epss}*

35S:NRG1.2^{EEAA}-HF, 35S:SAG101-Myc and 35S:EDS1-V5 were infiltrated into *N. benthamiana^{epss}* leaves at OD_{600} = 0.2, 1 and 0.05 respectively. After 48 hours, the leaves were infiltrated with 10 mM $MgCl_2$ (mock), Pf0-1_EV or Pf0-1_XopQ for 4 hours and frozen in liquid nitrogen. A detailed method for NRG1-HF protein extraction was optimised by a previous lab member Dr Joanna Feehan and can be found in Appendix 3. In brief, 30g of *N. benthamiana* tissue was ground to a powder in liquid nitrogen with a pestle and mortar. After incubation with extraction buffer, the protein solution underwent ultra-

centrifugation at 50,000 x g for 90 minutes and the supernatant collected. The protein sample was incubated twice with 500 µL of anti-FLAG® M2 affinity gel (Merck: A2220) beads to immunoprecipitate $NRG1^{EEAA}$-HF. Beads were washed and protein was eluted with 150 ng/µL of 3xFLAG peptide (Merck: F4799) for 30 minutes and with 250 ng/µL of 3xFLAG peptide overnight. Protein samples were diluted to reduce NP40 concentration and then concentrated first with a Amicon® Ultra 4 mL Centrifugal Filter (Merck) to 500 µL, followed by concentration to 60 µL with a 0.5 mL Vivaspin Centrifugal Concentrator membrane (Sartorious). A 10 µL aliquot was made up to a total of 40 µL with buffer (10 mM HEPES pH 7.5, 150 mM NaCl, 5 mM $MgCl_2$, 5 % Glycerol, 1 mM DTT) and used for phosphatase treatment as described in 2.4.1.6. The remaining sample was submitted for mass-spectrometry analysis.

2.4.2.6 Lambda protein phosphatase treatment

40 µL of protein sample was combined with 5 µL of 10X NEBuffer for Protein MetalloPhosphatases (PMP) (NEB) and 5 µL of 10 mM $MnCl_2$ and 1 µL of Lambda Protein Phosphatase (NEB). The samples were incubated at 30 °C for 30 minutes with shaking at 300 RPM. Samples were then boiled at 65 °C for 5 minutes in SDS buffer.

2.4.3 SDS-PAGE

SDS-PAGE (Sodium dodecyl sulfate polyacrylamide gel electrophoresis) gels were made with a resolving gel layer of 12% w/v polyacrylamide, 375 mM Tris-HCl pH 8.8 and 5% w/v SDS. Prior to pouring into Mini-PROTEAN 1.5 mm casting glass plates (Bio-Rad), 0.01 % (w/v) ammonium persulfate (APS) and 0.05 % Tetramethylethylenediamine (TEMED) was added to the acrylamide SDS solution. Isopropanol was added to remove bubbles and ensure an even polymerisation at the top of the resolving gel layer. The gels were left at room temperature for 30 minutes to polymerise, and the isopropanol was removed by washing with ddH20. The stacking gel layer (5 % w/v polyacrylamide, 125 mM Tris-HCl, pH 6.8 with 5 % (w/v) SDS, 0.01 % (w/v) ammonium persulfate and 0.1 % TEMED) was poured on top and plastic gel casting combs were added. SDS-page gels were either used immediately or wrapped in water-soaked paper and clingfilm and stored at 4 °C. Gel combs were removed, and denatured protein samples loaded into gel wells next to a PageRuler™ Prestained Protein Ladder (ThermoFisher). SDS-gels were run in a Bio-Rad miniPOTEAN tetra tank in SDS-running buffer (25 mM Tris-HCl, 250 mM NaCl, 0.1 % w/v SDS) for 1.5-2 hours at 110V.

2.4.3.1 Phos-tag SDS-PAGE gels

20 µM Phos-tag SDS-PAGE gels were made with a resolving gel solution containing 6% (w/v) Acrylamide, 20 µM Phos-tag™ Acrylamide AAL-107 (AlphaLabs), 375 mM Tris-HCl pH 8.8, 100 uM $MnCl_2$, 0.1% (w/v) SDS Solution, 0.01% TEMED, 0.05% (w/v) ammonium persulfate (APS). Acrylamide-SDS solution was poured into Mini-PROTEAN 1 mm casting glass plates (Bio-Rad) with an isopropanol layer on top. The gels polymerised at room temperature for 45 minutes and then isopropanol was removed by washing with ddH20. The stacking gel solution containing 4.5% (w/v) Acrylamide, 125 mM Tris-HCl pH 6.8, 0.1% (w/v) SDS Solution, 0.01% TEMED, 0.04% (w/v) APS, was poured on top of the resolving gel and plastic gel casting combs were added. The gel was left to polymerise for 45 minutes at room temperature. Gels were used the same day and run under a constant current condition (30 mA/gel) for 1.5 hours in Bio-Rad miniPOTEAN tetra tank in SDS-running buffer (25 mM Tris-HCl, 250 mM NaCl, 0.1 % w/v SDS). After electrophoresis the gels were washed in 50 mL SDS running buffer with 5 mM EDTA three times for 15 minutes to eliminate the manganese ions prior to transfer. The gel was washed once in 50 mL SDS running buffer for 10 min to remove EDTA before blotting onto a PVDF membrane as described in 2.4.4.

2.4.4 Immunoblotting (Western blot)

SDS-PAGE gels were run as described and proteins transferred to a 0.2 µM PVDF membrane (polyvinylidene difluoride, Bio-Rad) using semi-dry Trans-Blot® TurboTM Transfer System (Bio-Rad) and the 'Standard SD' programme according to the manufactures instructions. After transfer, membranes were blocked for 1 hour in TBS-T (50 mM Tris-HCl, pH 8.0, 150 mM NaCl, 0.1 % Tween®-20) with 5% (w/v) non-fat dried milk powder or 2% BSA (Bovine serum albumin) added. 2% BSA was used for membranes incubated with α – Streptavidin HRP and 5% milk was used for all other antibodies. Membranes were incubated overnight at 4 °C with required antibodies in TBS-T with either 5% (w/v) non-fat dried milk powder or 2% BSA with gentle agitation. Antibody concentrations used in this study are shown in Table 2.4. After overnight incubation, membranes were washed three times with TBS-T for 5 minutes. If needed, secondary anti-rabbit-horseradish-peroxidase (α-Rabbit-HRP) in 5% milk TBS-T was probed at room temperature for one hour. For chemiluminescence visualisation, 400 µL of HRP substrate (SuperSignal West Pico Plus or West Femto solution, Thermo Scientific) was added to the membranes and immediately imaged using an ImageQuant™ LAS 4010 (Life Sciences) or Amersham™ ImageQuant™ 800 biomolecular imager.

Table 2.4. Antibodies used for immunoblotting

Antibody	Dilution	Supplier
α-Flag HRP M2	1:10000	Sigma Aldrich
α-V5 HRP	1:5000	Sigma Aldrich
α-Streptavidin HRP	1:5000	ThermoFisher
α-GFP HRP	1:5000	Santa Cruz
α-HA HRP	1:3000	Sigma Aldrich
α-mCherry	1:3000	Abcam
α-Rabbit IgG HRP	1:10000	Sigma Aldrich
α-Phosphoserine-proline	1:4000	Abcam

2.4.5. Proximity labelling protein sample preparation for mass-spectrometry

2.4.5.1 On-bead digest using Mobicol columns

After precipitation of biotinylated proteins as described in 2.4.1.3, streptavidin beads were transferred into a Mobicol spin column inserted with a filter. The beads were bound to the column by centrifugation at 1300 x g. The column was washed twice with 500 µL 50 mM Tris pH 7.5 and twice with 2 M Urea in 50 mM Tris pH 7.5. The columns were plugged and incubated in 80 µL of Trypsin buffer (50 mM Tris pH 7.5, 1 M Urea, 1m M DTT, 200 ng Trypsin) for three hours at 25 °C with shaking at 300 RPM. The columns were inserted into 1.5 mL low bind Eppendorfs and centrifuged to collect the digest. 60 µL of 50 mM Tris pH 7.5, 1 M Urea, 1 mM DTT was added twice to the columns and digests collected. 0.8 µL of DTT was added to a final concentration of 4 mM and incubating at 25 °C for 30 minutes with shaking. The digests were alkylated by adding Iodoacetamide to a final concentration of 10 mM and incubated at 25 °C for 45 minutes with shaking. 200 ng Trypsin was added to the digest and incubated overnight at 25 °C with shaking.

2.4.5.2 C18 clean-up

After overnight trypsin digest, the digests were acidified with a final concentration of 1% formic acid and desalted using OMIX C18 pipette tips (10 – 100 µL, Agilent). The C18 desalting tips were activated by twice aspiring and discarding 200 µL buffer B2 (0.1 % formic acid, 50 % acetonitrile) and equilibrated by four times aspiring and discarding 200 µL buffer A2 (0.1 % formic acid). Peptides were

bound by aspiring and dispensing the sample eight times. Then, the tip was washed by 10 times aspiring and discarding 200 µL buffer A2. The peptides were eluted by aspiring and dispensing 200 µL buffer B2 in a new tube for eight times. The desalted peptides were dried in a speed vac and stored at -80°C.

2.4.5.3 Data dependent acquisition (DDA) measurement of biotinylated proteins

LC-MS/MS analysis was performed using a Orbitrap Eclipse trihybrid mass spectrometer (Thermo Scientific) and a nanoflow-UHPLC system (Dionex Ultimate3000, Thermo Scientific) Peptides were trapped to a reverse phase trap column (Acclaim PepMap, C18 5 µm, 100 µm x 2 c§m, Thermo Scientific) connected to an analytical column (nanoE MZ HSS T3 1.8um 75um x 250mm, Waters). Peptides were eluted in a gradient of 6-55 % acetonitrile in 0.1 % formic (solvent B) acid over 90 min followed by gradient of 40-80 % B over 6 min at a flow rate of 200 nL/min at 40 °C. The mass spectrometer was operated in positive ion mode with nano-electrospray ion source with ID 0.02mm fused silica emitter (New Objective). Voltage +2800 V was applied via platinum wire held in PEEK T-shaped coupling union with transfer capillary temperature set to 275 ºC. The Orbitrap, MS scan resolution of 120,000 at 400 m/z, range 300 to 1800 m/z was used, and automatic gain control (AGC) was set at 2e5 and maximum inject time to 50 ms. In the linear ion trap, MS/MS spectra were triggered with data dependent acquisition method using 'top speed' and 'most intense ion' settings. The selected precursor ions were fragmented sequentially in both the ion trap using CID and in the HCD cell. Dynamic exclusion was set to 15 sec. Charge state allowed between 2+ and 7+ charge states to be selected for MS/MS fragmentation. Peak lists in the format of Mascot generic files (.mgf files) were prepared from raw data using MSConvert package (Matrix Science). Peak lists were searched on Mascot server v.2.4.1 (Matrix Science) against either Araport11 or an in house Nbenth database and an in-house contaminants database. Tryptic peptides with up to 2 possible mis-cleavages and charge states +2, +3, +4, were allowed in the search. The following modifications were included in the search: oxidized methionine, biotinylation and lysine acetylation as variable modification and carbamidomethylated cysteine as static modification. Data were searched with a monoisotopic precursor and fragment ions mass tolerance 10ppm and 0.6 Da respectively. Mascot results were combined in Scaffold v. 4 (Proteome Software) and exported in Excel (Microsoft Office).

2.4.5.4 Proximity labelling data analysis

Three biological repeats of biotin labelling and MS analysis was carried out. Proteins were considered a protein interactor if they were present in at least two biological repeats. If protein biotinylation was not detected in the third biological repeat, the median value of the two biological repeats was used as a third value. An average was then calculated for the three values. Proteins were identified as an interactor if they were unique to EDS1, SARD1 or TPR1 or if they were enriched in biotinylation compared to the appropriate control NLS-GFP or mCherry (2x fold change, P-value < 0.05). Biotinylation was compared and interactors identified within each immunity treatment e.g. NLS-GFP mock vs SARD1 mock, providing a list of interactors for each treatment. Proteins were also compared between mock and PTI, ETI or PTI + ETI conditions to give a list of proteins with enhanced biotinylation (or unique interactors) upon immunity activation - "immunity induced". These proteins also had to be statistically different from the controls (2x fold change, P-value < 0.05). Some proteins were present in multiple biological repeats but only present once in each immunity treatment. Therefore, these proteins were classed as "grouped interactors" if they were also not present in the controls.

2.5 Dual luciferase assay

2.5.1 Transient luciferase expression in *Nicotiana tabacum*

Nicotiana tabacum leaves were infiltrated with *Agrobacterium* carrying SARD1 dual-luciferase constructs (Table 2.5) at OD_{600} = 0.25 and leaf discs taken after 48 hours. Leaf discs were ground to a powder in liquid nitrogen and 500 µL of ice-chilled 1X Passive Lysis Buffer (Promega) was added. Samples were vortexed and centrifuged at 23,000 x g at 4 °C for 30 seconds and the supernatant kept. Renilla luciferase and Firefly luciferase expression was quantified with Dual-Luciferase® Reporter Assay System (Promega) and a VarioSkan plate reader as described in 2.5.3.

Table 2.5. Components of dual-luciferase constructs. Luciferase constructs together with either SARD1 or mCherry were assembled into one plasmid using Golden Gate cloning.

Promoter	Gene	Tag
Ubi10	SARD1 (or SARD1 phospho-variants)	Hellfire
Ubi10	mCherry-NLS	N/A
35S	Renilla Luciferase (*Photinus pyralis)*	V5
EDS5	Firefly Luciferase (*Renilla reniformis)*	HA

2.5.2 Arabidopsis protoplast isolation and transformation

This protocol was adapted from (Wu et al., 2009). The upper epidermal surface was affixed to a strip of Time tape, while the lower epidermal surface cell layer was pulled away with Magic tape. The enzyme solution (0.4M Mannitol, 20 mM KCL, 20 mM MES) was first pre-heated in a 55 °C water bath before addition of 1% Cellulase R-10 and 0.25% Macerozyme R-10 enzymes. The solution was then cooled to room temperature before addition of 10 mM $CaCl_2$ and 0.1% BSA (Bovine serum albumin). The leaves, still adhering to the Time tape, were transferred to a Petri dish containing the prepared enzyme solution. The leaves were shaken at 40 RPM in the light for 40 minutes to release the protoplasts into the solution. The digested leaves were filtered through a 70 µM nylon filter into a 50 mL conical tube and centrifuged at 150 x g for two minutes at the lowest acceleration and deceleration. The pellets were washed twice with ice-cold W5 solution (154 mM NaCl, 125 mM $CaCl_2$, 5 mM KCL, 2mM MES). The pellets were then re-suspended in ice- cold W5 solution and incubated on ice for 30 minutes. The protoplasts were centrifuged, and pellets resuspended in MMG (0.4M Mannitol, 15mM $MgCl_2$, 4mM MES). 50 µL of protoplasts were used to calculate the concentration of protoplasts with a haemocytometer and diluted to 2 X 10^5 cells/ml. 100 µL of protoplasts and 1X (plasmid+protoplast) volume of 40% PEG solution (40% PEG4000, 100 mM $CaCl_2$, 0.2M Mannitol) were added to a 2 mL round-end microtube. 0.5 – 2 µg of dual-luciferase plasmids (Table 2.5) were added and mixed gently. Protoplasts were incubated for 30 minutes at room temperature, before dilution with 4X volume W5 solution (now at room temperature) and mixed gently. The diluted protoplasts were centrifuged at 200 x g for 2 minutes and pellets washed once in 400 µL W5 solution. Protoplasts were then re-suspended in 400 µL W5 and incubated over-night under a bench top light. After incubation, the protoplasts were spun down and W5 supernatant discarded. The cells were then frozen in liquid nitrogen and stored at – 80 °C. Dual-Luciferase® Reporter Assay System (Promega) and a VarioSkan plate reader were used for quantification of Renilla and Firefly luciferase expression. 100 µL of 1X Passive Lysis Buffer (Promega) was added and protoplasts disrupted by vortexing for 10 seconds. Cell debris was pelleted by centrifugation at 10,000 × g for 2 minutes and supernatant used for reporter assay or boiled in 3 x SDS buffer at 95 °C for 5 minutes and used for western blot.

2.5.3 Dual luciferase measurements

Firefly and Renilla luciferase were quantified with Dual-Luciferase® Reporter Assay System (Promega) sequentially using one reaction tube. 100 µL of Luciferase Assay Reagent II (Promega) was predisposed into wells of a 96-well plate. 20 µL of the cell lysate was added and mixed gently by pipetting. The Varioskan illuminator was programmed for a 10-second read time. 100 µL of Stop &

Glo® Reagent (Promega) was added, mixed and a second reading taken. Three technical repeats were measured, and the averages calculated. The Firefly luciferase measurement was normalised against the Renilla luciferase measurement.

2.6 Quantitative phospho-proteomic methods

2.6.1 Growth of seedling balls

20 mg of estradiol-inducible *AvrRps4* /SUPER-ETI (SETI), Col-0 or SETI_krvy seeds were grown in 50 mL of ½ MS liquid media in 250 mL conical flasks, on a rotator set at 120 RPM for 7 days, at 22 °C, 70% humidity and 16-hour light conditions.

2.6.2 Estradiol induction of *AvrRps4* expression in Arabidopsis seedling balls

7-day old seedling balls were given either 50 µM of estradiol resuspended in DMSO or the corresponding volume of DMSO (Mock). After three hours seedlings were then quickly patted dry with tissue before being flash frozen with liquid nitrogen and stored at – 80 °C before processing.

2.6.3 Cytosolic and microsomal protein extraction

This protocol was first described in (Zhang & Peck, 2011). Plant tissue was ground to a powder in liquid nitrogen and homogenised in extraction buffer (50 mM Tris pH7.5, 10% Glycerol, 2 mM DTT, 10 mM NaF, 10 mM Na_3VO_4, 5 mM EDTA, 50 mM B-Glycero-phosphate, 1 mM phenylmethylsulfonyl fluoride (PMSF), 10 µg Leupeptin, 5 µg Aprotinin) using a 30 mL Potter-Elvehjem homogenizer within an ice jacket. Samples were centrifuged at 4,000 x g for 60 mins at 4 °C (Thermo Heraeus X3R, TX-1000 rotor). The supernatant was transferred to 36 mL ultra-centrifuge tubes (Sorvall, Cat no. 03141, PA tubes) and centrifuged at 100,000 x g for 30 minutes at 4 °C (Sorvall WX Ultra 100 Series, Surespin 360 swinging buckets) to collect the cytosolic fraction (supernatant) and microsomal fraction (pellet). The pellet was resuspended in 1 mL of 8M urea/0.1M ammonium bicarbonate (ABC).

2.6.4 Trypsin digest of cytosolic and microsomal proteins

This protocol was first described in (Mithoe et al., 2016). A Bradford assay was carried out to determine protein concentration of samples, with 1.5 mg of total microsomal protein and 2 mg of cytosolic protein used for phospho-peptide enrichment. Protein samples were dissolved in buffer containing 50 mM ammonium bicarbonate (ABC) and 8 M urea. Proteins were then reduced by 5 mM Tris (2-carboxyethyl) phosphine (TCEP), vortexed and placed in 37 °C shaker for 20 minutes.

Cysteine residues were alkylated with 40 mM Iodoacetamide (IAA) at 200 RPM and 25 °C for 60 minutes and then diluted with 50 mM ABC to a final concentration of 1.6 M urea. Proteins were digested with trypsin (Promega; 1:100 enzyme to substrate ratio) overnight at 37 °C with 200 RPM shaking. Digests were stopped with 10% Trifluoroacetic acid (TFA) to make a final concentration of 1% TFA.

2.6.5 Nuclear protein extraction

Plant tissue was ground to powder with a pestle and mortar and for a further 5 minutes in a potter tube with lysis buffer (20 mM Tris-HCl (pH 7.4), 25% glycerol, 20 mM KCl, 2 mM EDTA, 2.5 mM $MgCl_2$, 250 mM sucrose, 1 mM DTT, 1 mM PMSF, 2 mM NaF, 2 mM Na_3VO_4, 2 mM B-glycero-phosphate, 10 µg Leupeptin and 5 µg Aprotinin). Homogenates were centrifuged at 4 °C at 1500 x g for 10 minutes and the nuclear pellets resuspended in nuclear resuspension buffer with Triton-X (NRBT) (20 mM Tris-HCl pH 7.4, 25% glycerol, 2.5 mM $MgCl_2$, 0.2% Triton X-100, 2 mM NaF, 2 mM Na_3VO_4, 2 mM B-glycero-phosphate and 10 µg Leupeptin and 5 µg Aprotinin) and incubated on ice for 10 minutes. Centrifugation and re-suspension of pellets in NRBT was repeated twice more. To remove Triton-X, the pellets were then resuspended in nuclear resuspension buffer (NRB) (20 mM Tris-HCl (pH 7.4), 25% Glycerol, 2.5 mM $MgCl_2$), centrifuged at 4 °C for 10 minutes and the pellets resuspended again in NRB with 50U/100µL Benzonase (Merck) and incubated at 4 °C for 30 minutes. Samples were then given 12x two-second pulses of sonication in an ice bath and finally centrifuged at 23,000 x g for 10 minutes. The supernatant was kept as the supernatant fraction, while the pellet was resuspended in low salt buffer (150mM NaCL, 20 mM Tris-HCl pH 7.4, 2.5 mM $MgCl_2$, 10 µg Leupeptin and 5 µg Aprotinin). Sonication was repeated and protein samples incubated at 4 °C for 1 hour. Samples were then centrifuged 23,000 x g for 10 minutes. The supernatant was kept as the low salt fraction and pellet resuspended in high salt buffer (500mM NaCL, 20 mM Tris-HCl pH 7.4, 2.5 mM $MgCl_2$, 10 µg Leupeptin and 5 µg Aprotinin). Samples were incubated on ice for 1 hour, centrifuged at 23,000 x g for 10 minutes, the supernatant kept as the high salt fraction and the final pellet fraction was resuspended in 20 mM Tris-HCl pH 7.4, 2.5 mM $MgCl_2$. A Bradford assay was then carried out to determine protein concentration, before freeze-drying the samples overnight.

Detergent was found in the first nuclear samples measured by mass spectrometry. S-trap columns (Protifi) were used successfully to remove detergent, with a small loss of peptides. Therefore, S-trap columns were used for all the remaining nuclear samples. After nuclear protein extraction, proteins were freeze-dried and re-suspended in 500 µL SDS solubilisation buffer (5% SDS, 50 mM TEAB pH 7.55, H_2O). DTT was added to a final concentration of 20 mM and samples were heated for 10 minutes at

95 °C. Protein solution was then cooled to room temperature before addition of iodoacetamide (IAA) to a final concentration of 100 mM and incubated in the dark for 30 minutes. Undissolved matter was removed by centrifugation for 8 minutes at 13,000 x g. 50 µL of 12% phosphoric acid was added to the supernatant, mixed, then 3.3 mL of S-Trap buffer (90% MeOH, 100 mM TEAB, pH 7.1) added and mixed. The supernatant fraction samples were combined with the high salt fraction for each sample. The acidified lysate/S-Trap buffer mix was then added to the S-Trap spin column in a flow-through tube and centrifuged for 1 minute at 4,000 x g. The column was washed with S-Trap buffer and centrifuged for 1 minute at 4,000 x g. This was repeated three times. The S-Trap spin column was placed in a clean 15 mL tube and trypsin added at 1:25 wt:wt in digestion buffer (50 mM TEAB, pH 8) and incubated for 1 hour at 47 °C in a water bath, with no shaking. To elute the digested proteins, digestion buffer was added to the S-Trap spin columns and centrifuged at 4,000 x g for 1 minute, followed by addition of 0.2% aqueous formic acid to the S-Trap columns, and a final elution with 50% ACN containing 0.2% formic acid was performed and elutions combined. The peptides were freeze-dried and TiO_2 enrichment carried out as described in 2.6.6.

2.6.6 C18 clean up and TiO_2 enrichment of phosphorylated proteins

This protocol was first described in (Mithoe et al., 2016). Microsomal, nuclear and cytosolic peptide digests were cleaned with C18 SepPak® silica reversed-phase chromatography columns (Waters™) in a vacuum manifold. The columns were first equilibrated with 100% MeOH, followed by 80% acetonitrile (ACN) and 0.1% trifluoroacetic acid (TFA) and washed four times with 2% ACN 0.1% TFA. Peptide samples were then loaded onto the columns, placed in 15 mL falcon tubes and pushed through with a modified 20 mL syringe with parafilm. The flow-through was then loaded a second time onto the column. Columns were then washed five times with 2% ACN 0.1% TFA using the vacuum manifold. Peptides were eluted twice with 40% ACN 0.1% TFA, followed by 60% ACN 0.1% TFA. Peptides were then freeze-dried overnight.

Enrichment of large numbers of phosphorylated peptides using TiO_2 is a well-established method (Stecker et al., 2014, Benschop et al., 2007, Reiland et al., 2011, Shao et al., 2021). Dried peptides were resuspended in Phtalic acid solution (10% phtalic acid, 80% ACN, 3% TFA), vortexed and sonicated in a water bath for ten minutes. Filters with added to Mobicol spin columns and inserted into 2 mL Eppendorf tube. 0.625% titanium dioxide (TiO_2, GL Science) suspension was added to the spin columns and the resin equilibrated with 100% MeOH and Phtalic acid solution. Dissolved peptides were then loaded onto the columns, the end plugged and wrapped with parafilm and the top of the column secured with a screw on cap and parafilm. The columns were then placed for 60 minutes on a head-over-tail rotor. Columns were centrifuged for one minute at 1500 x g and the flow-through kept as the

unbound fraction. The columns were washed twice with Phtalic acid solution, twice with 80% ACN 0.1% TFA and twice with 0.1% TFA. Phosphorylated peptides were eluted three times into low-bind Eppendorf tubes with 0.3 M NH4OH solution (pH 10.5). 10% TFA was then added to the eluted peptides to neutralize the NH_4OH solution to pH 2.5.

A final C18 peptide clean-up was carried out with MicroSpin Columns (C18 Silica 5 – 200 µL loading, 5 – 60 µg capacity, The Nest Group Inc). Columns were washed three times with 100% MeOH, three times with 80% ACN 0.1% TFA and three times with 2% ACN 0.1% TFA. One-third of the phospho-peptide solution was loaded onto the spin columns twice, repeated with the remaining peptide solution. Columns were then washed six times with 2% ACN 0.1% TFA and the phospho-peptides eluted twice with 40% ACN 0.1% TFA and once with 60% ACN 0.1% TFA. The cleaned peptides were then freeze-dried in a speed vac and resuspended with 40µl of 2% ACN 0.1% TFA before mass-spec measurement.

2.6.7 Data dependent acquisition (DDA) of microsomal, cytosolic, nuclear proteins

LC-MS/MS analysis was performed using a Orbitrap Fusion trihybrid mass spectrometer (Thermo Scientific) and a nanoflow-UHPLC system (Dionex Ultimate3000, Thermo Scientific) Peptides were trapped to a reverse phase trap column (Acclaim PepMap, C18 5 µm, 100 µm x 2 c§m, Thermo Scientific) connected to an analytical column (Acclaim PepMap 100, C18 3 µm, 75 µm x 50 cm, Thermo Scientific). Peptides were eluted in a gradient of 3-40 % acetonitrile in 0.1 % formic (solvent B) acid over 120 min followed by gradient of 40-80 % B over 6 min at a flow rate of 200 nL/min at 40 °C. The mass spectrometer was operated in positive ion mode with nano-electrospray ion source with ID 0.02mm fused silica emitter (New Objective). Voltage +2200 V was applied via platinum wire held in PEEK T-shaped coupling union with transfer capillary temperature set to 275 ºC. The Orbitrap, MS scan resolution of 120,000 at 400 m/z, range 300 to 1800 m/z was used, and automatic gain control (AGC) was set at 2e5 and maximum inject time to 50 ms. In the linear ion trap, MS/MS spectra were triggered with data dependent acquisition method using ‘top speed’ and ‘most intense ion’ settings. The selected precursor ions were fragmented sequentially in both the ion trap using CID and in the HCD cell. Dynamic exclusion was set to 15 sec. Charge state allowed between 2+ and 7+ charge states to be selected for MS/MS fragmentation. Peak lists in the format of Mascot generic files (.mgf files) were prepared from raw data using MSConvert package (Matrix Science). Peak lists were searched on Mascot server v.2.4.1 (Matrix Science) against an Araport11 database and an in-house contaminants database. Tryptic peptides with up to 2 possible mis-cleavages and charge states +2, +3, +4, were allowed in the search. The following modifications were included in the

search: oxidized methionine, phosphorylation on Serine, Threonine, Tyrosine as variable modification and carbamidomethylated cysteine as static modification. Data were searched with a monoisotopic precursor and fragment ions mass tolerance 10ppm and 0.6 Da respectively. Mascot results were combined in Scaffold v. 4 (Proteome Software) and exported in Excel (Microsoft Office).

2.6.8 PRM quantification of nuclear samples

Phosphorylated peptides were quantified by Dr Paul Derbyshire using Parallel Reaction Monitoring (PRM) as previously described (Guo et al., 2020). Mass to charge ratios (m/z) of selected phospho-peptides were filtered by the first quadrupole and fragment ions were scanned out in the orbitrap mass analyser over the duration of the elution profile. 20 control phospho-peptides were included to measure relative phospho-peptide abundance in each sample. Raw data was searched against Mascot server data bases and combined with chromatographic profiles in Skyline, allowing peak picking to quantify peptide intensities. Individual peptide intensities were normalised against the 20 control peptide intensities. Three technical repeats were carried out for each of the four biological repeats for SETI Mock and SETI estradiol and two biological repeats for SETI_krvy estradiol. Technical and biological averages were then calculated for each sample. Only S-trap prepared nuclear samples, without detergent, were used for PRM analysis.

2.6.9 MS1 quantification

MS1 quantification was performed with a reduced target list of peptides from the nuclear fraction. Paul Derbyshire quantified 119 peptides from WRKY transcription factors, Calmodulin-binding proteins, Topless-related proteins, and RNA-polymerase subunit II identified in the DDA dataset. MS1 precursor ions were quantified based on DDA chromatograph data imported into Skyline.

2.6.10. PRM data analysis

In each nuclear subcellular protein fraction (High salt, Low salt, Pellet), the 20 control peptides had different levels of abundance. Therefore, the intensities of each control peptide were plotted against all others in a pairwise comparisons and those that best matched each other in intensity for each nuclear fraction were used for normalisation. Consequently, the control peptides for normalisation are specific to each nuclear subcellular protein fraction.

Peptides were considered as differential if log2Fold change > 0.6 or < -0.6 and Pvalue < 0.05 between SETI estradiol and SETI Mock. From the peptides that didn't meet these criteria, they were considered

differential if they had a log2fold change > 1 or < -1 in phosphorylation in SETI estradiol compared to either SETI Mock or SETI_krvy estradiol if the peptide also had > 0.6 or < – 0.6 log2Fold change compared to the other control. Only peptides with measurements from two or more biological repeats for each genotype were considered.

Chapter 3

Investigating changes of protein phosphorylation upon ETI activation

3 Investigating changes of protein phosphorylation upon ETI activation

3.1 Introduction

3.1.1 Protein phosphorylation during immune signalling

Protein phosphorylation has an important role in pattern-triggered immunity (PTI) signal transduction (Bigeard et al., 2015). Large-scale quantitative phospho-proteomic studies have identified changes in protein phosphorylation, at specific phosphorylation sites, during PTI signalling (Benschop et al., 2007, Nühse et al., 2007, Rayapuram et al., 2014, Mattei et al., 2016, Rayapuram et al., 2021). Functional analysis of these phosphorylation sites has revealed their importance in PTI signal transduction. For example, flg22- induced phosphorylation of RESPIRATORY BURST OXIDASE PROTEIN D (RBOHD) is required for reactive oxygen species (ROS) production, as alanine mutations at phosphorylated serines inhibit RBOHD activity (Nühse et al., 2007).

Using selected reaction monitoring (SRM), BOTRYTIS-INDUCED KINASE1 (BIK1) was identified as the kinase responsible for pathogen-associated molecular patterns (PAMP)-induced RBOHD phosphorylation (Kadota et al., 2014). Targeted proteomic approaches also identified PAMP-induced BIK1 phosphorylation (Lu et al., 2010). The leucine-rich-repeat receptor-like-kinase (LRR-RLK) BRI1-ASSOCIATED RECEPTOR KINASE (BAK1) was shown to phosphorylate BIK1, however BIK1 also trans-phosphorylates BAK1 and FLAGELLIN-SENSITIVE 2 (FLS2) to further enhance PTI signalling (Lu et al., 2010). Phosphorylation of OSCA1.3, a member of the Hyperosmolality-gated calcium-permeable channels (OSCA) family, was first identified in a quantitative phospho-proteomic screen during flg22 signalling (Benschop et al., 2007). Further analysis showed that OSCA1.3 is phosphorylated by BIK1 leading to increased Ca^{2+} channel activity (Thor et al., 2020). Additionally, OSCA1.3 phosphorylation is required for PTI-induced stomatal closure (Thor et al., 2020).

The phosphorylation events that occur during effector-triggered immunity (ETI) signalling are less well defined. Phosphorylation changes have recently been identified during RPS2-mediated ETI with dexamethasone-inducible *AvrRpt2* expression (Kadota et al., 2019). Over 100 differential phosphorylation sites were identified in plasma membrane localised proteins using quantitative phospho-proteomics (Kadota et al., 2019). Phosphorylation sites in RBOHD induced during ETI overlap with sites phosphorylated during PTI (Kadota et al., 2019). BIK1 is important in RBOHD phosphorylation during PTI (Kadota et al., 2014). However, the ETI-induced phospho-sites in RBOHD were not affected in the *bik1* mutant, suggesting another kinase is involved in phosphorylating RBOHD during ETI (Kadota et al., 2019). Phospho-sites induced by both ETI and PTI were also found in AUTOINHIBITED CA^{2+} -ATPASE (ACA8) (Kadota et al., 2019). The calcium ATPase ACA8 forms a complex

with FLS2 and plays a role in regulating Ca^{2+} levels during flg22 induced PTI (Frei dit Frey et al., 2012). Novel ETI phosphorylation sites were also found in proteins such as PLASMA MEMBRANE INTRINSIC PROTEIN (PIP) aquaporins (Kadota et al., 2019). Although differential ETI phosphorylation sites during ETI have been identified, little functional analysis of ETI phosphorylation sites has been done. This highlights the vast difference in knowledge between the phosphorylation sites required for PTI and ETI signalling.

Kadota et al., 2019 is the first paper to investigate large-scale phosphorylation during ETI without PTI. However, only membrane-localised proteins were investigated. Many quantitative proteomics studies have focused on the microsomal fraction (Benschop et al., 2007, Nühse et al., 2007, Kadota et al., 2019) or whole cell lysates (Sugiyama et al., 2008). There have been fewer studies investigating phosphorylation of nuclear proteins (de la Fuente van Bentem et al., 2008, Jones et al., 2009, Bigeard et al., 2014) and there has only been one report of nuclear protein phosphorylation upon PTI activation (Rayapuram et al., 2021). Additionally, Kadota et al., 2019 explored phosphorylation downstream of CC-NLR activation localised to the plasma membrane. Signalling downstream of nuclear localised TIR-NLR activation may involve phosphorylation of different proteins, especially considering the different localisations of the NLRs. Therefore, there is a gap in the literature exploring nuclear protein phosphorylation changes upon TIR-NLR ETI activation.

3.1.2 Known ETI signalling components

Effector triggered immunity involves recognition of pathogen effectors by intracellular immune receptors, known as nucleotide-binding leucine-rich repeat receptors (NLRs). Both coiled-coil (CC)-NLRs e.g. HOPZ-ACTIVATED RESISTANCE 1 (ZAR1) and Toll/interleukin-1 (TIR)-NLRs e.g. Recognition of XopQ 1 (ROQ1) have been shown to form resistosomes, upon indirect or direct effector recognition (Wang et al., 2019a, Wang et al., 2019b, Martin et al., 2020). The ZAR1 resistosome contains a α-helical funnel-like structure, which forms a calcium channel in the plasma membrane to induce cell death (Wang et al., 2019a, Bi et al., 2021). Helper NLRs N REQUIREMENT GENE 1 (NRG1) and ACTIVATED DISEASE RESISTANCE 1 (ADR1) form complexes with downstream signalling partners. ENHANCED DISEASE SUSCEPTIBILITY 1 (EDS1), SENESCENCE-ASSOCIATED GENE 101 (SAG101) and NRG1 form heterocomplexes upon effector recognition, leading to NRG1 oligomerisation and activation of HR (Lapin et al., 2019, Sun et al., 2021, Feehan et al., 2023). Additionally, NRG1 forms a Ca^{2+} channel to activate cell death (Jacob et al., 2021). EDS1, PHYTOALEXIN DEFICIENT 4 (PAD4) and ADR1 form a separate complex to restrict bacterial growth and activate large-scale transcriptional changes (Bhandari et al., 2019, Lapin et al., 2019, Ding et al., 2020, Sun et al., 2021). Recently it was discovered

that binding of TIR-NLR-catalysed small molecules promotes EDS1-PAD4-ADR1 and EDS1-SAG101-NRG1 associations (Huang et al., 2022, Jia et al., 2022), establishing a link between TIR-NLR activation and downstream signalling molecules. However, it is unknown how EDS1-PAD4-ADR1 associations result in changes in transcription.

Phosphorylation changes have been shown to have a role in TIR-NLR activation (Guo et al., 2020). RESISTANT TO RALSTONIA SOLANACEARUM 1 (RRS1) and RESISTANT TO P. SYRINGAE 4 (RPS4) are a pair of nuclear-localised TIR-NLRs which function together to recognise PopP2 from *Ralstonia solanacearum* and AvrRps4 from *Pseudomonas syringae pv pisi* (Gassmann et al., 1999, Hinsch & Staskawicz, 1996, Deslandes et al., 2003, Narusaka et al., 2009). There are two alleles of RRS1; RRS1-R in Arabidopsis accession Ws-2 and RRS1-S in Col-0 (Deslandes et al., 2002). The RRS1-R allele requires phosphorylation at T1214 in the WRKY domain to maintain it in an inactive state (Guo et al., 2020). Phospho-dead mutants of RRS1-R at T1214 show constitutive defence activation (Guo et al., 2020). PopP2 acetylates RRS1-R at the same residue inhibiting phosphorylation, revealing an antagonistic role of phosphorylation and acetylation of RRS1-R (Guo et al., 2020). Furthermore, phosphorylation of RRS1-R at additional sites is required for PopP2-induced proximity of the RRS1-R TIR and C-terminal domain, leading to RRS1/RPS4 activation (Guo et al., 2020). The kinase responsible for RRS1-R phosphorylation has not been reported.

EDS1 is phosphorylated by the plasma-membrane receptor-like cytoplasmic kinase PBS1-LIKE 19 (PBL19) after chitin treatment and EDS1 phosphorylation is important for immunity to fungal infections (Li et al., 2022b). No further reports have been made of phosphorylation events of ETI downstream signalling proteins upon ETI-activation. Using large-scale phospho-proteomic approaches could reveal phosphorylation of known ETI components, as well as reveal novel ETI signalling components.

To study ETI, in the absence of PTI, estradiol-inducible AvrRps4 Arabidopsis lines have been created (Ngou et al., 2020). These were termed SUPER-ETI (SETI) lines (Ngou et al., 2020). Estradiol-inducible AvrRps4 leads to RPS4/RRS1-dependent induction of salicylic acid biosynthesis genes e.g. *ISOCHORISMATE SYNTHASE1 (ICS1)* and thus induction of the defence gene *PATHOGENESIS RELATED1* (*PR1)* (Ngou et al., 2020). The KRVY motif at the N-terminus of processed AvrRps4 is required for bacterial virulence (Sohn et al., 2009). These residues are also required for ETI activation, as AvrRps4_KRVY^{AAAA} is not recognised by RPS4 (Sohn et al., 2012). Therefore, *ICS1* and *PR1* genes are not induced upon expression of the *AvrRps4*_KRVY^{AAAA} mutant (SETI_krvy) (Ngou et al., 2020). SETI and SETI_krvy lines thus provide a useful tool for studying changes in phosphorylation of nuclear proteins upon ETI activation, downstream of nuclear-localised NLR activation.

3.1.3 Role of SARD1 in defence gene activation

SAR DEFICIENT 1 (SARD1) (CBP60h) and CALMODULIN BINDING PROTEIN 60-LIKE G (CBP60g) are in a family of calmodulin-binding protein homologs (CBP60s) (Wang et al., 2011). SARD1 is the only member that lacks a functional calmodulin-binding domain and therefore does not bind calmodulin (Wang et al., 2011). SARD1 and CBP60g are most closely related and act redundantly to regulate SA synthesis, through direct transcriptional regulation of *ICS1* expression (Zhang et al., 2010b). Overexpression of SARD1 leads to constitutively high levels of SA and enhanced disease resistance (Zhang et al., 2010b). SARD1 and CBP60g act as master transcription factors, as they regulate the expression of a large set of genes during both PTI and ETI (Sun et al., 2015, Ding et al., 2020). For example, SARD1 and CBP60g target the promoters of ETI signalling components *EDS1*, *ADR1* and *PAD4*, as well as PTI components *BAK1* and *BIK1* (Sun et al., 2015). SARD1 and CBP60g also target regulators of systemic acquired resistance (SAR) e.g. *FLAVIN-DEPENDENT MONOOXYGENASE 1* (*FMO1*) and *AGD2-LIKE DEFENSE RESPONSE PROTEIN 1* (*ALD1*) (Sun et al., 2015). Additionally, SARD1 and CBP60g regulate the expression of negative regulators of immunity e.g. *PLANT U-BOX 13* (*PUB13*) (Sun et al., 2015). Therefore, SARD1 and CBP60g are regarded as master transcriptional regulators of plant defence responses (Sun et al., 2015, Ding et al., 2020). ENHANCED DISEASE SUSCEPTIBILITY 5 (EDS5) is required for SA accumulation upon bacterial infection (Nawrath et al, 1999). EDS5 functions as a transporter involved in SA export from the chloroplast into the cytoplasm (Serrano et al, 2013). ChIP-Seq reveals SARD1 binds directly to the *EDS5* promoter (Sun et al., 2015). *EDS5* expression is enhanced upon pathogen infection but is reduced in the *sard1/cbp60g* mutant (Sun et al., 2015). Therefore, SARD1 binds to the *EDS5* promoter to promote *EDS5* expression upon pathogen infection (Sun et al., 2015).

3.1.4 Chapter aims and objectives

The work in this chapter addresses the role of protein phosphorylation during ETI signalling. We focused on protein phosphorylation downstream of a nuclear-localised pair of TIR-NLRs. We used estradiol-inducible AvrRps4 lines to study phosphorylation changes during ETI, in the absence of PTI. Phosphorylation in the nuclear fraction was quantified with parallel reaction monitoring (PRM) and phosphorylation changes of a few peptides were confirmed with MS1 quantification. To understand the role of phosphorylation changes during ETI signalling, the requirement of SARD1 phosphorylation for transcriptional regulation was further investigated. As *EDS5* expression has been shown to be induced via SARD1 during immunity, we selected EDS5 for a transcriptional activation assay to test the

role of SARD1 phosphorylation. This was performed using a dual-luciferase assay in Arabidopsis protoplasts.

3.2 Results

3.2.1 Subcellular enrichment of phosphorylated peptides for data-dependent mass-spectrometry analysis

Phospho-peptide extraction from seedling balls, for analysis by mass-spectrometry, has been previously reported (Mithoe et al., 2016). Nuclear phospho-proteins have also been previously extracted from seedlings for mass-spec analysis (Jones et al., 2009). Estradiol treatment of seedling balls enables uniform activation of *AvrRps4* expression in all seedlings at the same time. Therefore, we decided to investigate ETI signalling in seedlings. Extraction of nuclear proteins from seedlings after estradiol-induced expression of *AvrRps4* was selected as a suitable method for our study.

Estradiol-induction of *AvrRps4* expression leads to *ICS1* expression in 5-week-old Arabidopsis leaves (Ngou et al., 2020). To test if estradiol-inducible *AvrRps4* also activates *ICS1* gene induction in 7-day old seedlings, samples for RNA extraction and qPCR were taken 2 and 3-hours after estradiol or mock treatment (Figure 3.1). *ICS1* expression was found to be highly induced at 3-hours but not at 2 hours post estradiol treatment (Figure 3.1). There was also higher *AvrRps4* expression seen at 3-hours (Figure 3.1). Therefore, there is a delay from when estradiol is added to the transcription and translation of AvrRps4, perception of AvrRps4 protein by RRS1/RPS4 and activation of ETI. Higher *AvrRps4* expression will lead to activation of more RRS1/RPS4 proteins and a stronger downstream signal. This will then lead to a stronger transcriptional response of SA biosynthesis genes, explaining the higher levels of *ICS1* expression seen at 3-hours compared to 2 hours (Figure 3.1).

To capture the earliest ETI induced phosphorylation changes, that lead to the changes seen in *ICS1* mRNA accumulation, we chose a 3-hour time point for phospho-peptide extraction. 7-day old estradiol-inducible *AvrRps4* seedlings were given a 3-hour treatment of estradiol or mock and the protein extract split into cytosolic, microsomal or nuclear fractions (Figure 3.2). The nuclear pellets were sonicated, incubated with Benzonase and given a low and high salt buffer treatment to release weakly, or tightly bound chromatin associated proteins, resulting in four nuclear fractions: Supernatant, low salt, high salt and pellet (Figure 3.3). Using high and low salt buffers to extract chromatin associated phospho-proteins has previously been described (Bigeard et al., 2014). To remove detergent S-trap columns were used. The S-trap midi columns should only be used with protein content more than 100 µg. As the supernatant fraction samples were < 100 µg, these samples were combined with the high salt fraction for each sample. This resulted in three sub-cellular nuclear

fractions: high salt/supernatant (referred to as high salt), pellet and low salt. Proteins were digested into peptides with trypsin and enriched for phosphorylated peptides with titanium oxide (Figure 3.2). To identify the phosphorylated peptides that were present in each sample and protein fraction, the peptides were first measured by mass-spectrometry using a semi-quantitative data-dependent acquisition (DDA) method for three biological repeats.

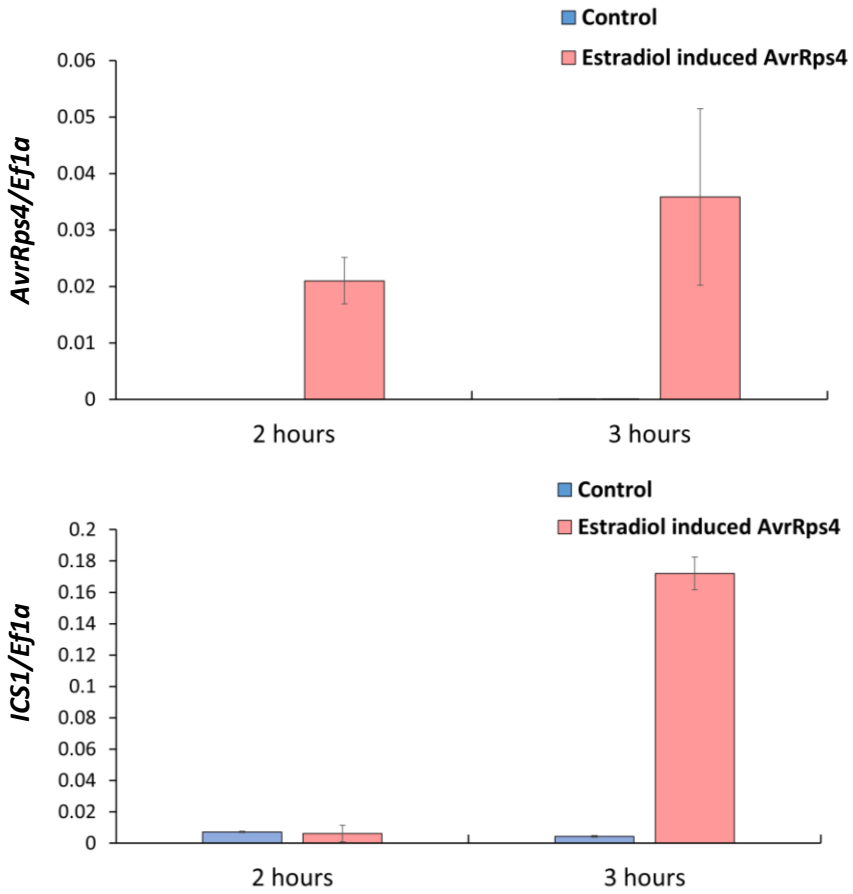

Figure 3.1. *AvrRps4* and *ICS1* expression is induced in estradiol- inducible *AvrRps4* seedlings. 7-day old estradiol-inducible *AvrRps4* (SETI) seedlings were given either estradiol or a DMSO mock treatment (Control) and harvested after 2 and 3 hours. Primers for *AvrRps4*, *ICS1* and *Ef1α*, a house-keeping gene, were used for qPCR after RNA extraction.

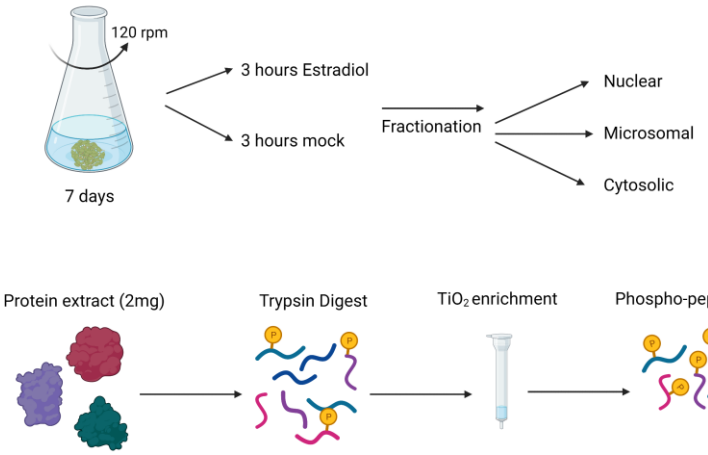

Figure 3.2. Workflow of sample preparation for mass-spectrometry (MS) proteomics. Proteins were digested with trypsin and phosphorylated peptides enriched with titanium dioxide (TiO_2).

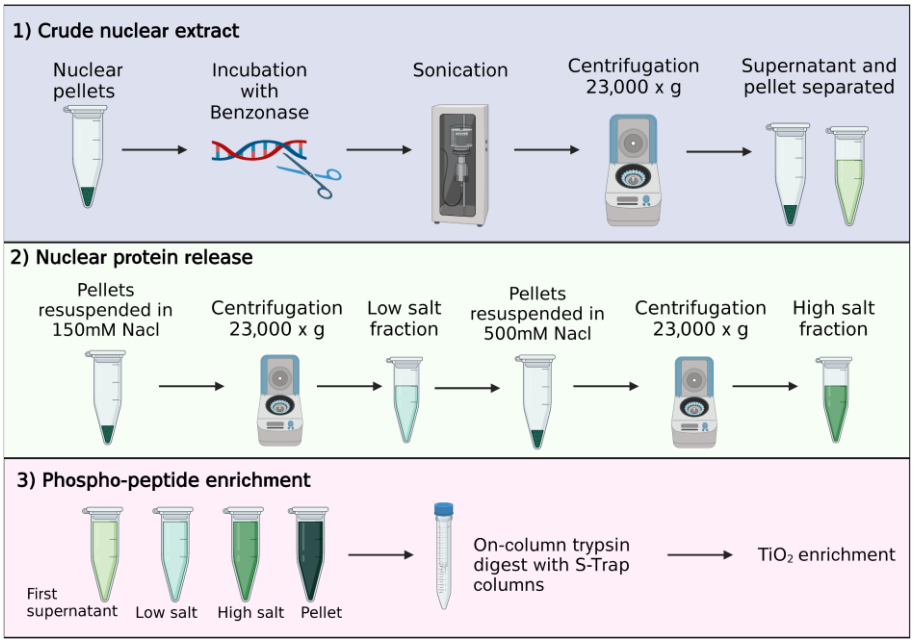

Figure 3.3. Experimental workflow of nuclear protein extraction and fractionation for mass-spectrometry analysis.

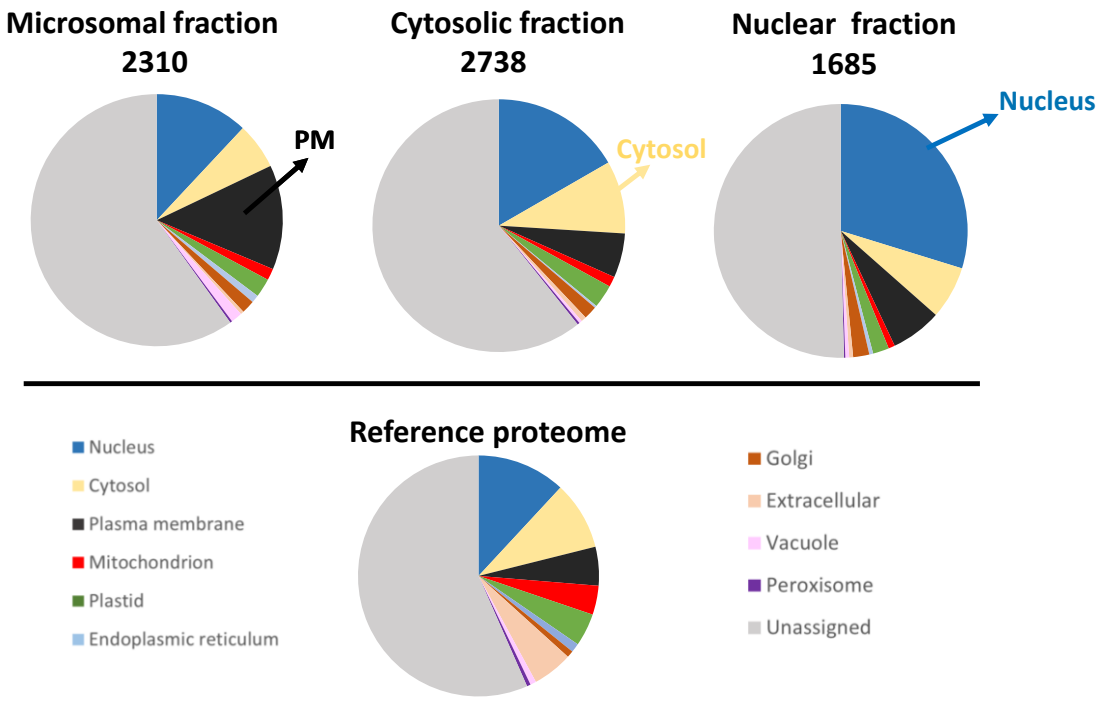

Figure 3.4. The proportional distribution of proteins in DDA data from each subcellular localisation. DDA data from microsomal, cytosolic and nuclear protein fractions analysed by mass-spectrometry. Localisation was predicted using SUBA4.

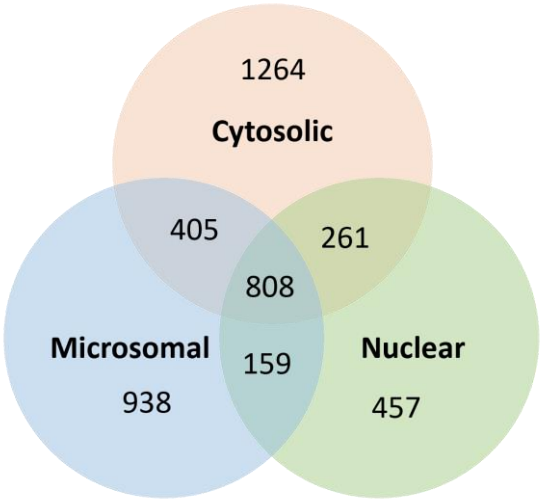

Figure 3.5. Overlap of proteins detected by data-dependent acquisition (DDA) in each protein fraction.

A high number of phosphorylated peptides were detected in each protein fraction (Figure 3.4). Over 1600 phosphorylated proteins were identified in the nuclear fraction and over 2300 in each of the microsomal and cytosolic fractions (Figure 3.4). SUBA is a subcellular database which uses experimental data and predictions to assign subcellular localisation information for Arabidopsis proteins (Heazlewood et al., 2007). Using this SUBA database, the microsomal fraction appears enriched for plasma membrane proteins and the nuclear fraction for nuclear localised proteins, compared to the SUBA4 reference proteome (Figure 3.4). The nuclear fraction was the fraction most highly enriched, with nearly half of all proteins in the nuclear samples assigned to nuclear proteins (Figure 3.4). As these were crude protein extractions, each fraction contains proteins from other protein fractions (Figure 3.5). A large proportion of microsomal and cytosolic proteins were unique to that fraction (Figure 3.5). Although many proteins from the nuclear fraction overlapped with other fractions, it contained 450 unique proteins (Figure 3.5). Overall, there was a successful enrichment in each protein fraction of the corresponding subcellular localised proteins.

3.2.2 Quantification of nuclear phosphorylation changes by parallel reaction monitoring

As RRS1 and RPS4, the TIR-NLR pair which recognises AvrRps4, are nuclear localised, we expect early ETI signalling to be occurring in the nuclear fraction. Additionally, very little known is known about the signalling pathways leading to transcriptional activation during ETI. Therefore, investigating phosphorylation of nuclear-localised proteins would give insight into ETI-induced transcriptional activation. We selected the nuclear fraction for quantitative proteomics using parallel reaction monitoring (PRM). PRM is a targeted approach, where target peptides are selected for quantification (Figure 3.6). To create a target list for PRM we ranked peptides on a few criteria. 1) Proteins known to be involved in immunity from previous literature, 2) Proteins with defence related GO-Terms 3) Proteins which showed a differential change in the DDA dataset and 4) Proteins with key words: kinase, transcription, and polymerase. 366 phospho-peptides were measured in the first PRM technical run. Additional peptides were included in the second technical repeat and a total of 448 peptides targeted. In the third run 344 peptides were quantified, with only those detected in the previous PRM runs included in the target list. Double the protein amount was injected into the mass-spec for the third technical run, to increase detection of low abundant peptides. Three technical repeats were carried out for each of the four biological repeats for SETI mock and SETI estradiol and two biological repeats for SETI_krvy estradiol. Unfortunately, many peptides were only detected in one SETI_krvy estradiol sample. Comparisons between SETI estradiol and SETI_krvy estradiol were only made if there was data for two biological samples. Therefore, the majority of the data analysis and identification of differential changes were done comparing SETI mock and SETI estradiol.

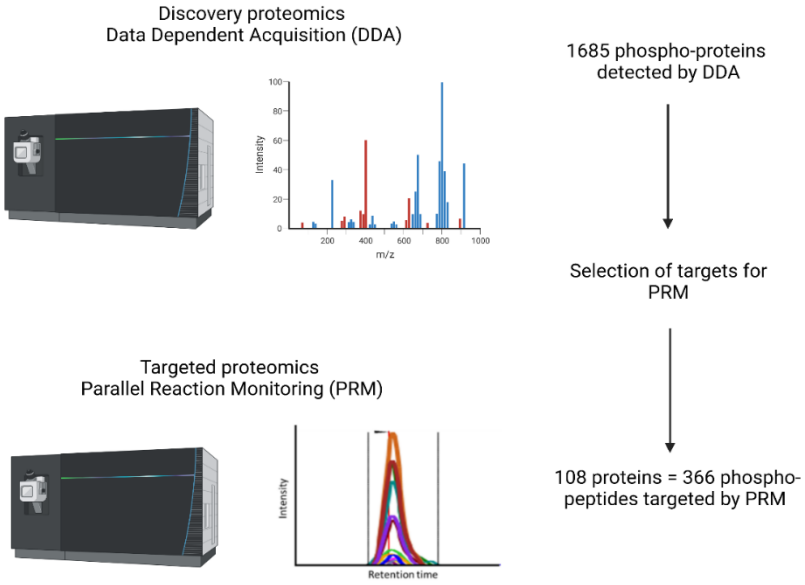

Figure 3.6. Flowchart of proteomic methods to quantify differential phosphorylation of nuclear proteins.

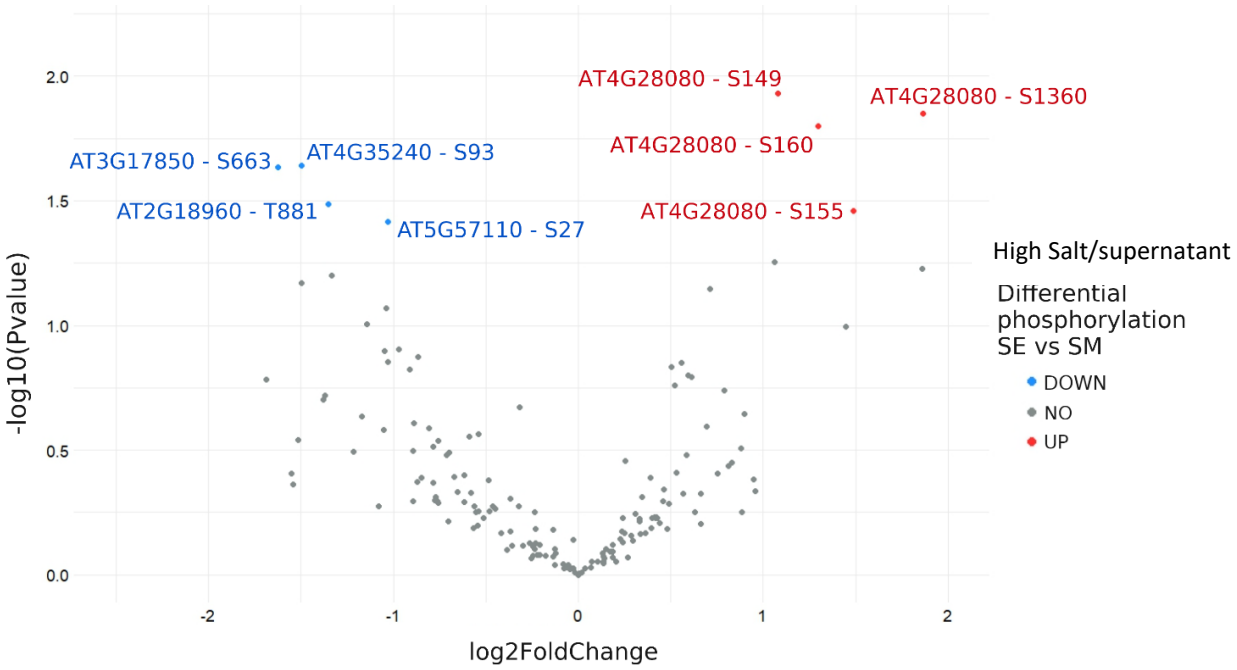

Figure 3.7. Differential phospho-sites in the high salt/supernatant nuclear fraction quantified by PRM. Differential phosphorylation between SETI mock (SM) and SETI estradiol (SE). Blue dots represent phospho-sites with log2FoldChange < - 0.6 and P-value of < 0.05. Red dots represent peptides with log2FoldChange > 0.6 and P-value of < 0.05. Represents data from 4 biological repeats, however some peptides may have only been detected in at least 2 repeats. The average peptide intensity from three technical PRM repeats was taken together with the average across at least two biological repeats.

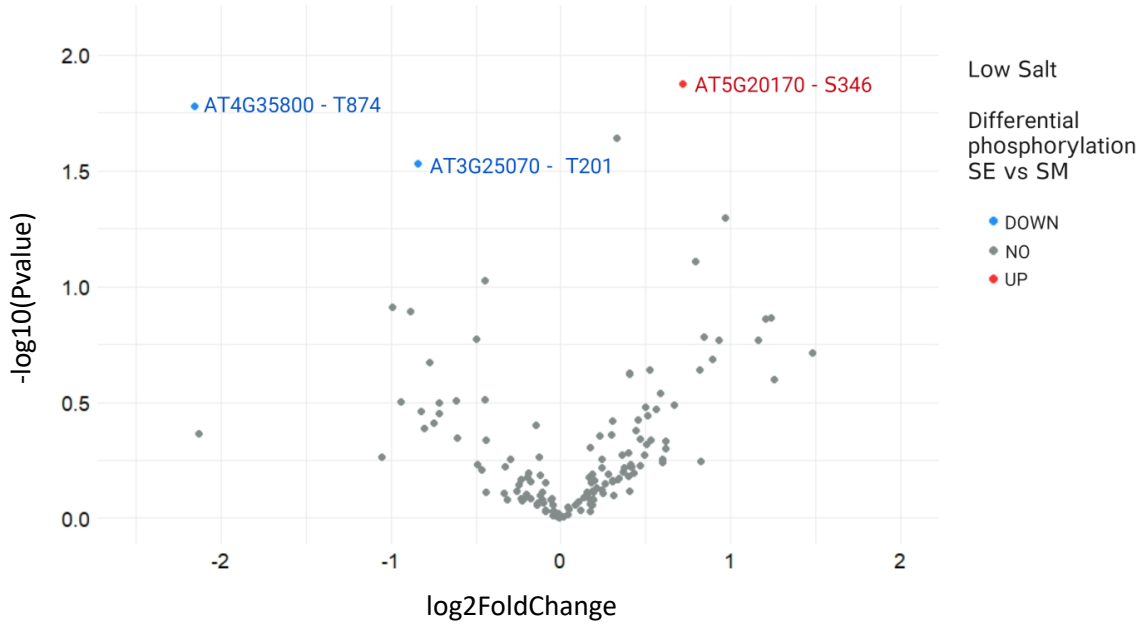

Figure 3.8. Differential phospho-sites in the low salt nuclear fraction quantified by PRM. Differential phosphorylation between SETI mock (SM) and SETI estradiol (SE). Blue dots represent phospho-sites with log2FoldChange < - 0.6 and P-value of < 0.05. Red dots represent peptides with log2FoldChange > 0.6 and P-value of < 0.05. Represents data from 4 biological repeats, however some peptides may have only been detected in at least 2 repeats. The average peptide intensity from three technical PRM repeats was taken together with the average across at least two biological repeats.

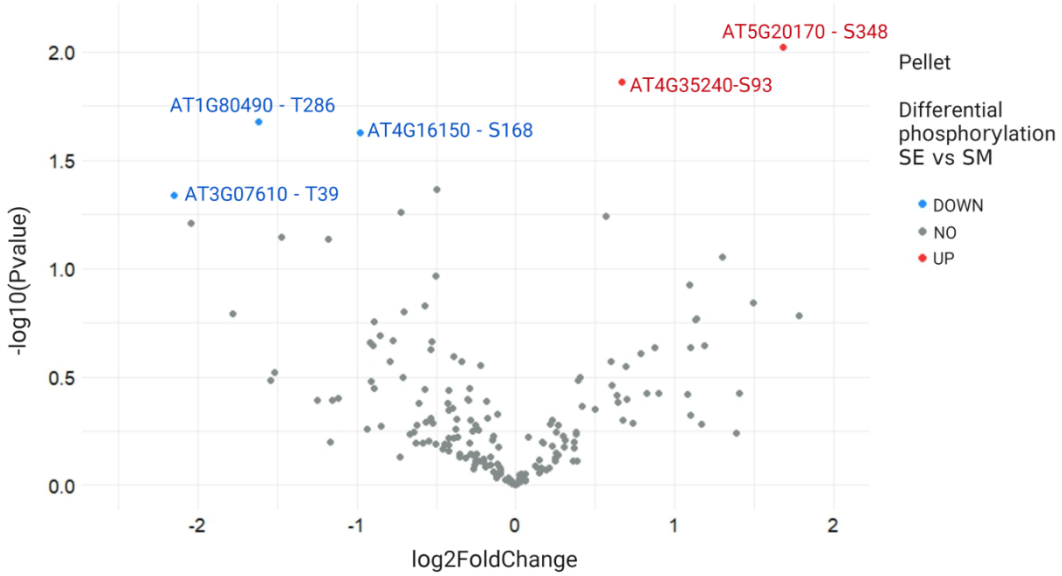

Figure 3.9. Differential phospho-sites in the pellet nuclear fraction quantified by PRM. Differential phosphorylation between SETI mock (SM) and SETI estradiol (SE). Blue dots represent phospho-sites with log2FoldChange < - 0.6 and P-value of < 0.05. Red dots represent peptides with log2FoldChange > 0.6 and P-value of < 0.05. Represents data from 4 biological repeats, however some peptides may have only been detected in at least 2 repeats. The average peptide intensity from three technical PRM repeats was taken together with the average across at least two biological repeats.

PRM-quantified peptide data was analysed in each nuclear subcellular fraction separately. From 344 quantified peptides, 8 peptides in the high salt/supernatant fraction, 5 peptides in the pellet fraction and 3 peptides in the low salt fraction have a statistically significant change in phosphorylation upon ETI activation between SETI estradiol and SETI mock (Figure 3.7-3.9, Table 3.1). 7 peptides show an increase in phosphorylation and 9 peptides show a decrease in phosphorylation (Figure 3.7-3.9). However, 4 phospho-sites show a different/ or no change in phosphorylation when comparing SETI estradiol with SETI_krvy estradiol (Table 3.1). For example, TPR1 T286 shows a decrease in phosphorylation in SETI estradiol, compared to SETI mock, but there is no difference in phosphorylation between SETI estradiol and SETI_krvy estradiol (Table 3.1). Additionally, AT4G35240 shows an increase in phosphorylation at S93 in SETI estradiol compared to SETI mock, but a decrease compared to SETI_krvy estradiol (Table 3.1). Therefore, these 4 phospho-sites should not be considered as differential and the data for these phospho-sites are not further discussed. We also considered those peptides with a non-statistically significant change in phosphorylation of at least a two-fold change (log2FC >1 or < -1) in phosphorylation (Table 3.1). From 344 quantified peptide, 41 peptides from 26 proteins show a two-fold change in phosphorylation (Table 3.1). 5 proteins have two phospho-sites listed in the same row (Table 3.1). In these instances either both phospho-sites were phosphorylated in the same peptide, or we were not able to determine which residues was phosphorylated in the peptide due to the pattern of fragment ions.

Table 3.1. Differential phospho-sites in the nuclear fraction quantified by PRM. Differential phosphorylation between SETI estradiol (SE) and SETI mock (SM) and SETI_krvy estradiol (KE). Statistically significant differential phospho-sites in **bold** with log2FoldChange (FC) < - 0.6 or > 0.6 and P-value of < 0.05 are represented in Figures 3.7-3.9. If data is available for KE in two biological repeats, the log2FC for SE/KE is also indicated. Phospho-sites highlighted in grey show a different trend when comparisons between SETI estradiol and SETI mock or SETI_krvy estradiol are made and should not be considered as differential. If P-value was > 0.05, then phospho-sites with log2FoldChange (FC) < - 1 or > 1 between SE and SM or KE are listed. The nuclear fraction where the phospho-site is differential is indicated. If a differential change of log2FC > 0.6 or < -0.6 was seen in an additional nuclear fraction, the log2FoldChange in this nuclear fraction is also indicated. Represents data from 4 biological repeats, however some peptides may have only been detected in at least 2 repeats. The average peptide intensity from three technical PRM repeats was taken together with the average across at least two biological repeats.

ID	Description	Phospho-site	Differential fraction	SE/SM P-value	SE/SM log2FC	SE/KE log2FC	Change in other fractions?	Known PTI and /or ETI sites?
AT4G35800	NRPB1, RNA polymerase II large subunit	S267	Pellet	0.3782	1.41 ↑	0.88 ↑	(HS) 0.66 ↑	No
AT4G35800	**NRPB1,RNA polymerase II large subunit**	**T874**	**Low Salt**	**0.0166**	**-2.15 ↓**	**N/A**	**(HS) 3.96 ↑**	No
AT4G35800	NRPB1, RNA polymerase II large subunit	S1508	Pellet	0.2304	1.10 ↑	N/A	(LS) -1.05 ↓	No
AT4G35800	NRPB1, RNA polymerase II large subunit	T1500, Y1502	Low Salt	0.1657	0.84 ↑	1.69 ↑	No	No
AT5G20170	MED17, RNA polymerase II transcription mediators	S346	High Salt	0.0989	-1.14 ↓	N/A	No	No
AT5G20170	**MED17, RNA polymerase II transcription mediators**	**S348**	**Pellet**	**0.0095**	**1.68 ↑**	**0.52**	**No data**	No
AT5G20170	**MED17, RNA polymerase II transcription mediators**	**S2346**	**Low Salt**	**0.0134**	**0.71 ↑**	**0.17**	**(HS) -1.57 ↓**	No
AT4G00450	MED12, RNA polymerase II transcription mediators	S1388	High Salt	0.2328	-1.17 ↓	N/A	No	No
AT4G00450	MED12, RNA polymerase II transcription mediators	S1394	High Salt	0.1981	-1.38 ↓	N/A	No	No
AT1G71080	RNA polymerase II transcription elongation factor	T182	Pellet	0.0939	-1.47 ↓	N/A	No data	No
AT4G35240	**DNA-directed RNA polymerase subunit beta**	**S93**	**Pellet**	**0.0138**	**0.67 ↑**	**-0.69 ↓**	**No data**	No
AT3G07610	**IBM1, protein with histone H3mK9 demethylation activity**	**T39**	**Pellet**	**0.0460**	**-2.15 ↓**	**N/A**	**No data**	No
AT2G31370	bZIP59, Basic-leucine zipper (bZIP) transcription factor	S160	Pellet	0.6309	-1.17 ↓	N/A	No data	PTI
AT1G80490	TPR1/TPL, TOPLESS-related 1/ Topless (AT1G15750)	T395	High Salt	0.4134	0.95 ↑	1.41 ↑	(LS) 1.37 ↑	No
AT1G80490	**TPR1, TOPLESS-related 1**	**T286**	**Pellet**	**0.0211**	**-1.62 ↓**	**-0.49**	**No**	No
AT1G80490	TPR1, TOPLESS-related 1	T286	Pellet	0.2206	-2.77 ↓	N/A	(LS) -0.94, (HS) -0.77 ↓	No
AT1G80490	TPR1, TOPLESS-related 1	T351	High Salt	0.0631	-1.34 ↓	N/A	No	No
AT3G16830	TPR2, TOPLESS-related 2	S681, S696	High Salt	0.1268	-1.05 ↓	N/A	No	No
AT3G16830	TPR2, TOPLESS-related 2	S1116	Pellet	0.4033	-1.25 ↓	N/A	No	No
AT3G16830	TPR2, TOPLESS-related 2	S1124	Low Salt	0.1057	1.26 ↑	N/A	(HS) -0.91 ↓	No
AT5G27030	TPR3, TOPLESS-related 3	T288	Pellet	0.0620	-2.04 ↓	-1.48 ↓	No data	PTI
AT2G32700	LUH, LEUNIG_homolog	S211	Pellet	0.3781	0.82 ↑	1.43 ↑	No	No
AT2G32700	LUH, LEUNIG_homolog	S355	High Salt	0.1800	-2.57 ↓	N/A	No	No
AT2G32700	LUH, LEUNIG_homolog	S358	High Salt	0.1905	-1.37 ↓	N/A	No	No
AT2G04880	WRKY1, zinc-dependent activator protein-1	S76, S79	High Salt	0.1643	-1.69 ↓	N/A	No	No
AT4G31800	WRKY DNA-binding protein 18	S86	High Salt	0.1213	2.37 ↑	N/A	(Pel) -1.54 ↓	No
AT3G01970	WRKY45, WRKY DNA-binding protein 45	T33	High Salt	0.1876	2.82 ↑	N/A	(Pel) 1.18 ↑	No
AT5G64220	CAMTA2, Calmodulin-binding transcription activator	S984	Low Salt	0.4328	-2.13 ↓	N/A	No	No
AT4G16150	**CAMTA5, Calmodulin binding transcription activator**	**S168**	**Pellet**	**0.0236**	**-0.98 ↓**	**-1.34 ↓**	**(HS) -0.66 ↓**	No
AT1G67310	Calmodulin-binding transcription activator, CG-1 + Ankyrin domains	S317	Pellet	0.3795	1.08 ↑	0.84 ↑	No	No
AT5G57110	**Tetratricopeptide repeat (TPR)-like superfamily protein**	**S27**	**High Salt**	**0.0384**	**-1.03 ↓**	**N/A**	**No**	PTI
AT4G35240	**Tetratricopeptide repeat (TPR)-like superfamily protein**	**S93**	**High Salt**	**0.0229**	**-1.50 ↓**	**N/A**	**No**	No
AT4G28080	**Tetratricopeptide repeat (TPR)-like superfamily protein**	**S146**	**High Salt**	**0.0117**	**1.08 ↑**	**N/A**	**(Pel) 1.09 ↑**	No
AT4G28080	**Tetratricopeptide repeat (TPR)-like superfamily protein**	**S155**	**High Salt**	**0.0347**	**1.49 ↑**	**N/A**	**(Pel) 1.49 ↑**	No
AT4G28080	**Tetratricopeptide repeat (TPR)-like superfamily protein**	**S160**	**High Salt**	**0.0158**	**1.30 ↑**	**N/A**	**(Pel) 1.13 ↑**	No
AT4G28080	Tetratricopeptide repeat (TPR)-like superfamily protein	S160	Pellet	0.1645	1.78 ↑	1.48 ↑	(HS) 1.86 ↑	No
AT4G28080	Tetratricopeptide repeat (TPR)-like superfamily protein	S162, S165	Low Salt	0.1361	1.23 ↑	0.62 ↑	(HS) 0.83 ↑	No
AT4G28080	Tetratricopeptide repeat (TPR)-like superfamily protein	T535	High Salt	0.3913	0.75 ↑	1.79 ↑	No	CC-NLR ETI
AT4G28080	**Tetratricopeptide repeat (TPR)-like superfamily protein**	**S1360**	**High Salt**	**0.0142**	**1.87 ↑**	**N/A**	**(Pel) 0.67 ↑**	No
AT4G28080	Tetratricopeptide repeat (TPR)-like superfamily protein	S1453	Pellet	0.5717	1.39 ↑	3.15 ↑	No	No
AT3G17850	IREH1, Protein kinase superfamily protein	S271	Pellet	0.4071	-1.15 ↓	N/A	No data	No
AT3G17850	**IREH1, Protein kinase superfamily protein**	**S663**	**High Salt**	**0.0232**	**-1.63 ↓**	**N/A**	**(LS) - 0.77 ↓**	No
AT2G05940	RIPK, Protein kinase superfamily protein	S426	High Salt	0.3212	-1.22 ↓	N/A	No	No
AT2G05940	RIPK, Protein kinase superfamily protein	S451	Pellet	0.2987	2.33 ↑	2.29 ↑	(HS) 1.45 ↑	No
AT5G04870	CPK1, calcium dependent protein kinase 1	S52	High Salt	0.0853	-1.04 ↓	N/A	No	PTI
AT3G02880	KIN7, receptor-like protein kinase	S626	High Salt	0.2890	-1.51 ↓	N/A	No	PTI
AT3G19100	Protein kinase superfamily protein	S37	High Salt	0.1396	-1.03 ↓	N/A	No	No
AT1G30270	CIPK23, CBL-interacting protein kinase 23	T190	Pellet	0.1614	-1.78 ↓	N/A	No	No
AT3G25070	**RIN4 | RPM1 interacting protein 4**	**T201**	**Low Salt**	**0.0295**	**-0.84 ↓**	**N/A**	**(HS) -0.81 ↓**	No
AT1G59870	PEN3, ABC-2 and Plant PDR ABC-type transporter family protein	S40	High Salt	0.2947	2.97 ↑	N/A	(Pel) 0.69 ↑	PTI, CC-NLR-ETI
AT3G46530	RPP13, NB-ARC domain-containing disease resistance protein	S156	High Salt	0.4359	-1.54 ↓	N/A	No	PTI
AT2G18960	**AHA1, PMA, OST2, HA1 | H(+)-ATPase 1**	**T881**	**High Salt**	**0.0325**	**-1.35 ↓**	**N/A**	**N/A**	PTI
AT4G31580	SRZ-22, serine/arginine-rich 22	S162, S160	High Salt	0.3941	-1.55 ↓	N/A	No	No
AT2G20960	pEARLI4, Arabidopsis phospholipase-like protein	S66	Low Salt	0.0503	0.97 ↑	1.07 ↑	No	No
AT2G20960	pEARLI4, Arabidopsis phospholipase-like protein	T190	Low Salt	0.1285	-0.88 ↓	-1.30 ↓	No	No
AT2G20960	pEARLI4. Arabidopsis phospholipase-like protein	S400	Pellet	0.5209	1.17 ↑	0.92 ↑	No	No

3 phospho-sites from WRKY DNA-BINDING PROTEIN 18 (WRKY18), TOPLESS RELATED 2 (TPR2) and RNA POLYMERASE II LARGE SUBUNIT (NRPB1) show an increase in phosphorylation in one fraction but a decrease in phosphorylation in another subcellular nuclear fraction at the same phospho-site (Table 3.1). For example, TPR2 S1124 increases in phosphorylation in the low salt fraction but decreases in phosphorylation in the high salt fraction (Table 3.1). Phosphorylation changes in these proteins may cause changes in subcellular localisation of the protein, explaining why phosphorylation is increasing in one fraction but decreasing in another nuclear fraction at the same residue. 27 phospho-sites changed in phosphorylation in just one subcellular nuclear fraction, with no change in phosphorylation in the other nuclear fractions (Table 3.1). Therefore, protein phosphorylation/dephosphorylation may only occur on a specific subcellular localised pool of proteins e.g. in the high salt fraction containing tightly bound chromatin-associated proteins. 15 phospho-sites had a differential change in phosphorylation in the same direction in two or more nuclear fractions (Table 3.1). For example, RPM1 INTERACTING PROTEIN 4 (RIN4) T201 shows a decrease in phosphorylation in both the low salt and high salt fraction but WRKY45 T33 shows an increase in phosphorylation in both the high salt and pellet fraction (Table 3.1). This would suggest WRKY45 is increasing in phosphorylation throughout the nucleus, whereas there is global dephosphorylation of RIN4.

5 phospho-sites were exclusively detected in just one subcellular nuclear fraction. For all 5 of these sites, this was the pellet fraction. e.g. TOPLESS RELATED 3 (TPR3) T288 (Table 3.1). Additionally, these 5 sites were each from proteins where only one phospho-site was identified as having differential phosphorylation. This may further highlight the requirement for sub-cellular specificity of a single phosphorylation pattern for ETI signalling. The proteins showing this pattern include an RNA polymerase transcription elongation factor, three transcription factors and a protein kinase (Table 3.1). As these were all seen in the pellet fraction, this could suggest a specific phosphorylation change is required for activation of transcription.

9 proteins have phosphorylation changes in two or more phosphorylation sites. E.g. AT4G28080 has phosphorylation changes at 8 phospho-sites, which all show an increase in phosphorylation. This protein may have increased in protein abundance upon ETI activation. Therefore, we must be careful when interpreting this increase in phosphorylation. However, AT2G20960 has an increase in phosphorylation at S400 in the pellet fraction and an increase at S66 in the low salt fraction, but a decrease in phosphorylation at T190 in the low salt fraction (Table 3.1). 6 of the 9 proteins show an increase in phosphorylation at one phospho-site and a decrease in phosphorylation at another phospho-site: TPR2, NRPB1, TOPLESS RELATED 1 (TPR1), RPM1-INDUCED PROTEIN KINASE (RIPK), LEUNIG HOMOLOG (LUH) and AT2G20960 (Table 3.2). Changes in phosphorylation in different

directions at different sites suggests changes in phosphorylation of these proteins are not due to changes in protein level.

3.2.2.1 Phosphorylation changes of transcription factors

Transcriptional changes are induced upon ETI signalling (Mine et al., 2018, Bhandari et al., 2019, Ding et al., 2020, Ding et al., 2021). Phosphorylation may play a role in activating these transcriptional changes. TPR1 shows a decrease in phosphorylation at T286 and T351 (Table 3.1). T286 is represented twice in the table, due to being present in two peptides, with different tryptic cleavage patterns (Table 3.1). TPR1 and TOPLESS (TPL) are transcriptional co-repressors and act redundantly as positive regulators of immunity, with 92% protein similarity (Zhu et al., 2010). The phospho-site T395, which increases in phosphorylation upon ETI activation, is within a conserved region of these proteins and therefore it is not possible to distinguish which protein the phospho-peptide was from. Another report found TPL S214 phosphorylation was induced upon flg22 treatment in a *mpk3* mutant (Rayapuram et al., 2021). S214 is a conserved serine between TPL and TPR1. S214 was quantified by PRM but did not show a change in phosphorylation upon ETI activation. TPR2 has three phospho-peptides showing a change in phosphorylation upon ETI activation (Table 3.1). TPR3 shows a decrease in phosphorylation at T288 (Table 3.1). TPR2 and TPR3 have been reported to act as negative regulators of immunity (Garner et al., 2021). TPR2 binds SUPPRESSOR OF NPR1-1 CONSTITUTIVE 1 (SNC1) and TPR1, preventing TPR1 repression of negative regulators of immunity e.g. DEFENSE NO DEATH 1 (DND1) (Zhu et al., 2010, Garner et al., 2021). Changes in TPR2 and TPR3 phosphorylation may be a mechanism to inhibit TPR2/TPR3 activity upon immunity activation, due to their role as negative regulators.

LUH is within the Gro/Tup1 family of transcriptional corepressors and is dephosphorylated and phosphorylated at different sites upon ETI activation (Table 3.1) LUH positively regulates the transcription of Jasmonic acid (JA)-responsive genes, through its function as a co-activator of MYC2, a master transcription factor in JA signalling (You et al., 2019). LUH functions as a scaffold for MED25 and HISTONE ACETYLTRANSFERASE OF THE CBP FAMILY 1 (HAC1) interactions during JA signalling (You et al., 2019). This contrasts the role of TPL, another member of the Gro/Tup1 family of transcriptional repressors, which acts to repress MYC2 activation (Pauwels et al., 2010). Broadly speaking, JA is important for resistance to necrotrophic pathogens but acts antagonistically to SA, which is important for resistance to biotrophic pathogens (Niki et al., 1998). However, a positive role for JA in ETI signalling was revealed (Liu et al., 2016). SA receptors NPR1-LIKE PROTEIN 3/4 (NPR3/NPR4) activate JA synthesis during NLR RPS4-mediated ETI (Liu et al., 2016). Therefore, the role of LUH in JA signalling during ETI needs to be explored to determine if LUH acts as a positive or negative regulator of ETI. In addition, the role of changing phosphorylation at different phospho-sites within LUH is not clear.

Three WRKY proteins show a change in phosphorylation: WRKY18, WRKY45 and WRKY1 (Table 3.1). WRKY18 acts as a positive regulator of immunity in response to the bacterial effector AvrRps4 (Schon et al., 2013). WRKY18 S86 shows a 3x fold increase in phosphorylation in response to dehydration stress (Umezawa et al., 2013). Therefore, WRKY18 could be phosphorylated in response to different stress signals. It has been reported that WRKY1 negatively regulates *Pst* DC3000 induced immunity (Fang et al., 2021b). WRKY1 binds to the promoter of *PR1* and represses *PR1* expression and *wrky1* plants showed increased resistance to *Pst* DC3000 (Fang et al., 2021b). There has been no report of WRKY45's role in immunity in Arabidopsis.

CALMODULIN-BINDING TRANSCRIPTION ACTIVATOR 2 (CAMTA2) is dephosphorylated upon ETI activation in PRM (Table 3.1). CAMTA2 acts redundantly with CAMTA1/3 to repress the expression of SA genes *ICS1*, *SARD1*, *CBP60g* and *PR1* (Kim et al., 2013). Therefore, phosphorylation may play a role in repressing this negative regulator of ETI signalling. CALMODULIN-BINDING TRANSCRIPTION ACTIVATOR (CAMTA5) also shows a decrease in phosphorylation (Table 3.1). CAMTA5 responds to a rapid decrease in temperature and promotes the expression of dehydration-responsive element binding proteins (*DREB1s*), which control cold-responsive gene expression (Kidokoro et al., 2017, Liu et al., 1998). The role of CAMTA5 in ETI signalling and specifically the role of CAMTA5 phosphorylation is not known.

The basic-leucine zipper (bZIP) transcription factor bZIP59 is dephosphorylated upon ETI activation (Table 3.1). bZIP59 is expressed in guard cells and is involved in stomatal immunity (Song et al., 2022). *bzip59* mutants have reduced *Pst* DC3000 and flg22-induced stomatal closure (Song et al., 2022). *bzip59* mutants are more susceptible to surface inoculated *Pst* DC3000 but *bzip59* plants have similar bacterial levels to Col-0 when *Pst* DC3000 was infiltrated into leaves (Song et al., 2022). No difference was seen in apoplastic ROS production in the *bzip59* mutants compared to Col-0, but *bzip59* plants are deficient in ROS production in guard cells after flg22 treatment (Song et al., 2022). bZIP59 represses the expression of two transcription factors involved in JA signalling, NAC DOMAIN CONTAINING PROTEIN 19 and 72 (*ANAC019* and *ANA072)*, to inhibit coronatine -induced stomata re-opening (Song et al., 2022). This suggests bZIP59 is involved in stomatal immunity but not involved in apoplastic defence responses (Song et al., 2022). Additionally, bZIP59 is involved in transcriptional regulation of many genes during flg22 responses (Song et al., 2022). The function of dephosphorylation in regulating bZIP59's role in stomatal immunity should be further investigated.

INCREASE IN BONSAI METHYLATION 1(IBM1), a histone demethylase, shows a decrease in phosphorylation (Table 3.1). IBM1 is a negative regulator of immunity, as the *ibm1* mutant has increased resistance to *Pst* DC3000 and elevated immune responses to flg22 (Lv et al., 2022).

Therefore, dephosphorylation may play a role to inhibit or activate this negative regulator during ETI signalling. Changes in phosphorylation of transcription factors with known and unknown roles in ETI give clues to the signalling pathways activated to facilitate transcriptional changes during ETI.

3.2.2.2 Role of RNA polymerase-associated protein phosphorylation

4 protein components of RNA polymerase show changes in phosphorylation: the RNA polymerase II large subunit NRPB1, two transcription mediators and an RNA polymerase II transcription elongation factor (Table 3.1). NRPB1 T874 shows a decrease in phosphorylation in the low salt fraction but an increase in phosphorylation in the high salt fraction. This may indicate a phosphorylation-induced localisation change, moving from loosely associated to a highly chromatin associated protein. This would correlate with the role of NRPB1 in transcription and the large transcriptional changes that occur during ETI signalling (Mine et al., 2018, Bhandari et al., 2019, Ding et al., 2020, Ding et al., 2021). NRPB1 has a total of 4 phospho-sites which change in phosphorylation upon ETI activation (Table 3.1). Changing phosphorylation at different sites within the same protein may be important for interacting with other members of the RNA polymerase complex e.g. at different stages of transcription. The C-terminal domain (CTD) of NRPB1 contains a tandem heptapeptide repeat region, with the most common repeat being YSPTSPS (Eick & Geyer, 2013). Phosphorylation of NRPB1 CTD has been previously reported, with different phosphorylation patterns of NRPB1 CTD recruiting different protein complexes (Ding et al., 2011). Different phosphorylation patterns of NRPB1 CTD are also associated with different stages of transcription e.g. initiation, elongation and termination (Ding et al., 2011). The phospho-sites on NRPB1 identified in our study were upstream of the CTD (Table 3.1). Most studies on RNA POLYMERASE II (Pol II) activity and CTD phosphorylation have been done in Drosophila, yeast or mammalian cells (Cramer et al., 2000, Eick & Geyer, 2013, Cramer, 2019). Very little work has been done with phosphorylation of Pol II in plants. PAMP-induced Arabidopsis CTD phosphorylation has been described (Li et al., 2014a). Flg22 treatment induced phosphorylation of RNA Pol II CTD in Arabidopsis seedlings (Li et al., 2014a). Cyclin-dependent kinases CDCK1 and CDCK2 phosphorylate Pol II CTD and *cdkc1/2* mutant plants are more susceptible to *Pst* infection (Li et al., 2014a).). Furthermore, MAP KINASE 3 (MPK3) and MPK6 directly phosphorylate CDCK1 upon flg22 treatment (Li et al., 2014a). Therefore, flg22 induced MAPK signalling results in CDCK1 phosphorylation by MPK3/6 and phosphorylation of Pol II CTD by CDCKs (Li et al., 2014a). C-TERMINAL DOMAIN PHOSPHATASE-LIKE 3 (CPL3) is a negative regulator of plant immunity and dephosphorylates NRPB1 CTD (Li et al., 2014a). Therefore, the phosphatase CPL3 and cyclin-dependent kinases act antagonistically to fine tune the transcriptional response to pathogen detection through phosphorylation changes of the Pol II CTD (Li et al., 2014a). Phosphorylation of NRPB1 has not been previously investigated during ETI activation.

Therefore, the phospho-sites identified in this study are novel ETI-induced NRPB1 phospho-sites. Novel ETI phosphorylation sites are important clues to how signalling differs between ETI and PTI. Whether the same or different kinases are responsible for NRPB1 phosphorylation during PTI and ETI signalling needs to be investigated.

MEDIATOR SUBUNIT 17 (MED17) is dephosphorylated upon ETI activation (Table 3.1). MED17 binds to the promoters of thermosensory genes, to promote H3K4me3 enrichment and increase RNA polymerase II occupancy at these genes (Agrawal et al., 2022). MEDIATOR SUBUNIT 12 (MED12) is also dephosphorylated upon ETI activation (Table 3.1). MED12, which forms part of the Mediator kinase module, acts as positive regulator of SA signalling (Huang et al., 2019). *med12* mutant plants have decreased SA accumulation and reduced *ICS1, NPR1* and *PR1* expression (Huang et al., 2019, Chen et al., 2019). *med12* plant are also defective in the establishment of Systemic Acquired Resistance (SAR) (Chen et al., 2019). ChIP-Seq revealed MED12 binds to the promoters of genes enriched for "Response to stimulus" and "Response to stress" GO terms (Liu et al., 2020). Therefore, MED12 and MED17 dephosphorylation may be required for transcriptional changes during ETI.

3.2.2.3 Phosphorylation of protein kinases upon ETI activation

7 protein kinases show a change in phosphorylation upon ETI activation (Table 3.1, 3.2). Protein kinase INCOMPLETE ROOT HAIR ELONGATION 1 (IREH1), which shows a decrease in phosphorylation upon ETI activation (Table 3.1), is involved in root skewing (Yue et al., 2019), but a role of IREH1 in immune signalling has not been previously reported. The receptor kinase 7 (KIN7) at S626 is dephosphorylated upon ETI activation (Table 3.1). This phospho-site is conserved amongst some members of the receptor kinase family in Arabidopsis and rice (Hsu et al., 2009). The same site is phosphorylated after 200 mM NaCl salt-stress (Hsu et al., 2009). Therefore, this may be a conserved phosphorylation site between different stress signals. KIN7 is localised to the plasma membrane and phosphorylates Two Pore K+ 1 (TPK1), a K+ channel involved in ABA-mediated stomatal closure (Isner et al., 2018). Further investigation is needed to determine a link between KIN7 phosphorylation, stomatal closure and immunity signalling.

CBL-interacting protein kinase 23 (CIPK23) T190 was dephosphorylated upon ETI activation (Table 3.1). The same site is also de-phosphorylated after auxin and ABA treatment (Zhang et al., 2013, Huang et al., 2023). The phospho-mimetic CIPK23^{T190D} promotes stomatal opening (Huang et al., 2023). Therefore, dephosphorylation of CIPK23 upon ETI activation may act to limit stomatal opening and restrict pathogen entry. CIPK23 phosphorylates the K^+ channel ATK1 (Xu et al., 2006a). The *M. oryzae* effector AvrPiz-t binds to OsAKT1, preventing OsCIPK23 interaction and inhibiting K^+ uptake (Shi et al.,

2018). Therefore, OsCIPK23 may have a positive role in rice immunity to *M. oryzae* by increasing K^+ levels (Shi et al., 2018). However, no difference was found in K^+ uptake in $CIPK23^{T190D}$ vs wildtype (WT) CIPK23 plants (Huang et al., 2023). Therefore, the role of CIPK23 phosphorylation in plant immunity signalling is unclear.

Calcium dependent protein kinase 1 (CPK1) is a positive regulator of immunity, as *cpk1* mutants are more susceptible to *P. syringae* and have reduced *PR1* expression (Coca & San Segundo, 2010). CPK1 is dephosphorylated upon ETI activation (Table 3.1). PHE AMMONIA LYASE 1 (PAL1), an enzyme involved in SA defence signalling, is phosphorylated by CPK1 (Cheng et al., 2001, Kim & Hwang, 2014). However, the role of PAL1 and CPK1 phosphorylation in immunity signalling is not known. The role of phosphorylation of these protein kinases during ETI signalling needs be further investigated.

3.2.2.4 Overlaps between TIR-NLR and CC-NLR phosphorylation

Several phospho-sites identified upon TIR-NLR RRS1/RPS4 activation, were also previously found after CC-NLR RESISTANT TO P. SYRINGAE 2 (RPS2) activation. T535 from tetratricopeptide repeat (TPR)-like superfamily protein (AT4G28080) increases in phosphorylation upon ETI activation (Table 3.1) T535 was found to also increase in phosphorylation after CC-NLR activation (Kadota et al., 2019). The function of the tetratricopeptide repeat (TPR)-like superfamily protein in plants has not been well studied. Therefore, although it may be a conserved signalling protein between CC-NLR and TIR-NLR immunity, we cannot comment on its role in ETI signalling. PENETRATION 3 (PEN3) S40 shows an increase in phosphorylation upon ETI activation (Table 3.1). Phosphorylation at the same site S40 increases in phosphorylation upon CC_NLR activation (Kadota et al., 2019). S40 also increases in phosphorylation after 10 minutes of flg22 or 10 minutes treatment with the fungal elicitor Xylanase (Benschop et al., 2007). PEN3 is involved in callose deposition in response to flg22 (Clay et al., 2009). This suggests PEN3 may be involved in both PTI and ETI signalling and could be a conserved signalling protein in multiple defence pathways. RIPK protein kinase shows an increase in phosphorylation at S451 (Table 3.1). RIPK was also found to increase in phosphorylation downstream of RPS2 activation but at a different phosphorylation site S433 (Kadota et al., 2019). RIPK is involved in ETI signalling and phosphorylates RIN4 to activate CC-NLR RESISTANCE TO P. SYRINGAE PV MACULICOLA 1 (RPM1) (Xu et al., 2017, Liu et al., 2011). The role of RIPK phosphorylation in TIR-NLR signalling remains unclear. Overall, there are limited overlaps between the CC-NLR and TIR-NLR datasets. This is partly due to the difference in subcellular fractions studied, with membrane proteins investigate upon CC-NLR activation (Kadota et al., 2019) and nuclear proteins investigated after TIR-NLR RPS4/RRS1 activation (Table 3.1). It would be useful to investigate ETI-triggered phosphorylation of another nuclear-

localised NLR or the nuclear fraction of a membrane or cytosolic-localised NLR, to understand conservation in phosphorylation signalling between activation of different NLRs.

3.2.2.5 The nuclear fraction contains differential phosphorylation of plasma membrane-localised proteins

Multiple plasma-membrane localised proteins were found to have differential phosphorylation in the nuclear protein fraction. These include KIN7, CIPK23 and PEN3 which have been previously discussed, as well as AHA1 and RIN4. The nuclear fraction was a crude extraction and therefore may have some contamination of microsomal proteins. H^+-ATPASE 1 (AHA1) is dephosphorylated at T881 upon ETI activation (Table 3.1). Phosphorylation of AHA1 T881 was found to rapidly decrease after flg22 treatment (Nühse et al., 2007), suggesting this may be a conserved phosphorylation site between ETI and PTI. AHA1 negatively regulates PR1 secretion into the apoplast upon bacterial infection (Baena et al., 2022). AvrB from *Pseudomonas syringae* promotes AHA1 activity to induce stomatal opening and increase bacterial virulence (Zhou et al., 2015). AHA1 also enhances JA signalling (Zhou et al., 2015). Therefore, AHA1 acts as a negative regulator of plant immunity. Whether dephosphorylation of AHA1 during ETI/PTI activation acts to repress AHA1 activity needs to be explored. RIN4, a plasma-membrane localised protein linked to RPM1-mediated immunity (Mackey et al., 2002), shows a decrease in phosphorylation at T201 in both the low salt and high salt fraction (Table 3.1). RIN4 is phosphorylated by RIPK at three other residues, in the presence of the bacterial effectors AvrB and AvrRpm1 (Liu et al., 2011). Therefore, whether RIN4 is also phosphorylated by RIPK at T201 in the presence of AvrRps4 should be tested.

3.2.3 Quantification of nuclear proteins by MS1 quantification

Another method of quantitative proteomics is MS1 quantification. Here the precursor ions are quantified, rather than the fragment ions which are quantified during PRM. A selection of peptides showing a differential phosphorylation in PRM were quantified by MS1. SARD1 S77 was also included for quantification by MS1 as the DDA looked promising, but the peptide was not detected in two biological samples in PRM. Phosphorylation changes in phospho-sites from TPR1, WRKY45, NRPB1 and WRKY1 seen in PRM were confirmed by MS1 quantification (Table 3.2). A decrease in phosphorylation of TPR2 S116 seen in PRM, was also seen in MS1 in SETI estradiol compared to SETI mock, but no change was seen compared to SETI_krvy estradiol (Table 3.2). Therefore, TPR2 S116 cannot be considered as differential by MS1. Another site in TPR2 S1124 showed no change in phosphorylation in MS1 (Table 3.2). NRPB1 T874 and RIPK S451 also showed no change in phosphorylation in MS1

(Table 3.2). CAMTA5 S168 showed a decrease in phosphorylation in the pellet and high salt fraction in PRM and no change in the low salt fraction (Table 3.1). However in MS1, CAMTA5 S168 showed an increase in phosphorylation in the low salt fraction and no change in the other two fractions (Table 3.2). PRM data is more sensitive and has less background than MS1. Therefore, for these sites the PRM data should be trusted over the MS1 data. WRKY18 S86 showed a decrease in phosphorylation in the pellet fraction, but an increase in phosphorylation in the high salt fraction in PRM (Table 3.1). MS1 quantification had no data for high salt or pellet fraction but showed an increase in phosphorylation in the low salt fraction (Table 3.2). The MS1 data for WRKY18 was much stronger than the PRM data. Therefore, the increase in phosphorylation of WRKY18 S86 seen in MS1 should be relied upon over changes seen in PRM.

SARD1 S77 shows a large increase in phosphorylation in the pellet fraction by MS1 quantification (Table 3.2). SARD1 regulates the transcription of many genes during ETI, PTI and SAR (Sun et al., 2015). CBP60g, which acts redundantly with SARD1, is phosphorylated upon PAMP treatment and CBP60g phosphorylation is required for SA signalling (Sun et al., 2022). CBP60g phosphorylation enhanced its transcriptional activity at the *ICS1* promoter (Sun et al., 2022). Therefore, phosphorylation of SARD1 could also be important for its role as a transcriptional regulator of ETI.

Table 3.2. Phospho-sites in the nuclear fraction quantified by MS1 quantification. A selection of proteins showing a differential phosphorylation by PRM were quantified by MS1. Log2FoldChange (FC) in phosphorylation between SETI estradiol (SE) and SETI mock (SM) or SETI_krvy estradiol (KE) is show. P value > 0.05 = NS. Represents data from 4 biological repeats, however some peptides may have only been detected in at least 2 repeats. If data is available for KE in two biological repeats, the log2FC for SE/KE is indicated. N/A = peptide was detected in only one KE sample. The peptide intensity across at least two biological repeats was averaged. Phospho-sites in grey indicate sites which do not show the same phosphorylation trend as that measured in PRM, or where the phosphorylation change in SM and KE compared to SE do not match.

ID	Description	Phospho-site	Differential protein fraction	SE/SM P-value	SE/SM log2FC	SE/KE log2FC
AT4G35800	NRPB1, RNA polymerase II large subunit	S267	Pellet	NS	2.17	1.66
AT4G35800	NRPB1, RNA polymerase II large subunit	T874	Low Salt	NS	-0.24	N/A
AT1G80490	TPR1, TOPLESS-related 1	T286	High Salt	NS	-0.87	N/A
AT1G80490	TPR1, TOPLESS-related 1/ TPL | Topless	T395	HS	NS	4.66	2.35
AT3G16830	TPR2, TOPLESS-related 2	S1116	Pellet	NS	-0.77	0.45
AT3G16830	TPR2, TOPLESS-related 2	S1124	Low Salt	NS	-0.03	0.26
AT2G04880	WRKY1, zinc-dependent activator protein-1	S76, S79	High Salt	NS	-1.2	-0.63
AT3G01970	WRKY45, WRKY DNA-binding protein 45	T33	Low Salt, Pellet	(Pel) 0.0205	(LS) 1.30, (Pel) 1.62	(Pel) 0.77
AT4G31800	WRKY18, WRKY DNA-binding protein 18	S86	Low Salt	NS	1	N/A
AT5G64220	CAMTA2, Calmodulin-binding transcription activator	S984	High Salt , Pellet	NS	(HS) 0.95, (Pel) 0.69	(Pel) 0.74
AT4G16150	CAMTA5, calmodulin binding;transcription regulators	S168	Low Salt	NS	1.16	N/A
AT2G05940	RIPK, Protein kinase superfamily protein	S451	Pellet	NS	0.30	N/A
AT1G73805	SARD1, SAR DEFICIENT 1	S77	Pellet	NS	1.82	N/A

To investigate the role of phosphorylation during ETI signalling, we selected proteins for functional analysis experiments. We wanted to investigate phosphorylation of proteins which were nuclear localised and already had a known role in ETI signalling. WRKY18 and TPR1 show changes in phosphorylation upon ETI activation (Table 3.1). WRKY18 and TPR1 are involved in immunity after AvrRps4 detection (Schon et al., 2013, Zhu et al., 2010). Therefore, we investigated the role of TPR1 and WRKY18 phosphorylation and this is further discussed in Chapter 4. SARD1 S77 showed an increase in phosphorylation in the nuclear pellet fraction using MS1 quantification. We chose to follow up on SARD1 phosphorylation because SARD1 is a master regulator of transcription during immunity (Sun et al., 2015). Additionally, the experimental materials (Arabidopsis mutants of *sard1*, *sard1*/*cbp60g*) were already available in the lab. Transient expression in protoplasts also provided a quick assay which did not require waiting for Arabidopsis stable lines to be created.

3.2.4 Functional analysis of SARD1 phosphorylation

3.2.4.1 SARD1 phospho-sites are conserved across plant species

SARD1 was phosphorylated upon ETI activation (Table 3.2). The SARD1 phosphorylation site is located at one of three serines: S75, S76 or S77. The location of the phosphorylated serine was not resolved due to the position of the fragment ions detected by MS. S75 and S77 are well conserved in SARD1 homologs from multiple plant species (Figure 3.10). However, S76 is not well conserved in SARD1 homologs from across the plant kingdom (Figure 3.10). This suggests S75 and S77 may be important for SARD1 function. SARD1 acts redundantly with CBP60g (Zhang et al., 2010b). S75 of SARD1 is conserved in an alignment with CBP60g (Wang et al., 2011a). However, no phosphorylation of CBP60g was detected in our phospho-proteomics study. To study the role of phosphorylation, amino-acid substitutions can be made at protein phosphorylation sites. Substitutions that mimic a phosphorylated residue are called phospho-mimetic e.g. Aspartic Acid and Glutamic acid chemically resemble a phosphorylated serine (Dissmeyer & Schnittger, 2011). Therefore, the protein is always in its phosphorylated form, allowing researchers to study the role of phosphorylation in regulating protein function. To make a phospho-dead substitution a non-phosphorylatable amino acid is used e.g. Alanine (Dissmeyer & Schnittger, 2011). As we were not certain which SARD1 serine was phosphorylated, we targeted all three serines to make single, double (S75+S77) or triple phosphorylation variants. The three serines were changed to Alanine (AAA) to make a phospho-dead variant or changed to Aspartic Acid (DDD) to make a phospho-mimic.

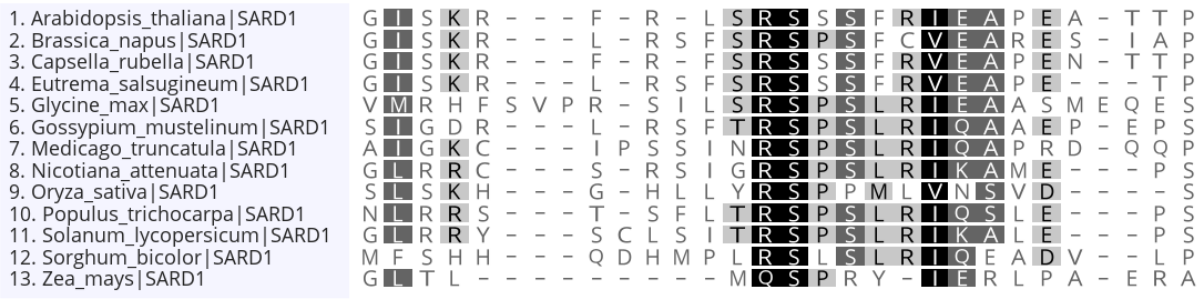

Figure 3.10. *At*SARD1 residues S75 and S77 are well conserved in SARD1 homologs. *At*SARD1 protein sequence was used in a protein BLAST and the top protein identity hits selected from across the plant kingdom are shown. Multiple protein sequence alignment was performed using T-Coffee and imported into Geneious.

3.2.4.2. SARD1 phospho-mimetic variants show enhanced binding to *EDS5* promoter

To study transcriptional regulation a dual-luciferase reporter assay can provide a quantitative output (Liu & Axtell, 2015) and can be combined with protoplast transfection to allow transient expression and analysis of transcription factor activity (Iwata & Koizumi, 2005, Fang et al., 2021a). The dual luciferase system utilises Firefly luciferase from *Photinus pyralis* (de Wet et al., 1985) and Renilla luciferase from the coral *Renilla reniformis* (Lorenz et al., 1991). The substrate of firefly luciferase is D-luciferin, whereas the substrate of Renilla is coelenterazine (Shifera & Hardin, 2010). The distinct substrates allow Renilla to act as an internal control.

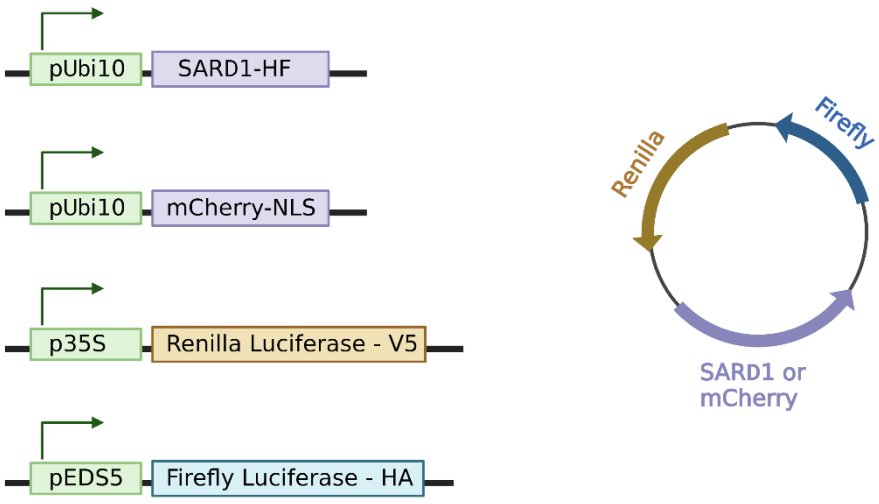

Figure 3.11. Schematic diagram of constructs used in dual-luciferase assay. Renilla luciferase and firefly luciferase were on a single plasmid, along with a SARD1 or mCherry construct.

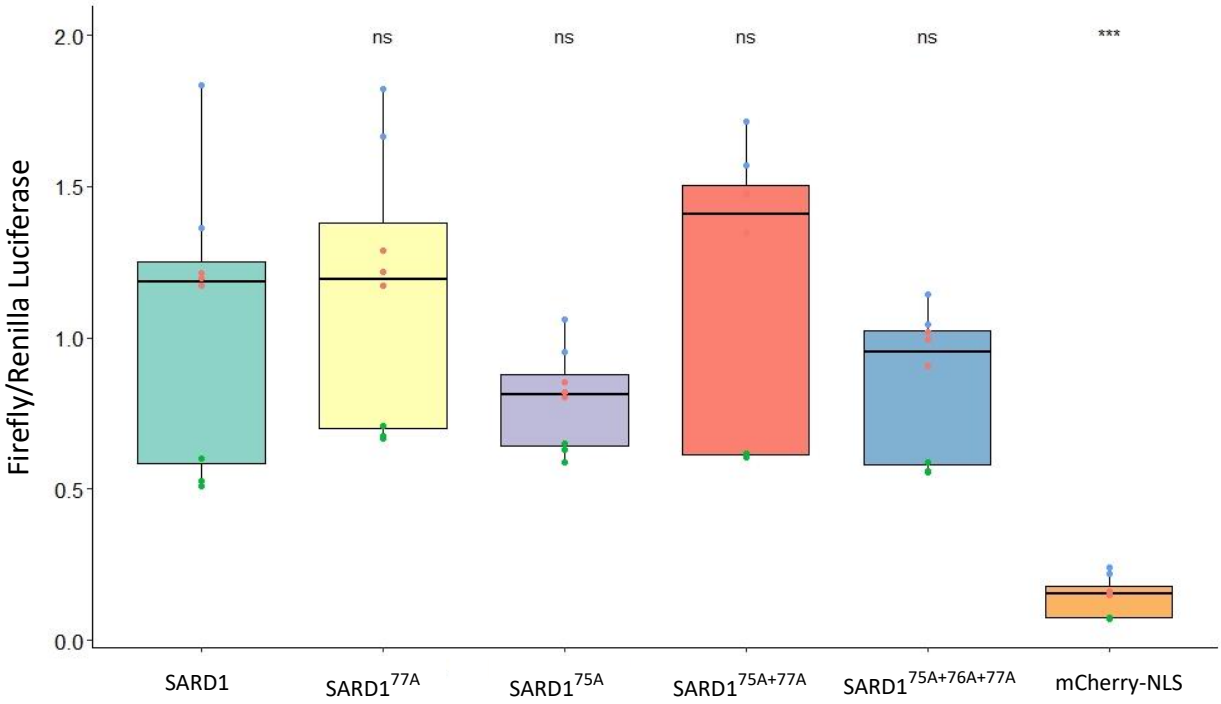

Figure 3.12. **mCherry NLS has reduced pEDS5:Firefly expression**. Dual-luciferase plasmids were transiently expressed in *N. tabacum* leaves at OD:0.25 and leaf discs taken after 48 hours. Renilla and Firefly luciferase expression was quantified with Promega Dual-Luciferase® Reporter Assay System and a VarioSkan plate reader. Three biological repeats represented (coloured dots). P-value *** < 0.001. ns = non-significant.

SARD1 binds directly to the *EDS5* promoter upon pathogen infection (Sun et al., 2015). To study the ability of SARD1 phospho-variants in binding to the *EDS5* promoter, a luciferase assay was performed with the *EDS5* promoter driving firefly luciferase expression. Ubi10 over-expression of SARD1 was used as a proxy for immunity activation. Firefly luciferase, Renilla luciferase and SARD1 phospho-variants or mCherry-NLS were assembled into one plasmid using Golden Gate cloning (Figure 3.11). The plasmids were cloned and assembled by Mark Youles of TSL Synbio service. Dual luciferase plasmids were transiently expressed in *Nicotiana tabacum*. After 48 hours leaf discs were taken and luciferase expression quantified with a Dual-Luciferase® Reporter Assay System. SARD1 wildtype had higher pEDS5:Firefly luciferase expression than mCherry-NLS (Figure 3.12). However, there was no difference between SARD1 wildtype and the SARD1 phosphorylation-dead variants (Figure 3.12). Endogenous *Nt*SARD1 in *N. tabacum* may be binding to the *EDS5* promoter, masking the differences seen between the *At*SARD1-varaints in promoting firefly expression. To study differences in luciferase expression between the *At*SARD1 variants, we completed dual luciferase assays in Arabidopsis Col-0: *sard1/cbp60g* protoplasts (Figure 3.13).

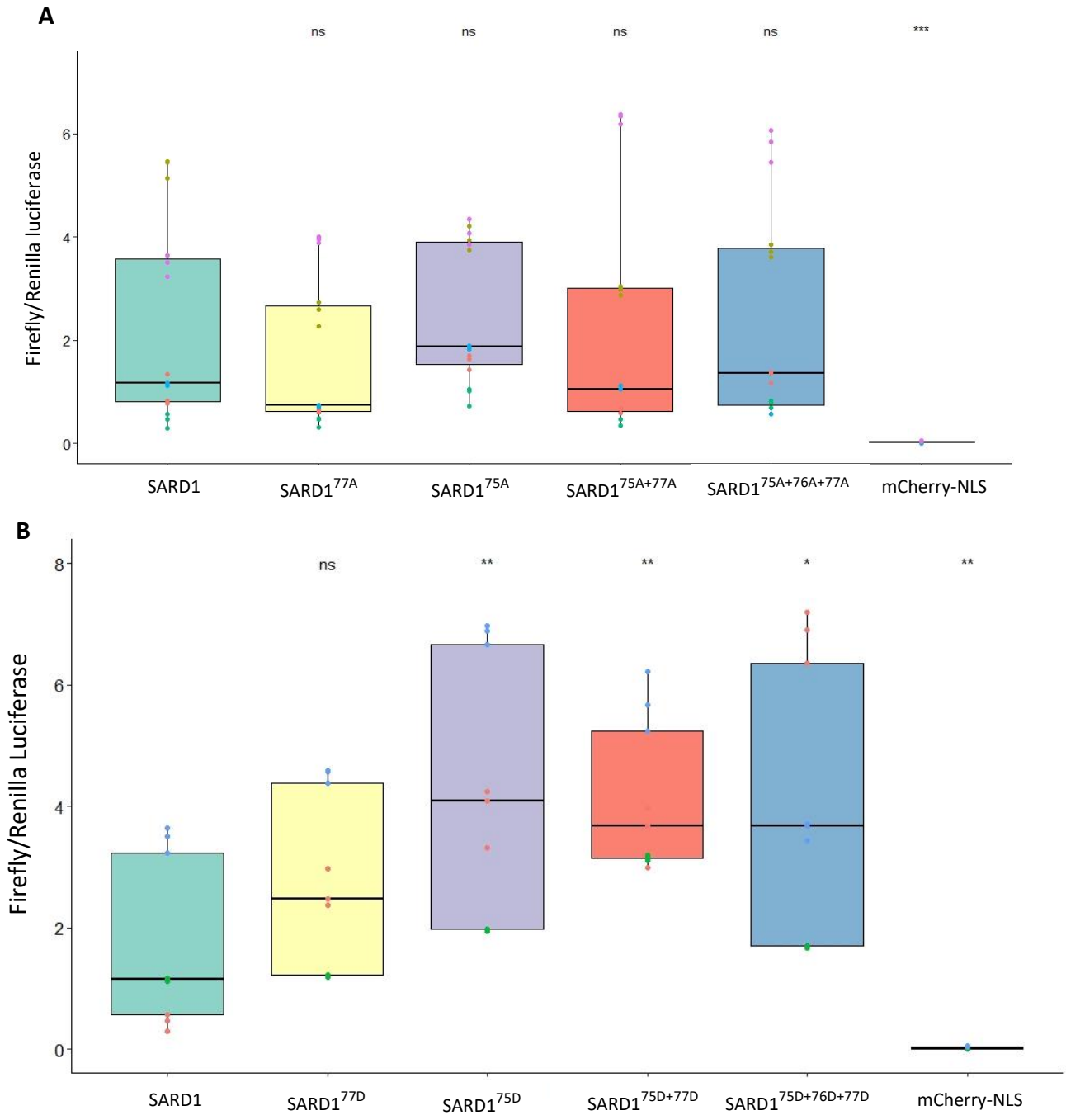

Figure 3.13. **Protoplasts transformed with SARD1 phospho-mimic variants have enhanced Firefly luciferase expression.** Arabidopsis Col-*0:sard1/cbp60g* protoplasts were isolated and transformed with 2 µg of dual-luciferase constructs with either **A)** Phospho-dead variants of SARD1 or **B)** Phospho-mimic variants of SARD1. Renilla and Firefly luciferase expression were quantified with Promega Dual-Luciferase® Reporter Assay System and a VarioSkan plate reader. Three biological repeats represented (coloured dots), each with three technical repeats T.Test P-value *< 0.05, ** < 0.01. ns = non-significant.

When Arabidopsis Col-0: *sard1/cbp60g* protoplasts are transformed with 2 µg of dual-luciferase plasmids, protoplasts transformed with SARD1$^{75D+76D_77D}$, SARD1$^{75D+77D}$ and SARD1^{75D} phospho-mimics have enhanced pEDS5:firefly luciferase expression compared to protoplasts with SARD1 wildtype (WT) (Figure 3.13B). There was no difference between SARD1 wildtype and SARD1^{77D} phospho-mimic (Figure 3.13B). SARD1 phospho-dead variants are not impaired in their ability to activate firefly expression, as all SARD1 phospho-dead variants induce similar pEDS5:firefly expression to SARD1 wildtype (Figure 3.13A). However, there was huge variation between biological repeats (Figure 13.3).

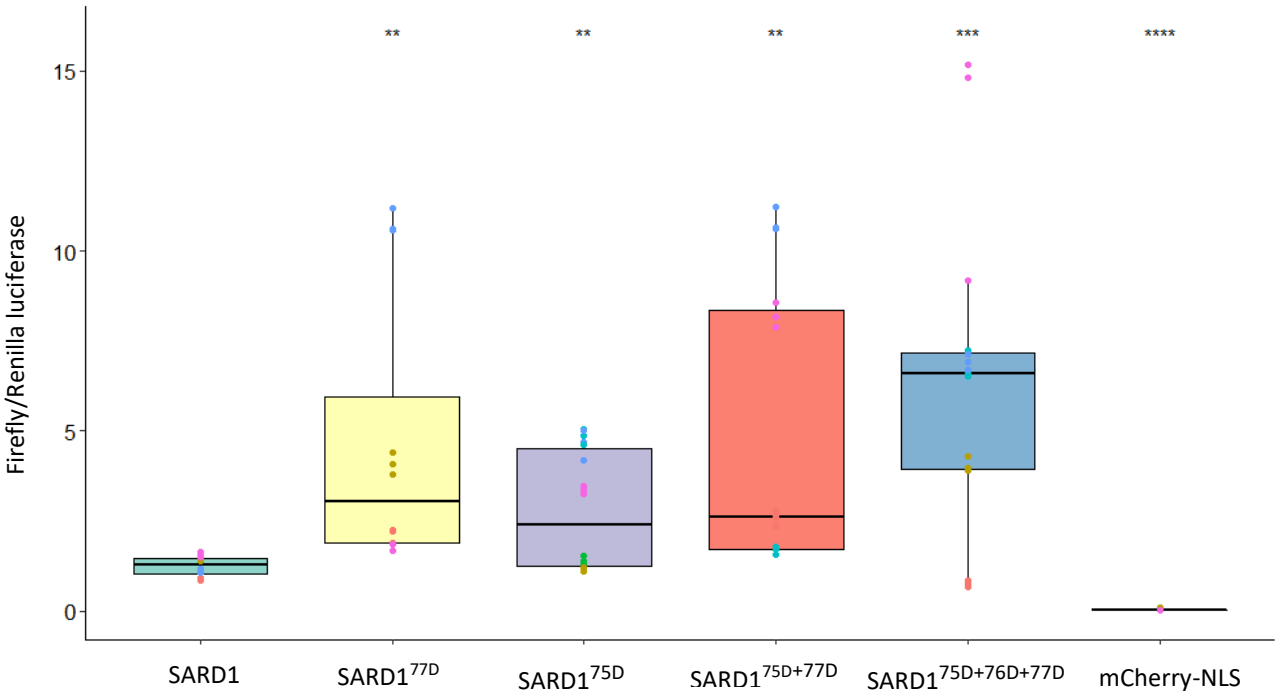

Figure 3.14. Protoplasts transformed with 0.5 µg of SARD1 phospho-mimic plasmids have enhanced Firefly luciferase expression. *Arabidopsis* Col-0:*sard1/cbp60g* protoplasts were isolated and transformed with 0.5 µg of dual-luciferase constructs. Renilla and Firefly luciferase expression were quantified with Promega Dual-Luciferase® Reporter Assay System and a VarioSkan plate reader. Three biological repeats represented (coloured dots), each with at least two technical repeats. T.test P-value ** < 0.01, *** < 0.001. ns = non-significant.

To test if luciferase expression was saturated due to a high plasmid concentration, we tested transforming protoplasts with 0.5 µg of dual luciferase plasmids (Figure 3.14). Similar to previous results with 2 µg of plasmid, SARD1 phospho-mimic variants enhance pEDS5:firefly expression when 0.5 µg of dual-luciferase plasmid is used (Figure 3.14). All SARD1 phospho-mimics lead to enhanced pEDS5 luciferase compared to SARD1 wildtype, including SARD1^{77D} (Figure 3.14). The phospho-dead variants were not tested with 0.5 µg of dual-luciferase plasmid and this is something that should be investigated. The lower dual-luciferase plasmid concentration may reveal a difference in pEDS5:firefly luciferase expression between the SARD1 WT and phospho-dead variants. Differences may have been hidden due to a saturation in firefly luciferase levels with the higher dual-luciferase plasmid concentrations.

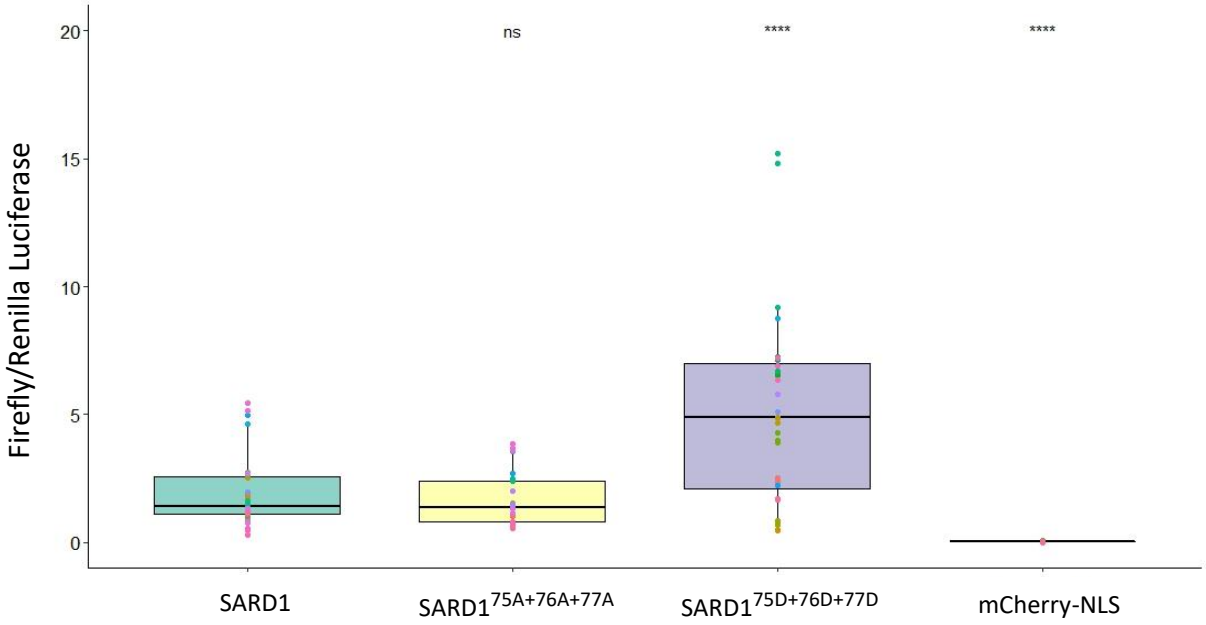

Figure 3.15. Ubi10 overexpression of phospho-mimic SARD1$^{75D+76D+77D}$ increases pEDS5:firefly expression. *Arabidopsis* Col-0:*sard1/cbp60g* protoplasts were isolated and incubated with 2 µg, 1 µg or 0.5 µg of dual-luciferase constructs overnight**.** Renilla and Firefly luciferase expression were quantified with Promega Dual-Luciferase® Reporter Assay System and a VarioSkan plate reader. Coloured dots represent different biological repeats. P-value **** < 0.0001. ns = non-significant.

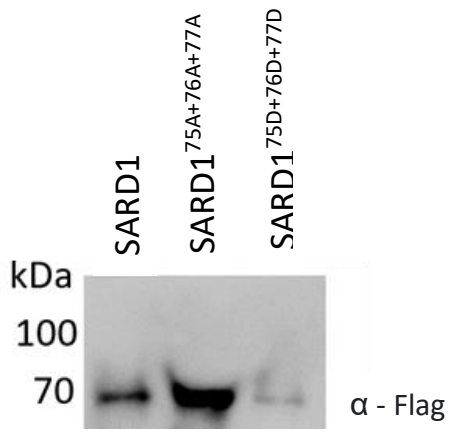

Figure 3.16. Phosphorylation may lead to differences in SARD1 protein stability. Protein expression of SARD1 phospho-variants. *Arabidopsis* Col-0:*sard1/cbp60g* protoplasts were isolated and transformed with 0.5 µg of luciferase constructs and SARD1 protein detected by western blot.

When biological repeats from all protoplast experiments are combined, using 2 µg, 1 µg or 0.5 µg of dual-luciferase plasmids, Ubi10 overexpression of phospho-mimic SARD1$^{7D5+76D+77D}$ increases pEDS5:firefly expression compared to Ubi10 overexpression of SARD1 WT (Figure 3.15). Protoplasts transformed with phospho-dead SARD1$^{75A+76A+77A}$ have the same levels of pEDS5:Firefly luciferase expression as those transformed with SARD1 WT (Figure 3.15). Therefore, this suggests that SARD1 phosphorylation at S75/S76/S77 enhances activation of *EDS5* promoter, but SARD1 phosphorylation at these sites is not necessary, as SARD1 phospho-dead variants are still functional. There may also be differences in stability between the SARD1 phospho-variants (Figure 3.16). SARD1$^{75D+76D+77D}$ had consistently lower protein expression compared to SARD1 WT (Figure 3.16). However, the expression of SARD1$^{75A+76A+77A}$ was variable compared to WT between different biological repeats. Staining with Ponceau did not show any rubisco bands and an anti-actin antibody was unable to detect any bands. Therefore, a protein loading control was unable to be included. There may be activation-induced degradation of SARD1. Therefore the stability of SARD1 protein before/after phosphorylation and immunity activation needs to be further investigated. Additionally, the western blot should be repeated with a negative control without SARD1 to confirm the protein band is SARD1 specific.

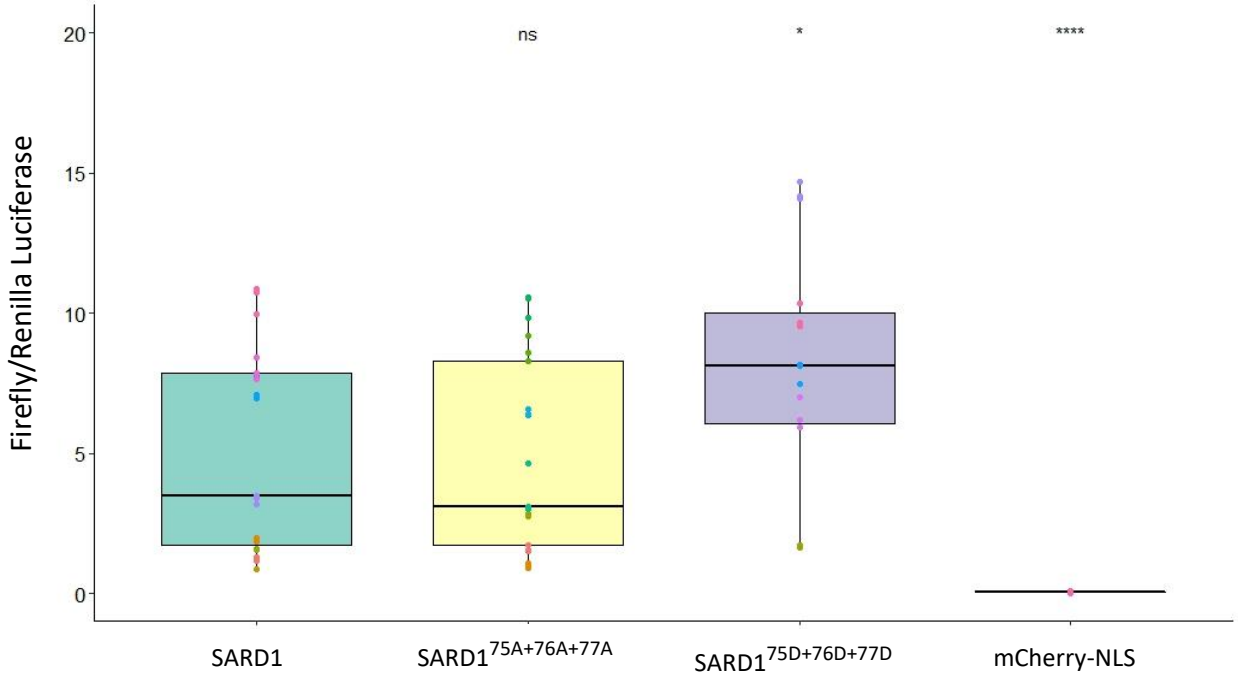

Figure 3.17. **SARD1$^{75D+76D+77D}$ enhances pEDS5:Firefly luciferase expression after flg22 treatment**. *Arabidopsis* Col-0:*sard1/cbp60g* protoplasts were isolated and incubated with 0.5 µg of dual-luciferase constructs overnight and then treated with 100 nM flg22 for two hours. Renilla and Firefly luciferase expression were quantified with Promega Dual-Luciferase® Reporter Assay System and a VarioSkan plate reader. At least three biological repeats represented by different coloured dots, each with at least two technical repeats. T.Test P-value * < 0.05, **** < 0.0001. ns = non-significant.

In the previous experiments, Ubi10 over-expression of SARD1 was used as a proxy for immunity activation. Next, we decided to look at the role of SARD1 phosphorylation in promoting pEDS5:firefly luciferase expression during PTI activation. After overnight transformation, Col-0:*sard1/cbp60g* protoplasts were treated with 2 hours of 100 nM flg22. Protoplasts transformed with SARD1 phospho-mimic SARD1$^{75D+76D+77D}$ show enhanced pEDS5:Firefly luciferase expression after flg22 treatment compared to protoplasts transformed with SARD1 WT (Figure 3.17). SARD1$^{75A+76A+77A}$ phospho-dead variant induces similar pEDS5:Firefly luciferase expression as SARD1_WT (Figure 3.17). Therefore, during PTI signalling, SARD1 phosphorylation enhances expression of EDS5, but phosphorylation is not necessary for SARD1 to activate EDS5 expression and SARD1 phospho-dead variants are still functional. To better understand the role of SARD1 phosphorylation during PTI activation, a SARD1 native promoter should be tested, instead of a constitutive over-expression promoter (Ubi10). This would allow PTI to be studied without the autoimmunity of SARD1 over-expression. Additionally, EDS5 expression needs to be compared before and after flg22 treatment for the different SARD1 variants within the same experiment/figure. This would allow us to make conclusions as to whether SARD1 phosphorylation leads to a strong induction of EDS5 expression upon flg22 treatment or if EDS5 expression is constitutively high with a SARD1 phospho-mimic and there is no change in EDS5 expression upon flg22 treatment. Furthermore, our phospho-proteomic analysis revealed SARD1 is phosphorylated during ETI alone. Therefore, if SARD1 is phosphorylated during PTI needs to be investigated.

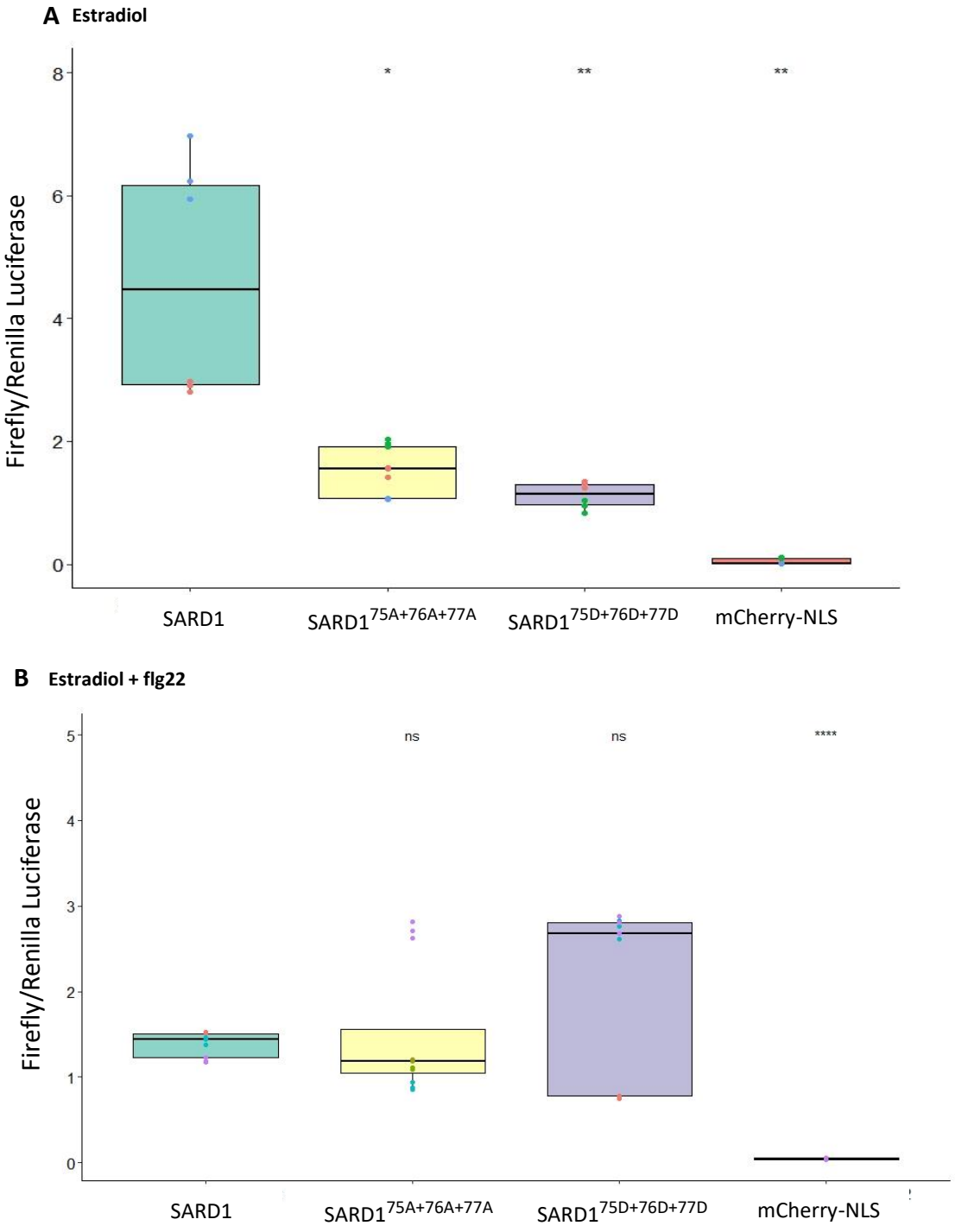

Figure 3.18. SARD1 phosphorylation does not enhance pEDS5:Firefly luciferase expression after PTI + ETI activation. Arabidopsis SETI:*sard1/cbp60g* protoplasts were isolated and incubated with 0.5 µg of dual-luciferase constructs overnight. **A)** Protoplasts treated with 50 µM estradiol for four hours. **B)** Protoplasts treated with 50 µM estradiol and 100 nM flg22 for four hours. Renilla and Firefly luciferase expression were quantified with Promega Dual-Luciferase® Reporter Assay System and a VarioSkan plate reader. Three biological repeats of SARD1 and SARD1 phospho-variants represented by different coloured dots. T.Test P-value * < 0.05, ** < 0.01, **** < 0.0001. ns = non-significant.

To investigate the role of SARD1 phosphorylation after ETI or PTI + ETI activation, SETI: *sard1/cbp60g* protoplasts were treated with 50 µM estradiol for 4 hours, with or without flg22 treatment (Figure 3.18). Protoplasts transformed with SARD1$^{75A+76A+77A}$ or SARD1$^{75D+76D+77D}$ both have reduced pEDS5:Firefly luciferase expression compared to SARD1 WT after estradiol treatment (Figure 13.18A). This could suggest phosphorylation of SARD1 reduces the activity of SARD1 at the *EDS5* promoter. However, that would not correlate with the increase in phosphorylation of SARD1 that we detected after ETI activation with MS1 quantification (Table 3.2). As both SARD1 phospho-mimic and phospho-dead variants lead to a reduction in EDS5 expression, this could suggest there is cyclic phosphorylation of SARD1 during immunity signalling, the specific function of which can't be revealed by this assay. After flg22 and estradiol treatment (PTI + ETI) there is no difference in pEDS5:Firefly luciferase expression between protoplasts transformed with SARD1 WT or SARD1 phospho-variants (Figure 3.18B). However, the timing of estradiol-inducible *AvrRps4* expression and ETI activation may be different in protoplasts compared leaves. Therefore, this needs to be checked, to ensure that ETI has been activated after 4 hours of estradiol treatment in protoplasts. In addition, creating stable Arabidopsis lines expressing pSARD1:SARD1 phospho-variants would allow bacterial growth assays and qPCR of defence genes to be performed. This may reveal a role of SARD1 phosphorylation in activating bacterial growth restriction or transcriptional changes during PTI, ETI or PTI + ETI that wasn't able to be detected with transient expression in protoplasts.

3.3 Discussion

3.3.1 ETI- induced phospho-sites suggest a role of phosphorylation in transcriptional regulation

ETI activation induced phosphorylation changes in proteins with known roles in immunity and in proteins with no previous link to immunity. Some of the TIR-NLR-induced phospho-sites have been previously described during PTI, suggesting an overlap between PTI and ETI signalling. Novel ETI sites were also identified. However, the kinases and phosphatases responsible for RRS1/RPS4 induced phosphorylation changes remain unknown. Changes in protein phosphorylation upon TIR-NLR ETI activation were identified in transcription factors, RNA polymerase/Mediator associated proteins and protein kinases. This may indicate a role of phosphorylation in activating transcriptional changes seen during ETI signalling. However, this may also reflect the types of proteins we selected for quantification by PRM. Other proteins not directly involved in transcriptional regulation may also change in phosphorylation, but as we did not select these for quantification, their phosphorylation changes were not identified. Phosphorylation changes were seen in different nuclear subcellular

fractions, with some protein phosphorylation increasing in one fraction and decreasing in another fraction. The importance of this specificity of phosphorylation changes in each subcellular fraction is not understood and needs to be further investigated. This large study revealed phosphorylation changes of multiple proteins, at multiple different phosphorylation sites, changing in different directions within different nuclear sub-cellular fractions. Therefore, it is challenging to extract meaning from this dataset. However, it does provide an insight into the type of proteins which are phosphorylated during ETI, and which proteins may play a role in ETI signal transduction.

3.3.2 There are fewer ETI-induced changes in phosphorylation compared to those induced during PTI

We identified fewer changes in phosphorylation upon ETI activation, compared to large changes in phosphorylation seen during PTI signalling (Benschop et al., 2007, Nühse et al., 2007, Rayapuram et al., 2014, Mattei et al., 2016, Rayapuram et al., 2021). Our dataset may be missing key changes in nuclear protein phosphorylation due to the targeted nature of selecting targets for PRM quantification. In addition, there might be large changes in phosphorylation in the cytosolic fraction upon TIR-NLR activation, but we did not quantify phosphorylation changes in this protein fraction. TIR-NLRs have NADase activity and produce TIR-catalysed small molecules which induce EDS1/PAD4/ADR1 or EDS1/SAG101/NRG1 heterotrimer formation (Wan et al., 2019, Huang et al., 2022, Jia et al., 2022). ADR1, ADR1-L1 and ADR1-L2 localise to the plasma membrane (PM) and ADR1 also localises to the endoplasmic reticulum membrane (Saile et al., 2021). Auto-active ADR1 remains localised to the PM (Saile et al., 2021). ADR1 localisation at the PM is interesting given its role in activating transcriptional changes. How ADR1 signals to nuclear-localised transcriptional machinery remains unknown. NRG1 is localised to the cytosol and endoplasmic reticulum and NRG1's localisation was not found to change upon pathogen detection (Wu et al., 2019). Additionally, auto-active NRG1 forms puncta at the PM (Jacob et al., 2021). Therefore, small molecules produced by nuclear-localised TIR-NLRs may be exported into the cytosol and diffuse throughout the cell to activate EDS1/PAD4/ADR1 or EDS1/SAG101/NRG1 heterotrimer formation. Therefore, there is early ETI signalling in multiple sub-cellular localisations. Future work should investigate phosphorylation changes in the cytosolic fraction before, during and after heterotrimer formation. Phosphorylation may be required for heterotrimer formation or required to transduce a signal from the cytosol to the nucleus. Therefore, further work would enhance our understanding in this area.

We chose to investigate ETI-induced phosphorylation at 3-hours post estradiol treatment. However, this time point may be too late. The majority of phosphorylation could be very transient and have disappeared by 3 hours after estradiol treatment. However, microsomal proteins upregulated in

phosphorylation downstream of a plasma-membrane localised CC-NLR showed a differential change at 3 hours (Kadota et al., 2019). Proteins downregulated in phosphorylation showed a differential change at 1 hour post dexamethasone induced AvrRpt2 expression (Kadota et al., 2019). Differences in timing in the kinetics of de-phosphorylation and phosphorylation upon CC_NLR activation are not understood. Our quantitative phospho-proteomic study should be repeated comparing PTI, ETI and PTI + ETI. When this study was first designed and carried out, the data on mutual potential between ETI and PTI had not been published (Ngou et al., 2021, Yuan et al., 2021). Both PTI and ETI are required for full defence activation (Ngou et al., 2021, Yuan et al., 2021). Estradiol-inducible AvrRps4 (ETI) leads to prolonged PTI-induced phosphorylation of MPK3 and RBOHD, suggesting phosphorylation has a role in defence potentiation (Ngou et al., 2021). Therefore, the presence of PTI activation may be required to provide the phosphorylation and potentiation of ETI signalling. A previous study in tomato compared PTI, ETI and PTI + ETI and found more ETI specific phosphorylation changes than PTI or PTI + ETI changes (Yu et al., 2021). This is surprising considering the extensive list of known phosphorylation changes seen during PTI in Arabidopsis (Benschop et al., 2007, Nühse et al., 2007, Rayapuram et al., 2014, Mattei et al., 2016, Rayapuram et al., 2021). This may be explained by the experimental design. PTI is known to induce phosphorylation within seconds (Schulze et al., 2010). As plants were harvested 6 hours after *Pst* DC3000 infiltration (Yu et al., 2021), PTI phosphorylation may have already returned to basal levels. The *Pst* DC3000 flagellin deficient strain (fliC) was used to activate ETI alone (Yu et al., 2021). This mutation will abolish flagellin/FLS2 signalling and FLS2-induced phosphorylation changes, however other PTI signalling may remain and therefore cannot be considered ETI alone. DC3000 delivers 28 effectors into its host (Cunnac et al., 2011). These 28 effectors may be contributing to effector-triggered susceptibility (ETS) and inhibition of PTI signalling components, many of which may overlap with ETI signalling. Therefore ETS may be interfering in the ETI alone phosphorylation changes investigated in the Yu et al., 2021 study. Studying ETI in combination with PTI and ETS is more representative of a natural infection. However, to study ETI alone-induced phosphorylation changes, an inducible effector system must be used.

3.3.3 Changes seen in protein phosphorylation after ETI activation may be due to changes in protein abundance

During ETI signalling, 10% of the Arabidopsis transcriptome shows differential gene expression changes (Ngou et al., 2021). Protein levels of PTI components BIK1 and MPK3 increase during ETI signalling. Additionally, changes in transcription and translation during ETI induction are broadly correlated (Meteignier et al., 2017, Yoo et al., 2020), suggesting that many of the changes seen in phosphorylation, could be due to changes in protein levels. Protein levels of the differential phospho-proteins before and after ETI induction need to be measured to determine if protein changes could

account for changes in protein phosphorylation. This could be done in a few ways. 1) If additional peptides from the same phospho-protein do not show a change in phosphorylation or show a change in phosphorylation in the opposite direction, then this would suggest the phosphorylation change is real. 2) TiO_2 flow-through samples of non-phosphorylated peptides could be measured by mass-spectrometry to measure the total protein levels of differential phospho-proteins. 3) Protein levels could be visualised by western blot using transient expression in *Nicotiana benthamiana* or using transgenic Arabidopsis, allowing for immunoprecipitation of the protein before/after immune activation. A study using ribosomal profiling found WRKY45, PEN3, IBM1, WRKY18, AT1G67310, LUH, CIPK23, SARD1 and CPK1 RNA increased in abundance and WRKY1 RNA decreased in abundance on ribosomes after ETI activation (Meteignier et al., 2017). Changes in ribosomal abundance can be used to predict changes in protein level. From those proteins that showed an increase in ribosome abundance, all show an increase in phosphorylation except IBM1, CIPK1 and CIPK23 which show a decrease (Table 3.1), suggesting the increase in phosphorylation of these proteins could be due to increases in protein translation. IBM1 increased in ribosome abundance (Meteignier et al., 2017) but shows a decrease in phosphorylation, suggesting the phosphorylation is not due to changes in protein abundance (Table 3.1). WRKY1 has a decrease in ribosome abundance and a decrease in phosphorylation, suggesting a decrease in protein translation could be responsible for the decrease in phosphorylation seen by PRM (Table 3.1). Protein kinase RIPK shows an increase in phosphorylation in one peptide at S451 and has a decrease in phosphorylation at another site S426. This suggests the increase/decreases in phosphorylation are not due to changes in protein abundance. AT4G28080, TPR1, AT3G17850, RNA polymerase II transcription elongation factor, CAMTA2, CAMTA5, TPL, AT1G67310, NRPB1, TPR2, WRKY1, LUH all had several additional phospho-peptides which did not show a change in phosphorylation, suggesting the phospho-peptides which do show a change in phosphorylation are not due to changes in protein abundance.

3.3.4 Role of SARD1 phosphorylation in transcriptional regulation during PTI/ETI needs further investigation

During SARD1 overexpression-induced autoimmunity, SARD1 phosphorylation enhances activation of the *EDS5* promoter. However, SARD1 phosphorylation is not necessary to induce *EDS5* expression, as SARD1 phospho-dead variants are still functional. During PTI activation, the SARD1 phospho-mimic enhances EDS5 expression, compared to SARD1 wildtype and SARD1 phospho-dead variant. However, the results from ETI and PTI + ETI activation are difficult to interpret, as there was no difference in EDS5 expression during ETI and PTI activation. 4 hours estradiol treatment in protoplasts may have not been long enough to induce *AvrRps4* expression. A previous study using rice protoplasts showed

estradiol-inducible gene expression increases by 2x from 12 hours to 48 hours after estradiol treatment (Schlucking et al., 2013). Another study looked at estradiol-inducible expression in Arabidopsis protoplasts after 15 hours (Chen et al., 2017). Therefore, the kinetics and timing of estradiol-inducible expression may be different in protoplasts compared to seedlings or leaves and needs to be further investigated.

The phosphorylation site identified in SARD1 at S77 is within a calcium-dependent protein kinase motif L-X-R/K-X-X-S/T (Kawamoto et al., 2015). It has been previously suggested that SARD1 may be directly regulated by calcium-dependent protein kinase 5 (CPK5), although so far there is no direct evidence of this (Guerra et al., 2020). CPK5 was shown to function upstream of SARD1 and SA signalling and acts as an important signalling component in the establishment of SAR (Guerra et al., 2020). The expression of SAR marker genes *AGD2-LIKE DEFENSE RESPONSE PROTEIN* 1 (*ALD1*) and *FLAVIN-DEPENDENT MONOOXYGENASE 1* (*FMO1)* were lower in *cpk5* mutant plants (Guerra et al., 2020). CBP60g, which acts redundantly with SARD1 (Zhang et al., 2010b), was found to be phosphorylated upon bacterial and fungal PAMP treatment (Sun et al, 2022). This phosphorylation is weakened in *bik1, pbl1* and *cngc2* mutants, suggesting phosphorylation of CBP60g is calcium dependent (Sun et al, 2022). A phospho-mimic variant of CBP60g showed enhanced binding activity to the *ICS1* promoter and the corresponding phospho-dead allele had reduced expression of *ICS1*, suggesting the phosphorylation status of CBP60g is important for SA signalling (Sun et al, 2022). CPK5 was found to directly phosphorylate CBP60g upon PAMP recognition (Sun et al, 2022). This further supports the suggestion that SARD1 may also be phosphorylated by CPK5. However, SARD1-TurboID discussed in Chapter 4 did not detect biotinylation of CPK5, suggesting CPK5 does not interact with or phosphorylate SARD1 during PTI or PTI + ETI and therefore may not be responsible for the ETI-induced SARD1 phosphorylation detected by MS1. CPK5 may phosphorylate SARD1 during SAR, as SAR was not investigated during the SARD1-TurboID or nuclear ETI phospho-proteomics studies.

To investigate ETI-induced phosphorylation, we selected SARD1 for functional analysis. However, additional proteins from this dataset should be followed up. WRKY1, bZIP59, CAMTA2 and MED12 also have known roles in defence activation and the role of ETI-induced phosphorylation in these proteins should be further explored. Extensive NRBP1 phosphorylation has also previously been reported, including phosphorylation induced during PTI (Li et al., 2014). However, NRPB1 PTI-induced phosphorylation is at a different residue to that found in our study during ETI. Functional analysis of NRPB1 phosphorylation would be challenging, as a NRPB1 mutant is lethal (Onodera et al., 2008). Therefore, to study the role of phosphorylation changes in RNA polymerase proteins, mediator subunit MED12 could be investigated.

This quantitative phospho-proteomic study gives an indication of the nuclear phospho-site changes induce upon ETI activation downstream of a TIR-NLR localised to the nucleus. Changes detected by PRM provides phospho-protein targets for which the role of ETI phosphorylation can be further explored in the future. The SARD1 phospho-sites identified by MS1 may be important for SARD1 transcriptional regulation of *EDS5* expression. However, the protoplast assays showed too much biological variation for firm conclusions to be made. To gather more consistent results, stable Arabidopsis lines with SARD1 phospho-variants have been made to study the role of phosphorylation in bacterial growth restriction and defence gene activation. These lines will soon be ready for testing. This study provides a useful dataset to which further research can build upon to widen our understanding of ETI signalling.

Chapter 4

Identifying novel interactors of immune proteins using proximity labelling

4 Identifying novel interactors of immune proteins using proximity labelling

4. 1 Introduction

4.1.1 Proximity labelling using TurboID

Protein complex formation is important for signalling during effector-triggered immunity (Lapin et al., 2019, Ma et al., 2020a, Sun et al., 2021, Wu et al., 2021). However, it is not known how these upstream protein complexes, e.g. EDS1-PAD4-ADR1 heterotrimers, activate downstream defence responses e.g. transcriptional changes. Therefore, protein interaction studies might shed new light on these important signalling networks. To study large-scale protein-protein interactions *in vivo* methods such as immunoprecipitation mass-spectrometry (IP-MS) or in-vitro methods such as yeast-2-hybrid screens can be used. In a yeast-2 hybrid screen, *Saccharomyces cerevisiae* strains are transformed with vectors carrying a bait protein with a DNA-binding domain and a prey protein with a transcription activation domain (Matiolli & Melotto, 2018). If the two proteins interact, this activates the transcription of a gene encoding an enzyme, allowing the yeast to grow on selective media (Matiolli & Melotto, 2018). A previous yeast-2 hybrid screen identified 126 *Ustilago maydis* effectors that interact with themselves, or other *U. maydis* effectors (Alcantara et al., 2019). However, yeast-2 hybrids can result in false-positive interactors or miss true interactors due to differences in protein folding and post-translational modifications in yeast compared to Arabidopsis. IP-MS involves immunoprecipitation of a protein of interest and analysis of protein interactors by mass-spectrometry. IP-MS has previously been used to identify interactors of immunity proteins (Sun et al., 2021). IP-MS confirmed that EDS1 forms exclusive heterodimers with PAD4-ADR1 and with SAG101-NRG1 (Sun et al., 2021). NRG1 was only found to interact with SAG101 and EDS1 after activation of TIR-NLR signalling (Sun et al., 2021). IP-MS also identified poly(A)-binding protein (PABP)-interacting proteins during PTI-induced protein translation (Wang et al., 2022). However, IP-MS does not capture weak or transient interactions and intact protein complexes must be isolated. Additionally, homogenization during IP-MS protein extraction can introduce false positive interactions, as proteins not in close contact in a cell are mixed together.

The biotin ligase BirA from *E.coli*, catalyses the covalent binding of biotin to a lysine in the biotin carboxyl carrier protein (BCCP) subunit of acetyl-CoA carboxylase, a key enzyme in metabolism (Chapman-Smith et al., 2001). A mutant of BirA has been created called BioID to identify protein interactors (Roux et al., 2012). BioID is fused to a protein of interest and catalyses biotin to form reactive biotinoyl-5'-AMP (bioAMP) (Roux et al., 2012). bioAMPs diffuse and covalently bind to lysine

residues of nearby proteins (Roux et al., 2012). Biotinylated proteins can then be affinity purified with streptavidin beads and analysed by mass-spectrometry to identify protein interactors *in vivo* (Roux et al., 2012). However, as BioID has low activity at room temperature, BioID requires labelling with biotin for 18 hours to produce sufficient biotinylated material, so the researcher is unable to study dynamic processes that occur within minutes or hours (Roux et al., 2012). Therefore, a new mutant version of BirA was created called TurboID (Branon et al., 2018). TurboID reduces the biotinylation window to 10 minutes at room temperature (Branon et al., 2018). Biotinylation efficiency of TurboID increases with biotin concentration and labelling time (Shioya et al., 2022, Melkonian et al., 2022). TurboID has been previously characterised in both Arabidopsis and *N. benthamiana* (Mair et al., 2019, Zhang et al., 2019, Lin et al., 2022). The first TurboID study in plants identified novel interactors of the TIR-NLR receptor N, including a putative E3 ubiquitin ligase UBR7 (Zhang et al., 2019). UBR7 was shown to negatively regulate N-mediated immunity, by reduction of N protein stability in a proteasome-dependent manner (Zhang et al., 2019). TurboID has also been utilised to understand MPK4 interactors after flg22 treatment and successfully identified the known interactor MKK1, in addition to 92 other interacting proteins, expanding the knowledge of PTI signalling (Lin et al., 2022). TurboID can also identify sub-cellular and cell type specific proteins e.g. in stomatal nuclei (Mair et al., 2019).

4.1.2 EDS1 interacts with key ETI signalling proteins

EDS1 is a key component of ETI signalling, forming two distinct heterotrimers with SAG101-NRG1 or PAD4-ADR1 to induce downstream signalling upon effector recognition (Lapin et al., 2019, Sun et al., 2021, Feehan et al., 2023). EDS1 interactor studies have focused on targeted proteomic methods e.g. Yeast-2-hybrid, bimolecular luminescence complementation assays or co-immunoprecipitations (co-IPs) (Feys et al., 2001, Chen et al., 2021). A yeast-2-hybrid assay can provide information on what specific protein domains are important for protein interactors e.g. the first 15 amino acids of PAD4 are required for an EDS1 interaction (Feys et al., 2001).

NPR1, a salicylic acid (SA) receptor, is reported to interact with EDS1 to recruit EDS1 to the PR1 promoter upon effector recognition and SA induction (Chen et al., 2021). This protein interaction was shown with co-IPs using transgenic Arabidopsis lines (Chen et al., 2021). The authors suggested a feedback loop mechanism between EDS1 and NPR1, whereby EDS1 stabilizes NPR1 protein and NPR1 directly upregulates *EDS1* transcription (Chen et al., 2021). Furthermore, they reported that EDS1 interacts with cyclin-dependent kinase 8 (CDK8), a component of the kinase module in the Mediator complex (Chen et al., 2021). Therefore, NPR1-EDS1 may recruit the Mediator complex to the PR1 promoter to induce transcriptional changes (Chen et al., 2021). However, several reports have shown

that EDS1 forms heterotrimers with PAD4-ADR1 and SAG101-NRG1 upon TIR-NLR NADase activity to activate downstream signalling (Lapin et al., 2019, Sun et al., 2021, Huang et al., 2022, Jia et al., 2022). Therefore, these additional results suggest it may be unlikely that EDS1 has activities, e.g. as a transcriptional activator, independent of SAG101 and PAD4.

Additional literature has reported an EDS1 interaction with negative regulators of ETI e.g. the protein kinase ENHANCED DISEASE RESISTANCE1 (EDR1), MYELOCYTOMATOSIS2 (MYC2) involved in Jasmonate (JA) signalling and EDS1-INTERACTING J PROTEIN1 (EIJ1) (Cui et al., 2018, Neubauer et al., 2020, Liu et al., 2021). EIJ1 negatively regulates immunity by interacting with EDS1, inhibiting trafficking of EDS1 to the nucleus (Liu et al., 2021). EDR1 associates with EDS1 to negatively regulate the interaction between PAD4 and EDS1, suppressing activation of defence responses (Neubauer et al., 2020). This inhibition of EDS1-PAD4 complex formation is not caused by phosphorylation of PAD4/EDS1 by EDR1, as a kinase-inactive EDR1 is still able to inhibit EDS1-PAD4 interaction (Neubauer et al., 2020). EDS1-PAD4 interact with MYC2 to prevent JA antagonism of SA signalling (Cui et al., 2018). This EDS1 inhibition of MYC2 protects a set of defence genes, including MPK3 and MPK2, from repression by MYC2 (Bhandari et al., 2019).

The SA receptors NPR1-LIKE PROTEIN 3/4 (NPR3/NPR4) are negative regulators of immunity (Ding et al., 2018). NPR3 and NPR4 form protein complexes with EDS1 and negatively regulate EDS1 protein stability by promoting EDS1 polyubiquitination (Zhang et al., 2006, Chang et al., 2019). The proteasome-mediated degradation of EDS1 is prevented by AVRPPHB SUSCEPTIBLE 3 (PBS3), another positive regulator of immunity (Warren et al., 1999, Chang et al., 2019). PBS3 is an enzyme involved in SA biosynthesis (Li et al., 2023). PBS3 is reported to form a complex with EDS1 in the nucleus and cytoplasm, disrupting the interaction of NPR3 and NPR4 with EDS1 (Chang et al., 2019). These EDS1-PBS3 complexes are specific to EDS1, and separate from other EDS1 heterodimers, as no interaction was found between PBS3 and PAD4 or SAG101 (Chang et al., 2019). As previously mentioned, there are many reports that EDS1 forms heterotrimers with SAG101/NRG1 or ADR1/PAD4 during immunity signalling (Lapin et al., 2019, Sun et al., 2021, Feehan et al., 2023). As the EDS1-PBS3 interactions were independent of SAG101 and PAD4, this casts some doubt in the validity of these results.

Although, some EDS1 interactors during ETI signalling are known, it is not known how EDS1 heterotrimers signal to activate downstream responses. A large-scale EDS1 protein interactor study has not been previously reported. Therefore, our study will reveal novel EDS1 interactors and give insight into downstream ETI signalling pathways. Additionally, our study will independently reveal if

the previously reported EDS1 interactions are true. As *At*EDS1 must signal with Arabidopsis alleles of NRG1 and SAG101 to activate HR, we decided it was important to carry out this EDS1 protein interaction study in transgenic Arabidopsis lines.

4.1.3 There is a knowledge gap in SARD1 protein interactors

SARD1 has a major role in transcriptional reprogramming during immune signalling (Sun et al., 2015, Ding et al., 2020). Therefore, previous studies have focused on the transcriptional activation function of SARD1, identifying chromatin target sites of SARD1 (Sun et al., 2015). Very limited research has been done to investigate SARD1 protein interactions during defence signalling. SARD1 and CBP60g have a clear positive role in immunity, through direct transcriptional regulation of many PTI and ETI defence genes. However, the protein complexes involved and how EDS1-PAD4-ADR1 heterotrimer formation activates SARD1 transcriptional regulation remain unknown. Therefore, any protein interactors discovered using SARD1-TurboID will be novel and will advance our understanding of the role of SARD1 in early immune signalling.

4.1.4 TPL/ TPRs are transcriptional co-repressors

Topless (TPL) and topless-related proteins (TPRs) are a Gro/Tup1 family of transcriptional corepressors (Liu & Karmarkar, 2008). TPL and TOPLESS RELATED 1 (TPR1) share 92% protein similarity and act redundantly during TIR-NLR immunity (Zhu et al., 2010). Co-repressors do not have the ability to bind DNA and are recruited to gene promoters by DNA-binding transcription factors. Topless was first reported in Arabidopsis in 2006, with a role in embryo development, with *tpl-1* mutants switching the fate of a shoot pole into a second root pole (Long et al., 2006). There are 4 close homologs to Topless: Topless-related 1 (TPR1), Topless-related 2 (TPR2), Topless-related 3 (TPR3) and Topless-related 4 (TPR4) (Long et al., 2006). Arabidopsis TPL/TPRs form two clades: TPL/TPR1/TPR4 and TPR2/TPR3 (Plant et al., 2021). TPL/TPR proteins are involved in diverse pathways during plant development in multiple plant organs e.g. seed germination, meristem maintenance, leaf development and stress responses (Plant et al., 2021).

TPL/TPRs contain three highly conserved N-terminal domains: Lissencephaly homology (LisH) motif, C-terminal to LisH (CTLH) motif and CT11-RanBPM (CRA) domain (Szemenyei et al., 2008, Martin-Arevalillo et al., 2017). The C-terminus contains a WD40 repeat region which form two β-propeller structures (Martin-Arevalillo et al., 2017). The N-terminal domains have been collectively termed the TOPLESS Domain (TPD) (Ke et al., 2015). A repression domain is located within the CRA domain of TPL

(Leydon et al., 2020). Furthermore, this repression domain of TPL directly interacts with Mediator and these interactions are required for the repression of genes involved in auxin-regulated development (Leydon et al., 2020). TPL acts to stabilise the Mediator complex to allow rapid transcription once released (Leydon et al., 2020). Additionally, histone deacetylation is involved in epigenetic repression and HISTONE DEACETYLASE 19 (HDA19) was found to associate with TPR1 *in vivo* (Zhu et al., 2010). TPR1 may form a complex with HDA19 and other transcriptional repressors during immunity (Zhu et al., 2010).

To understand the role of TPR1 during immunity-induced transcriptional reprogramming, ChIP sequencing (ChIP-Seq) was carried out in an autoimmune line with elevated defence responses (Griebel et al., 2020). ~ 1500 peaks in the genome were enriched for a TPR1 signal, including ICS1, PBS3, CBP60g and bound to genes enriched for Gene Ontology (GO)-terms associated with abiotic and biotic stress (Griebel et al., 2020). TPR1 was also bound to the promoters of transcription factors WRKY18 and WRKY60 (Griebel et al., 2020). 10% of TPR1 bound sites required EDS1, e.g. ICS1 and WRKY60, suggesting TIR-NLR signalling may be required to induce a small proportion of TPR1 promoter occupancy (Griebel et al., 2021). 27% of EDS1-dependent TPR1 bound genes had increased expression in autoimmune lines compared to an *eds1* mutant, whereas 4% were downregulated (Griebel et al., 2021). Additionally, many of the EDS1-dependent TPR1 bound genes had increased expression upon treatment with flg22 or *Pst* DC3000 AvrRps4 (Griebel et al., 2021). Therefore, there is increased binding of TPR1 to genes upregulated during immune activation. As TPL/TPRs are transcriptional repressors, TPR1 may have a role in reducing the induction of defence genes to prevent an over-response. Additionally, during immunity TPR1 is recruited to the promoters of and represses the activity of negative regulators of immunity DND1 and DND2 (Zhu et al., 2010). To test the role of TPL/TPRs in transcriptional regulation during PTI + ETI signalling, RNA-sequencing (RNA-seq) was carried out with *tpr1/tpr4/tpl* plants (Griebel et al., 2021). However, no statistically significant differences in gene expression were found between *tpr1/tpr4/tpl* and Col-0 plants (Griebel et al., 2021). In another study, an increase in expression of *ICS1*, *SARD1* and *PAD4* is seen in the *tpr1/tpl/tpr4* triple mutant upon Pf0-1:AvrRps4 treatment compared to WT, suggesting TPLs may act to suppress SA signalling during immune activation (Ding et al., 2020). The role of TPR1 as a transcriptional repressor during immune signalling remains unclear. Further research is needed to understand the role of TPL/TPRs in regulating transcriptional changes during PTI, ETI and PTI + ETI.

4.1.4.1 TPL/TPRs are recruited for transcriptional repression via an EAR-motif-containing protein

A transcriptional repression motif, known as Ethylene-responsive element binding factor-associated Amphiphilic Repression (EAR), has two consensus residue patterns: LxLxL or DLNxxP (Kagale & Rozwadowski, 2011). EAR motifs are present in 10-25% of transcriptional regulators (Kagale et al., 2010). 40% of EAR-domain containing proteins are negative regulators (Kagale et al., 2010). TPL/TPRs are recruited for transcriptional repression through EAR motifs in both transcription factors (Li et al., 2022a, Szemenyei et al., 2008), histone deacetylases (Wang et al., 2013) and through an EAR motif in the NINJA adaptor protein involved in JA signalling (Pauwels et al., 2010). NINJA acts as a negative regulator of JA signalling (Pauwels et al., 2010). The JASMONATE ZIM-DOMAIN (JAZ) repressor proteins recruit TPL/TPRs via an EAR domain in NINJA (Pauwels et al., 2010). All three leucine residues of the NINJA LxLxL motif are required for transcriptional repression (Ke et al., 2015). The LxLxL EAR-motif in NINJA is conserved within AUX/IAA proteins involved in Auxin signalling and in NINJA-related AFP proteins involved in ABA signalling (Pauwels et al., 2010). Interactions between TPL/TPRs and AFP proteins were also confirmed with Yeast-2-hybrid assays (Pauwels et al., 2010). Therefore, TPL/TPRs may have a general transcriptional repressive role during hormone signalling that is regulated by EAR-motif interactions.

4.1.4.2 EAR-motif containing effector proteins target TPL/TPRs to outcompete EAR-motif interactors and inhibit immune signalling

Multiple effectors from different pathogen species target TPL proteins via an EAR motif to enhance host susceptibility (Darino et al., 2019, Harvey et al., 2020, Navarrete et al., 2022). *U. maydis* effector proteins bind the same EAR-motif-binding hydrophobic groove in Maize REL-like 2 (RELK2) where host *Zm*IAA proteins bind RELK2 (Bindics et al., 2022). Therefore, these effector proteins compete with *Zm*IAA proteins for TPL binding, activating auxin signalling and increasing host susceptibility (Bindics et al., 2022). *U. maydis* effector protein Naked1 also interacts with TPL/TPRs via an EAR motif (Navarrete et al., 2022). Naked1-*Zm*TPL1 interaction prevents *ZmTPL1* interaction with *Zm*IAA5, leading to the repression of PTI-related genes e.g. MAPK and RBOHD and the upregulation of auxin-responsive genes (Navarrete et al., 2022). Naked1 interaction with TPL/TPRs also prevents a PTI-induced ROS burst (Navarrete et al., 2022). Therefore, TPL/TPR repression of auxin-signalling genes is required for the activation of a ROS burst upon PAMP perception and this is inhibited by Naked1 (Navarrete et al., 2022). The *Ustilago maydis* effector Jsi1 interacts via its EAR motif with the second WD40 domain (Darino et al., 2019). TPL binds the transcription factor ERF1 (Darino et al., 2019). The

interaction between ERF1 and TPL is weakened due to the presence of Jsi1, activating jasmonic acid and ethylene signalling in *Zea mays* (Darino et al., 2019).

The *Hyaloperonospora arabidopsidis* (*Hpa*) effector RxL21 interacts via an EAR motif with the CTLH TPL/TPR1 domain, to increase pathogen virulence (Harvey et al., 2020). The EAR motif is not sufficient for TPL interaction, as other *H.arabidopsidis* effectors with an EAR motif did not interact with TPL in a yeast-2 hybrid assay (Harvey et al., 2020). Increased host susceptibility, induced by RxL21 interaction with TPL, is not due to a large-scale inhibition of PTI responses, as flg22 was able to activate similar differentially expressed genes in the presence or absence of RxL21 EAR motif (Harvey et al., 2020). However, the few genes repressed by RxL21 also show an enrichment for TPR1 binding e.g. ICS1, PBS3 and WRKY46 (Harvey et al., 2020). Therefore, RxL21 maintains the repression of these genes by TPR1 and can inhibit specific components of immunity, resulting in increased host susceptibility (Harvey et al., 2020).

4.1.4.3 Additional roles of TPLs in plant defence responses

A gain-of-function mutation in the SUPPRESSOR OF NPR1-1, CONSTITUTIVE 1 (SNC1) TIR-NLR leads to an autoimmune dwarfed phenotype and increased resistance to *P. parasitica* Noco2 (now known as *Hpa*) (Zhang et al., 2003, Goker et al., 2009). TPR1 was found in a suppressor screen of the *snc1* mutant to act redundantly with TPL in *snc1* autoimmunity (Zhu et al., 2010). TPR1 and TPL are required for resistance to *Pst* DC3000 AvrRps4 and *Hpa* Cala2, mediated by the TIR-NLRs RRS1/RPS4 and RPP2 respectively, but are not required for resistance to *Pst* DC3000 expressing AvrRpt2, mediated by the CC-NLR RPS2 (Zhu et al., 2010). This suggests TPL/TPRs may act downstream of TIR-NLRs but not CC-NLRs during ETI (Zhu et al., 2010). Overexpression of TPR1 (TPR1-OE) leads to a dwarfed autoimmune phenotype with elevated *PR1* expression and high SA levels, which requires EDS1 and PAD4 (Zhu et al., 2010). The requirement of EDS1 supports the conclusions that TPR1 is only required in TIR-NLR mediated immunity and not CC-NLR immunity (Zhu et al., 2010). Furthermore, a suppressor screen of TPR1-OE found functional SNC1 is required for defence activation due to TPR1 overexpression (Zhu et al., 2010). TPR1 and SNC1 TIR-domain were also found to interact *in vivo* (Zhu et al., 2010). The activity of TPR1 is regulated by SIZ1-mediated SUMOylation (Niu et al., 2019). SIZ1 represses TPR1 activity to prevent autoimmunity and allow normal growth conditions in the absence of pathogens (Niu et al., 2019). SUMOylation was also found to enhance TPR1 interaction with TIR-NLR SNC1, possibly trapping SNC1 in a complex with TPR1 in a resting state (Niu et al., 2019). Therefore, if TPR1 acts downstream of SNC1 and other TIR-NLR activation, there could be a feedback loop in which high levels of TPR1

activates SNC1 and SNC1 activates another TPR1-independent immune signalling pathway required for the constitutive defence response seen in TPR1-OE.

TPL/TPRs have been shown to have a role in PTI, as *tpr1/tpr4/tpl* plants have a reduced flg22-induced ROS burst (Navarrete et al., 2022). As mentioned previously, despite TPR1 enrichment at 1000s of promoters, there is limited differences in transcriptional changes during ETI between WT and *tpl*/*tpr1*/tpr4 plants (Ding et al., 2020). Additionally, Topless proteins are not required for bacterial growth restriction, as there is little/no difference in bacterial growth between Col-0 and *tpr1/tpr4/tpl* plants (Griebel et al., 2021). However, *tpr1/tpr4/tpl* plants have increased electrolyte leakage compared to Col-0 plant at 24 hours after Pf0_AvrRps4 or Pf0-1_Empty Vector treatment (Griebel et al., 2021). Therefore, TPL/TPRs act to limit electrolyte leakage induced during both PTI and PTI + ETI responses (Griebel et al., 2021). *tpr1/tpr4/tpl* plants lost 30% of fresh weight 3 days after *Pst* infection, compared to 20% in Col-0, suggesting TPL/TPRs may have a role in limiting growth penalties during immunity activation (Griebel et al., 2021). Therefore the specific role of TPL proteins during PTI and ETI signalling remains elusive. The genetic redundancy between different TPR proteins and the unknown roles of interactions between the individual members makes interpretation of these results difficult.

4.1.4.4 Interactors of TPL/TPR1 during immune signalling

TPL has been the main focus of previous studies and a large number of protein interactors of TPL are known during different plant processes e.g. reproduction and hormone signalling (Plant et al., 2021). A large-scale yeast two-hybrid study was carried out which identified the majority of TPL/TPR interactors as transcription factors (TFs), including WRKY transcription factors WRKY61 and WRKY32 as TPR1 interactors (Causier et al., 2012). This is expected, as corepressors have no DNA binding domain and so form complexes with DNA-binding transcription factors to repress gene expression. The TFs came from 17 protein families, 40% of which are annotated as transcriptional repressors (Causier et al., 2012). This highlights the major role TPL/TPRs play in transcriptional repression in plants (Causier et al., 2012). Proteins involved in Jasmonic acid and ethylene hormone signalling were also found as interactors, including JAZ5, JAZ6, ERF3 and ERF4, in addition to MYB44 involved in ABA responses (Causier et al., 2012). No interactions were found with key PTI or ETI components e.g. BAK1, BIK1, NRG1, SAG101, EDS1 (Causier et al., 2012). An interaction between SNC1 or HDA19 and TPR1 was also not found in this yeast-two hybrid assay, which have been shown previously to interact with TPR1 (Zhu et al., 2010, Causier et al., 2012). Therefore, this highlights that yeast 2-hybrids may miss weak or transient interactors that occur in-planta.

Fewer studies have investigated TPR1 protein interactors involved in immune responses. TPR1 interacts with another member of the Topless family TOPLESS RELATED 2 (TPR2), which acts as a negative regulator of immunity, and both compete to interact with the TIR-NLR SNC1 (Zhu et al., 2010, Garner et al., 2021). A SUMO E3 ligase, SIZ1, was found to interact with TPR1 to represses TPR1 co-repression activity during immune activation (Niu et al., 2019). This interaction was investigated using split luciferase after transient expression in *N. benthamiana* leaves and co-IPs from TPR1-Myc Arabidopsis lines (Niu et al., 2019). There have not been any large-scale in-planta TPR1 interactor studies performed in the literature so far. Knowledge about TPR1 protein complexes is important for insights into how TPR1 functions to control changes in gene expression upon immune activation. TPR1 acts redundantly with other Topless family members TPL and TPR4 (Zhu et al., 2010). As homozygous Arabidopsis mutants of *tpr1/tpr4/tpl* were not available at the time of the experiments, we decided to perform TPR1-TurboID transiently in *N. benthamiana*.

4.1.5 WRKY18 and WRKY40 act redundantly to regulate transcriptional changes during immunity

WRKY transcription factors are defined by their conserved WRKYGQK sequence (Rushton et al., 1995). Arabidopsis has 71 WRKY proteins which form 5 phylogenetic clades (Eulgem et al., 2000, Wang et al., 2011b). WRKY18 forms a subgroup with WRKY40 and WRKY60 (Eulgem et al., 2000). WRKYs bind conserved W-box sequence elements, many of which are found in defence responsive genes e.g. PR1 (Rushton & Somssich, 1998). WRKY18 interacts with itself and with both WRKY40 and WRKY60 via a shared leucine zipper motif (Xu et al., 2006b). Interactions between WRKY18 and WRKY40 or WRKY60 enhanced their W-box binding activity (Xu et al., 2006b).

WRKY18 expression is induced after SA treatment (Yu et al., 2001). In the presence of SA, WRKY18 is recruited to the NPR1 promoter by NPR1 to positively regulate its own gene expression (Chen et al., 2019). WRKY18 binds W-box motifs in the *NPR1* promoter (Yu et al., 2001). Cyclin-dependent kinase 8 (CDK8), a component of the kinase module in the Mediator complex interacts with WRKY18 and facilitates RNA Polymerase II binding to the *NPR1* promoter (Chen et al., 2019, Chen et al., 2021). Therefore, CDK8 creates a molecular bridge between WRKY18 and RNA Pol II for transcriptional activation during SA signalling (Chen et al., 2019).

4.1.5.1 WRKY18/40 act as transcriptional repressors of flg22-induced genes

WRKY transcription factors are involved in transcriptional reprogramming during immunity. WRKY18 binds to 1403 sites in the Arabidopsis genome, and binding to 380 genes was found to be flg22-inducible (Birkenbihl et al., 2017). Many genes involved in PTI were found to be WRKY18 target genes e.g. *FLS2*, *BIK1*, *RBOHD*, as well as *ICS1* involved in SA biosynthesis and *EDS1* involved in SA signalling (Birkenbihl et al., 2017). 87% of WRKY18 target genes are also targeted by WRKY40, suggesting WRKY18 and WRKY40 are functionally redundant (Birkenbihl et al., 2017). Additionally, 426 differentially expressed genes were identified upon flg22 between WT and *wrky18/wrky40* double mutant seedlings, but only 6 and 108 DEGs were identified in the *wrky18* and *wrky40* single mutants respectively, further suggesting they act redundantly during PTI (Birkenbihl et al., 2017). WRKY18 and WRKY40 may act as negative regulators of immunity, as 61% of the DEGs in w*rky18/wrky40* were upregulated after flg22 treatment (Birkenbihl et al., 2017). Furthermore, genes with flg22-dependent WRKY binding were mainly upregulated in wild type plants e.g. *ICS1* (Birkenbihl et al., 2017). Therefore, WRKY18 and WRK40 may act to weaken the effect of positive regulators such as SARD1 (Birkenbihl et al., 2017). In support of this, WRKY18's transcriptional activator activity is abolished upon SA treatment, suggesting it may switch to a repressor upon defence activation (Chen et al., 2010).

WRKY18 and WRKY40 are reported to act as positive regulators of immunity in response to *Pst* DC3000 AvrRps4 (Schon et al., 2013). However, the direct role of WRKY18 during PTI or AvrRps4-triggered ETI signalling remains elusive. Furthermore, WRKY18/WRKY40 act as positive or negative regulators in response to different pathogens and during ETI triggered by different effectors (Xu et al., 2006b, Schon et al., 2013). Additionally, WRKY18 and WRKY40 act redundantly during PTI but can act antagonistically in autoimmune plants (Xu et al., 2006b, Birkenbihl et al., 2017). The role of WRKY18 and WRKY40 during ETI-triggered transcriptional changes has not been previously discussed and is further explored in this study.

4.2 Results

4.2.1 Investigating EDS1 protein interactors with proximity labelling

To identify novel EDS1 interactors we created EDS1-TurboID transgenic Arabidopsis lines. pEDS1-*At*EDS1-TurboID-V5 was transformed into the SETI:*eds1*-2 background (Table 4.1). The *eds1-2* allele was identified in fast neutron bombarded seeds and produces a truncated protein (Falk et al., 1999). Estradiol-inducible AvrRps4 (SETI) seedlings show growth inhibition and yellowing leaves when grown

on 50 µM estradiol supplemented ½ MS media (Ngou et al., 2020). The SETI:*eds1-2* mutant abolishes estradiol-induced *ICS1* expression (Ngou et al., 2020). SETI:*eds1-2* also abolishes the SETI growth phenotype (Figure 4.1). Therefore, to test if EDS1-TurboID-V5 complemented the SETI:*eds1-2* mutant, the EDS1-TurboID lines were sown on ½ MS media with 25 µM estradiol (Figure 4.1). EDS1-TurboID line #T1-4 T2-6 has yellowing leaves on estradiol plates, suggesting EDS1-TurboID-V5 is able to signal and activate ETI (Figure 4.1). However, there is not full complementation of the SETI phenotype as the EDS1-TurboID line #T1-4 T2-6 leaves are bigger than SETI leaves. This may be due to differences in EDS1 activity and/or localisation due to the addition of the TurboID tag. Line #T1-4 T2-6 also has induced *ICS1* expression after Pf0-1_AvrRps4 infection (Figure 4.2), suggesting ETI gene induction has been restored. Therefore, line #T1-4 T2-6 was chosen for EDS1-TurboID experiments. As EDS1 is localised to both the nucleus and cytoplasm (Garcia et al., 2010), we used mCherry-TurboID and NLS-GFP-TurboID transgenic Arabidopsis lines as controls for both cellular localisations. The two TurboID control transgenic plants were generated by other members of the lab group (Table 4.1).

Figure 4.1. EDS1-TurboID-V5 complements the *eds1-2* mutant in the SETI background. EDS1-TurboID-V5 line T1-4 T2-6 mimics the SETI phenotype. Seeds were grown on 25 µM estradiol ½ MS plates for 14 days.

Table 4.1. Transgenic Arabidopsis lines used for proximity labelling experiments

Promoter	Gene	Tag	Background	Selection Marker	Made by
*At*EDS1	*At*EDS1	TurboID-V5	Col-0: SETI: *eds1-2*	Basta	Sophie
*At*SARD1	*At*SARD1	TurboID-V5	Col-0: *sard1*	FAST Red	Sophie
35S	NLS-GFP	TurboID-V5	Col-0	Basta	Jianhua Huang
35S	mCherry	TurboID-V5	Col-0	Basta	Camille-Madeline Szymansky

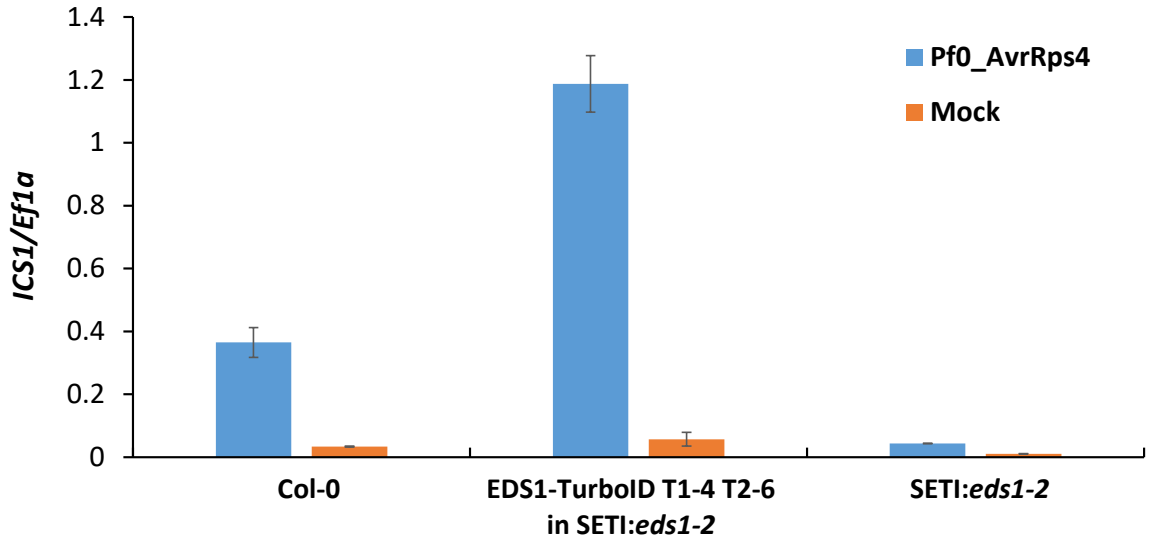

Figure 4.2. EDS1-TurboID induces expression of *ICS1* upon AvrRps4 recognition. RNA was extracted for RT-qPCR from 14-day old seedlings flooded with Pf0-1_AvrRps4 and harvested after 4 hours. Relative *ICS1* expression levels were normalized to *Ef1a*.

To compare differences in protein biotinylation between EDS1, mCherry and NLS-GFP-TurboID, it is important that they have similar levels of biotinylation activity and protein expression levels. NLS-GFP-TurboID-V5 and EDS1-TurboID-V5 have increased levels of biotinylated proteins after 4 hours of biotin treatment (Figure 4.3). NLS-GFP-TurboID-V5 has higher levels of protein expression than EDS1-TurboID-V5 and neither expression is changed upon biotin treatment (Figure 4.4A). EDS1-TurboID-V5 has higher levels of protein expression compared to mCherry-TurboID-V5, (Figure 4.4B). This needs to be considered when interpreting the biotinylation levels between EDS1, NLS-GFP and mCherry.

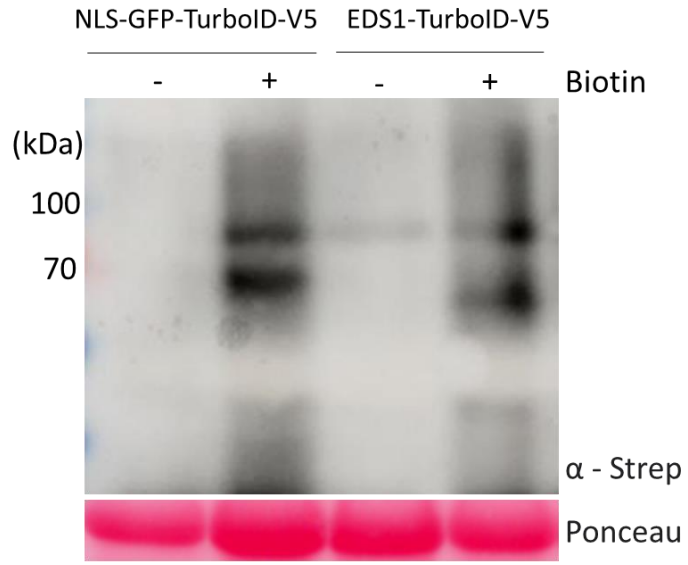

Figure 4.3. Increased levels of biotinylated proteins after 4 hours of biotin treatment. 5-week-old Arabidopsis leaves were treated with 50 µM biotin for 4 hours.

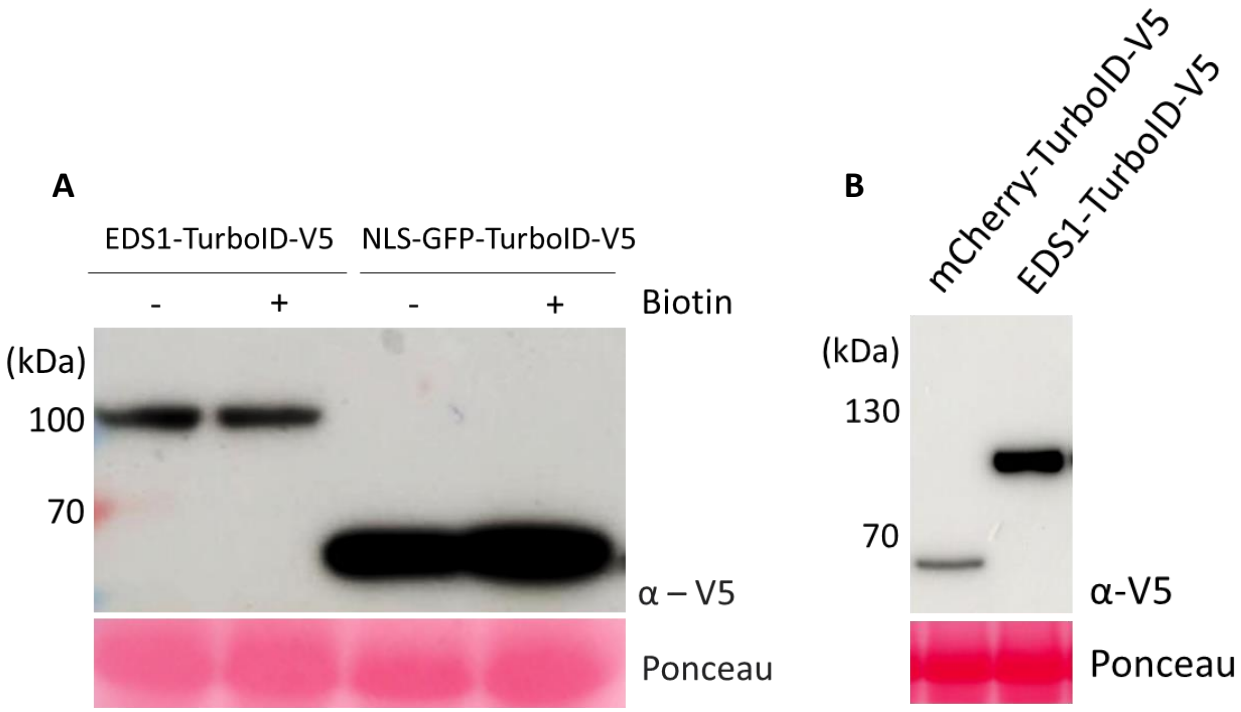

Figure 4.4. EDS1-TurboID-V5, NLS-GFP-TurboID-V5 and mCherry-TurboID-V5 plants have similar protein expression levels. A) 5-week-old Arabidopsis leaves were treated with 50 µM biotin for 4 hours. Samples were then taken for protein extraction. B) Protein extraction from 5-week-old Arabidopsis leaves of transgenic Arabidopsis lines.

To identify interactors of EDS1 during immune signalling, we treated SETI:EDS1-TurboID-V5 plants with mock, Pf0-1_Empty vector (EV) (PTI), 50 µM estradiol (ETI) or Pf0-1_AvrRps4 (PTI + ETI) (Figure 4.5). These were co-infiltrated with 50 µM biotin to label interactors during the early signalling events until 4 hours post infiltration. 50 µM of biotin has previously been used in other Arabidopsis TurboID experiments (Mair et al., 2019). After 4 hours of biotin labelling, proteins were extracted and desalted to remove excess biotin (Figure 4.5). Biotinylated proteins were then immunoprecipitated and digested into peptides for MS analysis (Figure 4.5). Proteins were considered EDS1 interactors if they were unique to EDS1-TurboID or showed a 2-fold increase in biotinylation compared to both NLS-GFP-TurboID and mCherry-TurboID and had a statistically significant difference P-value < 0.05. Proteins also had to be present in at least two biological repeats of EDS1-TurboID. Proteins were compared between EDS1 and NLS-GFP and mCherry during the different immunity treatments. Some proteins were found in multiple biological repeats but only once in each immunity treatment. Therefore, for these proteins we grouped the immunity treatments and considered these proteins as EDS1 interactors if they were unique to EDS1 (grouped interactors) (Supplementary Table 1).

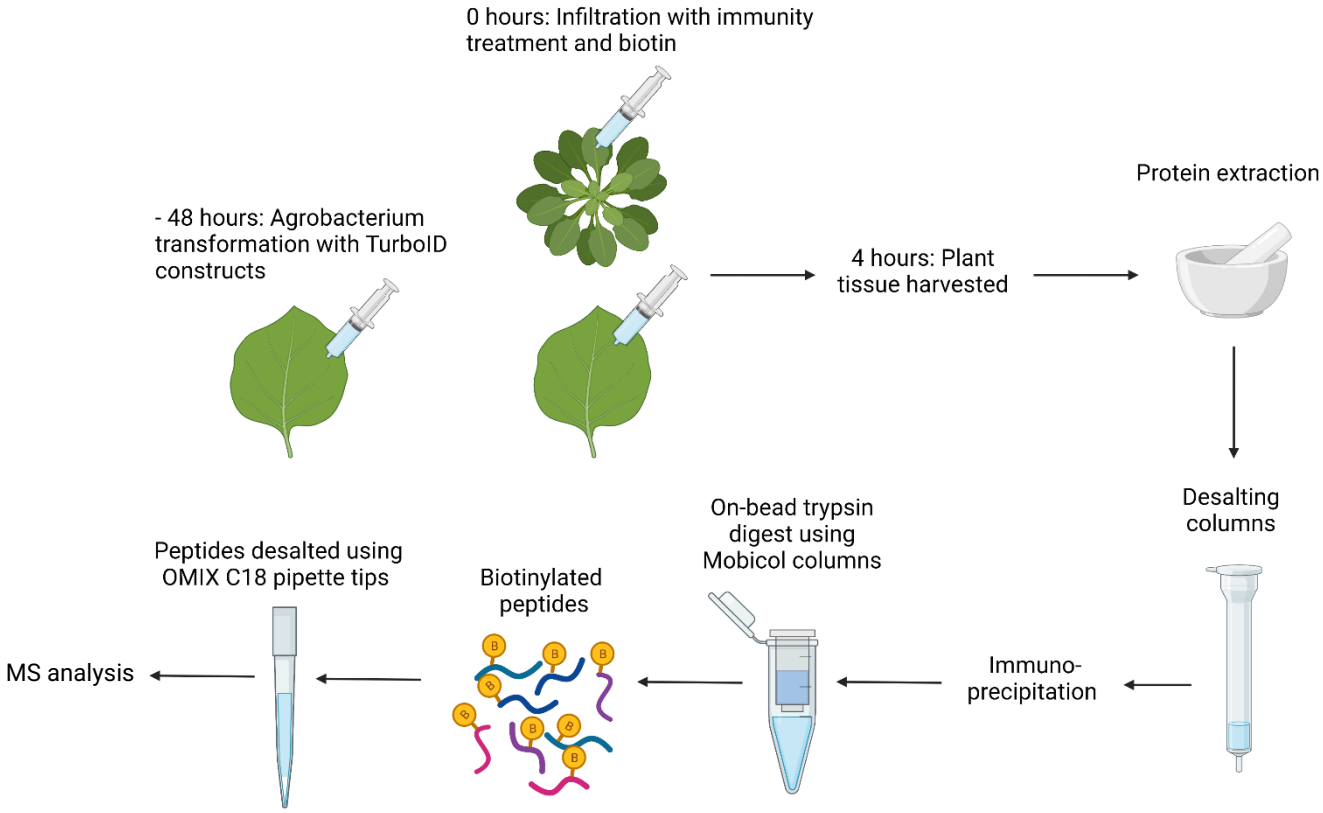

Figure 4.5. Schematic representation of proximity labelling experimental design. 4-week-old *N. benthamiana* plants were infiltrated with *Agrobacterium* carrying TPR1-TurboID or NLS-GFP-TurboID constructs 48 hours prior to 4 hours of Pf0-1 and biotin treatment. 5-week-old transgenic Arabidopsis plants were infiltrated with mock, estradiol or Pf0-1 in addition to biotin. Leaves were harvested after 4 hours. Proteins were extracted, desalted and biotinylated proteins immunopurified. Proteins were digested into peptides and peptides desalted. Samples were then analysed by MS.

SAG101 and PAD4 had the highest biotinylation of all EDS1 interactors, suggesting their interaction is very stable. SAG101 and PAD4 were found to be EDS1 interactors in mock, PTI, ETI and PTI + ETI samples (Figures 4.7-4.10), but no enrichment was found between mock and the different activation states. As SAG101 and PAD4 are both known interactors of EDS1 (Feys et al., 2001, Feys et al., 2005), they act as positive controls in this experiment.

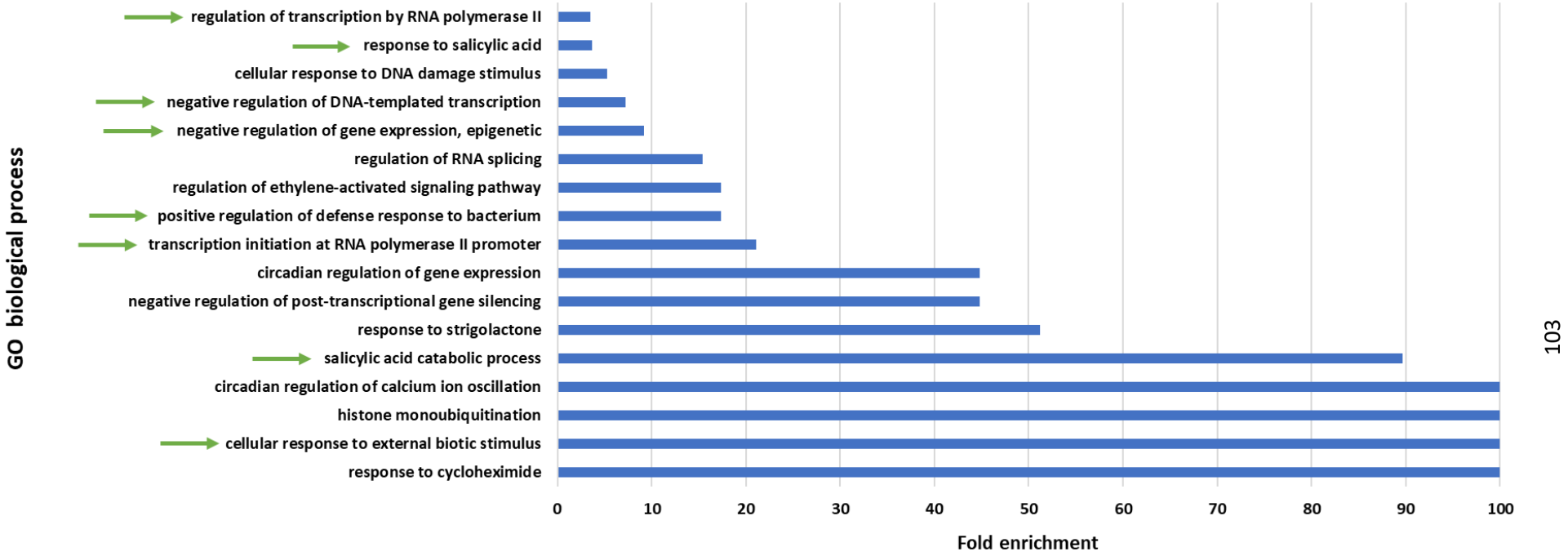

Figure 4.6. Go-term enrichment of EDS1 interacting proteins. Protein interactors of EDS1-TurboID were compared to all Arabidopsis proteins. Green arrows indicate GO-terms relating to plant immune responses. P-value < 0.05.

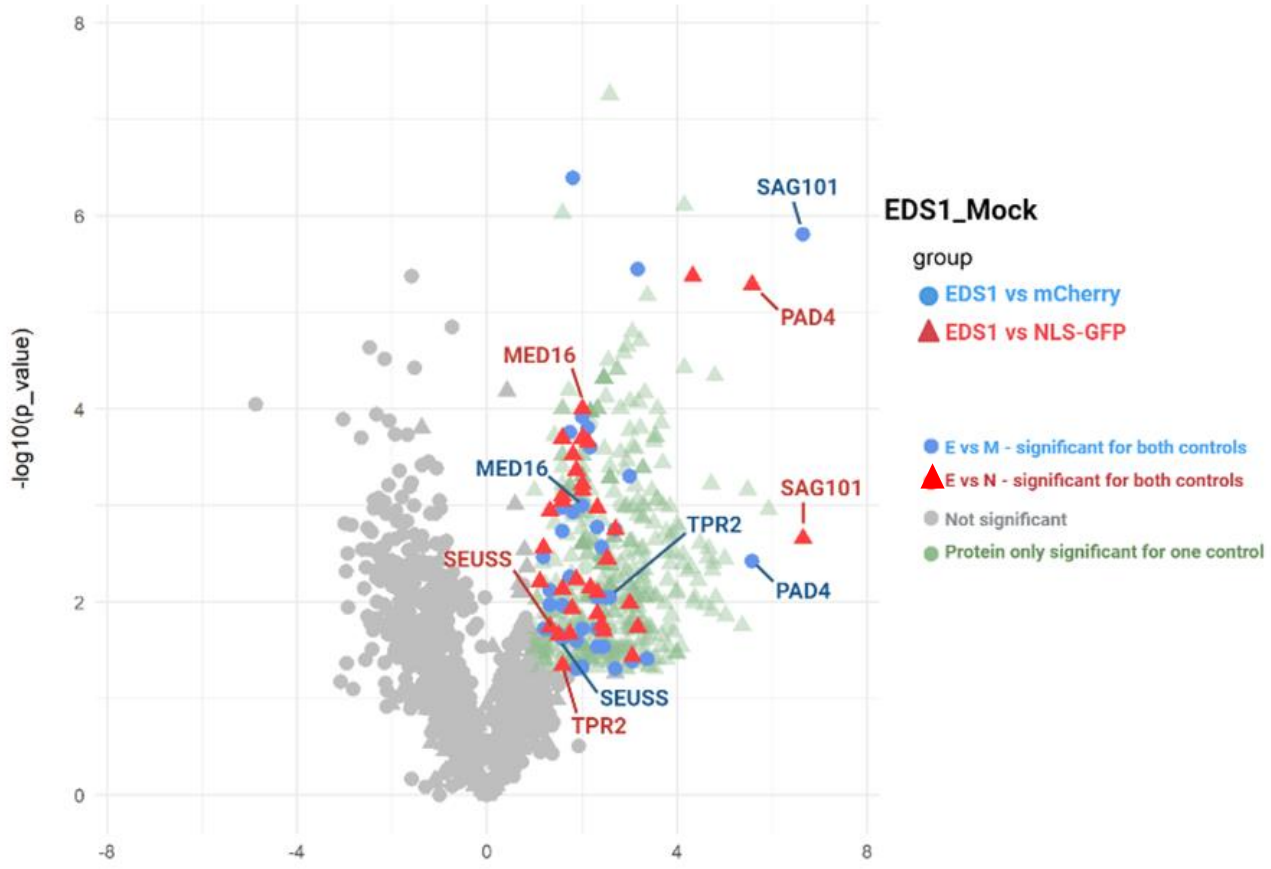

Figure 4.7. EDS1 interactors during mock treatment. Proteins were considered EDS1 interactors if they showed a 2-fold increase in biotinylation compared to both NLS-GFP-TurboID and mCherry-TurboID and had a statistically significant difference P-value < 0.05. Biotinylated proteins not significantly different are in gray. Proteins significantly different but only compared to one control are in **green.** Fold change and P-values significant for EDS1 interactors vs NLS-GFP are represented by ▲ and values for EDS1 interactors compared to mCherry are represented by ● .

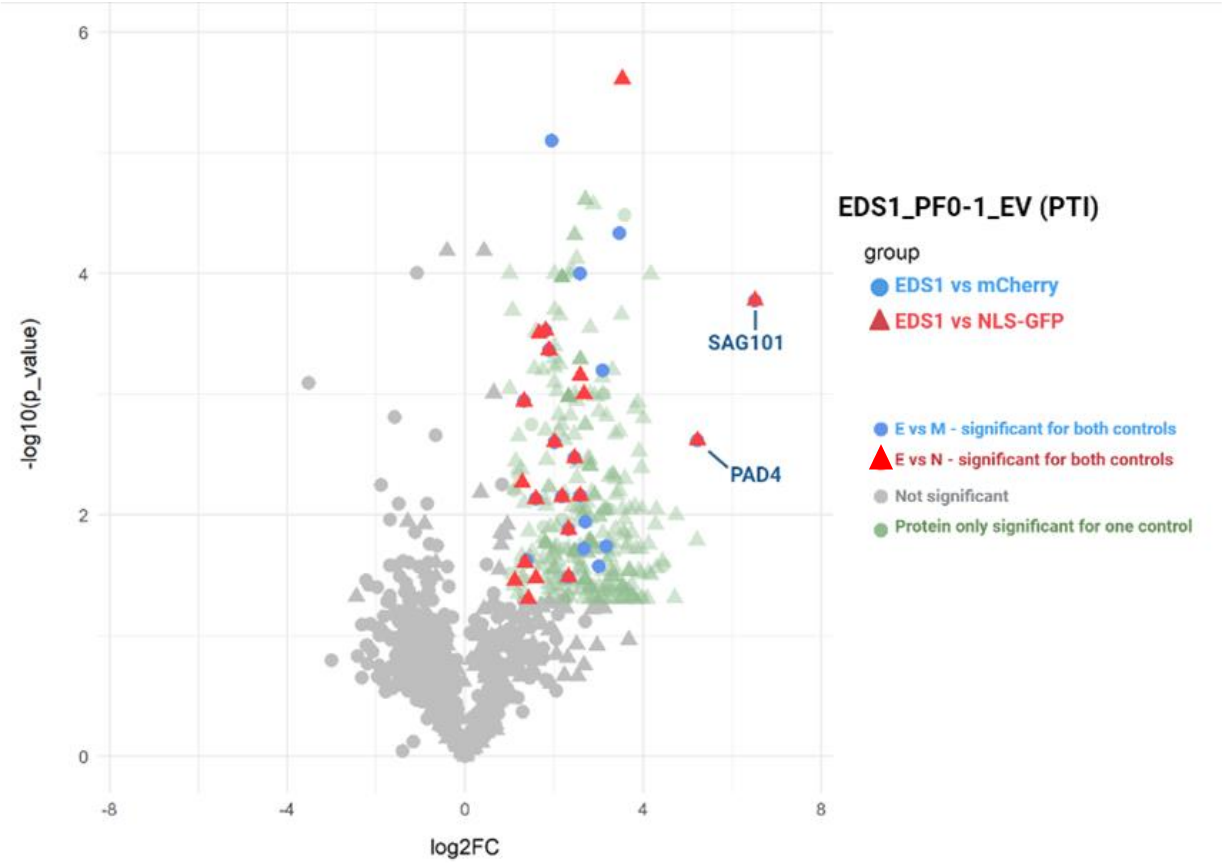

Figure 4.8. EDS1 interactors during PTI. Proteins were considered EDS1 interactors if they showed a 2-fold increase in biotinylation compared to both NLS-GFP-TurboID and mCherry-TurboID and had a statistically significant difference P-value < 0.05. Biotinylated proteins not significantly different are in gray. Proteins significantly different but only compared to one control are in **green.** Fold change and P-values significant for EDS1 interactors vs NLS-GFP are represented by ▲ and values for EDS1 interactors compared to mCherry are represented by ● .

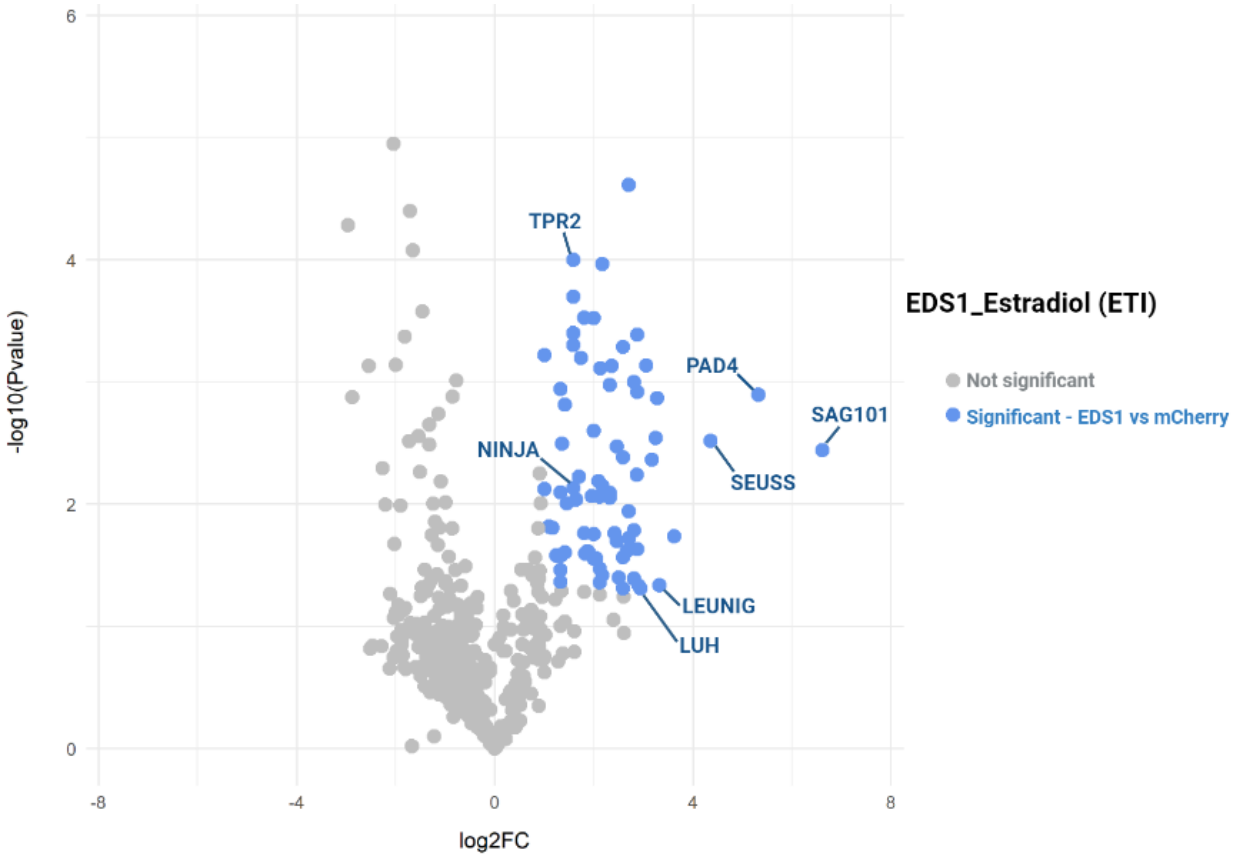

Figure 4.9. EDS1 interactors during ETI. Proteins were considered EDS1 interactors if they showed a 2-fold increase in biotinylation compared to NLS-GFP-TurboID and had a statistically significant difference P-value < 0.05. Biotinylated proteins not significantly different are in gray. Significant EDS1 interactors are represented in blue.

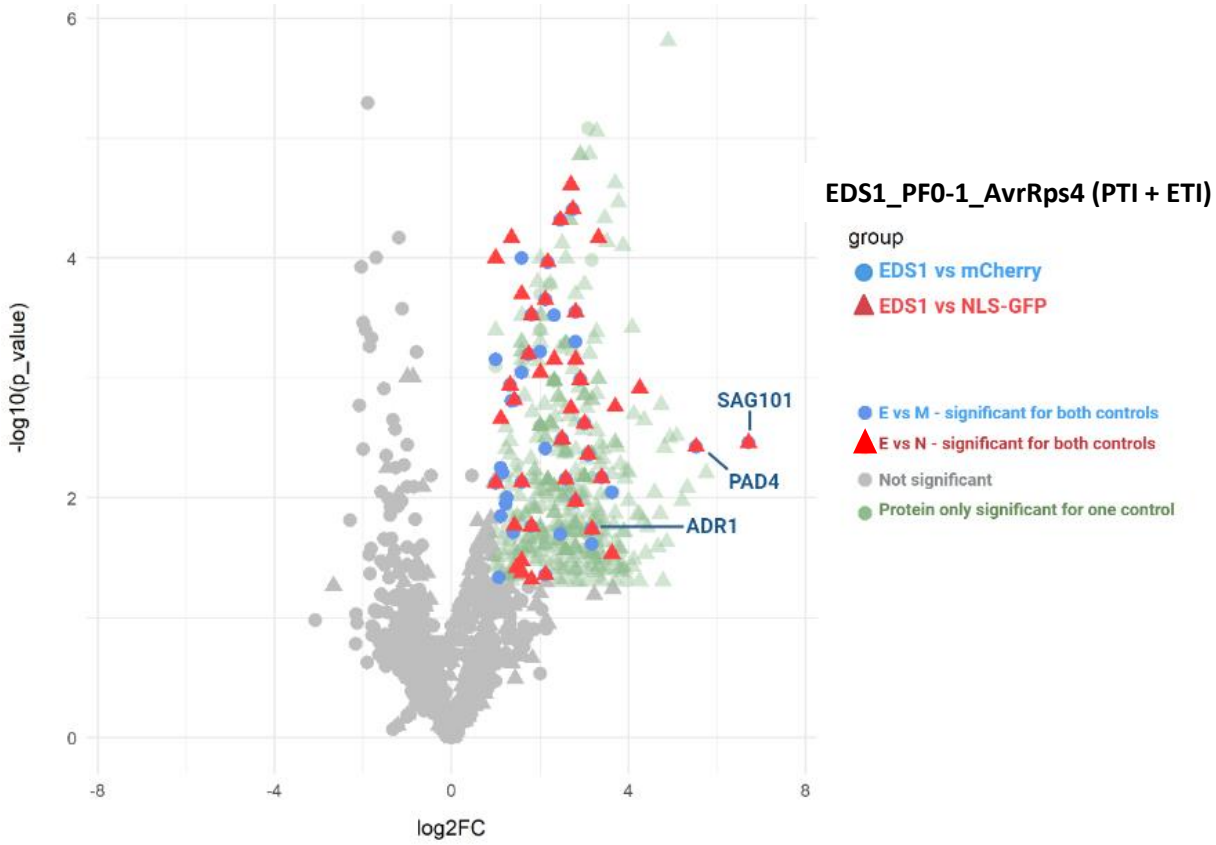

Figure 4.10. EDS1 interactors during PTI + ETI. Proteins were considered EDS1 interactors if they showed a 2-fold increase in biotinylation compared to both NLS-GFP-TurboID and mCherry-TurboID and had a statistically significant difference P-value < 0.05. Biotinylated proteins not significantly different are in gray. Proteins significantly different but only compared to one control are in **green.** Fold change and P-values significant for EDS1 interactors vs NLS-GFP are represented by ▲ and values for EDS1 interactors compared to mCherry are represented by ● .

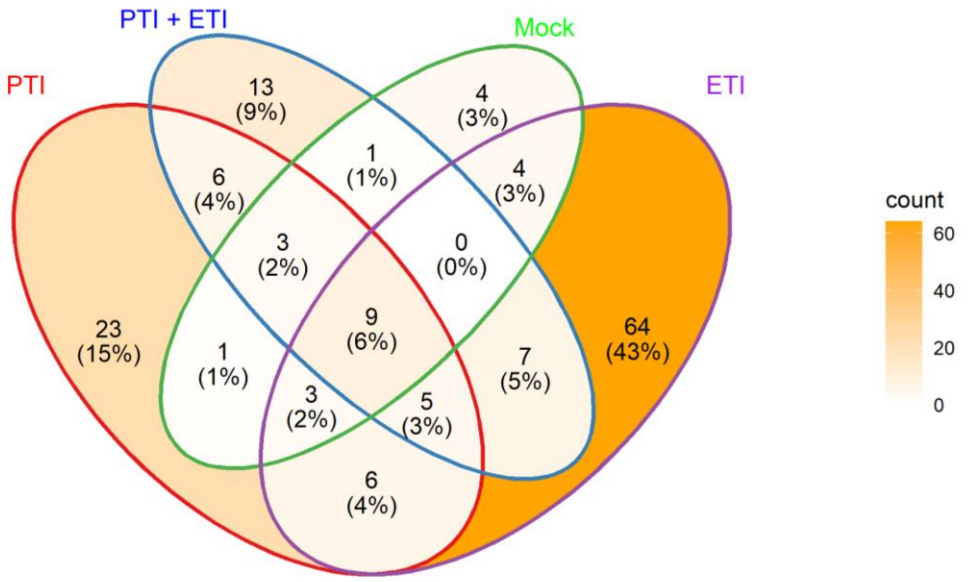

Figure 4.11. Many EDS1 interactors are unique to ETI signalling. Proteins were considered EDS1 interactors for each treatment if they were unique to EDS1-TurboID or showed a 2-fold increase in biotinylation compared to both NLS-GFP-TurboID and mCherry-TurboID and had a statistically significant difference P-value < 0.05. Protein interactors for each immunity treatment were compared to create a Venn diagram. Percentages represent total protein population of EDS1 interactors.

NRG1.1 and NRG1.2 are also reported interactors of SAG101-EDS1 upon effector recognition (Sun et al., 2021, Dongus et al., 2022, Feehan et al., 2023). However, NRG1.1 and NRG1.2 were not present in the EDS1-TurboID dataset and so were not identified as interactors. This reveals a limitation to the TurboID study, as we were not able to identify a known ETI-induced EDS1 interactor. However, this may be due to the low abundance of NRG1 proteins and therefore the low abundance of EDS1-NRG1 interactions. As mass-spectrometry (MS) analysis selects higher abundant peptides for measurement, the NRG1 biotinylated peptides may have been present in the sample but not detected by MS. Alternatively, NRG1 interacting with EDS1 may be further away than the 10-20 nm biotin cloud produced by the TurboID domain of EDS1. However, as the C-terminal EDS1 EP domain is important for NRG1 interaction (Dongus et al., 2022), we would expect NRG1 to close enough to be biotinylated by the C-terminally fused TurboID.

TurboID covalently labels proteins in proximity with biotin. Therefore, biotinylated proximal proteins give an indication as to which proteins may be interacting with EDS1. A total of 154 proteins were classed as EDS1 potential interacting proteins (Supplementary Table 2). EDS1 interactors were enriched for GO terms described as response to bacteria, response to SA and regulation of

transcription (Figure 4.6). This suggests the EDS1 interactors identified are proteins involved in immune response signalling. Most of the protein interactors identified were unique EDS1 interactors and were not biotinylated by NLS-GFP-TurboID or mCherry-TurboID (Supplementary Table 2). EDS1 biotinylated proteins were compared to NLS-GFP and mCherry during different immunity scenarios. 43 proteins during mock, 24 proteins during PTI, 98 proteins during ETI and 55 proteins during PTI + ETI activation were found to be EDS1 interactors (Figures 4.7-4.10, Supplementary Table 2). 43% of EDS1 interactors identified were unique to ETI treatment, providing an insight into the possible differences in signalling mechanisms between PTI, ETI and PTI + ETI (Figure 4.11). Despite a higher number of EDS1 interactors identified during PTI or ETI compared to mock, only 1 protein showed higher biotinylation during PTI, 3 during ETI and 5 during PTI + ETI compared to mock (Supplementary Table 1). Therefore, we were only able to identify a small number of proteins which show immunity-induced interactions with EDS1. WRKY30 and ADR1-like 1 showed an enrichment in EDS1-biotinylation upon PTI + ETI compared to mock (Supplementary Table 1). This supports previous literature that EDS1 interacts with ADR1 upon PTI + ETI activation (Lapin et al., 2019). PTI + ETI-induced biotinylation of ADR1-L1 in our study acts as a positive control, confirming that ETI has been activated in our samples and that EDS1-TurboID functions to biotinylate immune-related protein interactors. The role of WRKY30 in bacterial immunity is unknown but positively regulates resistance to Cucumber mosaic virus in Arabidopsis (Zou et al., 2019).

4.2.1.1 EDS1 interacts with transcriptional regulators

SEUSS is a transcriptional negative regulator of the floral homeotic gene AGAMOUS and functions together with LEUNIG, a transcriptional corepressor (Conner & Liu, 2000, Franks et al., 2002). LEUNIG represses transcription through direct interaction with components of the Mediator complex CDK8 and MED14 (Gonzalez et al., 2007). A LEUNIG mutant *lug*-3 results in upregulation of resistance genes RPP4, RPP5 and SNC1 (Gonzalez et al., 2007). LEUNIG HOMOLOG (LUH) positively regulates the transcription of Jasmonic acid (JA)-responsive genes (You et al., 2019). SEUSS, LEUNIG and LUH are EDS1 interactors during ETI activation (Figure 4.9, Supplementary Table 2). SEUSS also interacts with EDS1 in mock samples (Figure 4.7, Supplementary Table 2). This may reveal a novel role for these transcriptional regulators in immune signalling.

Novel Interactor of JAZ (NINJA) is as a negative regulator of JA signalling, through transcriptional repression of JA responsive genes (Pauwels et al., 2010). NINJA has not previously been directly linked to ETI signalling. NINJA is biotinylated by EDS1 during ETI activation suggesting EDS1 interacts with NINJA (Figure 4.9, Supplementary Table 2). However, there was no enhancement of NINJA

biotinylation upon ETI activation compared to mock. Therefore, the role of the EDS1-NINJA interaction during defence signalling is unclear.

C-terminal domain phosphatase-like 2 (CPL2) dephosphorylates the C-terminal domain (CTD) of RNA Polymerase II (Koiwa et al., 2004). Although no link to immunity has previously been reported. CPL2 interacts with EDS1 when sample treatments were grouped, as it was only present in one replicate per sample treatment, but in three samples across different immunity treatments. EDS1 also interacts with the mediator subunit MED16 in mock samples (Figure 4.7). MED16 positively regulates SA responses (Wang et al., 2016). Therefore, EDS1 interaction with MED16 and CPL2 could be a link between NLR activation and transcriptional regulation during plant immunity.

TPR2 is in a family of transcriptional co-repressors and is reported to be a negative regulator of immunity (Garner et al., 2021). TPR2 interacts with both SNC1 and TPR1 to inhibit SNC1-TPR1 interaction (Garner et al., 2021). TPR2 interacts with EDS1 during mock treatment and ETI activation in our study (Figure 4.7 and Figure 4.9, Supplementary Table 2). Therefore, TPR2 may also interact with EDS1 to suppress ETI defence induction.

Here we have described novel EDS1 interactions with proteins not previously linked to plant immunity. In addition, these proteins have a role in transcriptional regulation, suggesting these protein interactions may link upstream defence activation, and the formation of EDS1 heterotrimers, with downstream transcriptional changes. EDS1 also interacts with many additional proteins in the dataset not mentioned here, which have also not previously been linked to immunity. Therefore, this data set provides a resource for novel immunity proteins to be identified and to further our understanding of downstream signalling pathways.

4.2.1.2 Some reported EDS1 interactors were not identified in our study

EIJ1, a negative regulator of immunity, and PBS3, a positive regulator of immunity, have been previously reported to interact with EDS1 (Bhattacharjee et al., 2011, Chang et al., 2019, Chen et al., 2021, Liu et al., 2021). However, EIJ1 and PBS3 were not present in the EDS1-TurboID dataset.

EDR1 negatively regulates immunity through inhibition of the EDS1-PAD4 interaction (Neubauer et al., 2020). The interaction of EDR1 and EDS1 and the inhibition of the EDS1-PAD4 interaction was shown using a yeast-3-hybrid assay (Neubauer et al., 2020). However, an interaction between EDR1 and EDS1 has not been shown in-planta during immune activation (Neubauer et al., 2020). EDR1 was present in

the EDS1 TurboID dataset but had more biotinylation by mCherry than EDS1 and so EDR1 was not classed as an EDS1 interactor. EDS1 is reported to interact with NPR1 and the Mediator kinase module CDK8 to induce transcriptional changes (Chen et al., 2021). EDS1 interaction with CDK8 was shown after transient expression in *N. benthamiana* (Chen et al., 2021). We did not find CDK8 to be an EDS1-specific interactor as it was also biotinylated by NLS-GFP. EDS1 was shown to interact with NPR1 *in-vivo* (Chen et al., 2021). However, NPR1 was not biotinylated by EDS1 in our study. EDS1 was also reported to interact with MYC2 to prevent MYC2 repression of defence genes (Cui et al., 2018, Bhandari et al., 2019). MYC2 was only found in one biological replicate, so was not considered as an EDS1 interactor. As some proteins, previously identified as EDS1 interactors, were not biotinylated by EDS1 in our study, this could reflect a limitation of TurboID-MS in identifying weakly abundant interactions under our specific conditions. Despite these previously reported EDS1 interactions, whether EDS1 has activities during immunity activation independent of its interactors SAG101 and PAD4, remains an important question when interpreting these previous results. Although we did not identify NPR1, MYC2 or CDK8 as EDS1 potential interactors, we did identify other transcriptional regulators as EDS1 interactors e.g. LEUNIG, LUH, SEUSS, NINJA, CPL2 and Mediator subunit MED16. Therefore, EDS1 may have additional transcriptional activator activities to those previously described (Chen et al., 2021). We do not know if these EDS1 transcriptional activities are independent of SAG101 and PAD4 interactions. However, as the NRP1-EDS1 interaction and transcriptional activity at the PR1 promoter is PAD4/SAG101 independent (Chen et al., 2021), this suggests these additional transcriptional activities may also be independent of PAD4/SAG101. Alternatively, EDS1 may not directly control transcription at gene promoters but may be involved in signalling the activation of transcription, after heterotrimer formation. These additional EDS1 protein interactions may then trigger a structural change, sub-cellular localisation change or further interactions, leading to transcriptional changes. The role of EDS1 as a direct or indirect transcriptional regulator needs to be further explored. ChIP-Seq analysis would reveal if/which gene promoters are directly bound by EDS1.

4.2.2 TPR1 TurboID

4.2.2.1 TPR1 interacts with other transcription-related proteins

To identify TPR1 interactors, TPR1-TurboID was performed transiently in *N. benthamiana*. TPR1-TurboID-V5 and NLS-GFP-TurboID-V5 have similar protein expression levels in *N. benthamiana* (Figure 4.12B). There is increased protein biotinylation after 4 hours of biotin treatment in leaves transiently expressing TPR1-TurboID-V5 and NLS-GFP-TurboID-V5 (Figure 4.12A). This confirms that the proteins have good biotinylation activity. To compare proteins biotinylated by TPR1 upon PTI and PTI + ETI

activation, *N. benthamiana* leaves were infiltrated with *Agrobacterium* carrying TPR1-TurboID or NLS-GFP 48 hours before infiltration with biotin and either Pf0-1_Empty vector or Pf0-1_XopQ (Figure 4.5). Proteins were then extracted, biotinylated proteins purified and peptides analysed by MS (Figure 4.5). Proteins were compared between TPR1 and NLS-GFP for each immunity treatment. Proteins were considered TPR1 interactors if they were unique to TPR1 or if they had > 2x fold increase in biotinylation in TPR1 compared to NLS-GFP, with a P-value < 0.05. Samples were also grouped between immunity treatments if they were found in multiple biological repeats but only one per repeat per immunity treatment, as described previously for EDS1.

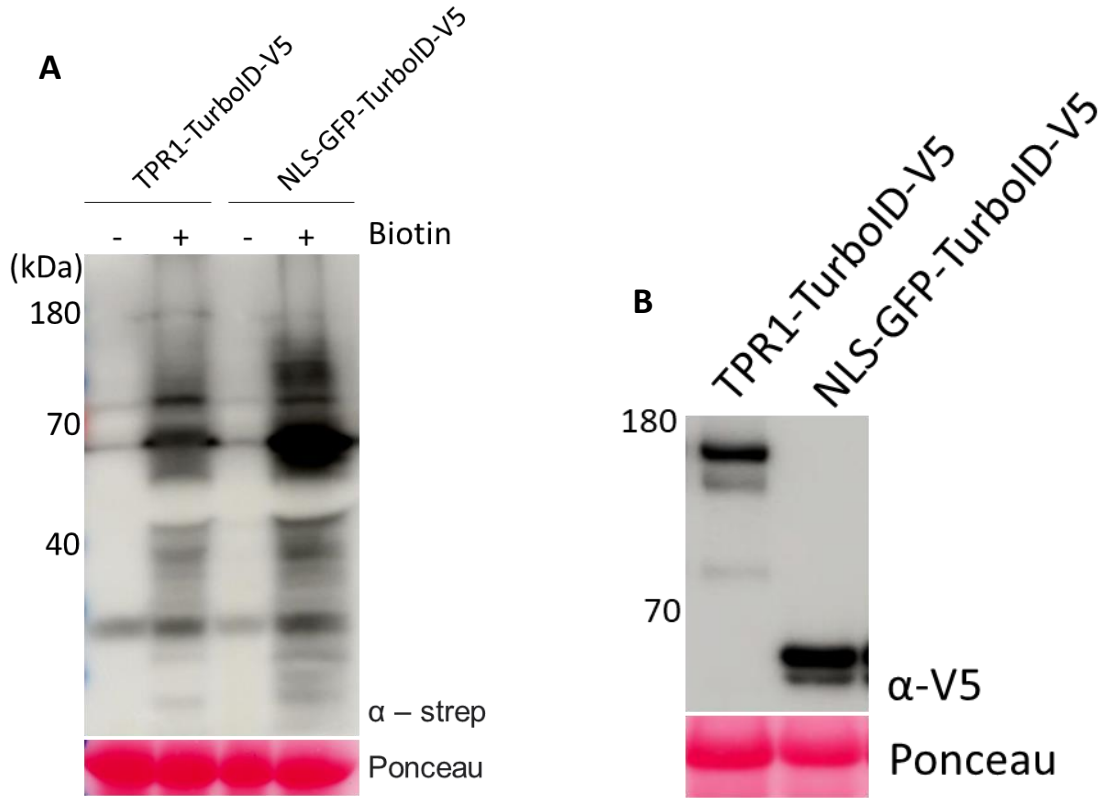

Figure 4.12. A) Increased levels of biotinylated proteins after 4 hours of biotin treatment. B) TPR1-TurboID and NLS-GFP-TurboID have similar levels of protein expression. A) Transient expression in N. benthamiana for 48 hours, followed by treatment with 50 µM Biotin for 4 hours**.** B) Transient expression in N. benthamiana for 48 hours.

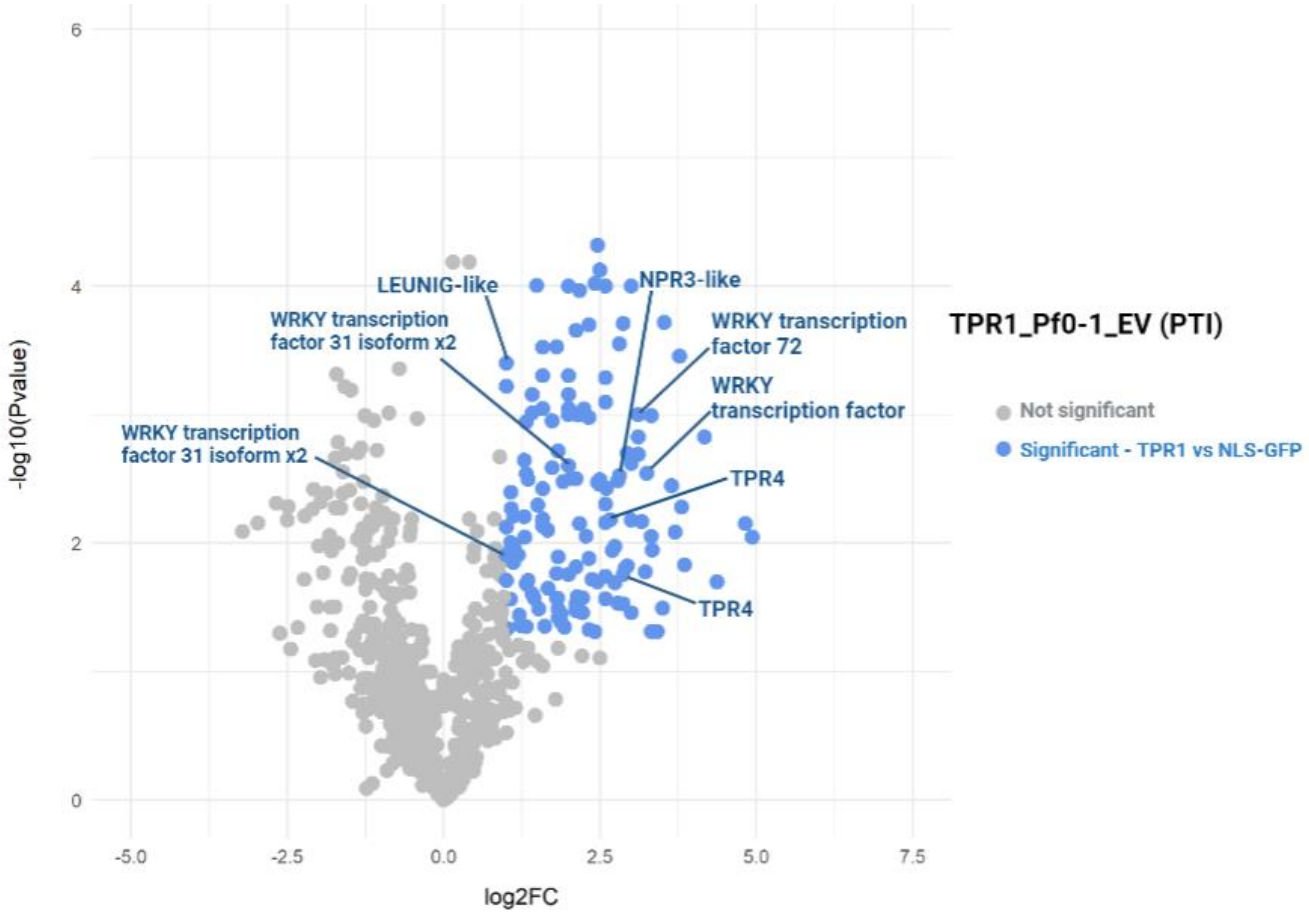

Figure 4.13. TPR1 interactors during PTI. Proteins were considered TPR1 interactors if they showed a 2-fold increase in biotinylation compared to NLS-GFP-TurboID and had a statistically significant difference P-value < 0.05. Biotinylated proteins not significantly different are in **gray**. Significant TPR1 interactors are represented in **blue**.

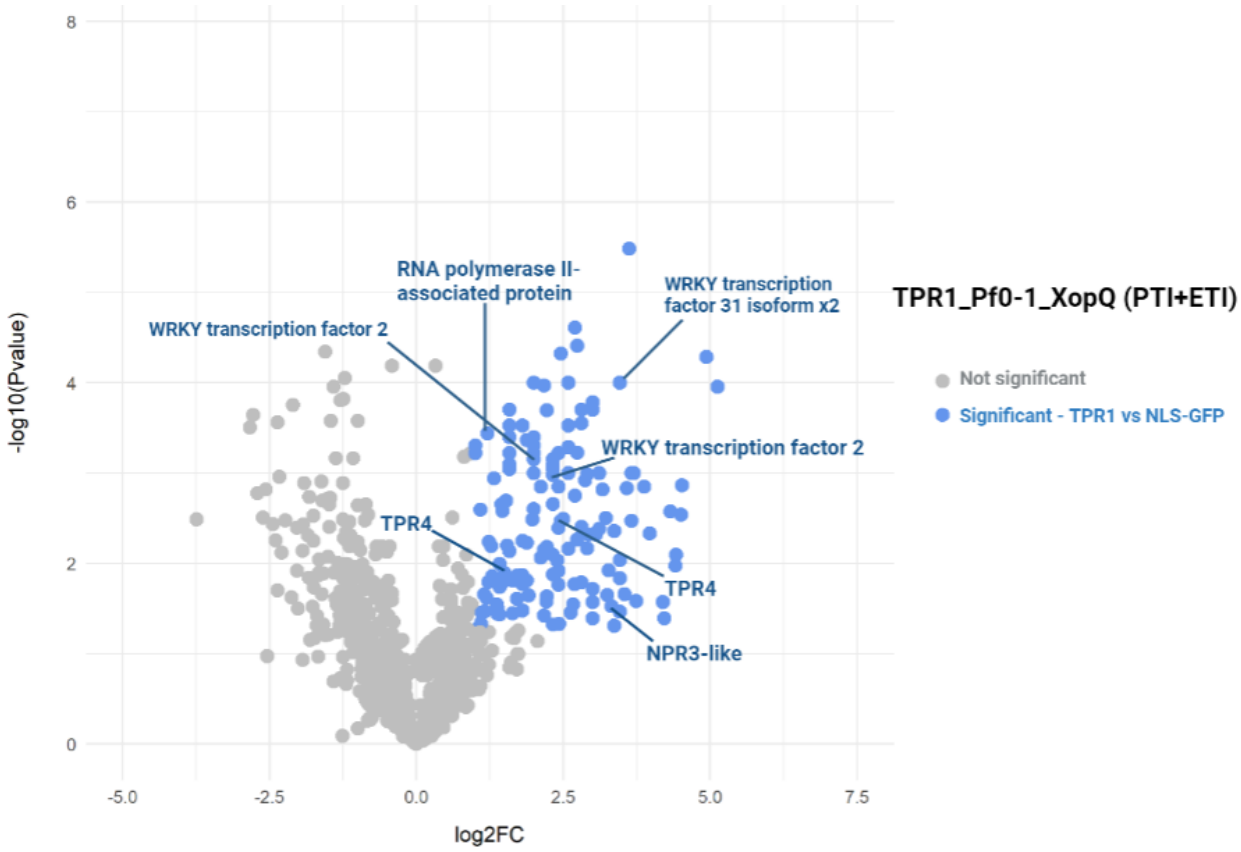

Figure 4.14. TPR1 interactors during PTI + ETI. Proteins were considered TPR1 interactors if they showed a 2-fold increase in biotinylation compared to NLS-GFP-TurboID and had a statistically significant difference P-value < 0.05. Biotinylated proteins not significantly different are in gray. Significant TPR1 interactors are represented in blue.

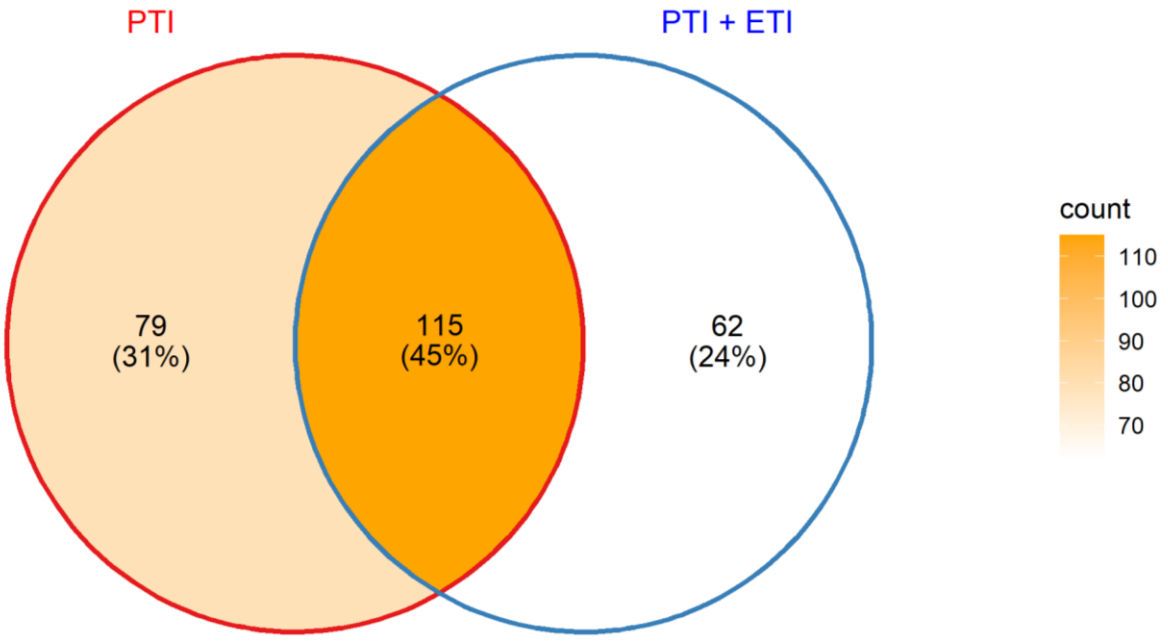

Figure 4.15. Many proteins were found to be TPR1 interactors during both PTI and PTI + ETI signalling. Proteins were considered TPR1 interactors for each treatment if they were unique to TPR1-TurboID or showed a 2-fold increase in biotinylation compared to NLS-GFP-TurboID and had a statistically significant difference P-value < 0.05. Protein interactors for each immunity treatment were compared to create a Venn diagram. Percentages represent total protein population of TPR1 interactors.

274 proteins were found to be potential TPR1 interactors during PTI or PTI + ETI activation (Supplementary Table 3). 176 proteins interact with TPR1 during PTI activation, 107 of these are unique to TPR1, with the remaining 69 showing an enhanced interaction with TPR1 compared to NLS-GFP (Figure 4.13, Supplementary Table 3). 194 proteins interact with TPR1 during PTI + ETI activation, 167 of which are unique to TRP1 (Figure 4.14, Supplementary Table 3). 45% of TPR1 interactors overlap between PTI and PTI + ETI (Figure 4.15). As we had no mock sample, we were unable to identify interactors induced upon PTI or PTI + ETI activation compared to mock. However, we did identify 3 proteins whose interaction was enhanced upon PTI + ETI activation compared to PTI activation and did not interact with NLS-GFP (Supplementary Table 4). These include two uncharacterised proteins and a Jasmonate ZIM domain protein (Supplementary Table 4). TPR1 also interacts with a NINJA-family protein during PTI activation (Figure 4.13). TPR1 has been previously shown to interact with NINJA to repress JA signalling (Pauwels et al., 2010, An et al., 2022). Therefore, our data provides in-vivo confirmation of TPR1-NINJA interaction during an immune response.

The SA receptor NPR1-LIKE PROTEIN 3 (NPR3) is a negative regulator of immunity and activates JA signalling (Liu et al., 2016, Ding et al., 2018). NPR3-like interacts with TPR1 during PTI and PTI + ETI activation (Figure 4.13, Figure 4.14 and Supplementary Table 3). This supports the role of TPR1 in regulating JA signalling, possibly by interacting with NPR3 to inhibit NPR3 activity.

TPR1 interacts with 29 proteins described as involved in transcription in their gene name. 6 WRKY proteins interact with TPR1 during PTI or PTI + ETI activation and the *At*WRKY18 and *At*WRKY40 homolog, *Nb*v6.1trA137700 probable WRKY40, was found as a TPR1 interactor when the immunity treatments were grouped (Figure 4.13, 4.14 and Supplementary Table 3 and 4). This suggests TPR1 interacts with multiple WRKY proteins as a possible mechanism to regulate transcriptional changes during immune activation. Two *Nb*TPR4 proteins interact with TRP1 during PTI and PTI + ETI activation (Figure 4.13 and 4.14). *At*TPR4 has been described as acting redundantly with TPL and TPR1 as a positive regulator of immunity (Zhu et al., 2010). However, the molecular activities of TPR4 have not been previously described. Therefore TPR1-TPR4 may interact to positively regulate immunity signalling. LEUNIG and LEUNIG homolog are in the same transcriptional co-repressor family as TPR1. *Nb*LEUNIG-like was found as a TPR1 interactor during PTI activation (Figure 4.13). The identification of TPR1 interaction with TPR4, LEUNIG, NPR3, and WRKY transcription factors provides promising leads for further investigation, to improve our understanding of TPR1 and defence-induced transcriptional changes. TPR1 also interacted with an RNA polymerase II-associated protein during PTI + ETI activation (Figure 4.14 and Supplementary Table 3), providing a direct link between TPR1 and transcriptional regulation upon ETI activation.

4.2.2.2 Some reported TPR1 Interactors were not identified in our study

SIZ1, a SUMO E3 ligase, was shown to interact with TPR1 *in vivo* in Arabidopsis plants to suppress plant immunity (Niu et al., 2019). SIZ1 was biotinylated by TPR1 but does not show a 2x fold increase in biotinylation compared to NLS-GFP. TPR1 was previously found to interact with HDA19 *in vivo* in transgenic Arabidopsis plants (Zhu et al., 2010). However, we did not identify HDA19 biotinylation in our study. These interactions may have been weak and under the detection limit of the MS.

4.2.2.3 WRKY18 and TPR1 interact but the interaction is not dependent on immune status or via an EAR domain

The *At*WRKY18 and *At*WRKY40 homolog Nbv6.1trA137700 was identified as a TPR1 interactor. *At*WRKY18 acts a positive regulator in response to *Pto* DC3000 AvrRps4 and has been proposed as a

negative transcriptional regulator in response to flg22 (Schon et al., 2013, Birkenbihl et al., 2017). Therefore, we further investigated the interaction between TPR1 and WRKY18. A co-immunoprecipitation (co-IP) was carried out and confirmed an interaction between *At*TPR1 and *At*WRKY18, after transient expression in *N. benthamiana* (Figure 4.16). This interaction is not enhanced or weakened after Pf0-1_XopQ treatment, suggesting the interaction does not change upon PTI + ETI activation (Figure 4.16). Therefore, the role of the interaction during immunity signalling is not known. TPR1 has been shown to interact with proteins containing an EAR domain (Szemenyei et al., 2008, Pauwels et al., 2010, Wang et al., 2013, Li et al., 2022a). *At*WRKY18 contains an EAR domain at the N-terminus of the protein (Figure 4.17) (Kagale et al., 2010). The *At*WRKY18 EAR DLNxxP motif is conserved in the *N. benthamiana* homolog which interacts with *At*TPR1. EAR domains are also present in two other TPR1 interacting *Nb*WRKYs: Nbv6.1trA202784 WRKY72 and Nbv6.1trP14772 WRKY31 isoform x2, as well as in 6 other transcription related proteins biotinylated by TPR1 (Supplementary Table 3). This suggests an EAR domain could be important for TPR1 interactions. Therefore, we tested the hypothesis that TPR1 and WRKY18 interact via an EAR domain in WRKY18. We first tested if the DLN motif in WRKY18 is important for its interaction with TPR1 (Figure 4.16). An alanine mutant in the WRKY18 EAR domain (WRKY18$^{DLN\text{-}AAA}$-GFP) does not weaken the interaction with TPR1-HF (Figure 4.16). We then made a N-terminal deletion of WRKY18, removing the first 16 amino acids after the start codon (Figure 4.17). This deletion encompasses the DLN motif and a LxIxL motif, which could represent another EAR domain (Figure 4.17). WRKY18$^{\triangle EAR}$-GFP interacts with TPR1-HF as strongly as WRKY18-GFP wildtype (Figure 4.18), suggesting the EAR domain and first 16 amino acids in WRKY18 are not required for TPR1 interaction. Therefore, TPR1 and WRKY18 interact via another domain.

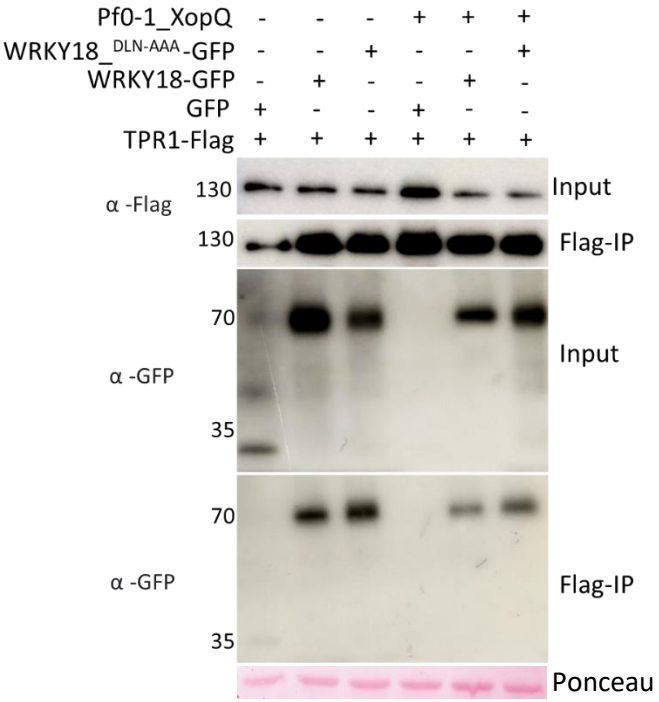

Figure 4.16. WRKY18-GFP and WRKY18$^{DLN-AAA}$-GFP interact with TPR1-HF. Transient expression in *N. benthamiana* and immunoprecipitation of Flag proteins. GFP was used as a negative control. 48 hpi, Pf0-1_XopQ was infiltrated and samples were collected after 4 hours. Similar results seen in two independent biological repeats.

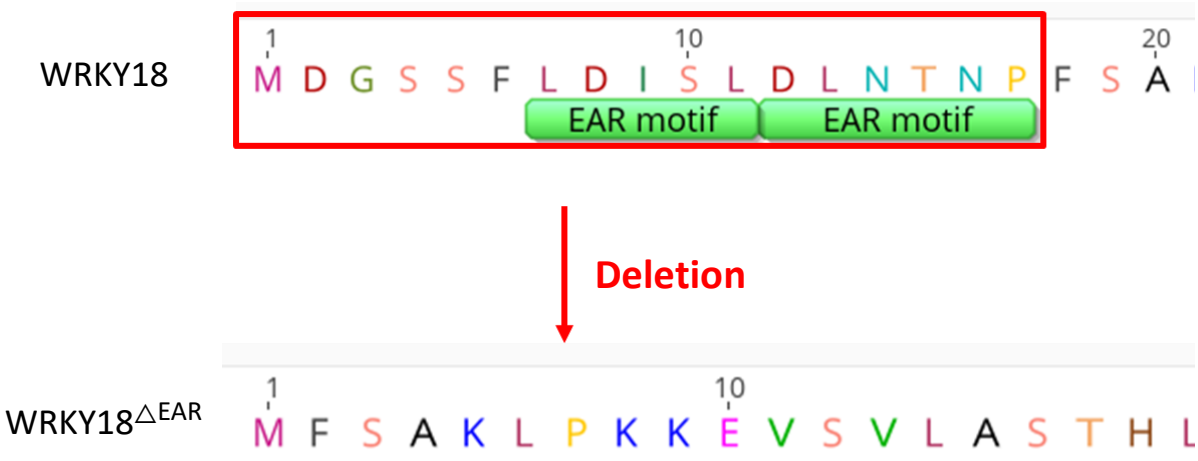

Figure 4.17. Localisation of EAR motifs in WRKY18. The N-terminus of WRKY18 was deleted to create a WRKY18$^{\triangle EAR}$ mutant.

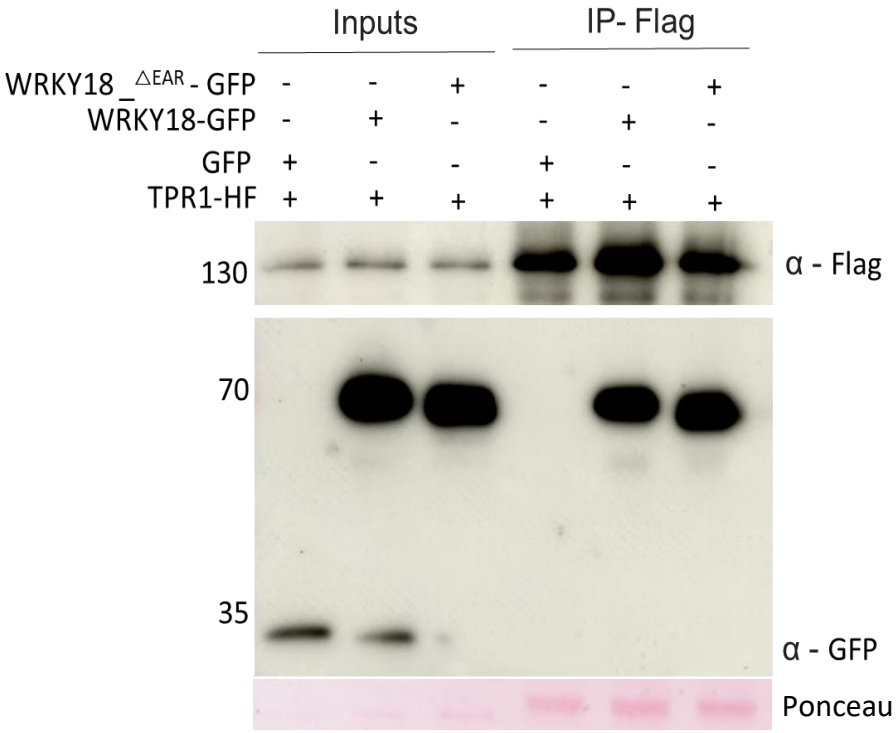

Figure 4.18. WRKY EAR domain deletion does not disrupt interaction with TPR1-HF. Transient expression in *N. benthamiana* and immunoprecipitation of Flag proteins. GFP was used as a negative control. Samples were collected 48 hpi. Similar results seen in three independent biological repeats.

4.2.2.4 The WRK18 EAR domain is important for TPR1 puncta co-localisation

To investigate if WRKY18-GFP and TPR1-mCherry have the same localisation pattern, confocal images were taken 48 hours after transient expression in *N. benthamiana* leaves. WRKY18-GFP has previously been shown to localise to the nucleus of onion epidermal cells (Xu et al., 2006b). In *N. benthamiana* WRKY18 localises as puncta in the nucleus (Figure 4.19). The number and size of the WRKY18 nuclear puncta was found to vary between cells (Figure 4.19). WRKY18 has previously been found to localise as nuclear puncta in *N. benthamiana* leaves and Arabidopsis protoplasts (Geilen & Bohmer, 2015). The EAR domain deletion in WRKY18 does not impact its ability to localise as nuclear puncta (Figure 4.19). When TPR1-mcherry is co-infiltrated with GFP, TPR1 has an even expression across the whole nucleus (Figure 4.19). When co-expressed with WRKY18-GFP, TPR1 forms the same puncta pattern and co-localises with WRKY18-GFP (Figure 4.19). However, TPR1 is unable to localise as puncta when co-infiltrated with WRKY18$^{\triangle EAR}$-GFP, suggesting the EAR domain of WRKY18 is required for TPR1 to co-localise with WRKY18 in nuclear puncta.

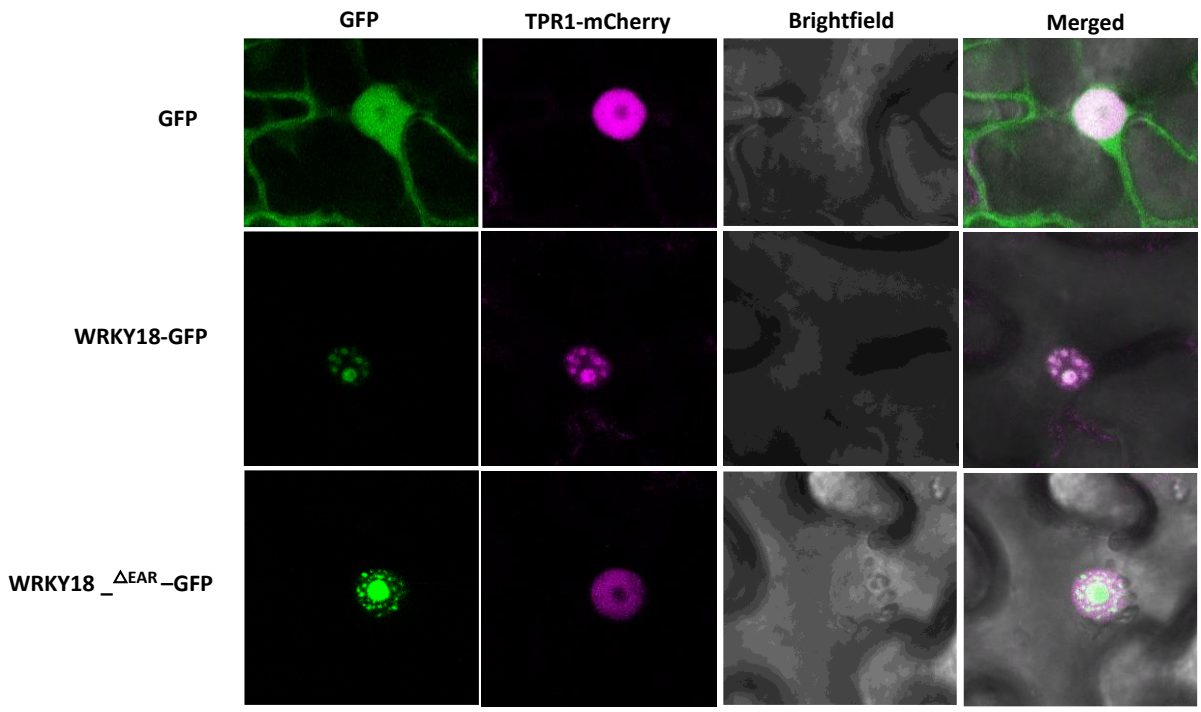

Figure 4.19. TPR1-mCherry forms nuclear puncta when co-expressed with WRKY18-GFP. TPR1-HF, GFP, WRKY18-GFP or WRKY18$^{\triangle EAR}$-GFP were transiently expressed in *N. benthamiana*. GFP was used as a negative control. Samples were collected 48 hpi. Represents three independent biological repeats. Images taken by SP5 Confocal microscope and processed by ImageJ.

4.2.2.5 There is no change in TPR1 or WRKY18 localisation upon Pf0-1 XopQ treatment

To test if ETI activation alters WRKY18 or TPR1 nuclear puncta localisation, *N. benthamiana* leaves co-infiltrated with WRKY18-GFP and TPR1-HF were infiltrated with Pf0-1_XopQ after 48 hours and leaves imaged 4 hours later. There is no change in WRKY18-GFP or WRKY18$^{\triangle EAR}$-GFP localisation after Pf0-1_XopQ treatment (Figure 4.20). In addition, TPR1 localisation does not change after Pf0-1_XopQ treatment (Figure 4.12).

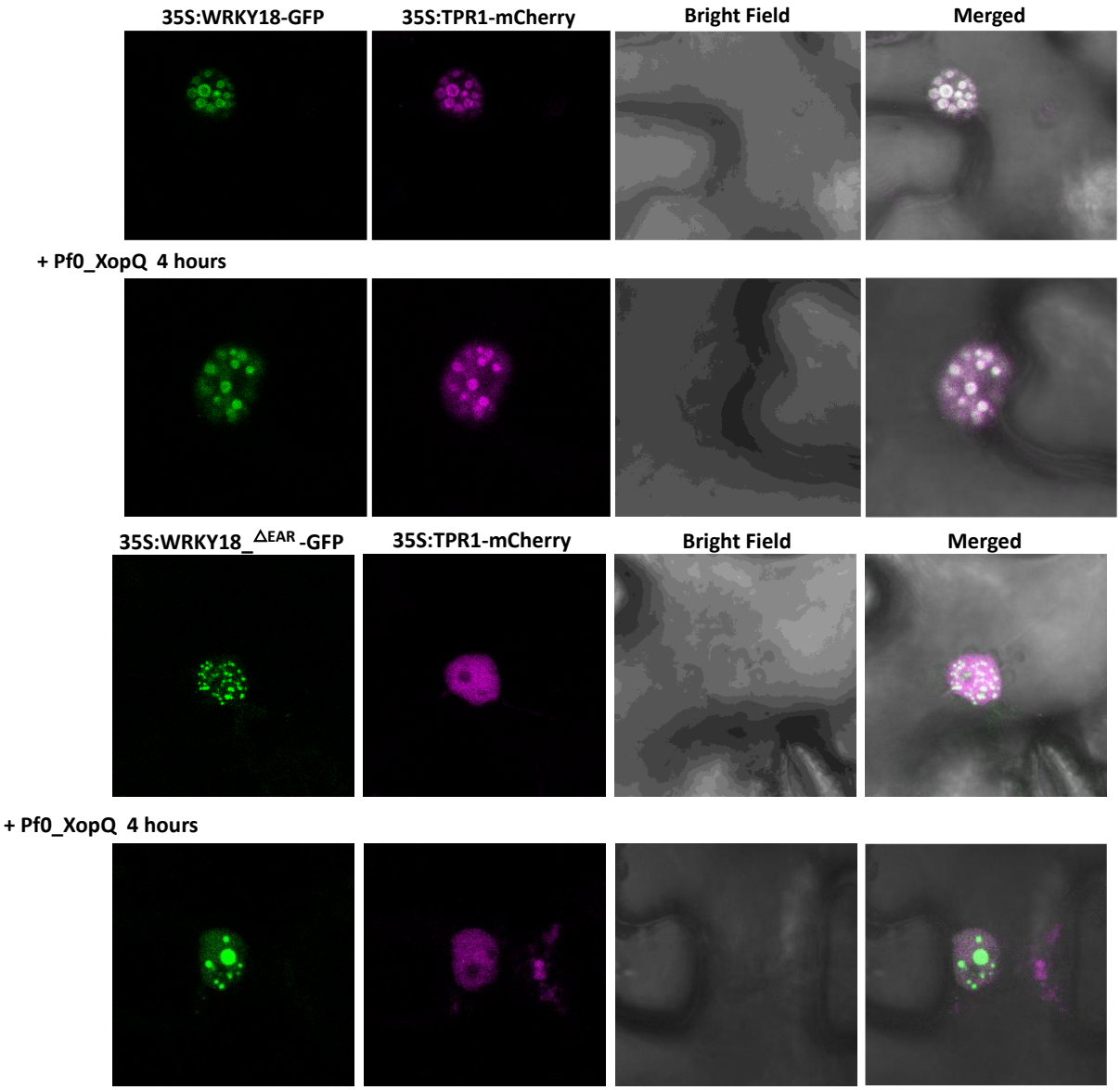

Figure 4.20. Localisation of TPR1-HF, WRKY18-GFP or WRKY18$^{\Delta EAR}$-GFP does not change after Pf0-1_XopQ treatment. Transient expression in *N. benthamiana*. 48 hpi, Pf0-1_XopQ was infiltrated and leaves were imaged after 4 hours. Similar results seen in three independent biological repeats, where 6 nuclear images were taken for each repeat. Images taken by SP5 Confocal microscope and processed by ImageJ.

4.2.2.6 The phosphorylation status of TPR1 or WRKY18 does not alter their interaction

In Chapter 3, TPR1 and WRKY18 were found to change in phosphorylation upon ETI signalling. TPR1 residues T286 and T289 are well conserved in flowering plants, suggesting they may be important for TPR1 function (Figure 4.21). TPR1 T286 is also well conserved within other Arabidopsis Topless proteins (Figure 4.21). TPR1 T395 is not well conserved across flowering plants suggesting it may not

be as important for TPR1 function (Figure 4.21). The conservation of the WRKY18 phosphorylation sites was checked within the phylogenetic clade WRKY IIa which WRKY18 lies within (Wang et al., 2011b). S86 and S89 are conserved in WRKY60 but are not conserved in other WRKYs from the IIa clade, including WRKY40, with which WRKY18 acts redundantly (Birkenbihl et al., 2017) (Figure 4.22). WRKY18 S86 is well conserved across homologs in other flowering plants and S89 is less conserved, suggesting S86 may be more important for WRKY function (Figure 4.23).

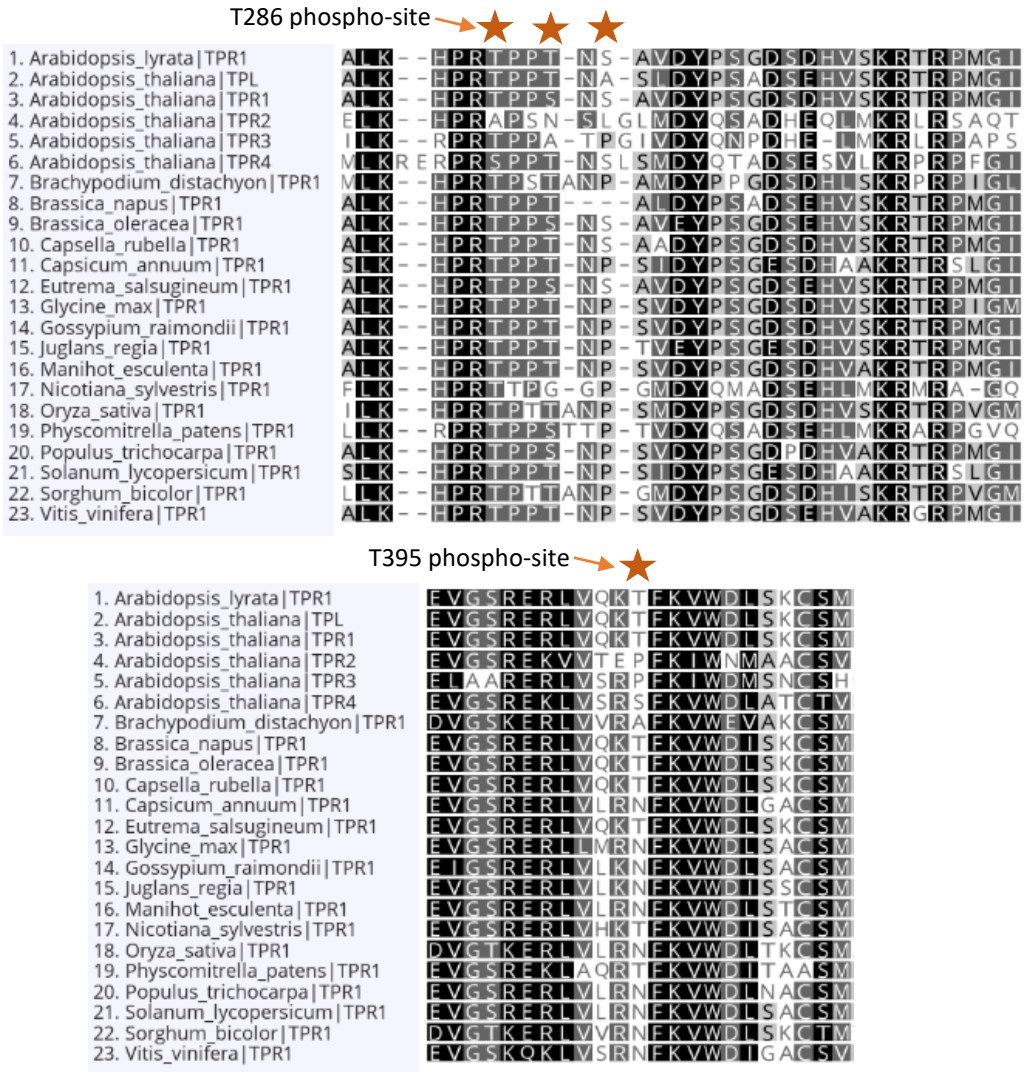

Figure 4.21. TPR1 T286 is conserved across different plant species. AtTPR1 protein sequence was used in a protein BLAST and the top protein identity hits from across the plant kingdom are shown. Multiple protein sequence alignment was performed using T-Coffee and imported into Geneious Prime. ★ highlights the T286, T289, S291 and T395 residues in *At*TPR1.

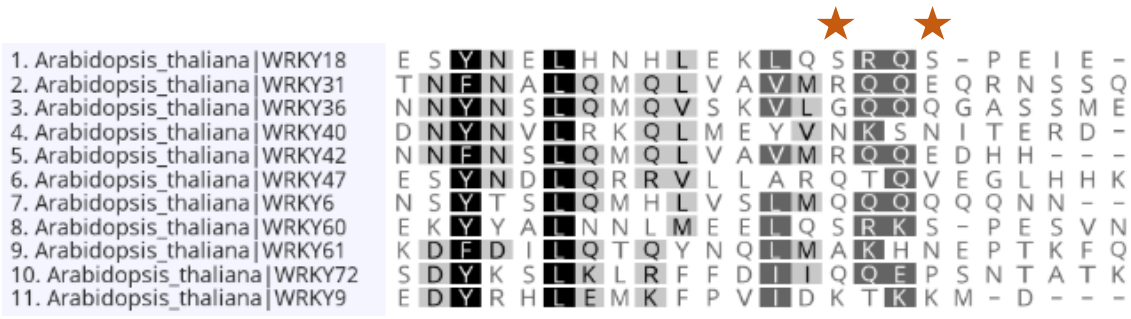

Figure 4.22. WRKY18 S86 and S89 are not conserved within the WRKY IIa clade. Alignment of WRKY18 phosphorylation peptide, identified by PRM, within the WRKY IIa clade. Protein sequences were downloaded from TAIR and multiple protein sequence alignment was performed by T-coffee. Alignment was imported into Geneious Prime. ★ highlights the S86 and S89 residues in *At*WRKY18.

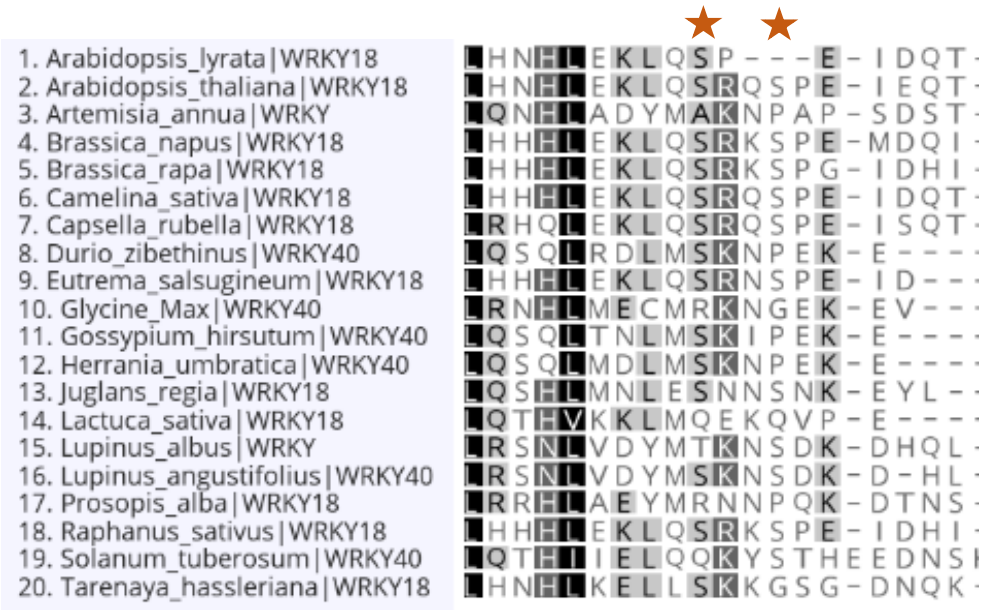

Figure 4.23. WRKY18 S86 is conserved in many plant species. Alignment of phosphorylation peptide within WRKY proteins from across flowering plants. A protein Blast was performed with the *At*WRKY18 protein sequence and the top protein sequence hits were downloaded from NCBI. A multiple protein sequence alignment was performed by T-coffee and imported into Geneious Prime. ★ highlights the S86 and S89 residues in *At*WRKY18.

WRKY18 has a leucine zipper motif important for WRKY-WRKY protein interactions (Xu et al., 2006b). The final leucine of this motif is L84, located two amino acids before the S86 phosphorylation site. Therefore, due to the close proximity of the phosphorylation site, WRKY18 phosphorylation may have a role in protein-protein interactions. To test if the phosphorylation sites in TPR1 and WRKY18 are important for their interaction during ETI signalling, phospho-variants of TPR1 and WRKY18 were made. To ensure we removed all possible phosphorylation sites, TPR1 T286, T289, and S291 were all targeted to make a TPR1 triple phospho-mimic ($TPR1^{DDD}$) or a triple phospho-dead variant ($TPR1^{AAA}$). A phospho-variant of another TPR1 phospho-site T395 was also made separately. Both TPR1 phospho-mimic and phospho-dead variants at the two phosphorylation regions show an interaction with WRKY18 similar to wildtype TPR1 (Figure 4.24). Their interaction does not change upon Pf0-1_XopQ treatment and subsequent ETI signalling activation (Figure 4.24). The TPR1_DDD-HF protein band appears reduced upon Pf01-_XopQ treatment compared to the other variants of TPR1 (Figure 4.24). However, we did not find this to be a consistent reduction in an additional repeat. This suggests these TPR1 phosphorylation sites are not important for the WRKY18 interaction. WRKY18 phospho-sites S86 and S89 were mutated to create a double phospho-dead ($WRKY18^{AA}$) and a double phospho-mimic ($WRKY18^{DD}$). Both WRKY18 phospho-variants interact with TPR1 and show no change upon Pf0-1_XopQ treatment, suggesting these phospho-sites are not important for WRKY18 interaction with TPR1 (Figure 4.25). Additionally, there is no difference in the nuclear puncta localisation of WRKY18 between the wildtype WRKY18-GFP and a phospho-mimic or phospho-dead variant of WRKY18-GFP (Figure 4.26). This suggests phosphorylation at S86 or S89 is not important in WRKY18's ability to form nuclear puncta. There is also no significant difference in the puncta size (area) or GFP intensity between WRKY18-GFP and WRKY18-GFP phospho-variants (Figure 4.27). Next it would be important to test it the phosphorylation sites of WRKY18 and TPR1 are important for their co-localisation as nuclear puncta, as seen for the $WRKY18^{\triangle EAR}$ mutant.

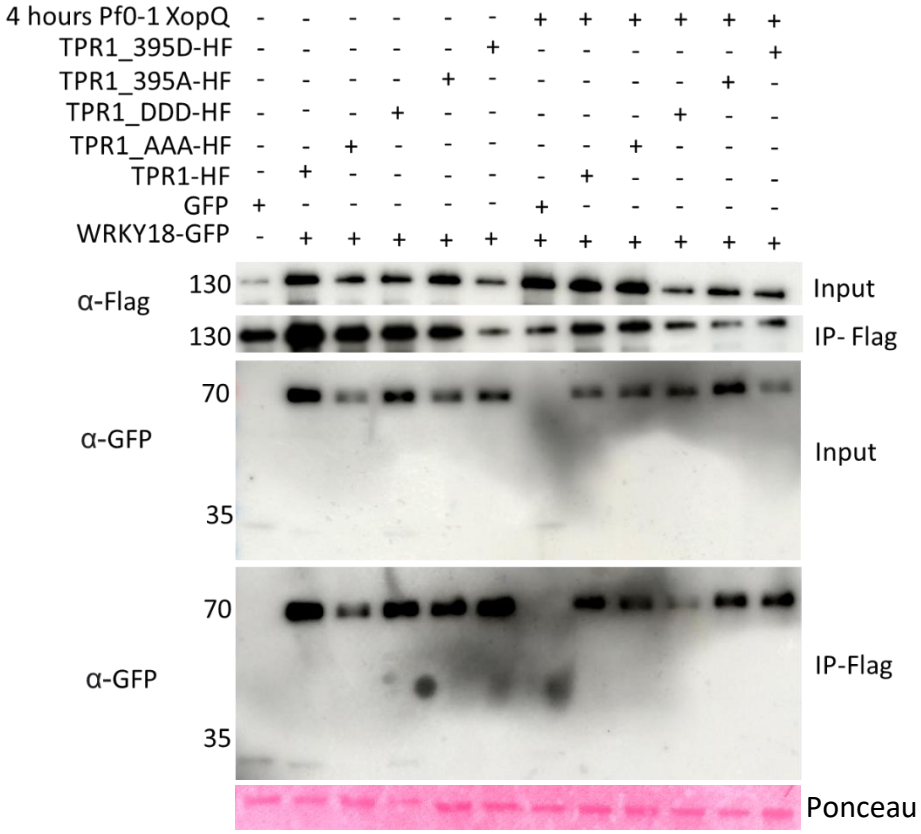

Figure 4.24. TPR1-HF phospho-variants interact with WRKY18-GFP. Interaction between WRKY18-GFP and TPR1-HF phospho-variants after transient expression in *N. benthamiana* and immunoprecipitation of Flag proteins. TPR1 triple phospho-mimic (TPR1_DDD) = TPR1 D286, D289, and D291. TPR1 triple phospho-dead variant (TPR1_AAA) = TPR1 A286, A289, and A291. GFP was used as a negative control. 48 hpi, Pf0-1_XopQ was infiltrated, and samples were collected after 4 hours. Similar results seen for two independent biological repeats.

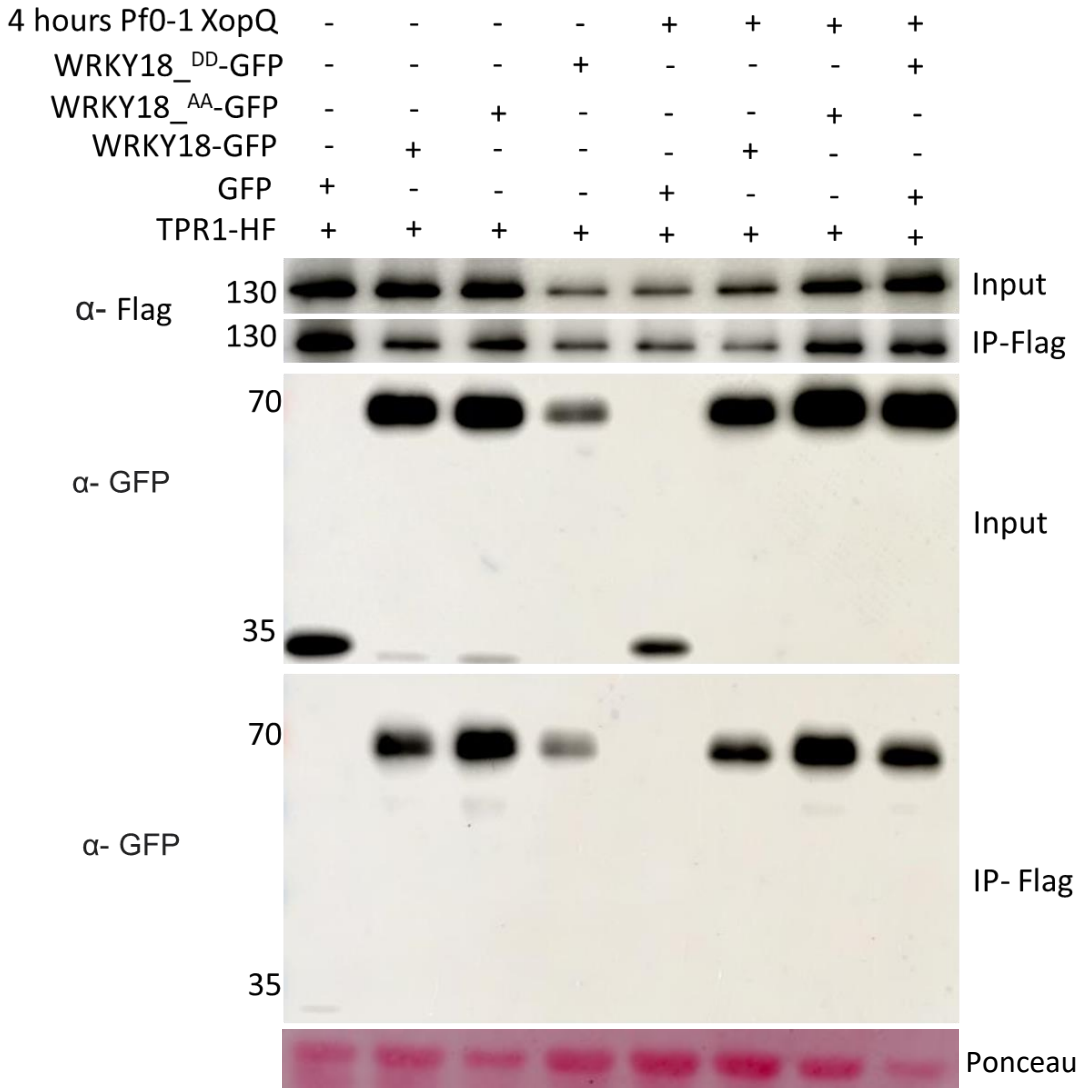

Figure 4.25. WRKY18 phospho-variants can interact with TPR1. Interaction between TPR1-HF and WRKY18-GFP, WRKY18^{DD} phospho-mimic or WRKY18^{AA} phospho-dead after transient expression in *N. benthamiana* and immunoprecipitation of Flag proteins. WRKY18 phospho-sites S86 and S89 were mutated to alanine (AA) or Aspartic acid (DD). GFP was used as a negative control. 48 hpi, Pf0-1_XopQ was infiltrated and samples were collected after 4 hours. Similar results seen for three independent biological repeats.

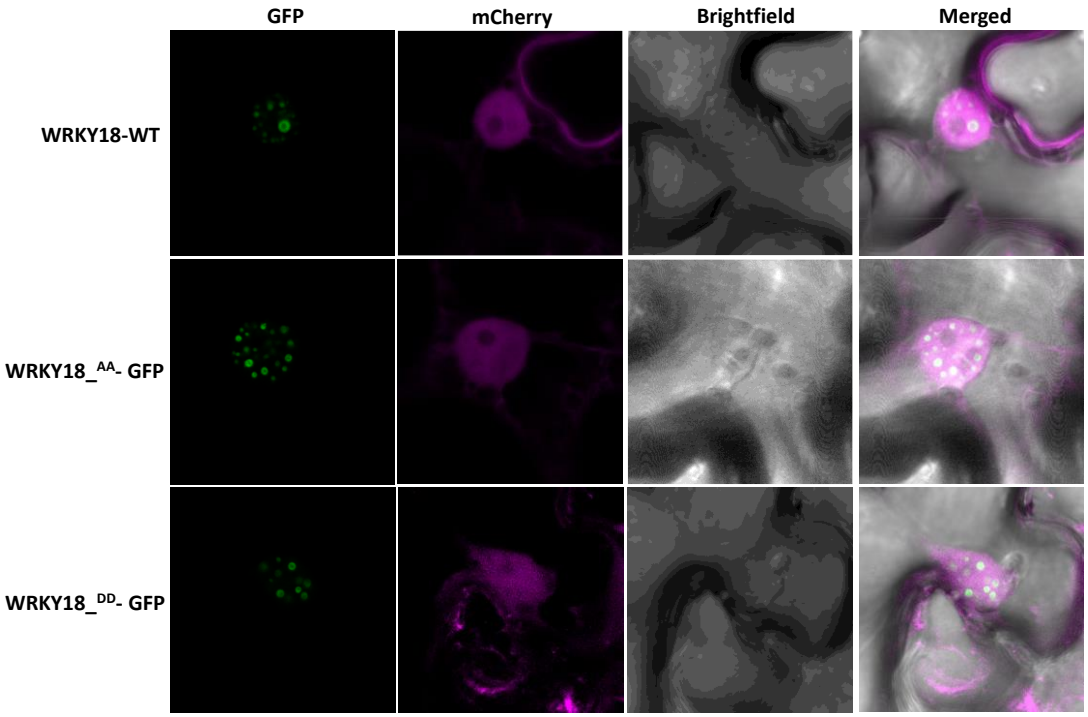

Figure 4.26. WRKY18 phospho-variants have similar localisation pattern to WRKY18 WT. Localisation of WRKY18-GFP, WRKY18^{AA}-GFP or WRKY18^{DD}-GFP after transient expression in *N. benthamiana*. mCherry was included as a nuclear localisation control. Represents three independent biological repeats. Images were taken 48 hpi by a SP5 Confocal microscope and processed by ImageJ.

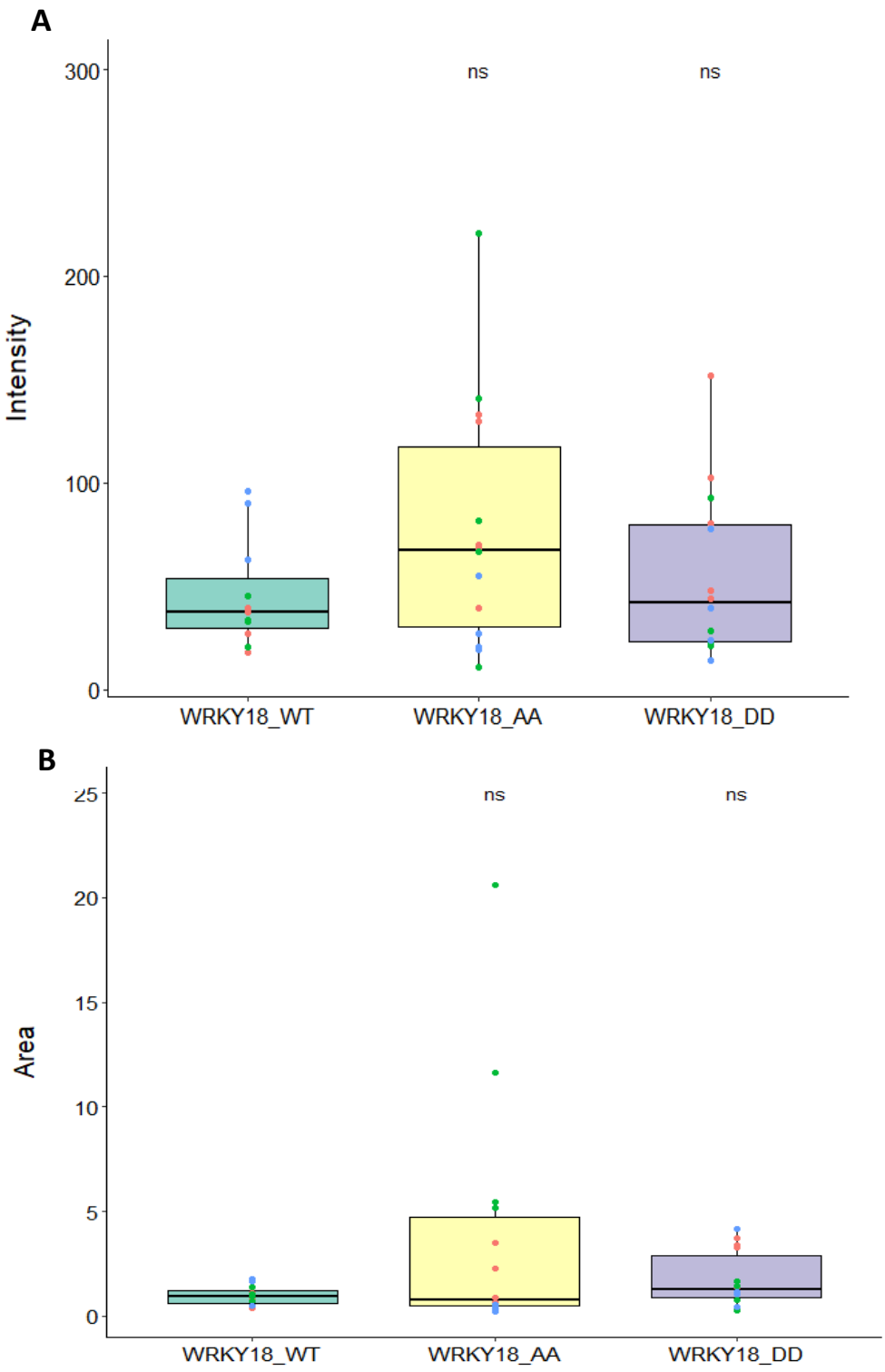

Figure 4.27. There is no difference in nuclear puncta GFP fluorescence intensity or puncta area between WRKY18 wildtype and phospho-variants. A) GFP fluorescence intensity of WRKY18-GFP, WRKY18^{AA}-GFP or WRKY18^{DD}-GFP nuclear puncta was measured after transient expression in *N. benthamiana*. B) The area of WRKY18-GFP, WRKY18^{AA}-GFP or WRKY18^{DD}-GFP nuclear puncta after transient expression in *N. benthamiana*. Represents data from three independent biological repeats. Images were taken 48 hpi by a SP5 Confocal microscope and individual puncta area and GFP fluorescence calculated by ImageJ.

4.2.2.7 What is the role of WRKY18 during PTI and ETI?

4.2.2.7.1 Transcriptional changes during PTI in *wrky18/40* mutants in response to flg22

To test the role of WRKY18 during PTI transcriptional changes, the expression of 5 PTI-induced genes was checked in the Col-0:*wrky18/40* mutant. Col-0:*wrky18/40* seeds were provided by Imre Somssich, Max Planck Institute. PEN3, CNGC3, WRKY51, CAD1, and MYB31 show increased expression 90 minutes after flg22 treatment (Bjornson et al., 2021). These genes also had enhanced WRKY18 binding to their promoters upon flg22 treatment (Birkenbihl et al., 2017). This suggests WRKY18 could regulate their expression upon PTI activation. 10-day old seedlings were treated with flg22 for 90 minutes and RNA extracted for RT-qPCR. PTI defence gene FRK1 expression is high in both Col-0 and wrky18/40 mutants showing that PTI has been activated in the seedlings (Figure 4.28). WRKY40 expression is induced upon PTI activation, whereas WRKY18 is not, suggesting that the two genes are regulated differently during PTI activation (Figure 4.29).

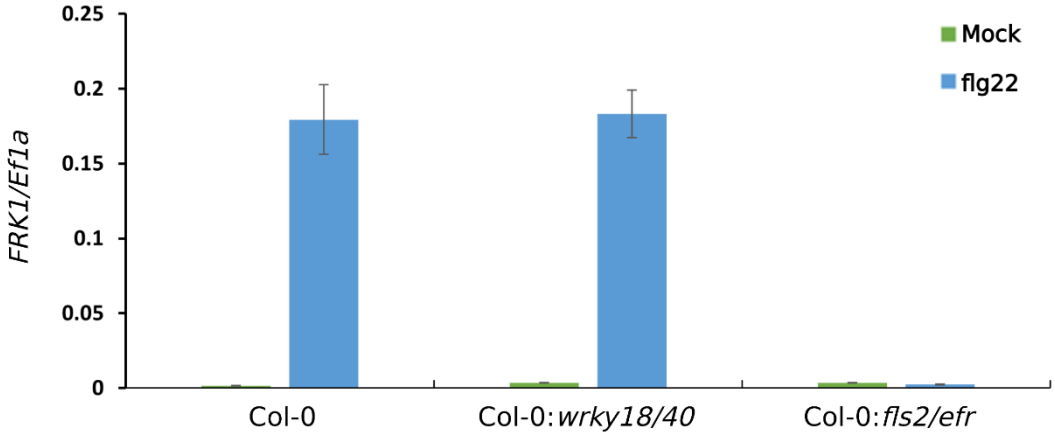

Figure 4.28. Flg22- induced FRK1 expression is not reduced in Col-0:*wrky18/40.* FRK1 expression in 10-day old seedlings incubated with 100 nM flg22 for 90 minutes. RNA extracted and used for RT-qPCR. Ef1a was used a control. Similar results were seen in three independent biological repeats.

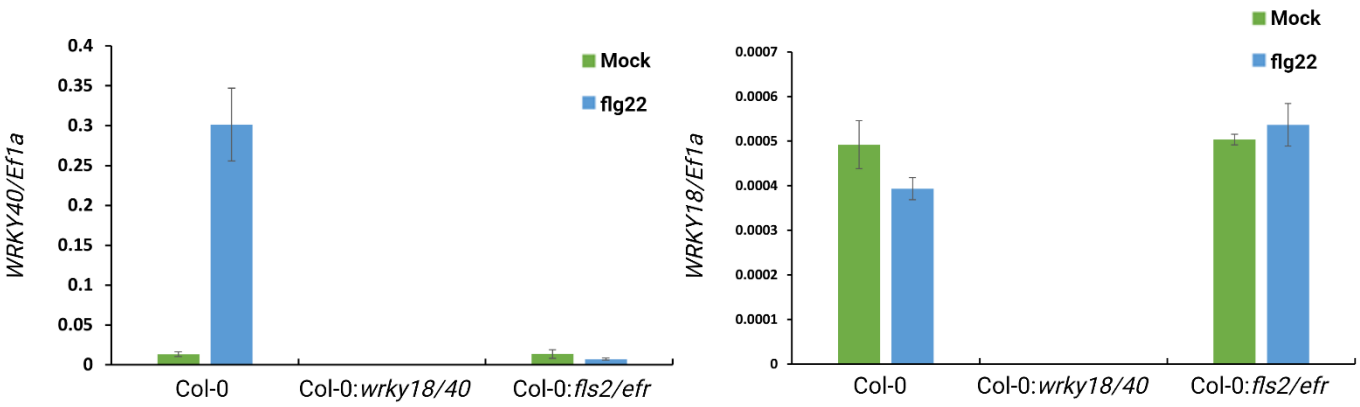

Figure 4.29. *WRKY40* gene expression, but not *WRKY18*, is induced upon PTI activation. WRKY18 and WRKY40 expression in 10-day old seedlings incubated with 100 nM flg22 for 90 minutes RNA extracted and used for qPCR. Ef1a used a control. Similar results seen in three independent biological repeats.

The 5 PTI induced genes have no difference in expression in *wrky18/40 mutants* compared to Col-0 (Figure 4.30). This suggests that WRK18 and WRKY40 are not solely responsible for inducing their expression upon flg22 detection, despite binding to their promoters. Therefore, the direct role of WRKY18/WRKY40 in PTI transcriptional regulation remains unknown.

4.2.2.7.2 Transcriptional changes during PTI + ETI in *wrky18/40* mutants

To investigate if WRKY18/WRKY40 are involved in transcriptional changes during PTI + ETI activation, *wrky18/40* mutants were infiltrated with Pf0-1_AvrRps4 or Pf0-1_AvrRps4_EEAA for 4 hours. Pf0-1_AvrRps4_EEAA is not recognised by RRS1/RPS4 and therefore, only PTI is activated (Sohn et al., 2012). ICS1 expression is increased in the *wrky18/40* mutant, suggesting WRKY18 and WRKY40 act as negative regulators of *ICS1* expression (Figure 4.31). However, *SARD1* expression is reduced in the *wrky18/40* mutant compared to Col-0, upon PTI + ETI activation (Figure 4.32). This suggests WRKY18 and WRKY40 act to differentially regulate two genes involved in SA biosynthesis. We predict that this could be due to protein complexes made at gene promoters e.g. with transcriptional regulators such as TPR1, that determine if WRKY18 acts to repress or activate transcription. RNA-seq upon ETI activation would reveal if there is a global role of WRKY18 in ETI transcriptional changes. Additionally, WRKY40 interactions with TPR1/TPL should be checked.

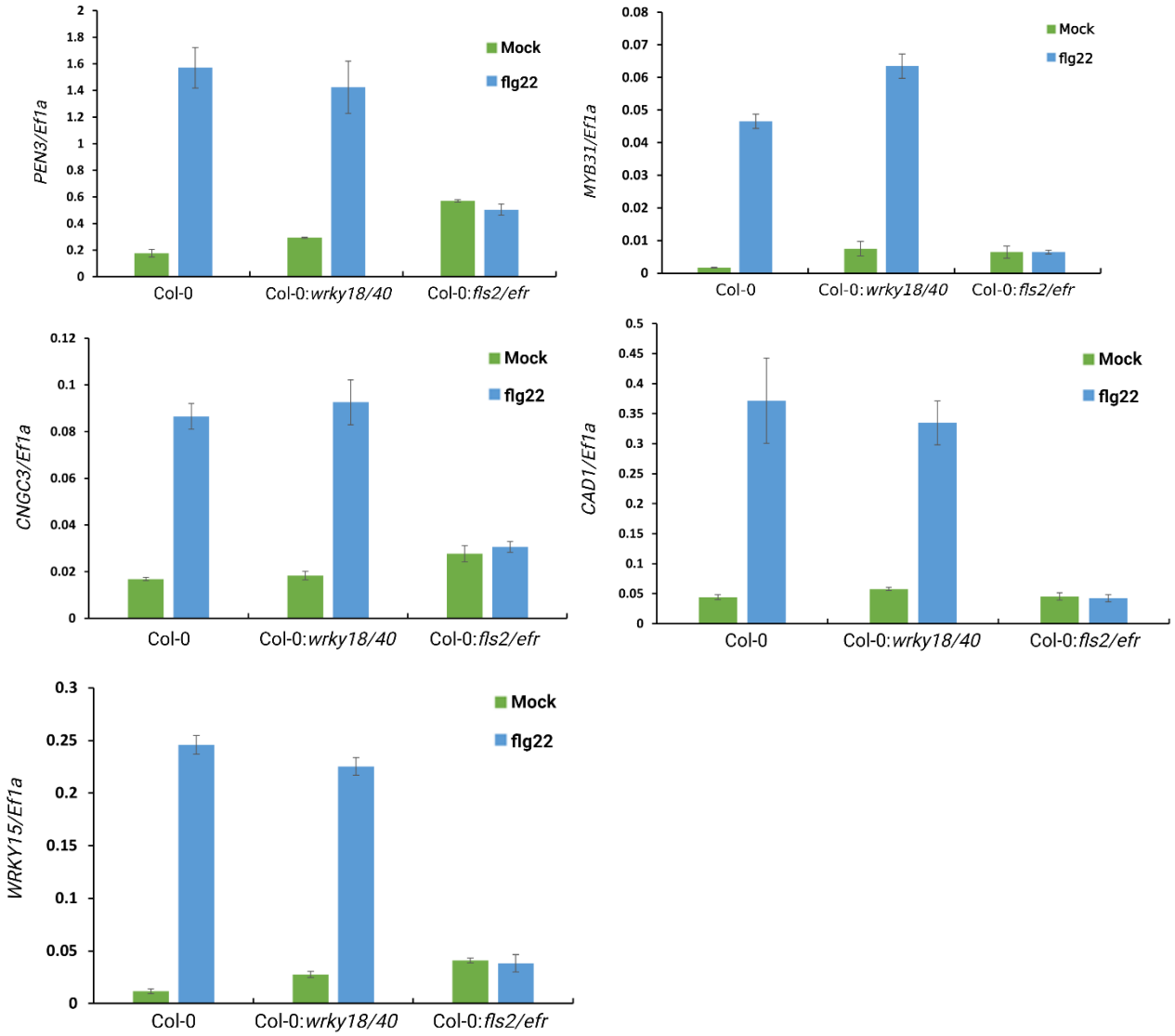

Figure 4.30. PTI gene expression of 5 selected PTI genes is not reduced in Col: *wrky18/40*. 10-day old seedlings were treated with 100 nM flg22 for 90 minutes RNA extracted and used for qPCR. Ef1a used a control. Similar results seen in three independent biological repeats.

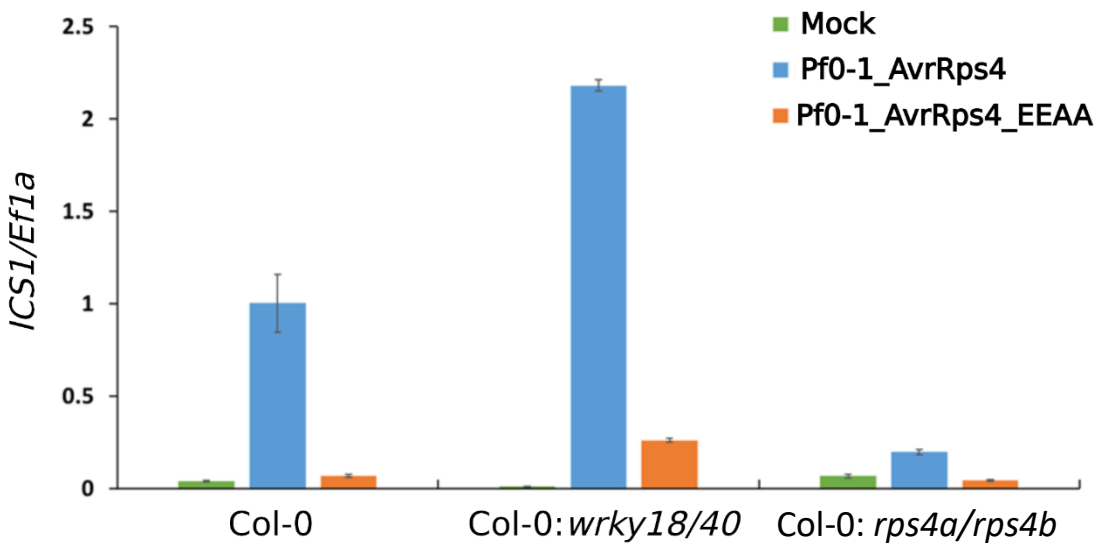

Figure 4.31. Col: *wrky18/40* has increased *ICS1* expression. *ICS1* expression in 5-week-old Arabidopsis plants infiltrated with mock or Pf0-1 and harvested after 4 hours. RNA extracted and used for qPCR. Ef1a used a control. Similar results seen in three independent biological repeats.

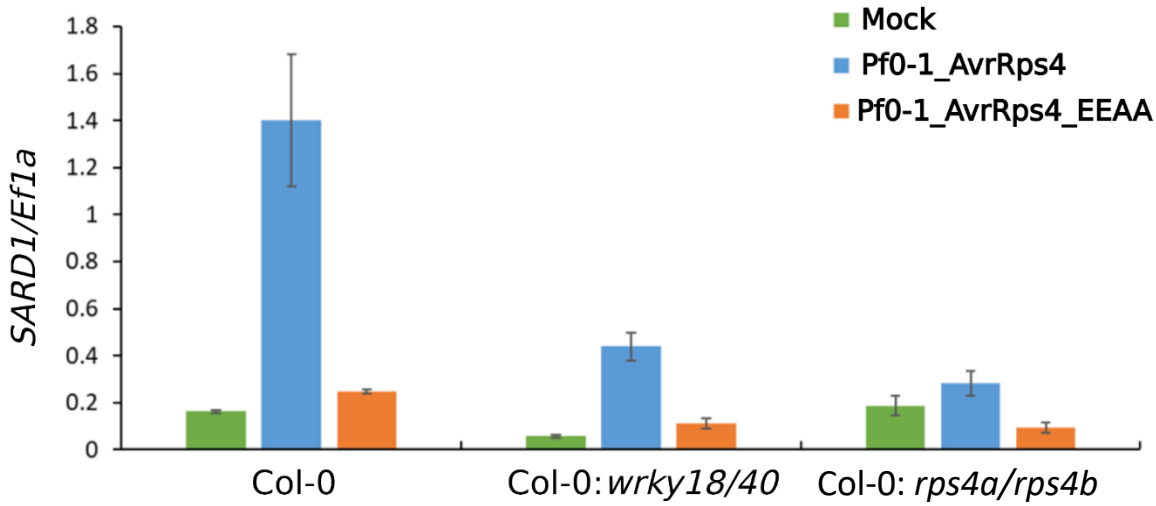

Figure 4.32. Col: *wrky18/40* has reduced *SARD1* expression. *SARD1* expression in 5-week-old Arabidopsis plants infiltrated with mock or Pf0-1 and harvested after 4 hours. RNA extracted and used for qPCR. Ef1a used a control. Similar results seen in three independent biological repeats.

4.2.3 SARD1-TurboID identified novel protein interactors

SARD1 has been reported to be a master regulator of PTI and ETI induced transcriptional changes (Sun et al., 2015). Despite this, little is known about the SARD1 protein interactions required to induce these changes. To investigate SARD1 protein interactions, SARD1-TurboID-V5 transgenic Arabidopsis plants were used for proximity labelling. Transgenic NLS-GFP-TurboID-V5 lines were used as a negative control, as SARD1 localises to the nucleus (Zhang et al., 2010b). SARD1-TurboID-V5 and NLS-GFP-TurboID-V5 biotinylate proteins upon exogenous biotin application (Figure 4.33). Biotinylated SARD1-TurboID-V5 and NLS-GFP-TurboID-V5 bands are indicated, confirming that they can biotinylate themselves as well as other proteins in close proximity after 4 hours of biotin treatment (Figure 4.33). SARD1-TurboID-V5 and NLS-GFP-TurboID-V5 have similar protein expression levels and their protein expression does not change upon biotin treatment (Figure 4.34).

Proteins were considered SARD1 interactors if they were unique to SARD1 or showed a 2x fold change increase in SARD1 compared to NLS-GFP with P-value < 0.05. 169 protein interactors of SARD1 were identified. These SARD1 interactors were enriched for GO-terms such as regulation of defence response, regulation of transcription as regulation of SA (Figure 4.35). This suggest SARD1 interactors have a similar role as SARD1 during defence activation.

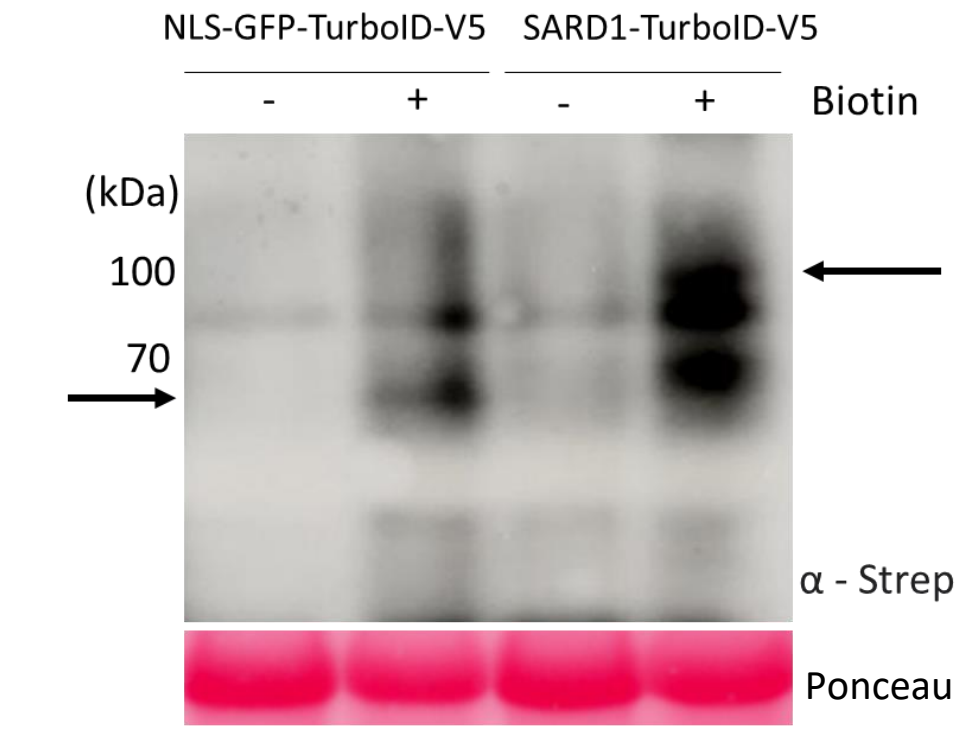

Figure 4.33. Increased levels of biotinylated proteins after 4 hours of biotin treatment. 5-week-old Arabidopsis leaves were infiltrated with 50 µM Biotin and leaves harvested after 4 hours**.**

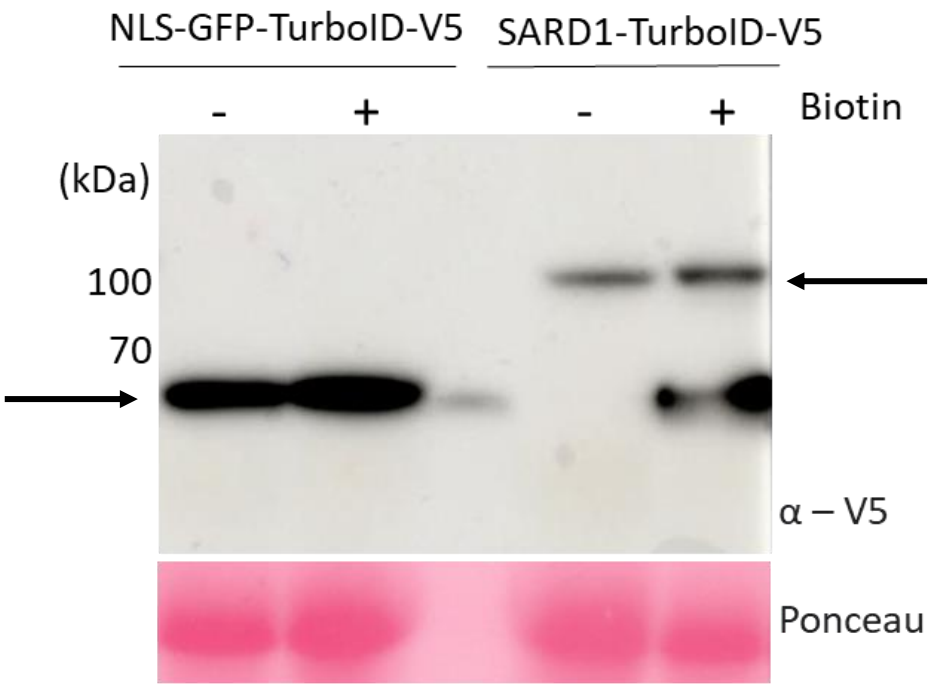

Figure 4.34. NLS-GFP-TurboID and SARD1-TurboID have similar protein expression levels. 5-week-old Arabidopsis leaves were infiltrated with 50 µM Biotin and leaves harvested after 4 hours**.**

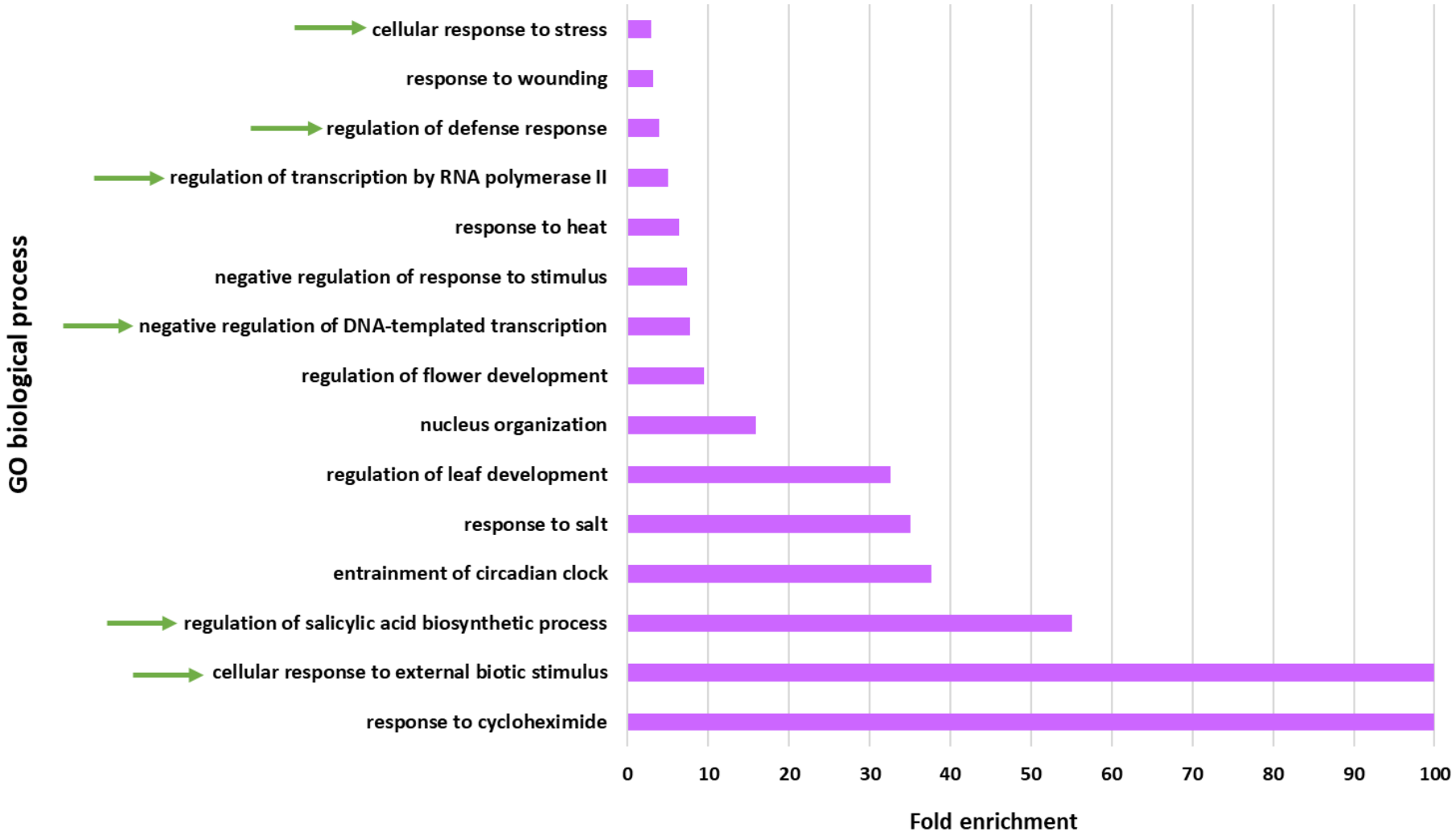

Figure 4.35. Go-term enrichment of SARD1 interacting proteins. Protein interactors of SARD1-TurboID were compared to all Arabidopsis proteins. Green arrows indicate GO-terms relating to plant immune responses. P-value < 0.05.

.

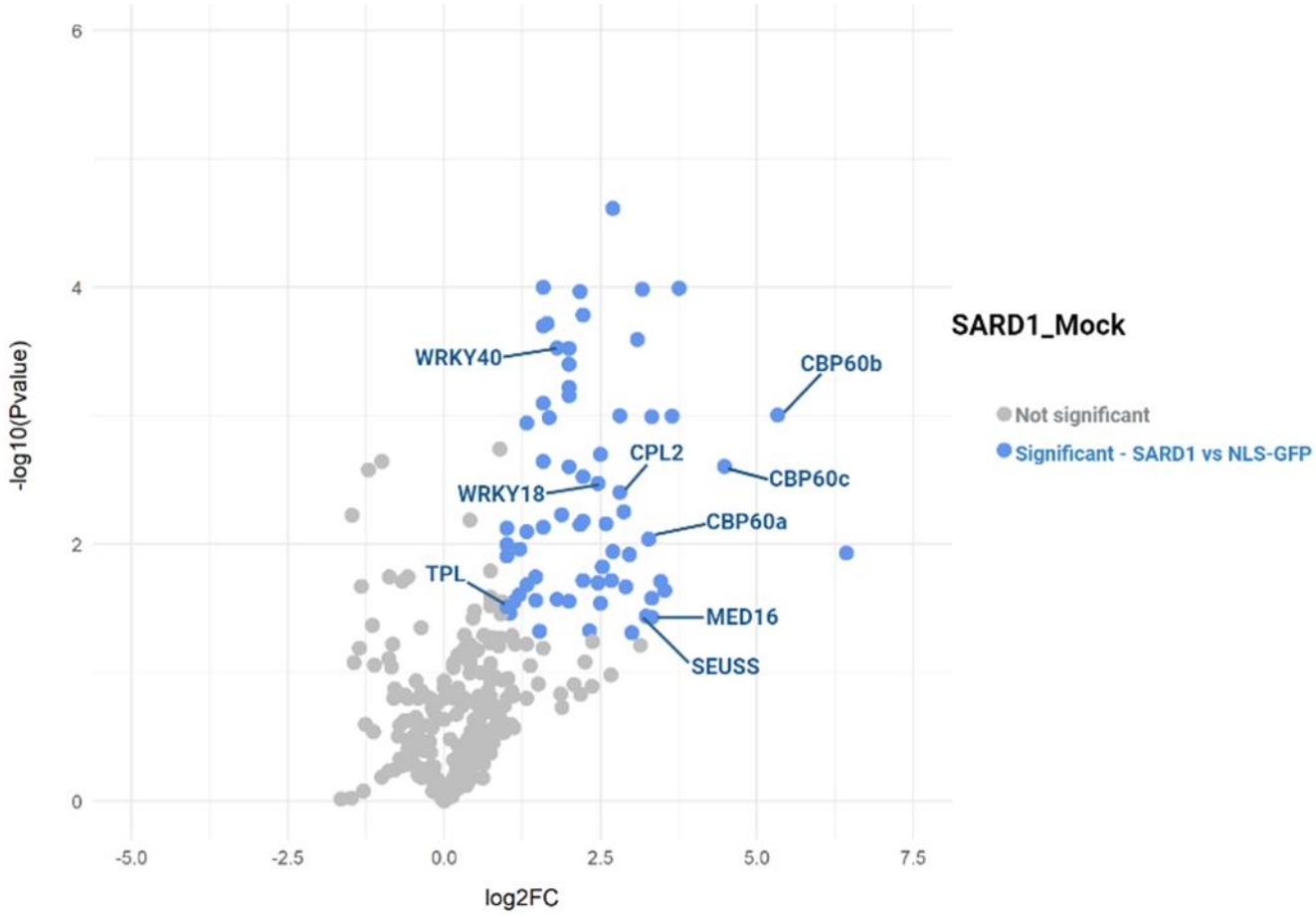

Figure 4.36. SARD1 interactors during mock treatment. Proteins were considered SARD1 interactors if they showed a 2-fold increase in biotinylation compared to NLS-GFP-TurboID and had a statistically significant difference P-value < 0.05. Biotinylated proteins not significantly different are in gray. Significant SARD1 interactors are represented in blue.

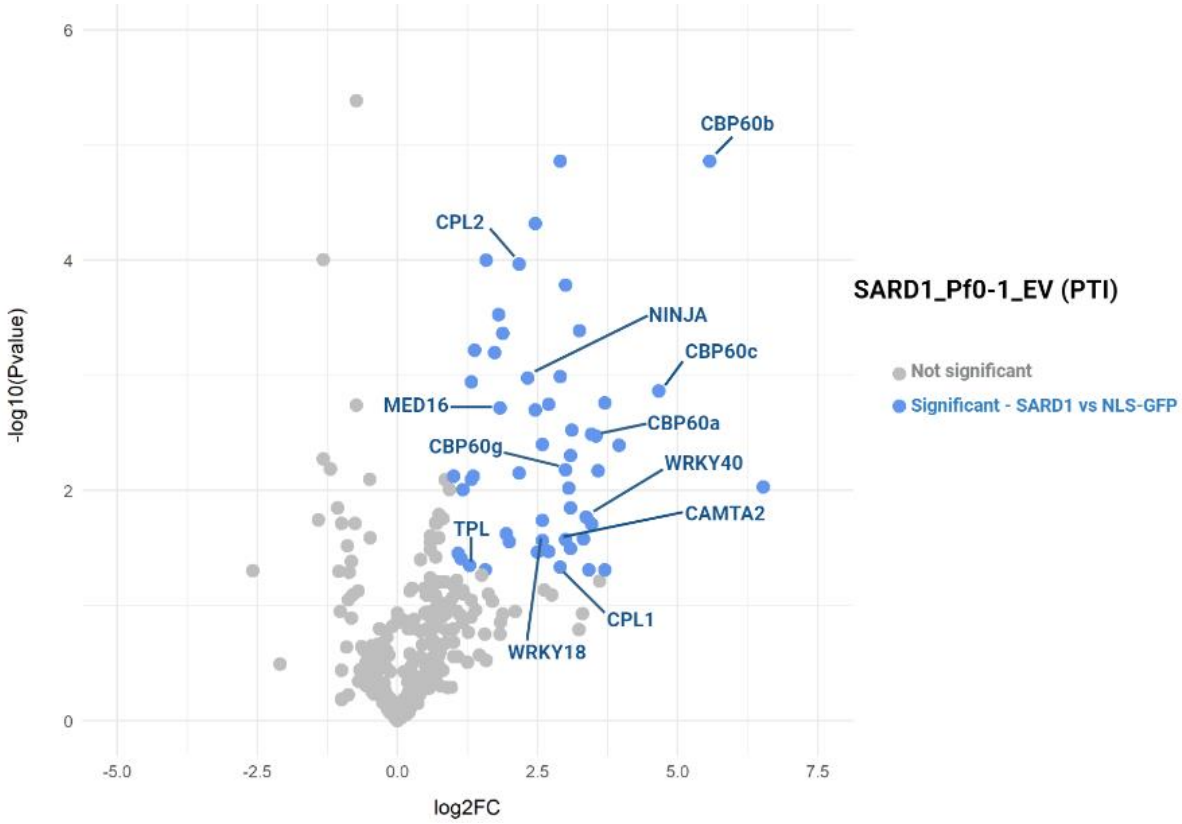

Figure 4.37. SARD1 interactors during PTI. Proteins were considered SARD1 interactors if they showed a 2-fold increase in biotinylation compared to NLS-GFP-TurboID and had a statistically significant difference P-value < 0.05. Biotinylated proteins not significantly different are in gray. Significant SARD1 interactors are represented in **blue**.

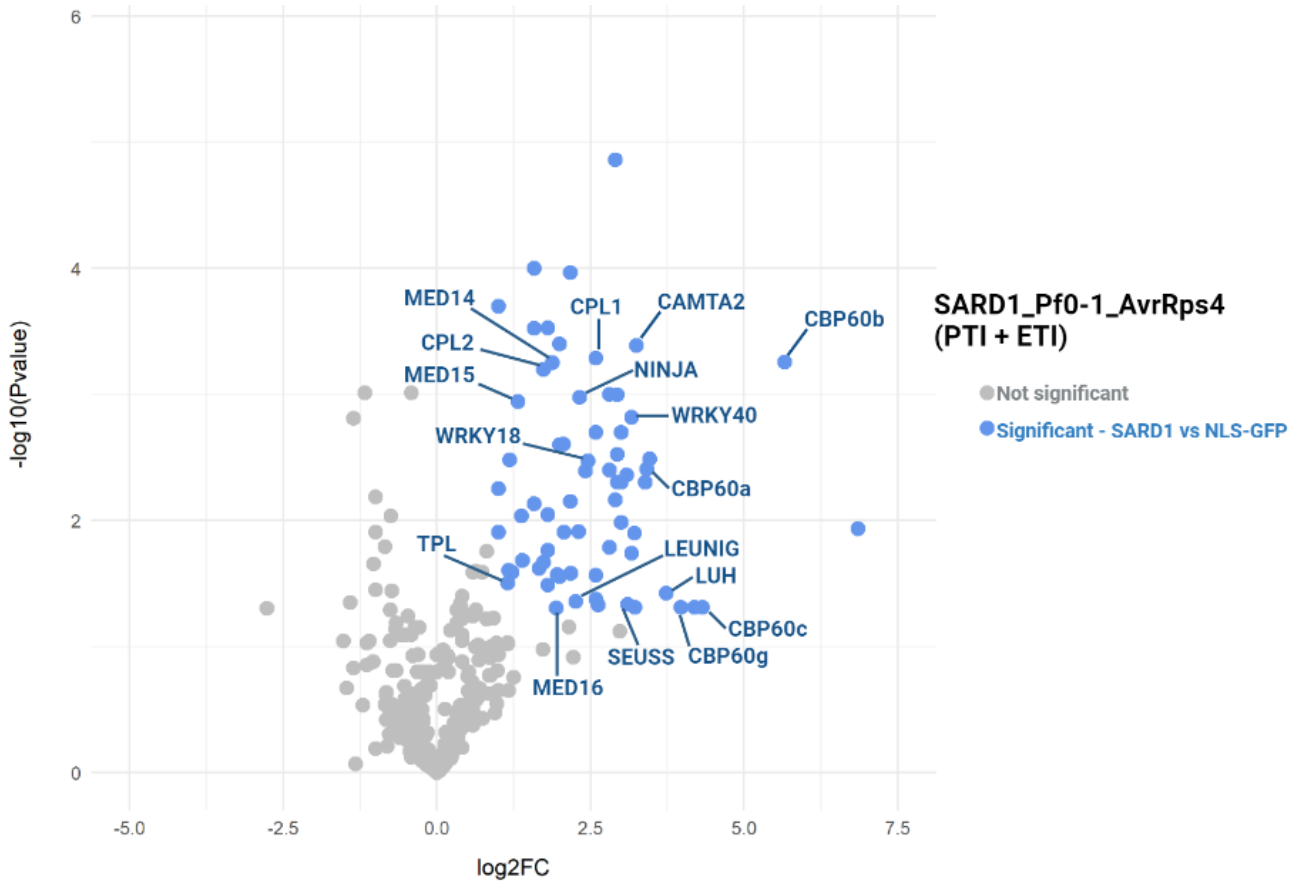

Figure 4.38. SARD1 interactors during PTI + ETI. Proteins were considered SARD1 interactors if they showed a 2-fold increase in biotinylation compared to NLS-GFP-TurboID and had a statistically significant difference P-value < 0.05. Biotinylated proteins not significantly different are in gray. Significant SARD1 interactors are represented in blue.

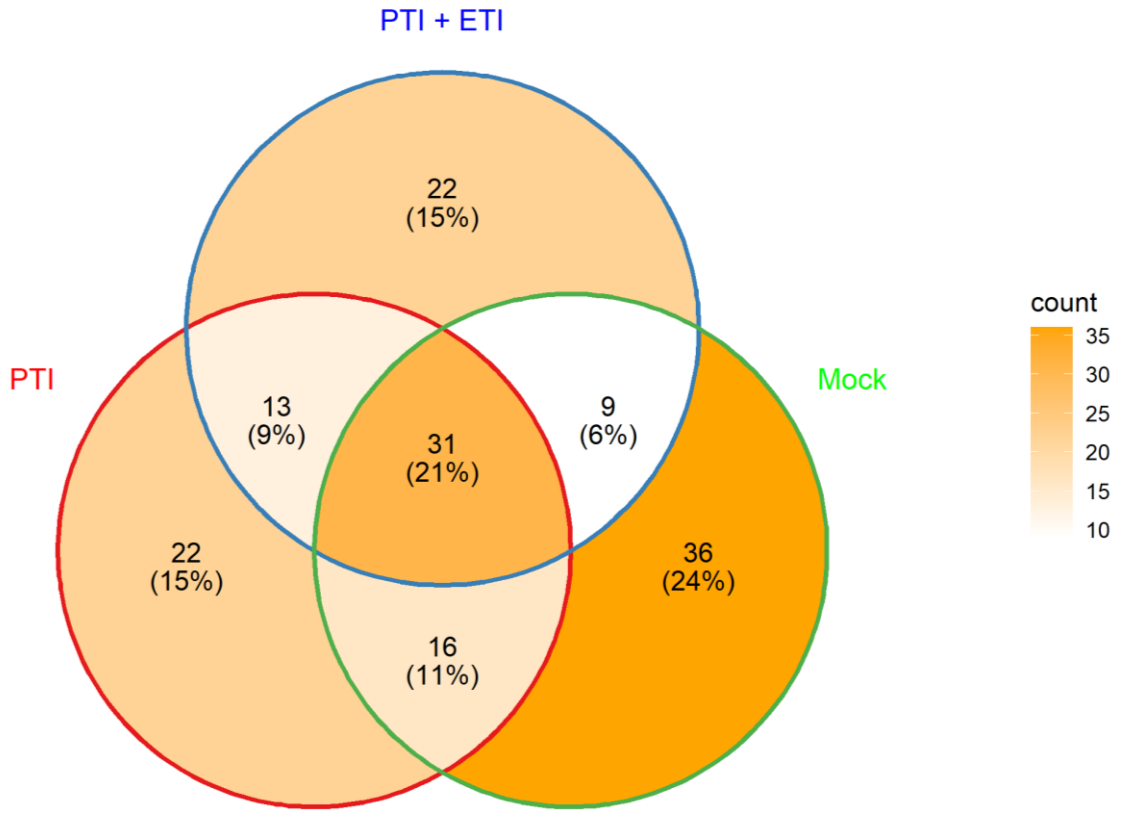

Figure 4.39. Some SARD1 proteins interactors are common between mock, PTI and PTI + ETI treatments , in addition to some unique to each treatment. Proteins were considered SARD1 interactors for each treatment if they were unique to SARD1-TurboID or showed a 2-fold increase in biotinylation compared to NLS-GFP-TurboID and had a statistically significant difference P-value < 0.05. Protein interactors for each immunity treatment were compared to create a Venn diagram. Percentages represent total protein population of SARD1 interactors.

92 proteins interact with SARD1 in mock samples, 74 proteins interact during PTI signalling and 81 during PTI + ETI signalling (Supplementary Table 6). Many SARD1 protein interactors overlap between PTI and PTI+ ETI signalling (Figure 4.39). There are also some proteins unique to each signalling treatment (Figure 4.39), providing an insight into how SARD1 signalling may differ between the immunity treatments. 6 proteins had higher biotinylation upon PTI activation and 10 proteins upon PTI + ETI activation compared to mock (Supplementary Table 5). CBP60g has enhanced interaction during both PTI and PTI + ETI activation compared to mock (Supplementary Table 5). SARD1 works redundantly with CBP60g as master transcriptional regulators of immunity (Sun et al., 2015, Ding et al., 2020). Therefore, they may interact to positively regulate each other and further enhance defence signalling.

SARD1 interacts with other calmodulin binding proteins in the same protein family. CBP60a, CBP60b, CBP60c all interact with SARD1 in mock, PTI and PTI + ETI samples (Figures 4.36-38 and Supplementary Table 6). CBP60b was highly biotinylated by SARD1 in all samples, suggesting the interaction is very abundant. CBP60b acts a positive regulator of plant defence and directly promotes *SARD1* expression (Huang et al., 2021). CBP60b is partially redundant with CBP60g and SARD1 and binds to the same promoters e.g. *SID2* and *PAD4* (Li et al., 2021) (Li et al., 2021). Therefore, SARD1 may interact with CBP60b to enhance immune responses.

When the immunity treatments are grouped, CBP60d was also identified as a SARD1 interactor. The role of CBP60c and CBP60d is currently unknown. CBP60a is reported to be a negative regulator of plant immunity (Truman et al., 2013). Another calmodulin-binding protein CAMTA2 also interacts with SARD1 in PTI and PTI + ETI samples (Figures 4.37 and 4.38). CAMTA2 was first reported to be a negative regulator of SA genes *ICS1*, *SARD1*, *CBP60g* and *PR1* (Kim et al., 2013). Therefore, the role of SARD1 interaction with CBP60a, CBP60b, CBP60d and CAMTA2 during immune responses should be further explored.

SARD1 interacts with mitogen-activated protein kinase 11 (MPK11) during PTI activation (Figure 4.37 and Supplementary Table 6). MPK11 is activated upon flg22 detection (Bethke et al., 2012). Therefore, this finding might provide insight into how MAPK activation leads to downstream responses, through SARD1 interaction. ZIN1 is suggested to be a DNA-binding protein with topoisomerase-like activity and acts as a susceptibility gene in Arabidopsis, targeted by multiple effectors to enhance pathogen virulence (Schreiber & Lewis, 2021). ZIN1 interacts with SARD1 during PTI activation (Figure 4.37 and Supplementary Table 6).

4.2.3.1 SARD1 interacts with components of mediator

Two mediator subunits (MED14 and MED15) show enhanced SARD1 interaction upon PTI or PTI + ETI activation compared to mock (Supplementary Table 5). Another mediator subunit MED16 interacts with SARD1 in mock, PTI and PTI + ETI treated samples (Figures 4.36-4.38 and Supplementary Table 6). MED14, MED15 and MED16 are required for SA induction of *PR1* expression (Wang et al., 2016). Additionally, MED14, MED15 and MED16 repress JA-induced responses to fine tune defence responses (Wang et al., 2016). Therefore, MED14, MED15 and MED16 may positively regulate SA responses by interacting with SARD1. CDK8, a component of the kinase module in the Mediator complex, also interacts with SARD1 during PTI + ETI activation, but this interaction was not statistically significant to mock treatment. Another mediator subunit (MED12) was found to be a SARD1 interactor

when the immunity treatments were grouped, as it was only present once in each immunity treatment but present in multiple biological repeats (Supplementary Table 5). As SARD1 interacts with five mediator subunits, this suggests SARD1 forms a complex with mediator to activate PTI + ETI-induced transcriptional changes.

C-terminal domain phosphatase-like 1 (CPL1) has enhanced interaction with SARD1 during PTI and PTI + ETI activation compared to mock, suggesting the interaction is important for defence signalling (Supplementary Table 5). CPL2 also interacts with SARD1 during mock, PTI and PTI + ETI (Figures 4.36-4.38 and Supplementary Table 6). CPL1 and CPL2 have been shown to dephosphorylate Arabidopsis RNA polymerase II (Koiwa et al., 2004). Therefore, SARD1 may interact with CPL1 and CPL2 to regulate the activity of RNA polymerase II during an immune response and activate transcriptional changes.

4.2.3.2 SARD1 interacts with other transcriptional regulators

SEUSS, LUH and Leunig are very highly biotinylated by SARD1 compared to controls suggesting their interaction is strong (Supplementary Table 6). LUH and Leunig interact with SARD1 during PTI + ETI activation (Figure 4.38). SEUSS-L1, SEUSS-L2 and SEUSS interact with SARD1 in mock, PTI and PTI + ETI treated samples (Figures 4.36-4.38 and Supplementary Table 6). This suggests a role novel for these proteins in transcriptional programming during immune responses.

Topless family proteins were found to be SARD1 interactors (Supplementary Table 6). TPL, TPR1, TPR2 and TPR3 interact with SARD1 in mock samples and interact with SARD1 during PTI and/or PTI + ETI activation (Figures 4.36-4.38 and Supplementary Table 6). This suggests Topless-related proteins may act to fine tune transcriptional responses through interactions with SARD1, with TPR2/TPR3 acting to suppress ETI and TPR1/TPL acting as positive regulators.

WRKY40 has enhanced biotinylation during PTI + ETI compared to mock, suggesting its interaction with SARD1 is enhanced during PTI + ETI signalling (Supplementary Table 5). SARD1 also interacts with WRKY18 in mock samples and during PTI and PTI + ETI activation (Figures 4.36-4.38). SARD1 only interacts with WRKY6 during PTI + ETI activation (Figure 4.38 and Supplementary Table 5), suggesting this interaction is induced by upstream PTI + ETI signalling. Therefore, SARD1 may interact with WRKY proteins to regulate transcriptional responses.

NINJA interacts with SARD1 during PTI and PTI + ETI activation (Figures 4.37, 4.38 and Supplementary Table 6). NINJA negatively regulates JA responses (Pauwels et al., 2010). Therefore, SARD1 may

interact with NINJA to activate NINJA-induced inhibition of JA signalling. NINJA also interacts with EDS1, suggesting that both EDS1 and SARD1 interact with NINJA to promote NINJA activity, suggesting a novel pathway whereby JA signalling is repressed upon ETI activation.

4.2.3.3 WRKY18 EAR motif is not required for SARD1 interaction

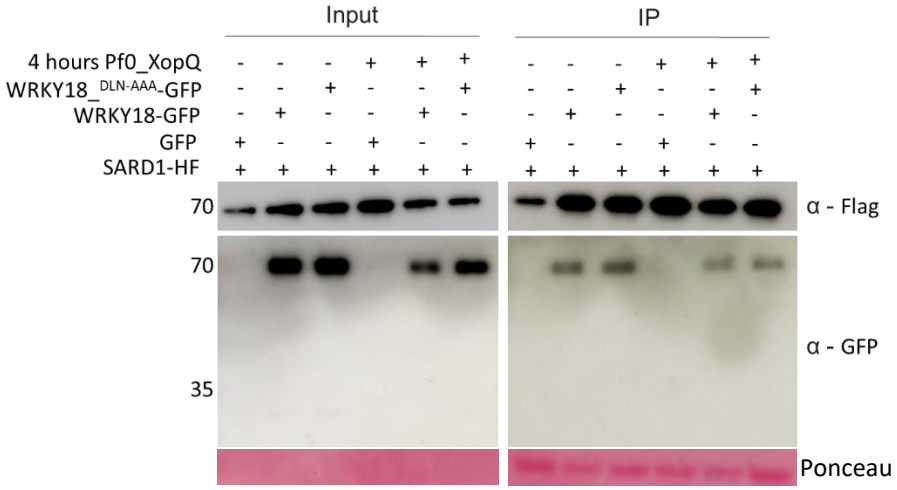

Figure 4.40. SARD1-HF interacts with WRKY18 and WRKY18$^{DLN-AAA}$-GFP. SARD1-HF and WRKY18-GFP or WRKY18$^{DLN-AAA}$-GFP were co-expressed in *N. benthamiana* and Flag proteins immunoprecipitated. GFP was used as a negative control. 48 hpi leaves were infiltrated with Pf0-1_XopQ and samples harvested 4 hours later. Similar results seen for two independent biological repeats.

WRKY18 was identified as a SARD1 interactor by TurboID. Therefore, we tested and confirmed the interaction by co-immunoprecipitation after transient expression in *N. benthamiana* (Figure 4.40). The interaction was not found to change upon Pf0-1_XopQ treatment, suggesting ETI does not enhance the interaction (Figure 4.40). Additionally, the WRKY18 DLN or LxIxL EAR motif is not required for interaction with SARD1 (Figure 4.40 and 4.41). Therefore, another interaction domain facilitates the WRKY18-SARD1 interaction. The role of SARD1-WRKY18 interaction during ETI activation and regulating transcriptional changes needs to be further explored. As SARD1 localises to the nucleus (Zhang et al., 2010b), it would be interesting to test if co-expression of WRKY18 alters SARD1 localisation into nuclear puncta, as seen for TPR1.

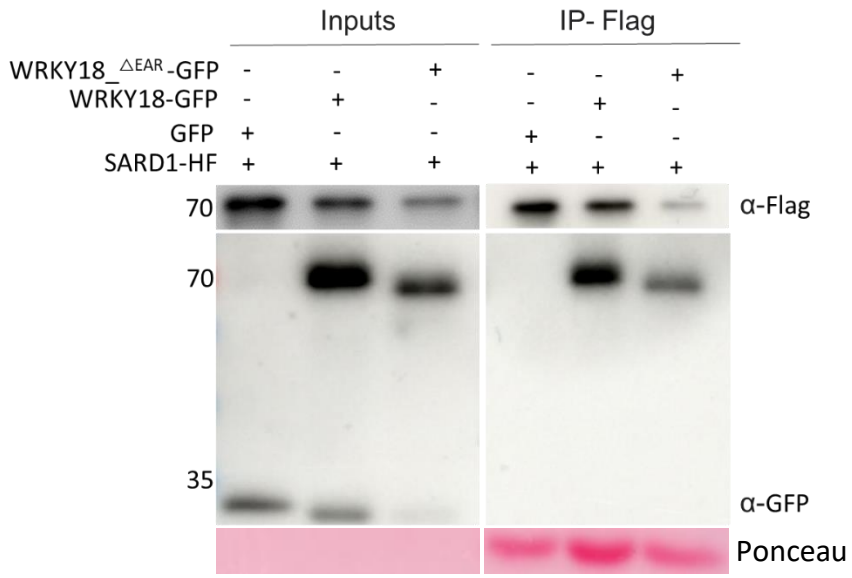

Figure 4.41. WRKY18 EAR domain deletion does not disrupt interaction with SARD1-HF. SARD1-HF and WRKY18-GFP or WRKY18$^{\triangle EAR}$-GFP were transiently co-expressed in *N. benthamiana*, followed by immunoprecipitation of SARD1-HF. GFP was used as a negative control. Samples were harvested 48 hpi. Represents three independent biological repeats.

4.3 Discussion

4.3.1 Proximity labelling reveals novel interactors of SARD1, EDS1 and TPR1

We utilised a proximity labelling method to independently test some reported interactions and to confirm known protein interactions, in addition to identifying novel interactions upon defence activation. ADR1-L1 interacts with EDS1-PAD4 upon TIR-NLR NADase activation that leads to pRIB-ADP/AMP synthesis, to activate downstream signalling (Lapin et al., 2019, Saile et al., 2020, Pruitt et al., 2021, Huang et al., 2022). ADR1-L1 interacts with EDS1 upon immune activation in our study. ADR1-L1 was biotinylated upon PTI activation, but biotinylation increased upon ETI activation. This supports previous literature where ETI activation increased the amount of EDS1 biotinylation by ADR1-L1-TurboID (Wu et al., 2021). However, the enhanced biotinylation was not found when an NADase-dead TIR-NLR was used, confirming that TIR-NLR NADase activity induces EDS1-PAD4-ADR1 heterotrimer formation (Wu et al., 2021, Huang et al., 2022). ADR1-L1 acts redundantly with ADR1 and ADR1-L2 during NLR-mediated immunity (Bonardi et al., 2011, Saile et al., 2020). Therefore, we would expect to find ADR1 and ADR1-L2 biotinylated by EDS1 in addition to ADR1-L1. However, ADR1 and ADR1-L2 were not biotinylated by EDS1 in our dataset. A previous protein interactome study reported ADR1-L1 interaction with PAD4 (Dongus et al., 2022). However, the paper did not report an interaction between PAD4 and ADR1, or ADR1-L2. Therefore, the EDS1-PAD4-ADR1-L1 association

may be stronger than the EDS1-PAD4 association with ADR1 or ADR1-L2, revealing differences between these redundant helper NLR proteins.

TPR1 and TPL act redundantly as transcriptional co-repressors. However, the exact role of TPL/TPR1 is difficult to unpick, with *tpl/tpr1/tpr4* mutants showing few differences compared to WT in transcriptional regulation or defence activation. We identified TPR1 interactors during PTI and PTI + ETI activation, including WRKYs, NINJA and LEUNIG-like. 10% of TPR1 interactors are described as transcription-related, suggesting TPR1 may form complexes with transcription factors to regulate transcriptional changes during immune responses. Therefore, our TPR1-TurboID dataset provides insight into how TPR1 may signal during defence activation. One limitation of our study is that we did not include a mock TurboID sample. Therefore, we were not able to identify protein interactors that were induced upon PTI or PTI + ETI activation and absent in mock.

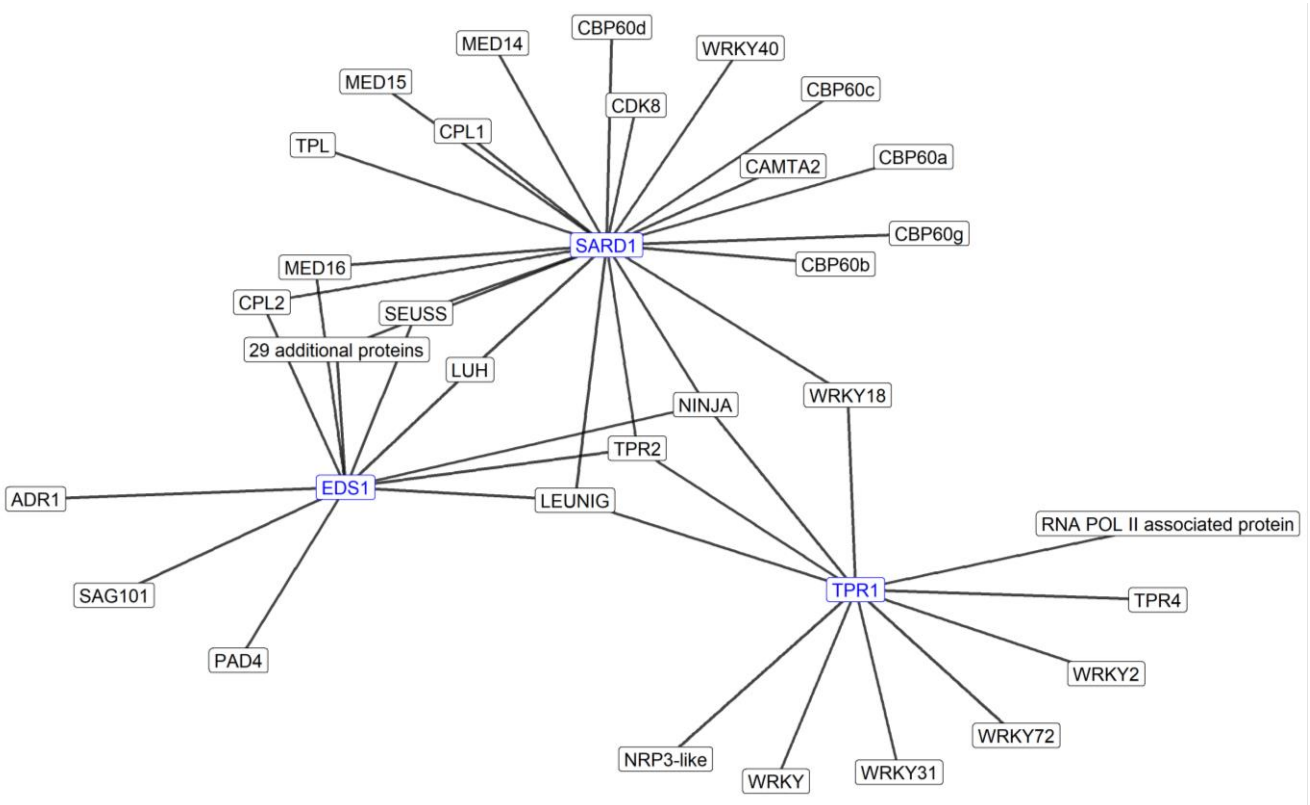

Figure 4.42 EDS1, TPR1 and SARD1 share common protein interactors. Network of proteins classed as protein interactors of SARD1, EDS1 and TPR1 by TurboID proximity labelling.

We found common protein interactors between TPR1, EDS1 and SARD1, including 36 proteins which interact with both EDS1 and SARD1, suggesting a core signalling hub for regulation of defence gene transcription (Figure 4.42). Mediator subunits and RNA polymerase II C-terminal domain phosphatase-like 2 (CPL2) both interact with EDS1 and SARD1 (Figure 4.42), suggesting a mechanism whereby transcriptional responses are activated upon upstream ETI activation. LEUNIG-homolog (LUH) and NINJA were found to be common interactors of SARD1, EDS1 and TPR1 (Figure 4.42). In addition, SEUSS and LEUNIG interacted with both EDS1 and SARD1 (Figure 4.42). The activity of SEUSS and LEUNIG during plant immunity has not been reported. However, LEUNIG mutant *lug*-3 results in upregulation of immune receptor genes RPP4, RPP5 and SNC1, suggesting LEUNIG is a negative regulator of plant defence (Gonzalez et al., 2007). Therefore, SARD1 and EDS1 may interact with LEUNIG to inhibit its activity as a negative regulator. MED14, CDK8 and LEUNIG interact during LEUNIG-mediated transcriptional repression (Gonzalez et al., 2007). SEUSS was also found to interact with MED14 and CDK8 (Gonzalez et al., 2007). Additionally, HDA19 interacts with LEUNIG to repress gene transcription (Gonzalez et al., 2007). We found SARD1 to interact with HDA19, CDK8, MED14, LEUNIG and SEUSS. Therefore, SARD1 may be interacting with the SEUSS-LEUNIG-MED14-CPK8 complex and with SEUSS-LEUNIG-HDA19 to regulate their transcriptional repression activity. Whether these protein complexes function to repress negative or positive regulators of plant defence is not clear. However, HDA19 has been reported to deacetylate histones at the PR1 promoter to repress PR1 gene expression both before and after pathogen infection (Choi et al., 2012). Therefore, SARD1 may interact with these protein complexes to relieve repression of defence genes. Our study reveals potential novel mechanisms for transcriptional regulation during plant immunity.

EDS1 and SARD1 both interact with the negative regulator of plant immunity TPR2, suggesting these two positive regulators may inhibit TPR2 activity. Alternatively, TPR2 may be targeting EDS1 and SARD1 to inhibit ETI defence activation. Therefore, the role of TPR2-EDS1 and TPR2-SARD1 interaction needs to be investigated to further understand the mechanisms of negative regulators of defence.

We found very few proteins with an enhanced interaction upon PTI, ETI or PTI + ETI activation compared to mock. This may be due to small changes in protein interactions upon defence activation which cannot be detected by the TurboID-based PL-MS method. Additionally, some protein interactions may be constitutive and defence-induced cellular signals (e.g. Ca^{2+} or ROS) may induce conformational changes within the protein complexes to activate downstream signalling.

4.3.2 The importance of the EAR-motif dependent TPR1 puncta localisation needs to be further investigated

We have shown that TPR1 and WRKY18 co-localise to the nucleus in puncta when co-expressed in *N. benthamiana*. This co-localisation is lost in the WRKY18$^{\triangle EAR}$ mutant, suggesting the EAR motif is important for TPR1 co-localisation. The mechanism behind this is not clear, as the EAR motif is not required for their interaction as assayed by Co-IP. One possibility is that the WRKY18 EAR motif is important for interaction with a third protein, bringing that protein into close proximity to TPR1, which then alters TPR1 localisation into nuclear puncta. To test if the WRKY18 EAR domain does play a role in protein interactions, we have made WRKY18-TurboID and WRKY18$^{\triangle EAR}$– TurboID constructs. This will allow us to identify EAR-domain dependent protein interactors.

The nuclear localisation of TPR1 has previously been reported. During low levels of SA, TPR1 is localised to the cytosol (Xu et al., 2021). High levels of SA promote TPR1 accumulation in the nucleus (Xu et al., 2021). However, TPR1 nuclear accumulation is inhibited by Exportin-4 (XPO4), a protein which facilitates the translocation of signalling molecules through the nuclear pore complex (Xu et al., 2021). TPR1 localisation was determined by protein extraction and fractionation, showing TPR1 levels in the different protein fractions by immunoblotting (Xu et al., 2021). We found nuclear TPR1 localisation in untreated (Agro-induced PTI) and PTI + ETI treated (Pf0-1_XopQ) *N. benthamiana* leaves. Our data suggest TPR1 nuclear localisation does not change upon ETI activation and therefore upon induction of high SA levels. One explanation for the contrasting results may be that *At*TPR1 cannot be exported out the nucleus by *Nb*XPO4. The XPO4 homolog in *N. benthamiana* Nbv6.1trP2126 (*Nb*blastn) was not found to interact with *At*TPR1 in our study, supporting this suggestion. Therefore, TPR1 nuclear localisation should be further investigated in Arabidopsis with confocal images, before and after ETI activation.

4.3.3 The role of EAR domains in TPR1 protein interactions

TPR1 biotinylates a NINJA-family protein during PTI activation, suggesting it is interacting with TPR1. NINJA has previously been found to interact with TPL/TPRs via an EAR domain in NINJA (Pauwels et al., 2010). Additionally, the NINJA EAR motifs are required for transcriptional repression (Ke et al., 2015). Therefore, whether the EAR domain in NINJA is important for TPR1 interaction and activation of transcriptional repression during PTI responses should be investigated. Hydrophobic grooves in the TPL CTLH N-terminal domain are important for interaction with EAR-motif interactors e.g. auxin protein INDOLE-3-ACETIC ACID INDUCIBLE 12 (IAA12) and plant growth factor WUSCHEL (Martin-

Arevalillo et al., 2017, Szemenyei et al., 2008). NINJA EAR motif also binds hydrophobic grooves in the TPD of the rice protein OsTPR2 (Ke et al., 2015). OsTPR2 forms a tetramer and each monomer binds a NINJA EAR motif (Ke et al., 2015). The binding groove in OsTPR2 TPD is also conserved in interactions with other LxLxL EAR-containing proteins e.g. IAA10 and IAA1 (Ke et al., 2015). The TPL/TPR TPD also binds to nucleosomes (Ma et al., 2017). Repressive methylation signatures H3 K9 and H4 K20 increased TPD binding to histones, confirming their role as transcriptional co-repressors (Ma et al., 2017). The EAR motif in the protein DWARF53 (D53) involved in strigolactone signalling, binds two sites in the N-terminal TPD of TPL/TPRs (Ma et al., 2017). The first is the binding groove conserved with NINJA interaction and the second site is located at the TPR2 dimerization interface (Ma et al., 2017). D53 interaction promotes TPR2 tetramer-tetramer interaction (Ma et al., 2017). TPL/TPRs interaction with nucleosomes is stabilised by interacting with the D53 EAR motif but not with the NINJA EAR motif, suggesting the tetramer-tetramer interaction, induced by D53 EAR binding at two sites, is required to enhance nucleosome interaction stability (Ma et al., 2017). Therefore, EAR motif interactions induce TPL/TPR oligomerisation, interactions with the nucleosome and possible formation of higher complexes. Additionally, binding grooves in the TPD of TPL/TPRs provide a conserved interaction interface for EAR-motif proteins. We identified 29 potential TPR1 interacting proteins described as involved in transcription in their gene name, in addition to an RNA polymerase II-associated protein. 10 of these proteins contain an EAR motif, including RNA POL II-associated protein. Therefore, it should be investigated if these EAR domains are important for TPR1 interaction and if they are required for TPR1-regulated transcriptional repression during immune signalling.

A non-EAR motif containing protein RELATED TO ABI3/VP1 1 (RAV1) interacts with the first nine WD40 repeats in TPL (Collins et al., 2019). Despite 92% protein similarity and high genetic redundancy between TPL and TPR1, RAV1 does not bind TPR1, suggesting sequence differences in the WD40 region are important for interaction with TPL (Collins et al., 2019). Another protein VERNALIZATION 5 (VRN5) interacts with the latter eight WD40 repeats (Collins et al., 2019). Therefore, there are protein interaction domains within both the TPL/TPR N-terminal TPD and C-terminal WD40 repeat domains. Therefore, the requirement of the N-terminal TPD or WD40 repeat region in protein interactions during PTI + ETI signalling should be tested, by mutating different regions of the N-terminal TPD or WD40 C-terminus of TPR1 and performing Co-IPs or Yeast-2-hybrid assays with TPR1 potential interactions. If multiple immune-related proteins share a conserved TPR1 interface, this may provide insight into structural mechanisms behind transcriptional regulation.

4.3.4 The role of WRKY18 in transcriptional regulation during PTI or PTI + ETI signalling is not clear.

WRKY18 was identified as an interactor of both TPR1 and SARD1 using proximity labelling. We confirmed both these interactions using Co-IP. Unfortunately, we were not able to identify a change in the protein interactions upon Pf0-1_XopQ treatment, suggesting PTI + ETI does not weaken or strengthen their interaction. Therefore, the biological role of this interaction is not clear.

WRKY18 was found to be enriched at a set of defence gene promoters upon flg22 treatment. (Birkenbihl et al., 2017). However, we found no difference in gene expression between Col-0 and *wrky18/wrky40* plants in the five genes we tested, suggesting WRKY18 and WRKY40 are not solely required for their expression. WRKY18 has often been reported as redundant with and studied alongside WRKY40 (Schon et al., 2013, Birkenbihl et al., 2017). However, phylogenetic trees place WRKY60 and WRKY18 most closely related, followed by WRKY40 (Wang et al., 2011b, De Paolis et al., 2020). Additionally, WRKY18 and WRK60 share 58% protein similarity, whereas WRKY18 and WRKY40 only share 41% (T-Coffee alignment). Therefore, this may explain why we did not see a difference in gene expression in the *wrky18/wrky40* mutant. To test if WRKY60 acts redundantly with WRKY18, to regulate gene expression upon flg22 treatment, a *wrky18/wrky40/wrky60* triple mutant should be investigated.

Elevated expression of WRKY18 leads to stunted growth, resistance to DC3000 and high PR1 levels (Chen & Chen, 2002). However, constitutive overexpression of both WRKY18 and WRKY40 or WRKY60 resulted in more susceptible plants and abolished the constitutive *PR1* expression in 35S:WRKY18 plants (Xu et al., 2006b). This suggests 35S:WRKY60 and 35S:WRKY40 antagonise 35S:WRKY18 resistance (Xu et al., 2006b). Therefore, the relationship between WRKY18, WRKY40 and WRKY60 during different immunity states is complex and needs further investigation in order to understand the role of each WRKY protein during plant immunity signalling.

WRKY18 has previously been found to bind the *ICS1* promoter (Birkenbihl et al., 2017). No enrichment of binding was found after flg22 treatment, suggesting WRKY18 does not mediate PTI-induced increases in *ICS1* expression (Birkenbihl et al., 2017). However, *ICS1* expression was increased in the *wrky18/40* mutant compared to wildtype plants after flg22 treatment (Birkenbihl et al., 2017). This suggests WRKY18 and WRKY40 negatively regulate *ICS1* expression during PTI activation, supporting our finding that WRKY18 and WRKY40 negatively regulate *ICS1* expression upon PTI + ETI activation. However, we also found that WRKY18 and WRKY40 positively regulate *SARD1* expression. Therefore,

how WRKY18 differentially regulates different SA biosynthesis genes is not clear. WRKY18 may form different heterodimers with other transcription factors, which determine if WRKY18 activates or represses transcription of SA genes. WRKY18-TurboID would provide insight into these different protein interactors, enhancing our understand of the mechanisms underpinning transcriptional regulation.

WRKY18 and WRKY40 act as negative or positive regulators of immunity in response *to* different pathogens (Xu et al., 2006b, Schon et al., 2013). *wrky18*, *wrky18/40* and *wrky18/40/60* plants have enhanced resistance to DC3000, suggesting they are negative regulators of immunity to *Pst* DC3000 (Xu et al., 2006b). However, WRKY18 and WRKY40 are positive regulators of immunity in response to *Pst* DC3000 AvrRps4, as *wrky18/40* plants are more susceptible (Schon et al., 2013). This requirement of WRKY18 and WRKY40 is specific against *Pst* DC3000 AvrRps4 and not specific to *P. syringae* or for TIR-NLR signalling, as resistance was not compromised in *wrky18/wrky40* plants in response to *Pst* AvrRpm1 or *Pst* HopA1 (Schon et al., 2013). No direct interactions between RPS4 and WRKY18 and WRKY40 could be observed (Schon et al., 2013). The specific requirement of WRKY18 and WRKY40 during AvrRps4 immunity and why WRKY18 and WRKY40 appear to have no function in response to AvrRpm1 or HopA1 needs to be further explored.

WRKY18 is recruited to the NPR1 promoter during SA signalling (Chen et al., 2019). It has been proposed that WRKY18 acts as a transcriptional activator of NPR1 expression (Chen et al., 2019). It would be interesting to test this, to further understand WRKY18's role as a transcriptional regulator of ETI signalling. In addition, WRKY18 interacts with the kinase CDK8 (Chen et al., 2019). Conceivably, CDK8 phosphorylates WRKY18 and CDK8 could be responsible for the ETI-induced phosphorylation sites identified in Chapter 3. WRKY18 also binds to the EDS1 promoter, but no change was found after flg22 treatment (Birkenbihl et al., 2017). As WRKY18 binds to the promoters of important ETI proteins, the role of WRKY18 in regulating transcriptional changes during ETI activation needs to be more extensively investigated with RNA-seq.

This proximity labelling study provides some interesting new leads and reveals novel protein interactions during PTI + ETI activation. We have identified multiple proteins which interact with both an upstream defence protein that interacts with helper NLRs (EDS1), and a downstream transcription factor regulating gene expression upon defence activation (SARD1 and TPR1). Additionally, we have identified novel protein interactors unique to each protein. Therefore, these novel protein interactors could help further develop our understanding of ETI signalling and in particular, how heterotrimer

formation induces transcriptional activation. The protein interactions identified in this study need be further tested in Arabidopsis, testing co-localisation, a role in regulating EDS1 heterotrimer/resistosome formation, identifying important protein interaction domains or performing transcriptional reporter assays to reveal their biological importance.

Chapter 5

Effector-triggered hypersensitive response is dependent on phosphorylation of NRG1

5 Effector-triggered hypersensitive response is dependent on phosphorylation of NRG1

5.1 Introduction

5.1.1 NRG1 requires PTI + ETI activation for oligomerisation

Hypersensitive response (HR) is a localised cell death at the site of pathogen entry, to prevent pathogen spread throughout the whole leaf (Stakman, 1915). HR is associated with resistance triggered by nucleotide-binding and leucine-rich repeat intracellular receptor (NLR)-effector recognition. N REQUIREMENT GENE 1 (NRG1) is a helper NLR, which functions downstream of TIR-NLRs (Qi et al., 2018, Castel et al., 2019). Upon effector recognition and TIR-NLR activation, NRG1 forms heterotrimers with SENESCENCE-ASSOCIATED GENE 101 (SAG101) and ENHANCED DISEASE SUSCEPTIBILITY 1 (EDS1) to activate HR (Lapin et al., 2019). Effector-triggered immunity (ETI), in the absence of pattern-triggered immunity (PTI), is sufficient to induce NRG1-EDS1-SAG101 associations in Arabidopsis (Feehan et al., 2023). However, both ETI and PTI are required to form NRG1-EDS1-SAG101 resistosomes and induce NRG1 oligomerisation (Feehan et al., 2023). Therefore, we hypothesise there must be biochemical signatures(s) during PTI + ETI, but not ETI alone, required for NRG1 oligomerisation. Phosphorylation plays an important role in PTI signalling (Benschop et al., 2007). PTI + ETI leads to prolonged phosphorylation of PTI signalling components e.g. MITOGEN-ACTIVATED PROTEIN KINASES (MAPK) and RESPIRATORY BURST OXIDASE PROTEIN D (RBOHD) (Ngou et al., 2020a, Yuan et al., 2020). This stronger phosphorylation is caused by the potentiation of PTI by ETI, as estradiol-inducible *AvrRps4* (ETI alone) does not lead to the phosphorylation of MAPK (Ngou et al., 2021). Therefore, the PTI signal required for NRG1 oligomerisation could involve phosphorylation of NRG1, which is then potentiated by ETI, potentially explaining why both PTI and ETI are required for NRG1 oligomerisation.

5.1.2 Targeted phospho-proteomic methods

There are several methods which can be used to reveal protein phosphorylation. Large-scale discovery phospho-proteomic studies can identify 1000s of phospho-sites (Benschop et al., 2007, Nühse et al., 2007, Rayapuram et al., 2014, Mattei et al., 2016, Kadota et al., 2019, Rayapuram et al., 2021). However, as the mass-spectrometer is selective towards higher abundance peptides, lower abundance phospho-peptides are not detected and measured. We were not able to identify phosphorylated NRG1 peptides in either the nuclear, cytosolic, or microsomal phospho-proteomic

datasets discussed in Chapter 3. Therefore, to study phosphorylation of a lower abundance protein, such as NRG1, targeted proteomic approaches must be used.

Protein phosphorylation can be studied with in-vitro kinase assays (Liu & Zhang, 2004, Bethke et al., 2009, Mao et al., 2011, Roux et al., 2015, Sun et al., 2022). An in-vitro kinase assay revealed that WRKY33 is phosphorylated by MITOGEN-ACTIVATED PROTEIN KINASES 3/6 (MPK3/6) to regulate camalexin biosynthesis genes upon pathogen infection (Mao et al., 2011). In-vitro kinase assays can also be coupled with mass-spectrometry (MS) to identify the specific phosphorylation sites. Multiple BOTRYTIS-INDUCED KINASE1 (BIK1) autophosphorylation sites and transphosphorylation sites by BRI1-ASSOCIATED RECEPTOR KINASE (BAK1) were identified using this method (Lin et al., 2014). However, this requires protein purification, and the knowledge of what kinase may be responsible for the protein phosphorylation. Additionally, a protein may be phosphorylated at multiple residues and a chain of phosphorylation/de-phosphorylation may be required for phosphorylation to occur at each site. This cannot easily be studied using in-vitro methods. Another method that has been previously used is isotope labelling of phosphate groups (O'Donoghue & Smolenski, 2022). This is very sensitive but identification of multiple phospho-sites can only be observed from signal intensity (O'Donoghue & Smolenski, 2022).

Immunoprecipitation mass-spectrometry (IP-MS) involves detecting phosphorylation sites from immunopurified proteins. Proteins can be immunoprecipitated using epitope tagged proteins e.g. by means of FLAG-tagging. IP-MS of tagged proteins has been used to identify phosphorylation sites induced after pathogen infection (Gong et al., 2019, Sun et al., 2022). CHITIN ELICITOR RECEPTOR KINASE 1 (CERK1) was IP-enriched from flg22 treated protoplasts to identify flg22-induced phosphorylation sites by mass spectrometry (Gong et al., 2019). Only a small percentage of a protein population may be phosphorylated in response to a stimulus. Therefore, phosphorylated peptides tend to be much lower abundance compared to non-phosphorylated peptides. Detection of phosphorylated peptides by IP-MS requires a large amount of protein. This requires a large volume of infiltrated (immune activated) plant tissue, which can be labour intensive.

Protein phosphorylation in IP-enriched samples can also be detected visually by immunoblotting with anti-phosphoserine/tyrosine antibodies (Guo et al., 2018, Li et al., 2018, Lee et al., 2020, Luo et al., 2020). An anti-phosphoserine antibody was used to detect receptor kinase FERONIA-dependent MYC2 phosphorylation (Guo et al., 2018). In-vitro kinase assays were combined with anti-phosphoserine/tyrosine antibodies to show that the protein kinase PBL13 phosphorylates the C-terminus of RBOHD (Lee et al., 2020). Once a phospho-site has been identified by MS, phospho-site specific antibodies can be used. p44/p42 antibodies were used to detect phosphorylation of MPK3

and MPK6 upon elicitor treatment (Saijo et al., 2009, Galletti et al., 2011). However, phospho-antibodies may lead to unspecific binding due to similarity between phospho-sites, especially if the phospho-site is within a conserved kinase motif.

To identify protein phosphorylation by immunoblotting, without the need for phospho-antibodies, a phosphate binding tag (Phos-tag) was developed (Kinoshita et al., 2004). Phos-tag acrylamide and either Zn^{2+} or Mn^{2+} are added into the resolving SDS gel (Kinoshita et al., 2004). Phos-tag binds the phospho-group of phosphorylated proteins as they migrate through the gel (Kinoshita et al., 2004). This leads to the slower migration of hyper-phosphorylated proteins during electrophoresis compared to hypo-phosphorylated proteins. Therefore, non- or hypo-phosphorylated and hyper-phosphorylated protein populations can be seen as two or more protein bands (Kinoshita et al., 2004). Phos-tag gels containing Mn^{2+} revealed multiple phosphorylated beta-casein bands (Kinoshita et al., 2006). Migration speed can vary with the number of phosphorylated sites but also the position of the phosphorylated site within the protein (Kinoshita et al., 2016). Therefore, multiple phosphorylation sites can be observed with Phos-tag. Phos-tag gels can also give an indication to the stoichiometry of phosphorylation, revealing the ratio of phosphorylated to non-phosphorylated protein species (Kinoshita et al., 2004). However, as chelated Mn^{2+} ions interfere in membrane transfer, inefficient transfer may alter the ratio of phosphorylated species seen on the membrane. Both Zn^{2+} and Mn^{2+}can be used with Phos-tag gels, however, Zn^{2+} requires a neutral pH and no band shifts occur under alkaline conditions (Kinoshita et al., 2006).

Phos-tag gels cannot give information about the molecular weight of the protein due to mobility shifts caused by Phos-tag. When Phos-tag SDS-PAGE gels and SDS-PAGE gels are run separately, it is unclear if the lower band of a Phos-tag gel (hypo-phosphorylated species) has also had a mobility shift due to Phos-tag. To solve this, a new method termed Phos-tag diagonal electrophoresis was developed, enabling SDS-PAGE and Phos-tag SDS-PAGE patterns to be seen on the same gel (Okawara et al., 2021). This can be done by combining SDS-PAGE in the first-dimension and Phos-tag SDS-PAGE in the second-dimension (Okawara et al., 2021).

Phos-tag gels have been used to successfully identify immunity-induced changes in protein phosphorylation in plants (Bethke et al., 2009, Mao et al., 2011, Sun et al., 2022). Phos-tag gels revealed phosphorylated WRKY33 protein bands upon *Botrytis cinerea* infection (Mao et al., 2011). Multiple CBP60g bands were observed after flg22 or chitin treatment in Phos-tag gels (Sun et al., 2022). This was then followed up with in vitro kinase assays which revealed that CALCIUM DEPENDENT PROTEIN KINASE 5 (CPK5) phosphorylates CBP60g after PTI activation and MS analysis revealed the specific phosphorylation sites within CBP60g (Sun et al., 2022).

To identify phosphorylation of NRG1, we initially chose to use Phos-tag gels. Due to the sensitive nature of immunoblotting, Phos-tag gels require smaller volumes of leaf tissue, compared to IP-MS. Therefore, we used Phos-tag gels to first identify NRG1 phosphorylation bands, before moving towards the more labour-intensive IP-MS to identify specific NRG1 phosphorylation sites.

5.1.3 Chapter aims and objectives

ETI alone can induce EDS1-SAG101-NRG1 heterotrimers. However, both PTI and ETI are required for activation of HR, NRG1 oligomerisation and EDS1-SAG101-NRG1 resistosome formation. One of the earliest hallmarks of PTI-induced changes is protein phosphorylation. This chapter aimed to test the hypothesis that PTI-induced phosphorylation of NRG1 is required for NRG1 dependent HR. There have been no previous literature reports of NRG1 phosphorylation. Therefore, we first had to test if NRG1 is phosphorylated. We used Phos-tag gels to identify and visualise NRG1 phosphorylation changes upon PTI, ETI and PTI + ETI signalling. NRG1 phosphorylation sites were identified by IP-MS and changes upon immune activation quantified by MS1. The role of these NRG1 phospho-sites in HR activation were then tested in *N. benthamiana.*

5.2 Results

5.2.1 Phos-tag gels reveal multiple slower migrating bands of NRG1.2 after PTI activation

Arabidopsis carries three gene copies of NRG1: NRG1.1 (A), NRG1.2 (B) and NRG1.3 (C) (Castel et al., 2019). *At*NRG1.1 and *At*NRG1.2 are functionally redundant (Castel et al., 2019). Previous research by Dr Joanna Feehan focused on the oligomerisation of NRG1.2 (Feehan et al., 2023). Joanna created a transgenic Arabidopsis NRG1.2-HF line for her research (Table 5.1). This line utilised the XVE system for estradiol-inducible *AvrRps4* expression to activate ETI (Table 5.1). This allowed us to study phosphorylation changes during ETI alone, in addition to PTI and PTI + ETI treatments.

Table 5.1. Transgenic Arabidopsis line used for targeted NRG1.2 phosphorylation experiments. Multiple genes were inserted into Col-0: *sag101* in one T-DNA and one transformation event. The line was generated by Dr Joanna Feehan.

Background: Col-0: *nrg1.1/nrg1.2/sag101*

Promoter + 5' UTR	**Gene**	**Tag**
pEDS1	*At*EDS1	V5
pSAG101	*At*SAG101	HA
pNRG1.2	*At*NRG1.2	HF
pLexAop:35S	AvrRps4	mCherry
pAtActin2	XVE	-
pAtOleosin	gAtOleosin (FastRed)	RFP

To identify differences in phosphorylation between PTI and ETI activation, 5-week-old Arabidopsis NRG1.2-HF plants were infiltrated with mock (10 mM $MgCl_2$), Pf0-1_Empty Vector (EV), 50 uM estradiol, or Pf0-1_AvrRps4 for 4 hours. Total protein extract was loaded onto Phos-tag gels and immunoblotted with a Flag antibody for NRG1.2-HF detection. Only one NRG1.2 band could be detected using Phos-tag gels after total protein extraction (Figure 5.1).

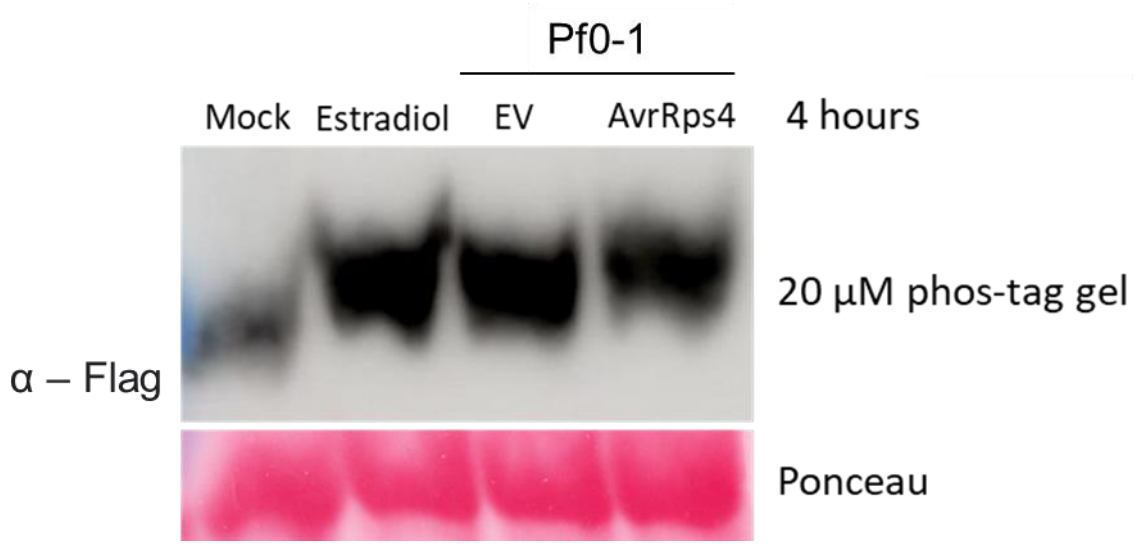

Figure 5.1. NRG1.2 phosphorylation was not detected in total extracts (using Phos-tag gels). Arabidopsis leaves were treated for 4 hours with mock (DMSO in 10 mM $MgCl_2$ and 0.01% Silwet® L-77), 50 μM β-Estradiol + 0.01% Silwet® L-77 (ETI), Pf0-1_Empty vector (EV) (PTI) or Pf0-1_AvrRps4 (PTI + ETI). Represents three biological repeats. Total protein extract was run on Mn^{2+} 20 μM Phos-tag gels and immunoblotted for NRG1.2-HF.

As we were unable to detect phosphorylated NRG1.2 from the total extracts, we IP-enriched NRG1.2-HF. We hoped to increase the yield of NRG1.2, thereby also increasing the yield of phosphorylated NRG1.2 species in our sample, enabling phosphorylated NRG1.2-HF to be detected by immunoblot. NRG1.2-HF was IP-enriched from mock (10 mM $MgCl_2$), Pf0-1_EV (PTI), estradiol (ETI) or Pf0-1_AvrRps4 (PTI + ETI) treated plant tissue. NRG1.2-HF IP samples show multiple slower migrating protein bands on Phos-tag gels (Figure 5.2 and 5.3). To conclude that protein band shifts seen in Phos-tag gels are due to phosphorylation, protein samples were treated with lambda phosphatase. If upper protein bands in Phos-tag gels are phosphorylated species, then the bands should disappear in the lambda phosphatase treated samples. The NRG1.2-HF IP samples were split in two and half the NRG1.2 protein sample was given lambda-phosphatase and all samples were incubated at 30 °C for 30 minutes. NRG1.2 slower migrating bands disappear after lambda phosphatase treatment, suggesting these protein bands are phosphorylated species of NRG1.2 (Figure 5.2 and Figure 5.3). The stoichiometry between phosphorylated and non-phosphorylated NRG1.2 bands differs between biological repeats (Figure 5.2 and 5.3). This may be due to the Mn^{2+} ions reducing transfer efficiency of phosphorylated proteins onto the membrane. The lower NRG1.2 protein bands in Figure 5.3 are not aligned, as samples not treated with lambda phosphatase were also not given the NEB 10x buffer

or incubated for 30 minutes at 30 °C (Figure 5.3). Therefore, this resulted in differing migration speeds between samples in the Phos-tag gels (Figure 5.3). This difference was not seen when all samples were given the NEB 10x buffer and incubated for 30 minutes at 30 °C (Figure 5.2). Therefore, it is difficult to conclude if there is a difference in migration speeds and therefore differences in phosphorylation of NRG1.2 between immunity-induced treatments in this repeat. Multiple (up to three) slower migrating NRG1.2 bands were seen in the PTI and PTI + ETI samples, that are not all present in the mock or ETI samples (Figure 5.2 and 5.3). This suggests NRG1.2 is phosphorylated at additional sites upon PTI signalling, in addition to sites possibly phosphorylated during ETI, or weakly present in mock treated samples.

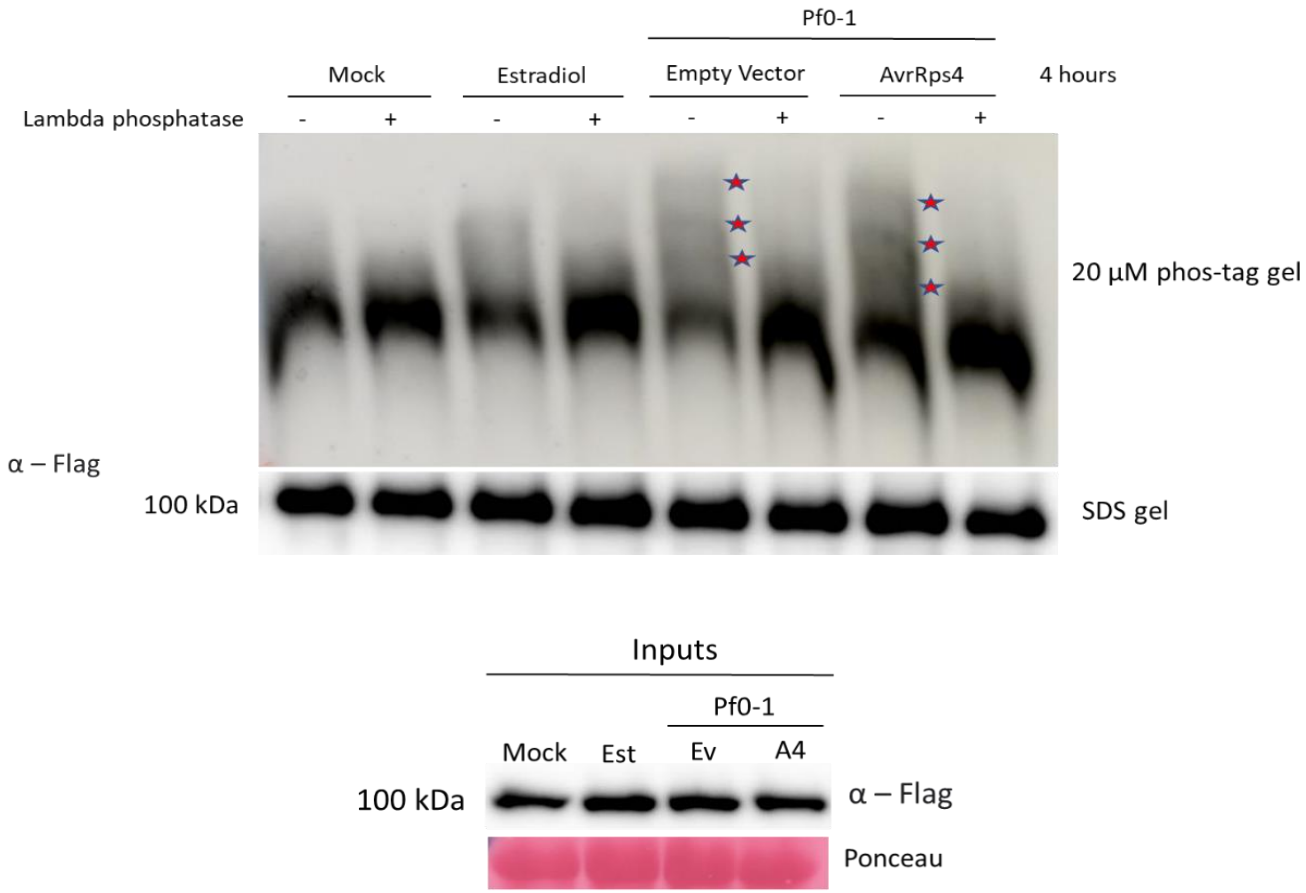

Figure 5.2. Multiple slower migrating NRG1.2-HF bands detected after PTI activation. NRG1.2-HF immunoprecipitated from leaves treated for 4 hours with mock (DMSO in 10 mM $MgCl_2$ and 0.01% Silwet® L-77), 50 µM β-Estradiol + 0.01% Silwet® L-77 (Est) (ETI), Pf0-1_Empty vector (EV) (PTI) or Pf0-1_AvrRps4 (A4) (PTI + ETI). NRG1.2-HF IP protein samples were split in half and half the protein sample treated with lambda phosphatase. Both lambda phosphatase treated and non-treated samples were then incubated for 30 minutes at 30 °C. Samples were run on Mn^{2+} 20 µM Phos-tag gels. Represents three biological repeats. ★ indicates slower migrating bands of NRG1.2.

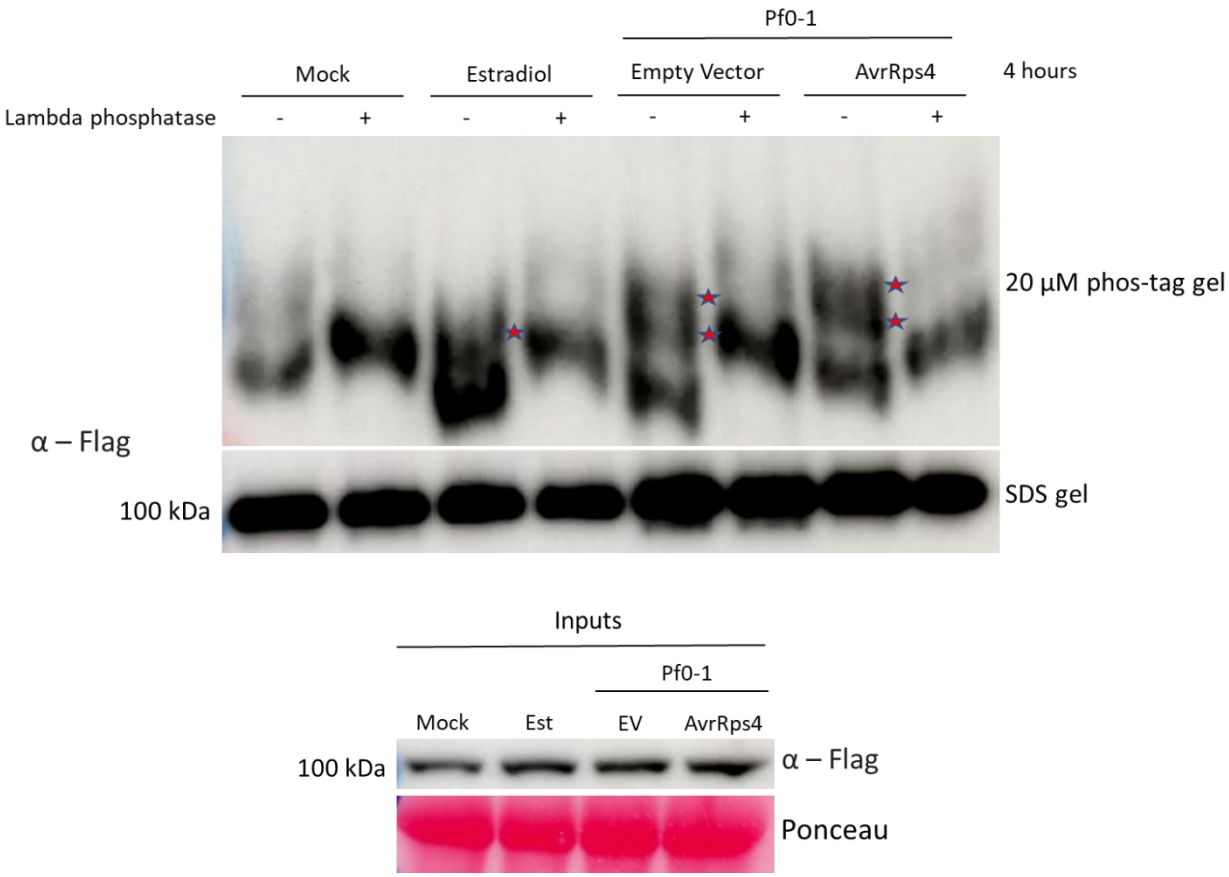

Figure 5.3. The stoichiometry between phosphorylated and non-phosphorylated NRG1.2 bands is different between biological repeats. NRG1.2-HF immunoprecipitated from leaves treated for 4 hours with mock (DMSO in 10 mM $MgCl_2$ and 0.01% Silwet® L-77), 50 µM β-Estradiol + 0.01% Silwet® L-77 (EST) (ETI), Pf0-1_Empty vector (EV) (PTI) or Pf0-1_AvrRps4 (PTI + ETI). NRG1.2-HF IP protein samples were split in half and half the protein sample was treated with lambda phosphatase for 30 minutes at 30 °C. Samples were run on 20 µM Phos-tag gels with Mn^{2+}. Represents two biological repeats. ★ indicates slower migrating bands of NRG1.2.

We next wanted to test if NRG1.2 phosphorylation could be induced by flg22 and elf18 treatment, in addition to the Pf0-1_Empty vector treatment seen in Figure 5.2 and 5.3. flg22 is a 22 amino-acid peptide from the N-terminus of flagellin (Felix et al., 1999). flg22 induces PTI activation through recognition by the receptor-like-kinase FLAGELLIN-SENSITIVE 2 (FLS2) (Gomez-Gomez & Boller, 2000). Elf18 is an acetylated 18-amino acid peptide from the N-terminus of the conserved bacterial translation protein Elongation Factor Thermo Unstable (EF-Tu) (Kunze et al., 2004). Elf18 is recognised by the leucine-rich repeat-receptor kinase EF-Tu Receptor (EFR) in Arabidopsis (Zipfel et al., 2006). 14-

day old seedlings were treated with both flg22 and elf18 for 5, 10 or 30 minutes. Multiple additional NRG1.2-HF bands can be seen in Phos-tag gels after flg22 and elf18 treatment compared to mock (Figure 5.4.). However, these bands do not disappear after lambda phosphatase treatment, suggesting the upper bands are not phosphorylated species of NRG1.2 (Figure 5.4). Therefore, the identity of the slower migrating bands of NRG1.2 is unclear.

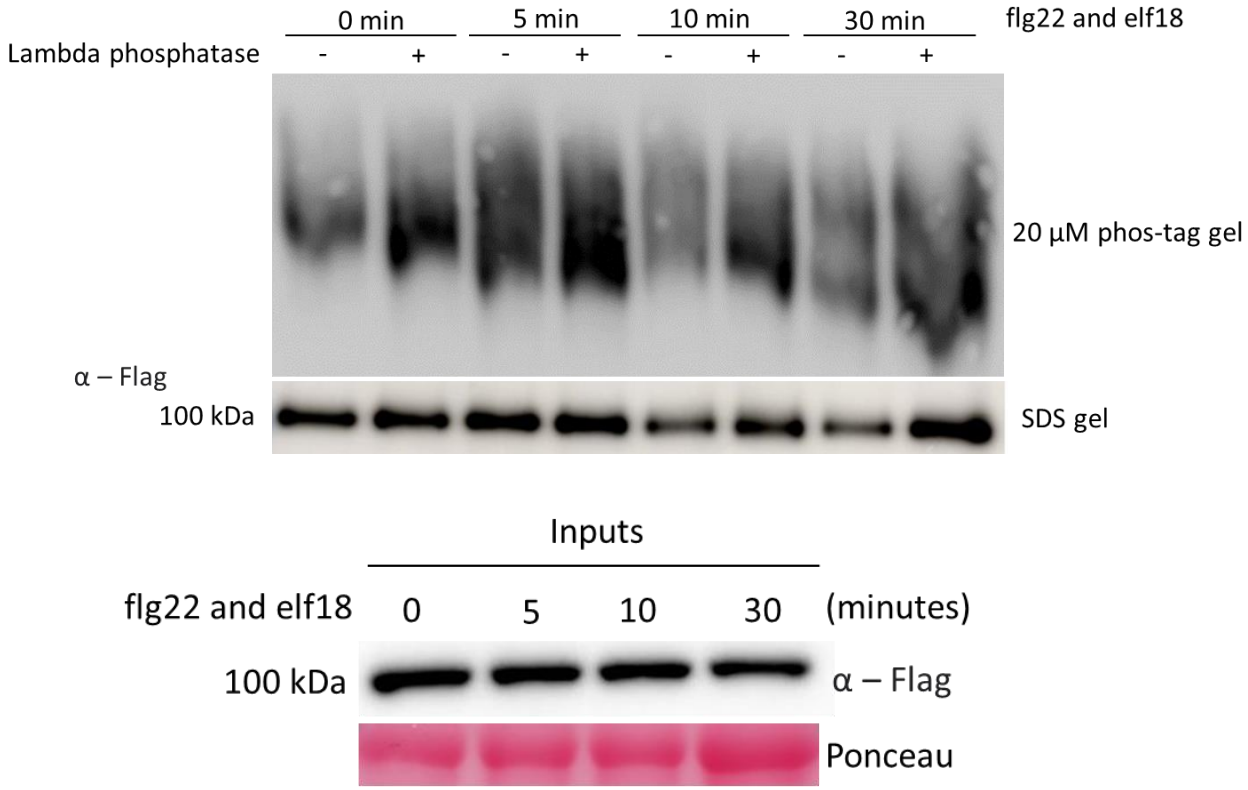

Figure 5.4. Slower migrating bands of NRG1.2-HF in PTI treated samples do not disappear after phosphatase treatment. NRG1.2-HF immunoprecipitated from Arabidopsis seedlings treated with mock or 200 µM flg22 and 200 µM elf18 for 5, 10 or 30 minutes. NRG1.2-HF protein samples were split in half and half the protein sample treated with lambda phosphatase. Both lambda phosphatase treated and non-treated samples were then incubated for 30 minutes at 30 °C. NRG1.2-HF protein samples were run on Mn^{2+} 20 µM Phos-tag gels. Represents two biological repeats.

5.2.2 Phosphorylated NRG1.1 bands were not detected with Phos-tag gels

As *At*NRG1.1 and *At*NRG1.2 are functionally redundant (Castel et al., 2019), we hypothesised that both NRG1.2 and NRG1.1 are phosphorylated during PTI and PTI + ETI signalling. To investigate NRG1.1 phosphorylation, NRG1.1-V5 Arabidopsis lines were used (Table 5.2). These lines were created by Dr Baptiste Castel. 5-week-old Arabidopsis leaves were treated for 4 hours with mock (10 mM $MgCl_2$), Pf0-1_Empty vector (EV) (PTI) or Pf0-1_AvrRps4 (PTI + ETI). NRG1.1-V5 was immunoprecipitated and protein samples run on Phos-tag gels (Figure 5.5). Only one band of NRG1.1 was detected, suggesting NRG1.1 is not phosphorylated after 4 hours of PTI or PTI + ETI activation, or its phosphorylation is not revealed by this assay (Figure 5.5). This suggests there may be different methods of activation of NRG1.1 and NRG1.2 during PTI + ETI signalling.

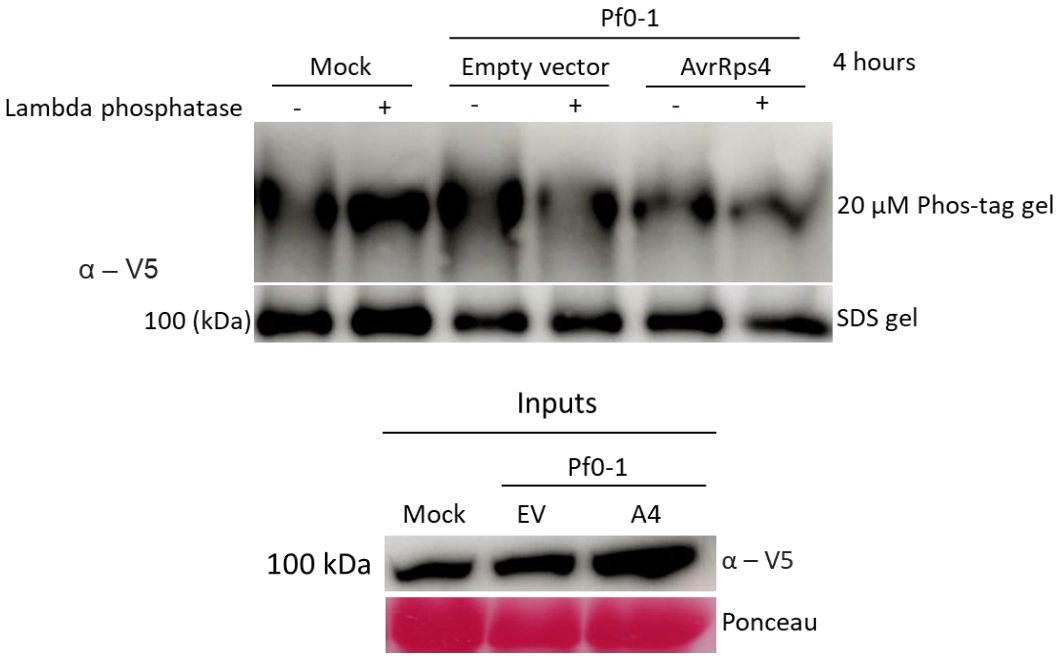

Figure 5.5. Slower migrating NRG1.1-V5 protein bands are not seen by Phos-tag gels. NRG1.1-V5 was immunoprecipitated from leaves treated for 4 hours with mock (10 mM $MgCl_2$), Pf0-1_Empty vector (EV) (PTI) or Pf0-1_AvrRps4 (A4) (PTI + ETI). NRG1.1-V5 protein samples were split in half and half the protein sample treated with lambda phosphatase. Both lambda phosphatase treated and non-treated samples were then incubated for 30 minutes at 30 °C. NRG1.1-V5 protein samples were run on Mn^{2+} 20 µM Phos-tag gels. Represents two biological repeats.

Table 5.2. Transgenic Arabidopsis line for NRG1.1 phosphorylation experiments

Background: Ws-2: *nrg1.1/1.2*

Promoter + 5' UTR	**Gene**	**Tag**
pNRG1.1	*At*NRG1.1	V5
pCsVMV	Bar (Basta)	-

5.2.3 MS1 quantification of NRG1.2 phosphorylation reveals similar levels between mock and 4 hours of PTI or PTI + ETI activation

To identify which residues are phosphorylated within NRG1.2, protein samples were analysed by mass-spectrometry. Data-dependent analysis identified phosphorylation at two sites within NRG1.2: S152 and S433 (Figure 5.6). These phospho-sites are not located within the conserved NRG1.2 protein domains: NB, LRR or RPW8 (Figure 5.6). S152 and S433 are both conserved between *At*NRG1.1, *At*NRG1.2 and within *Brassicaceae* NRG1 homologs (Figure 5.7). S152 is also conserved in the *Nb*NRG1 homolog (Figure 5.7). Conservation of phosphorylation sites between NRG1 Arabidopsis alleles and *Brassicaceae* homologs could indicate that the phosphorylation sites are important for NRG1 function. As S152 is located next to a proline in *At*NRG1.2, a Phosphoserine-Proline antibody (Abcam: ab9344) was tested on NRG1.2-HF protein samples but no bands were detected after SDS-PAGE immunoblotting. This suggests phosphorylated S152 may be too low abundance to be detected by immunoblotting or the antibody was not specific enough to be able to bind to phosphorylated S152. Additionally, despite S152 conservation, the proline at S153 in *At*NRG1.2 is not conserved in *At*NRG1.1 or in *Brassicaceae* homologs (Figure 5.7). Therefore, this suggests *At*NRG1 S152 phosphorylation is not a conserved site for proline-directed protein kinase phosphorylation e.g. by MAPK (Bardwell, 2006).

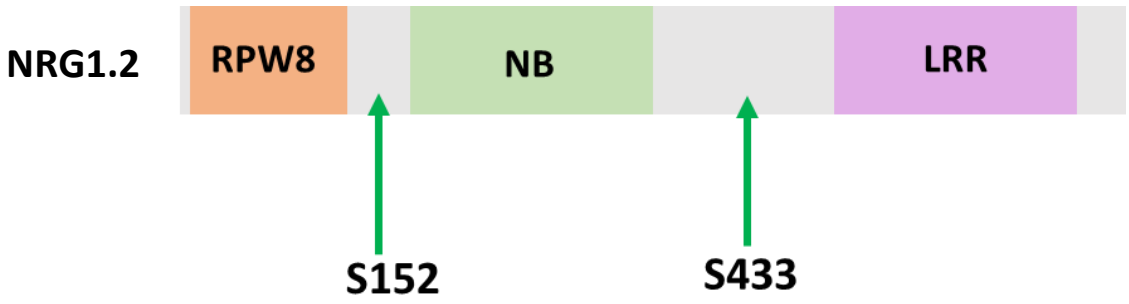

Figure 5.6. Location of *At*NRG1.2 phospho-sites identified by mass spectrometry analysis. Adapted from (Wu et al., 2022).

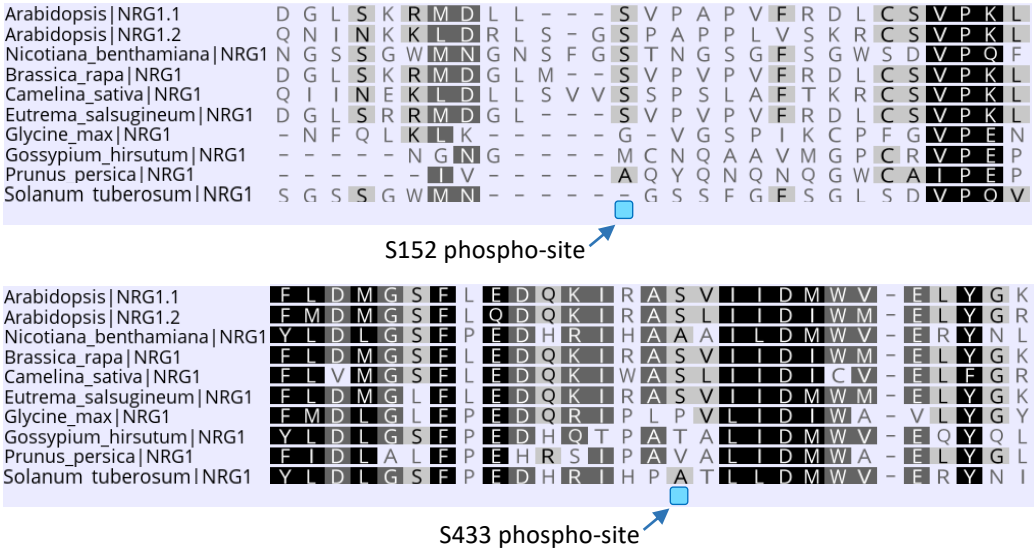

Figure 5.7. S152 and S433 are conserved between *At*NRG1.1, *At*NRG1.2 and in NRG1 within the *Brassicaceae*. Protein sequences were downloaded from NCBI. Multiple protein sequences were aligned with T-coffee and imported into Geneious.

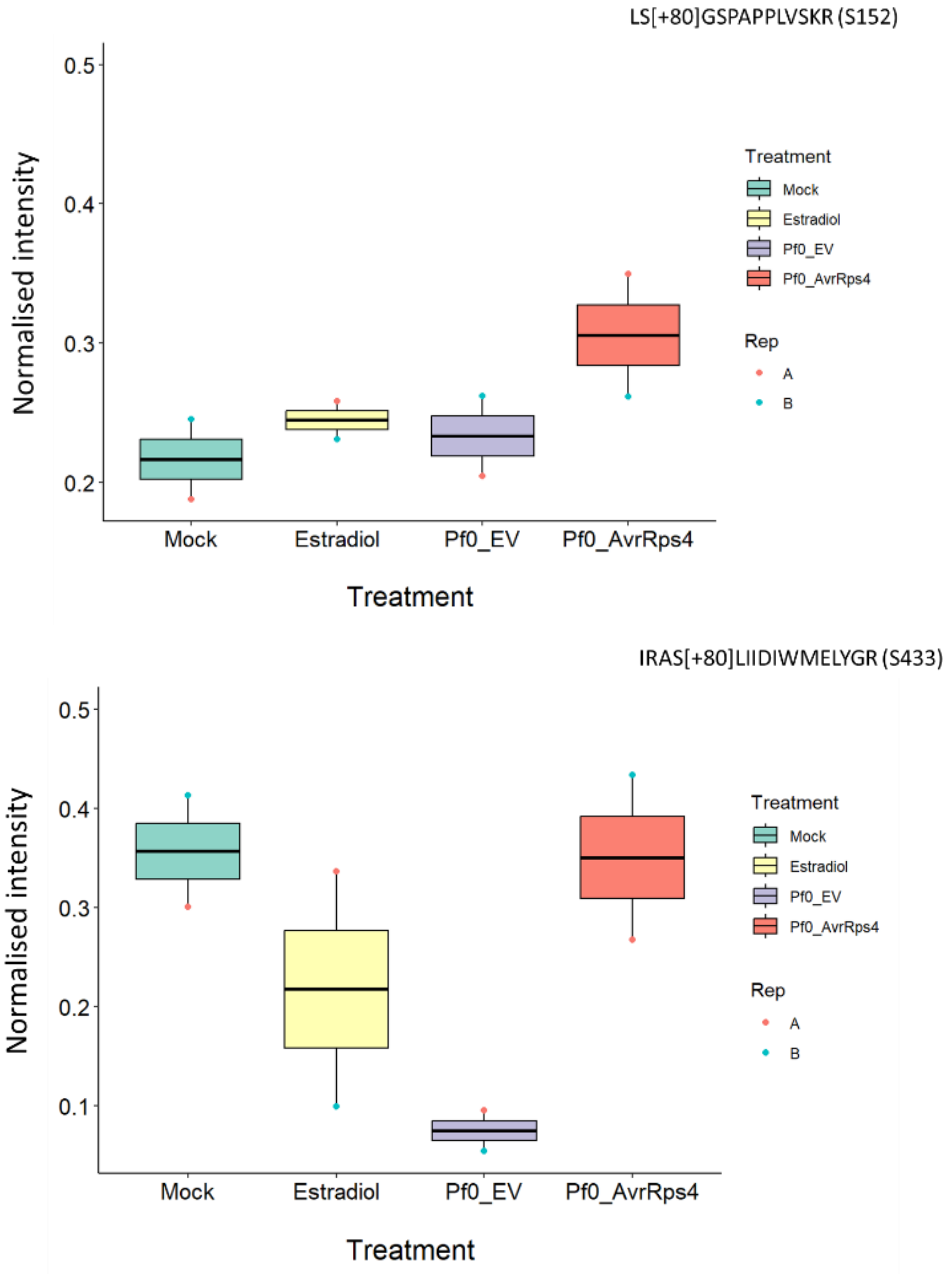

Figure 5.8. Phosphorylation of *At*NRG1.2 at S152 and S433 does not change after PTI, ETI or PTI + ETI activation. NRG1.2-HF immunoprecipitated samples were analysed by mass-spectrometry. Phosphorylated *At*NRG1.2 peptides were quantified by MS1 quantification. NRG1.2 phosphorylated peptide intensity was normalised against the intensity of 45 non-phosphorylated NRG1.2 peptides to account for differences in protein amount between samples. Intensity is scaled to the total intensity for each phospho-peptide (Total = 1). Data from two biological repeats.

To quantify differences in NRG1.2 phosphorylation between mock, PTI, ETI or PTI + ETI, the two phospho-sites were quantified by MS1 quantification by Dr Paul Derbyshire. Phosphorylated peptide intensity was measured and normalised against the intensity of 45 non-phosphorylated NRG1.2 peptides. This revealed no difference in NRG1.2-HF phosphorylation between the different immune activated treatments (Figure 5.8). One repeat did show an increase in S152 phosphorylation upon PTI + ETI activation, but this was not seen in the second repeat. Therefore, as only two replicates were carried out, further replication is needed to allow statistical analysis and determine if there is any difference in S152 phosphorylation upon PTI + ETI activation. As no quantitative difference was found by MS1, S152 and S433 may not be the phospho-sites responsible for the slower migrating bands seen in the Phos-tag gels upon PTI and PTI + ETI activation.

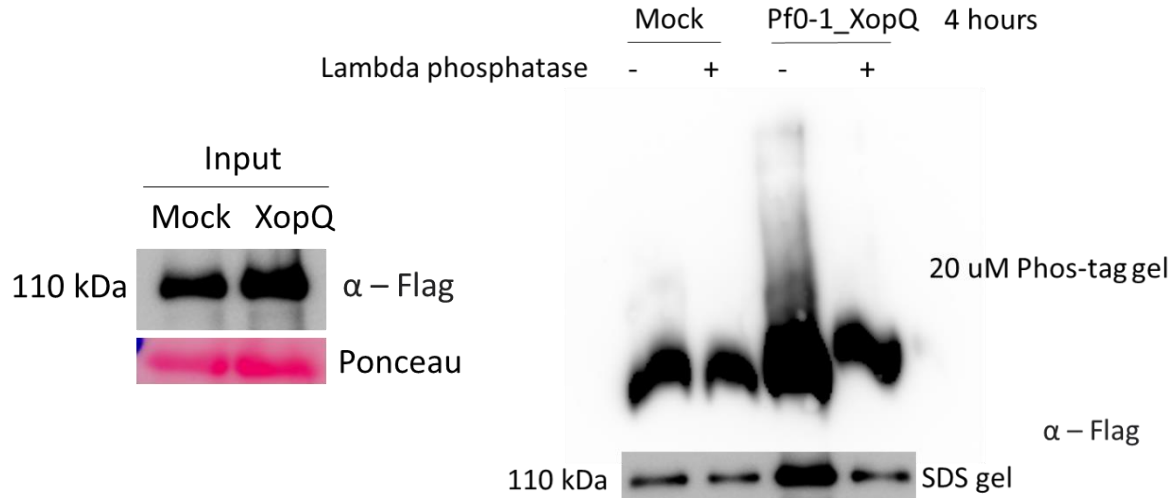

Figure 5.9. Transient expression of *At*NRG1.2 in *N. benthamiana* reveals phosphorylated AtNRG1.2 bands after Pf0-1_XopQ treatment. Transient expression of *At*NRG1.2^{EEAA}, *At*SAG101 and *At*EDS1 in *N. benthamiana* leaves for 48 hours. Leaves were infiltrated with Pf0-1_XopQ or mock (10 mM $MgCl_2$) for 4 hours. *At*NRG1.2-HF protein was immunoprecipitated and samples were run on Mn^{2+} 20 μM Phos-tag gels. Represents one biological repeat.

To investigate if *At*NRG1.2 can be phosphorylated by *N. benthamiana* protein kinases, *At*NRG1.2 was transiently expressed in *N. benthamiana* (Figure 5.9). *At*NRG1.2^{EEAA}, a funnel pore mutant of NRG1.2 which still oligomerises but does not trigger HR was used to increase the abundance of activated *At*NRG1.2 in the harvested plant tissue (Sun et al., 2021). *At*NRG1.2^{EEAA}, *At*SAG101 and *At*EDS1 were transiently co-expressed for 48 hours. Leaves were then infiltrated with Pf0-1_XopQ or mock (10 mM $MgCl_2$) and samples harvested after 4 hours. *At*NRG1.2^{EEAA}-HF was immunoprecipitated and an aliquot

of the *At*NRG1.2 protein sample was run on Phos-tag gels with/without lambda phosphatase treatment (Figure 5.9). Multiple slower migrating bands of NRG1.2-HF can be seen in the Pf0-1_XopQ treated samples, which disappear upon lambda phosphatase treatment (Figure 5.9). This suggests *At*NRG1.2 can be phosphorylated by *N. benthamiana* kinases. There is quite a significant difference in *At*NRG1.2 protein abundance between the non-phosphatase treated Pf0-1_XopQ sample and the other three samples, which may account for the increased signal of slower migrating NRG1.2 bands (Figure 5.9). Only one biological repeat has been carried out and therefore these results must be interpreted carefully. However, this provides a direction for future research of this project. The *At*NRG1.2 IP samples from *N. benthamiana* were measured by MS. *At*NRG1.2 S433 was phosphorylated in the Pf0-1_XopQ treated samples, suggesting *At*NRG1.2 can be phosphorylated by an *N. benthamiana* protein kinase at the same residue as Arabidopsis kinases. However, this serine residue is not conserved between *At*NRG1.2 and *Nb*NRG1. Therefore, a different residue may be important for *Nb*NRG1 activation. Only 30% of the *At*NRG1.2 protein was detected by MS. Therefore, there may be additional *At*NRG1.2 phosphorylation sites phosphorylated by *N. benthamiana* kinases that were not detected by MS. Higher volumes of *At*NRG1.2 protein need to be extracted from larger quantities of infiltrated *N. benthamiana* leaf tissue to increase the *At*NRG1.2 protein coverage measured by MS.

5.2.4 Phosphorylation of *At*NRG1.2 S152 and S433 are important for HR activation in *N. benthamiana*

To investigate the role of the *At*NRG1.2 phosphorylation sites identified by MS, phospho-variants of *At*NRG1.2 were created. Phosphorylated serines were changed to Aspartic acid (D) to create a phospho-mimic or to Alanine (A) to create a phospho-dead variant. We tested the requirement of these sites for activation of HR in *N. benthamiana*. *N. benthamiana* deficient in *Nb*EDS1, *Nb* PHYTOALEXIN DEFICIENT 4 (*Nb*PAD4), *Nb*SAG101a and *Nb*SAG101b (*Nb_epss*) was used (Lapin et al., 2019). Arabidopsis alleles of EDS1, SAG101 and NRG1 can reconstitute HR in *Nb_epss* (Lapin et al., 2019). However, all Arabidopsis alleles or all *N. benthamiana* alleles are required, as *Nb*NRG1 is unable to signal and trigger HR with *At*EDS1 and *At*SAG101 (Lapin et al., 2019). These proteins have co-evolved within each plant species and cannot signal with EDS1/SAG101/NRG1 proteins from other plant species. Therefore, the requirement of *At*NRG1 phosphorylation can be tested using Arabidopsis alleles of EDS1, SAG101 and NRG1 in *Nb_epss.*

AvrRps4 effector from *Pseudomonas syringae* is not recognised by *N. benthamiana* due to the absence of RRS1/RPS4 NLRs. Therefore, co-infiltration of AvrRps4, with *At*EDS1 and *At*SAG101 and *At*NRG1.2 phospho-variants, does not trigger HR (Figure 5.10). This confirms that *At*NRG1.2 phospho-variants

are not auto-active in *N. benthamaiana* (Figure 5.10). *At*NRG1.2 wildtype (WT) and *At*NRG1.2 phospho-variants have similar protein expression levels in *N. benthamiana* (Figure 5.11). Therefore, any differences seen in HR scores are not due to differences in *At*NRG1.2 phospho-variant protein expression.

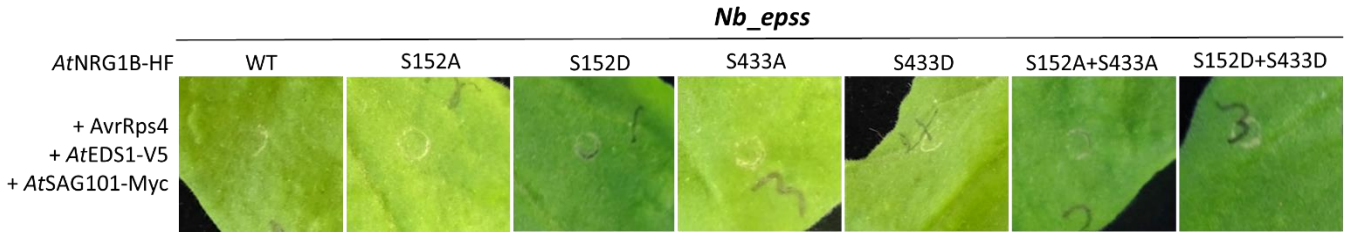

Figure 5.10. *At*NRG1.2 phospho-variants are not auto-active. 4-week-old *Nb_epss* leaves were co-infiltrated with *At*EDS1, *At*NRG1.2 phospho-variants, *At*SAG101 and AvrRps4 and images taken 6dpi. OD_{600} of NRG1.2, SAG101 and EDS1 was 0.2, 1 and 0.05 respectively. Represents three biological repeats.

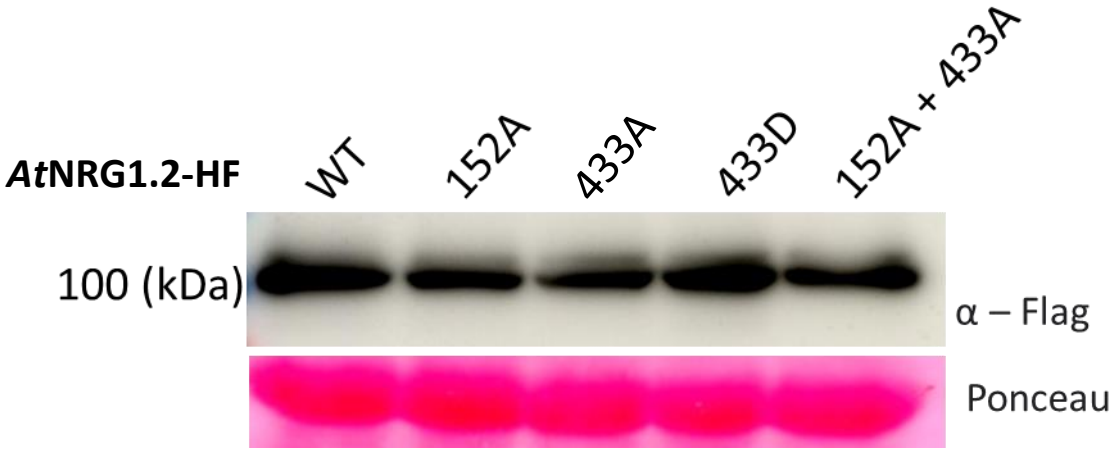

Figure 5.11. *At*NRG1.2 WT and *At*NRG1.2 phospho-variants have similar protein expression in *N. benthamiana.* 4-week-old *Nb_epss* leaves were infiltrated with *At*NRG1.2 phospho-variants and protein extracted after 48 hours.

To study HR in *N. benthamiana* different NLR- effector recognition systems can be used. The effector protein XopQ from *Xanthomonas* is recognised by TIR-NLR RECOGNITION OF XOPQ 1 (ROQ1) in *N. benthamiana* and triggers HR activation (Schultink et al., 2017). The oomycete *Albugo candida* effector CCG28 is recognised by WHITE RUST RESISTANCE 4A (WRR4A) to confer resistance in Arabidopsis (Redkar et al., 2023). Transient expression of CCG28 and WRR4A triggers HR in *N. benthamiana* (Redkar et al., 2023). Therefore, we utilised both these NLRs to investigate the role of *AtNRG1* phosphorylation in HR activation.

*At*NRG1.2 phospho-variants all activate HR in the presence of XopQ effector and there is no difference in the strength of HR between *At*NRG1.2 WT and the *At*NRG1.2 phospho-variants (Figure 5.12 and 5.13). This may be caused by high variability in the strength of HR between different leaves, including in the *At*NRG1.2 WT. Therefore, we tested HR in response to the CCG28 effector, which is known to cause a stronger and more reproducible HR. WRR4A and CCG28 were co-expressed in *N. benthamiana* with *At*NRG1.2, *At*EDS1 and *At*SAG101 (Figure 5.14). *At*NRG1.2 is required for activation of HR triggered by WRR4A recognition of CCG28 (Figure 5.14). We then looked for differences in HR strength between the *At*NRG1.2 phospho-variants when co-infiltrated with CCG28 and WRR4A and scored 6 days after infiltration (Figure 5.15). To reduce the strength of the HR response to reveal differences between the WT and phospho-variants, we also reduced the OD_{600} of NRG1.2, SAG101 and EDS1 to 0.05, 0.2 and 0.0125 respectively (Figure 5.15). This work was carried out by a pre-doc in the lab Renzo Villena-Gaspar, supervised by myself. We found a quantitative reduction in HR in the *At*NRG1.2^{152A} phospho-dead variant and WT-like HR in the *At*NRG1.2^{152D} phospho-mimic (Figure 5.15 and 5.16). This suggests NRG1 S152 phosphorylation is important for HR activation and the reduction in HR seen in the *At*NRG1.2^{152A} variant is due to the absence of NRG1 phosphorylation. We also found a reduction in HR in the *At*NRG1.2$^{152A+433A}$ and *At*NRG1.2^{433A} phospho-dead variants (Figure 5.15 and 5.16). However, there was also a reduction in HR strength in the respective phospho-mimics *At*NRG1.2^{433D} and *At*NRG1.2$^{152D+433D}$ (Figure 5.15 and 5.16). The reduction in HR in both the 433A phospho-dead and 433D phospho-mimic could suggest there is cyclic phosphorylation of NRG1. As HR activated by *At*NRG1.21^{152D} has a similar strength to WT, the *At*NRG1.2^{433D} mutant in the *At*NRG1.2$^{152D+433D}$ variant may be reducing the HR strength activated by *At*NRG1.2^{152D}. Cyclic phosphorylation is difficult to study in HR assays or those with longer time points post immune activation. Therefore, future studies investigating the role of NRG1 phosphorylation should focus on NRG1 S152.

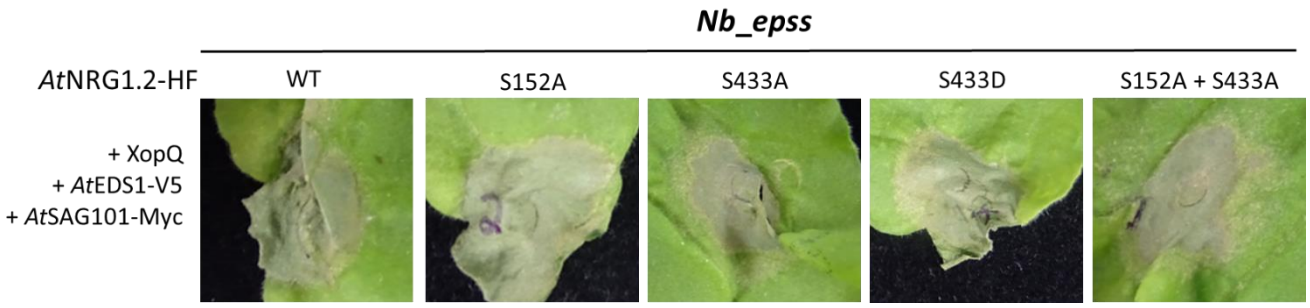

Figure 5.12. *At*NRG1.2 phospho-variants trigger HR in response to Pf0-1_XopQ. 4-week-old *Nb_epss* leaves were co-infiltrated with *At*EDS1, *At*NRG1.2 phospho-variants, *At*SAG101 and XopQ. OD_{600} of NRG1.2, SAG101 and EDS1 was 0.2, 1 and 0.05 respectively. Images taken 6 dpi. Represents three biological repeats.

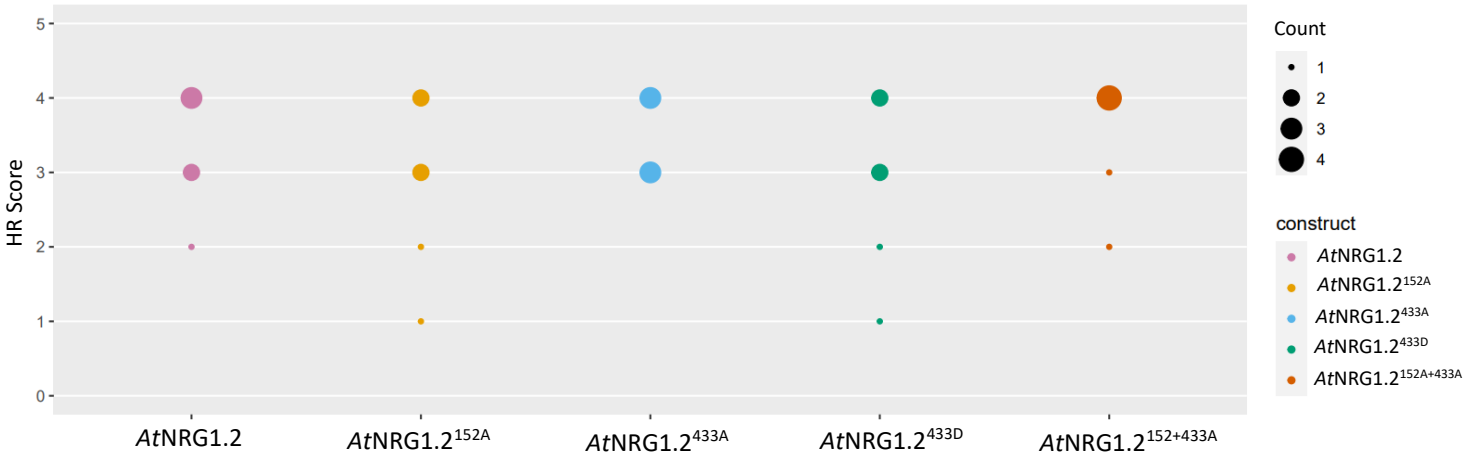

Figure 5.13. NRG1.2 WT and NRG1.2 phospho-variants give rise to indistinguishable HR strength in response to XopQ. HR scores for Figure 5.12. HR was scored 6 dpi on 6 leaves using the following HR score scale: 0 = no HR, 1 = chlorosis, 2 = mild HR, 3 = moderate HR, 4 = severe HR, 5 = very severe HR. HR scores are presented as dot plots, with the size of each dot proportional to the number of samples with that score (Count). Similar results were seen for three biological repeats. The besthr R package was used for statistical tests (MacLean, 2019). Bootstrap resampling tests were carried out using an upper significance cut-off of 0.975 and a lower cut-off of 0.025. Mean ranks of test samples falling outside of these cut-offs in the NRG1.2-HF WT bootstrap population were considered significant. Significant differences between NRG1.2-HF WT and the NRG1.2 phosphorylation variants are indicated with an asterisk (*).

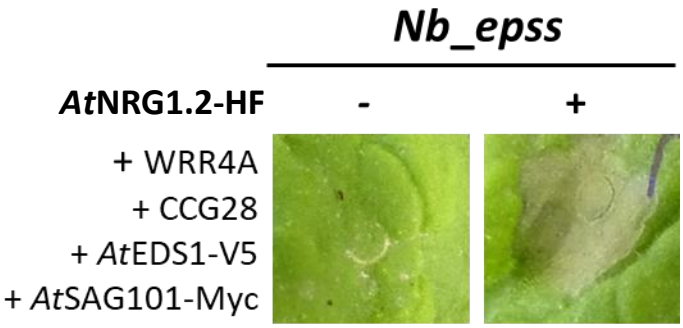

Figure 5.14. *At*NRG1.2 is required for HR induced by WRR4A recognition of CCG28. 4-week-old *Nb_epss* leaves were co-infiltrated with *At*EDS1, *At*NRG1.2, *At*SAG101, WRR4A and CCG28. OD_{600} of NRG1.2, SAG101 and EDS1 was 0.2, 1 and 0.05 respectively. Images were taken 6dpi. Represents three biological repeats.

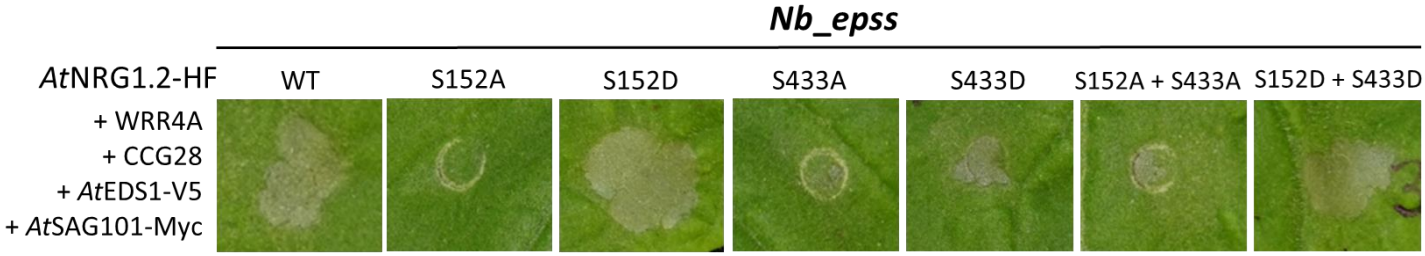

Figure 5.15. *At*NRG1.2 phospho-dead variants show a quantitative reduction in HR induced by CCG28 recognition. 4-week-old *Nb_epss* leaves were co-infiltrated with *At*EDS1, *At*NRG1.2 phospho-variants, *At*SAG101, WRR4A and CCG28. OD_{600} of NRG1.2, SAG101 and EDS1 was 0.05, 0.2 and 0.0125 respectively. Images were taken 6dpi. Represents three biological repeats.

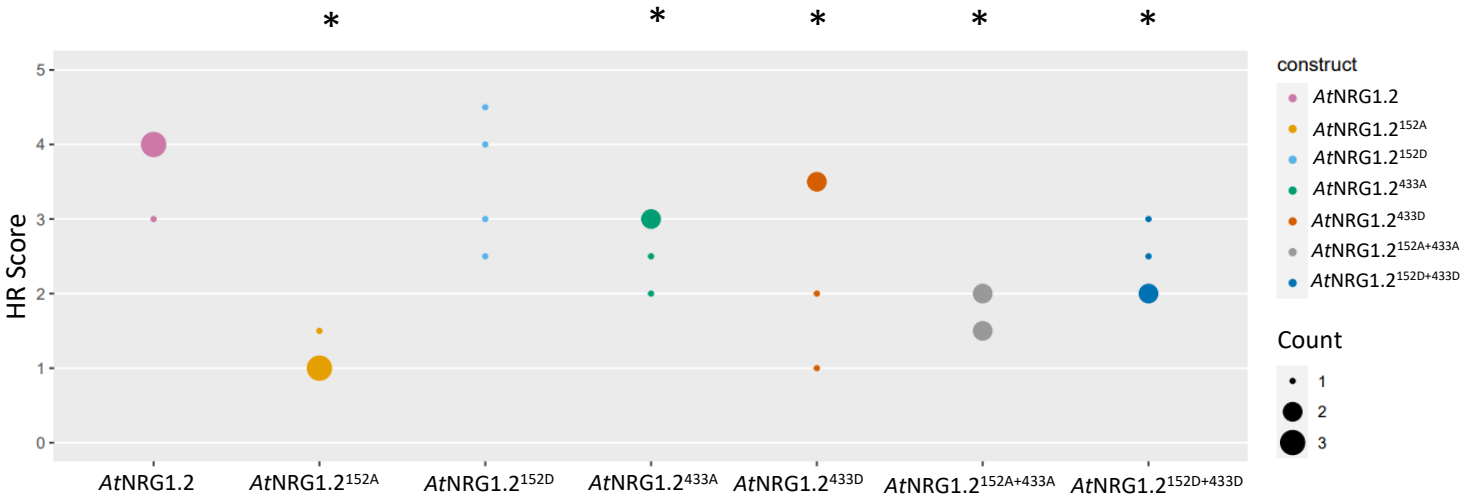

Figure 5.16. There is a reduction in HR strength induced by NRG1.2 phospho-dead variants after CCG28 recognition. HR scores for Figure 5.15. HR was scored 6 dpi on 4 or 6 leaves using the following HR score scale: 0 = no HR, 1 = chlorosis, 2 = mild HR, 3 = moderate HR, 4 = severe HR, 5 = very severe HR. HR scores are presented as dot plots, with the size of each dot proportional to the number of samples with that score (Count). Similar results were seen for three biological repeats. The besthr R package was used for statistical tests (MacLean, 2019). Bootstrap resampling tests were carried out using an upper significance cut-off of 0.975 and a lower cut-off of 0.025. Mean ranks of test samples falling outside of these cut-offs in the NRG1.2-HF WT bootstrap population were considered significant. Significant differences between NRG1.2-HF WT and the NRG1.2 phosphorylation variants are indicated with an asterisk (*).

5.3 Discussion

5.3.1 Additional NRG1.2 phospho-sites, not detected by MS, may be responsible for the slower migrating protein bands seen in Phos-tag gels

PTI and PTI + ETI treatment leads to multiple slower migrating NRG1.2 protein bands in Phos-tag gels, with upper bands not seen in mock or ETI treatments. The slower migrating NRG1.2 bands disappear upon phosphatase treatment, suggesting these protein bands are phosphorylated NRG1.2 and there is PTI-induced NRG1 phosphorylation. Phosphorylated peptides represented less than 1% of NRG1 peptides identified by MS across the 4 treatments, suggesting only a very small population of NRG1.2 is phosphorylated. This does not match the stoichiometry of non-phosphorylated/phosphorylated NRG1.2 protein seen in the Phos-tag gels. However, this would correlate with the small proportion of NRG1.2 protein that forms higher-order complexes (Feehan et al., 2023). The MS1 data does not

correlate with the Phos-tag gels, as there is no difference in phosphorylation at S152 and S433 between Mock and PTI, ETI or PTI + ETI with MS1 quantification. PTI does not enhance phosphorylation of NRG1.2 at S152 or S433. Therefore, there may be additional phosphorylation sites responsible for the slower migrating NRG1.2 bands, that are not detected by MS, due to the nature of tryptic cleavage. Protein samples are digested with trypsin into peptides before MS analysis. Trypsin cleaves at arginine and lysine residues. Depending on the amino acid sequence, protein cleavage with trypsin can produce some peptides which are too long or too short to be detected by MS. We therefore tested NRG1.2 protein cleavage with AspN, which has a different cleavage pattern, and repeated MS analysis. This did not reveal any additional phosphorylation sites. MS analysis detected NRG1.2 peptides with a protein-coverage of 60%. Therefore, there may be additional phospho-sites within NRG1.2 which were not detected by MS. As the same samples were used for Phos-tag gels and IP-MS, we expected the phosphorylated peptides responsible for the slower migrating bands to be more abundant in the MS data. Therefore, S433 and S152 may not be the phospho-sites responsible for the slower migrating bands in the Phos-tag gels. Phos-tag gels with phospho-dead NRG1.2 at S152 (NRG1.2^{152A}) would reveal if the slower migrating bands of NRG1.2 are due to phosphorylation at S152 or at additional unknown phosphorylation sites. In summary, we cannot exclude that additional phospho-sites could be present within NRG1.2 that, when cleaved by trypsin cannot be measured by MS.

NRG1 WT activates HR in *N. benthamiana* after co-infiltration of AtSAG101, AtEDS1, CCG28 and WRR4A. However, NRG1.2^{152A} phospho-dead variant has a reduction in HR. This strongly suggests that *N. benthamiana* kinases can phosphorylate *At*NRG1.2. S152 is also conserved in *Nb*NRG1, suggesting this residue may also be important for *Nb*NRG1 signalling. S152 and S433 are also conserved in NRG1.1. Therefore, further investigation needs to be done to see if the same phosphorylation sites are important for NRG1.1 activation of HR. MS1 quantification revealed there are no differences in NRG1.2 phosphorylation levels between mock, PTI, ETI or PTI + ETI activation at S152 and S433. Therefore, it is not currently clear why a phospho-dead mutation at S152 and S433 lead to reductions in HR. These residues may interfere with NRG1.2 interaction with an unknown signalling molecule required for HR and is something that needs to be further explored. Additionally, there may be differences in phosphorylation at S152 and S433 but at a different time point after defence activation.

Additional post-translational modifications (PTMs) of NRG1 could also be involved in NRG1 signalling e.g. ubiquitination. BIK1 is monoubiquitinated 10 minutes after flg22 treatment to positively regulate plant immunity (Ma et al., 2020b). BIK1 phosphorylation and monoubiquitination are both required for BIK1 dissociation from the FLS2 complex and production of reactive oxygen species (Ma et al., 2020b). Therefore, it may be possible that a combination of PTMs are required for NRG1 signalling. Further IP-MS analysis could reveal additional PTMs of NRG1.

5.3.2 Phosphorylation of *At*NRG1.2 and *At*NRG1.1 at additional time points should be investigated

NRG1.1 and NRG1.2 act redundantly in pathogen and HR assays in Arabidopsis (Castel et al., 2019). However, recently NRG1.1 was reported to interact with SAG101 significantly stronger than NRG1.2 (Dongus et al., 2022). Therefore, there may be differences between NRG1.1 and NRG1.2 in defence signalling that we do not yet understand, although single mutants of NRG1.1 or NRG1.2 show a wildtype defence phenotype, consistent with redundancy. Phosphorylation of NRG1.1 was not detected by Phos-tag gels after Pf0-1_Empty vector or Pf0-1_AvrRps4 treatment for 4 hours. The timing of NRG1.1 phosphorylation could be earlier and more transient than NRG1.2. Therefore, phosphorylation of NRG1.1 should be investigated at earlier time points, in addition to looking at phosphorylation after flg22/elf18-induced PTI.

PTI induced by Pf0-1_Empty vector treatment for 4 hours induced slower migrating bands of NRG1.2, which disappear upon phosphatase treatment. PTI induced by 30 minutes of flg22 and elf18 treatment of seedlings, also induced slower migrating bands of NRG1.2. However, these bands do not disappear with phosphatase treatment. Lambda protein phosphatase (NEB) has activity against phosphorylated serines, tyrosines and threonines. One possible explanation is the lambda protein phosphatase (NEB) had lost activity due to multiple freeze/thaw events. Therefore, these two PTI treatments need to be compared side-by-side on the same Phos-tag gel to determine if the slower migrating bands induced by flg22/elf18 are the same phosphorylated species of NRG1.2 induced after 4 hours of Pf0-1_ Empty vector treatment. Additionally, there are timing differences between the two PTI treatments: 4 hours for Pf0-1_EV and 30 minutes for flg22/elf18. A time-course with Pf0-1_EV would reveal if NRG1.2 phosphorylation is induced by PTI earlier than 4 hours and provide information about when NRG1 phosphorylation is at its strongest. Additionally, there may be differences between phosphorylation induced in leaves (PF0-1_EV treated samples) and seedlings (flg22/elf18 treated samples). Therefore, flg22/elf18 induced phosphorylation of NRG1.2 should also be investigated in 5-week-old leaf samples.

We chose to study phosphorylation 4 hours after infiltration, as a strong EDS1-SAG101-NRG1 association is detected at 4 hours post infection (hpi) (Sun et al., 2021). However, association is enhanced at 8 hpi and NRG1.2 oligomerisation was observed at 8 hpi (Sun et al., 2021, Feehan et al., 2023). Therefore, the timing of NRG1.2 phosphorylation needs to be further explored with an extended time-course. An enhancement of phosphorylation at certain phospho-sites may be very transient, which could be a reason why we did not detect a difference in phosphorylation levels at 4 hours by MS1 quantification. Phosphorylation may also be an important signal for NRG1.2

oligomerisation or EDS1-SAG101-NRG1 resistosome formation, suggesting the later time point of 8 hpi needs to be investigated.

5.3.3 The role of NRG1.2 S152 phosphorylation in activating NRG1 higher-order complex formation needs to be explored

ETI alone induces EDS1-NRG1-SAG101 heterotrimer formation (Feehan et al., 2023). However, both PTI and ETI activation are required for EDS1-SAG101-NRG1 resistosome formation and NRG1 oligomerisation (Feehan et al., 2023). Additionally, estradiol-inducible *AvrRps4*, does not induce macroscopic cell death (Ngou et al., 2020). Therefore, PTI is needed for NRG1 higher-order complex formation and HR activation. As phosphorylation is a key signal in PTI signal transduction, NRG1 phosphorylation could be required for HR activation, by triggering NRG1 higher-order complex formation. PTI alone may lead to NRG1 phosphorylation, and we know that ETI alone activates EDS1-NRG1-SAG101 heterotrimer formation. Therefore, we speculate that it is only when you have both ETI-induced heterotrimer formation + PTI-induced phosphorylation, that NRG1 forms resistosomes and oligomerises to activate HR. To determine if the phosphorylation residues identified in this study are required for NRG1.2 oligomerisation, blue-native page gels with phospho-dead NRG1 could be performed, to test if *At*NRG1.2^{152A} can still oligomerise or form resistosomes with EDS1 and SAG101. Additionally, Arabidopsis lines with two copies of NRG1.2, *At*NRG1.2^{152A}-HF and *At*NRG1.2^{152A} -V5, could also be used to test if these residues are important for NRG1.2 self-association. Identifying the kinases responsible for NRG1 phosphorylation would further our understanding of signalling pathways activated in PTI + ETI and may reveal further links between PTI and PTI + ETI signalling. For example, BIK1 phosphorylation of NRG1 could be tested with in-vitro kinase assays. Comparing WT NRG1.2 and phospho-dead NRG1.2^{152A} would also reveal if this residue is phosphorylated by BIK1. NRG1.2-TurboID Arabidopsis lines are being generated to help us to identify kinases responsible for NRG1 phosphorylation and further our understanding of NRG1.2 signalling. Furthermore, it is important to know if NRG1.2 S152 is important for HR activation and pathogen resistance in Arabidopsis. Stable transgenic lines with *At*NRG1.2^{152A} in a *nrg1.1/1.2* background would need to be made. Overall, this work provides the basis for future investigations into the role of NRG1.2 phosphorylation in NRG1 oligomerisation and HR activation.

Chapter 6

General discussion

6 General discussion

Effector-triggered immunity (ETI) signalling and NLR biology have seen major advances in the last four years. In 2019 the first plant NLR resistosome structure was solved with cryo–electron microscopy for the CC-NLR ZAR1 (Wang et al., 2019a, Wang et al., 2019b). Since then multiple CC- and TIR-NLR structures have shown many similarities to ZAR1 in their activation mechanisms (Ma et al., 2020a, Martin et al., 2020, Forderer et al., 2022, Zhao et al., 2022). Oligomerisation has also been shown for helper NLRs NRG1 and NRCs (Jacob et al., 2021, Contreras et al., 2022, Ahn et al., 2023, Feehan et al., 2023, Wang et al., 2023). CC-NLR resistosomes form Ca^{2+} channels in the plasma membrane to induce cell death (Bi et al., 2021, Jacob et al., 2021, Forderer et al., 2022, Wang et al., 2023). Additionally, TIR-NLR NADase activity and the production of small molecules has advanced our understanding of how effector recognition and NLR activation trigger downstream defence signalling (Horsefield et al., 2019, Wan et al., 2019, Huang et al., 2022, Jia et al., 2022). The observation of mutual potentiation between PTI and ETI (Ngou et al., 2021, Yuan et al., 2021) and discovery that both PTI and ETI activation are required for NRG1 oligomerisation (Feehan et al., 2023) has revealed links between what were previously regarded as separate immune pathways. However, there still remains a large black box in ETI signalling. For example, it is still unknown how EDS1-PAD4-ADR1 heterotrimer formation leads to transcriptional changes and pathogen growth restriction. Our study aimed to further understand ETI signalling, by studying ETI-induced phosphorylation changes and protein interactions of important ETI proteins.

6.1 Does ETI-induced phosphorylation play a role in transcriptional regulation?

Phosphorylation changes during pattern-triggered immunity (PTI) have been extensively studied. Many PTI-induced phosphorylation sites have been discovered with quantitative phospho-proteomic approaches (Benschop et al., 2007, Nühse et al., 2007, Rayapuram et al., 2014, Mattei et al., 2016, Rayapuram et al., 2021). Further analysis has revealed the importance of phosphorylation changes for the activation of PTI signalling pathways e.g. FLS2 and BAK1 phosphorylation of BIK1, RBOHD phosphorylation and production of ROS, activation of MAPKs and transcriptional changes (Asai et al., 2002, Lu et al., 2010, Zhang et al., 2010a, Mao et al., 2011, Kadota et al., 2014, Li et al., 2014b, Lin et al., 2014). Some phosphorylation sites have been identified after activation of CC-NLR mediated ETI (Kadota et al., 2019). To understand if phosphorylation is also important during TIR-NLR mediated ETI, we studied phosphorylation changes in nuclear proteins after estradiol-inducible *AvrRps4* expression (ETI alone) (Chapter 3). We identified fewer changes in phosphorylation after activation of ETI alone, compared to large changes previously seen during PTI signalling (Benschop et al., 2007, Nühse et al.,

2007, Rayapuram et al., 2014, Mattei et al., 2016, Rayapuram et al., 2021). Due to mutual potentiation between PTI and ETI and prolonged phosphorylation of BIK1, RBOHD and MPK3 during PTI + ETI (Ngou et al., 2021, Yuan et al., 2021), we would expect larger phosphorylation changes to be detected upon PTI + ETI compared to ETI alone. Both PTI and ETI are required for full defence activation (Ngou et al., 2021, Yuan et al., 2021). Therefore, to further understand the different signalling pathways activated between ETI and PTI + ETI, future quantitative phospho-proteomic studies should be repeated comparing PTI, ETI and PTI + ETI. One of the key outputs after estradiol-inducible *AvrRps4* expression is transcriptional activation (Ngou et al., 2020, Ngou et al., 2021, Yuan et al., 2021). Many of the ETI-induced phosphorylated proteins we identified are involved in transcription (Chapter 3). Therefore, our phospho-proteomic data provides leads into which proteins may be responsible for these ETI-induced transcriptional changes, and how transcriptional changes are activated through phosphorylation. However, these data reflect the proteins we selected as targets for parallel reaction monitoring (PRM) quantification and our focus on the nuclear protein fraction. There may be additional classes of nuclear proteins, e.g. nuclear export proteins, that are phosphorylated upon ETI activation which were not identified as phosphorylated, as we did not select them for quantification.

Additional post-translational modifications (PTMs) may also play a role in transcriptional regulation (Ramirez-Prado et al., 2018, Kang et al., 2022). Histone deacetylase 6 (HDA6) represses gene expression of defence genes PR1, PR2 and WRKY38 through chromatin modification (Wang et al., 2017). The histone demethylase JmjC DOMAIN-CONTAINING PROTEIN 27 (JMJ27) regulates methylation levels at the promoter of PR1 to increase expression of PR1 upon infection with *P. syringae* (Dutta et al., 2017). Therefore, phosphorylation is not the only process by which ETI-induced transcriptional changes are regulated. It would be informative to investigate these PTMs of nuclear proteins during ETI activation and study how they are different during PTI or PTI + ETI signalling. Additionally, the transcriptional activity of Topless (TPL) is regulated by acetylation (An et al., 2022). Acetylation of TPL at K689 is mediated by the histone acetyltransferase General Control Non-Depressible 5 (GCN5) (An et al., 2022). Acetylated TPL has an enhanced interaction with Novel Interactor of JAZ (NINJA) and increased corepressor activity at MYC2 target genes (An et al., 2022). In response to JA, TPL is deacetylated by HISTONE DEACETYLASE 6 (HDA6), weakening its interaction with NINJA, leading to transcriptional activation of JA responsive genes (An et al., 2022). During *Botrytis cinerea* infection, *HDA6* gene expression levels increase and this is correlated with a decrease in the levels of acetylated TPL (An et al., 2022). Additionally the GCN5 loss of function mutant *hga1-6* has increased ETHYLENE RESPONSE FACTOR 1 (ERF1) defence gene activation and decreased *B. cinerea* lesion area (An et al., 2022). Conversely, the HDA6 loss-of-function mutant *axe1-4* has reduced *EFR1*

expression and a larger lesion area (An et al., 2022). This suggests TPL is deacetylated by HDA6 upon pathogen infection, to inhibit TPL corepressor activity at defence gene promoters (An et al., 2022). Therefore, TPR1 and other transcriptional corepressors may also be regulated by acetylation during defence activation. Whether acetylation and phosphorylation work together or antagonistically to activate TPR1 activity during immune responses needs to be explored and would provide insight into the mechanisms controlling transcriptional activation.

Two Mediator subunits MED12 and MED17 are de-phosphorylated upon ETI activation. Phosphorylation of Mediator subunits has previously been linked to activation of transcriptional changes in other systems. Phosphorylation of the Mediator subunit MED1 enhances its interaction with Mediator and correlates with increased transcription during hormone signalling (Pandey et al., 2005, Belakavadi et al., 2008). The yeast *Saccharomyces cerevisiae* Mediator is phosphorylated on 17 of its 25 subunits and phosphorylation of the subunit MED15 were shown to suppress gene expression under non-stress (Miller et al., 2012). Therefore, ETI-induced phosphorylation of MED17 and MED12 may be important for transcriptional regulation.

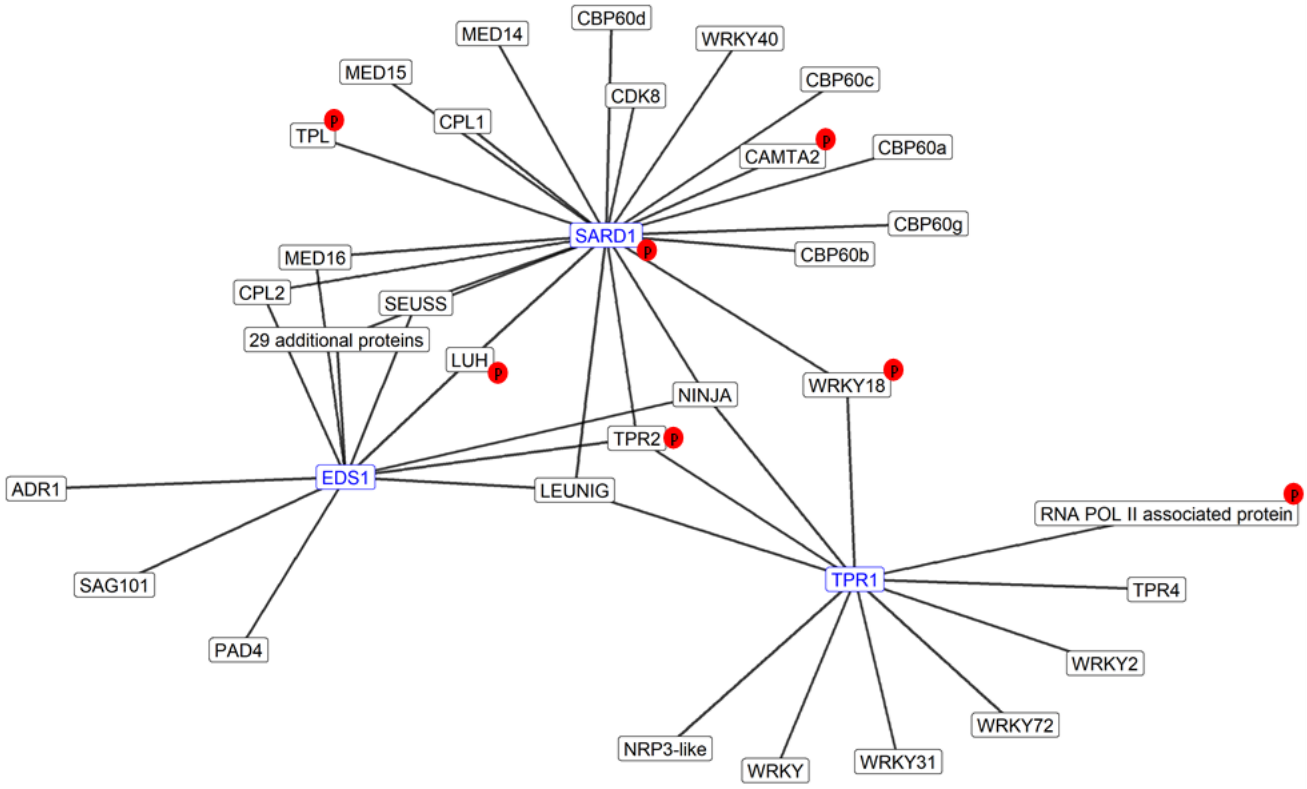

Figure 6.1 EDS1, TPR1 and SARD1 share common protein interactors, some of which are also phosphorylated and/or dephosphorylated upon ETI activation. Network of proteins classed as protein interactors of SARD1, EDS1 and TPR1 by TurboID proximity labelling. Proteins with a change in phosphorylation (increase or decrease) are labelled with P .

Upon PRR activation, MAPKs phosphorylate transcription factors e.g. WRKY DNA-BINDING PROTEIN 33 (WRKY33) to induce transcription of defence genes (Mao et al., 2011). It is not known how transcriptional changes are activated during ETI or PTI + ETI signalling. Therefore, the results from our study provide further insight into this research area. LEUNIG homolog (LUH), CAMTA2, mediator subunit MED12, TPR1, TPR2, TPR3 and WRKY18 show changes in phosphorylation upon ETI activation (Chapter 3, Figure 6.1). These proteins also all interact with SARD1 (Chapter 4, Figure 6.1), a master transcriptional regulator of PTI and ETI (Sun et al., 2015, Ding et al., 2020). Therefore, this suggests these phosphorylated proteins could be important ETI signalling components and that their activity might be regulated by phosphorylation. In addition, all these proteins are transcriptional regulators. Additional SARD1 interactors may also show a change in phosphorylation upon ETI activation but were not targeted for quantification by PRM. Until now it was not known how SARD1 regulates transcription, though ChIP-seq data show it can bind the promoters of defence gene targets e.g. EDS5, EDS1, WRKY70 (Sun et al., 2015). Therefore, we have identified not only putative components of ETI-transcriptional regulation but also putative SARD1 protein interactors, providing novel insights into potential mechanisms for transcriptional regulation. Functional characterisation of these SARD1 interactions is needed to understand their importance.

37 proteins interacted with both SARD1 and EDS1 (Chapter 4). However, SARD1 and EDS1 were not found to interact with each other, suggesting SARD1 and EDS1 form separate protein complexes with these proteins during ETI signalling. We found EDS1 to interact with the transcriptional regulators SEUSS and NINJA, as well as the mediator subunit MED16 and RNA polymerase II C-terminal domain phosphatase-like 2 (CPL2) (Chapter 4), suggesting a link between EDS1 heterotrimer formation and transcriptional activation. SEUSS and NINJA have not previously been directly linked to plant immunity, suggesting a potential new role for these proteins. NINJA is reported to act as a negative regulator of JA signalling, through repression of MYC2 target genes (Pauwels et al., 2010). Whether these transcriptional repressors repress negative or positive regulators of immunity and the biological function of their interactions with EDS1, is an important question. MED16 is a positive regulator of immunity and regulates SA-induced defence, including *PR1* gene expression (Zhang et al., 2012). Therefore, MED16 may positively regulate SA-induced defence responses, through interactions with EDS1 and SARD1. These results suggest EDS1 may have additional roles in transcriptional regulation, through interactions with these proteins. Whether these EDS1 interactions are independent to the EDS1-SAG101-NRG1 or EDS1-PAD4-ADR1 heterotrimers is not known and needs to be investigated, to determine if EDS1 has independent activities during ETI signalling.

Both our quantitative phospho-proteomics study and proximity labelling study give insights into how transcriptional regulation is controlled during ETI activation. Therefore, both these proteomic methods have been useful tools to identify promising leads for further investigation. Whether SEUSS, LEUNIG, NINJA and EDS1 have a direct role in regulating ETI-induced transcription needs to be tested with transcriptional reporter assays, qPCRs and ChIP-Seq, revealing if these proteins bind to defence gene promoters. ChIP-Seq would also reveal if the SARD1 interactors are binding at the same sites as SARD1, supporting the hypothesis for the formation of a SARD1 protein complex which regulates transcription. Additionally, whether phosphorylation of these proteins is important for ETI-induced transcriptional activation and/or SARD1 or EDS1 interaction should be further tested with *in vivo* studies. The impact of creating phospho-mimic or phospho-dead variants of these proteins on transcription and protein interactions, should be investigated. Although our study gives an insight into how transcriptional changes may be regulated, through protein interactions and changes in phosphorylation, additional experiments would address if ETI-induced phosphorylation does indeed induce transcriptional regulation.

6.2 Investigating the role of ETI-induced phosphorylation changes

During PTI activation, transcription factors are phosphorylated to induce transcriptional changes. WRKY33 is phosphorylated by MPK3/MPK6 to activate the expression of camalexin biosynthesis genes (Mao et al., 2011). *Nb*WRKY8 is phosphorylated by MAPKs, activating RBOHB expression, and a ROS burst in response to the INF1 elicitor from *Phytophthora infestans* (Ishihama et al., 2011, Adachi et al., 2015). Additionally, a phospho-mimic of WRKY8 strongly induces cell death (Adachi et al., 2015). Therefore, previous literature suggests that phosphorylation of transcription factors, particularly WRKYs, is important for transcriptional regulation and activation of defence pathways. The results from our phospho-proteomics approach described in chapter 3 suggest that ETI-induced phosphorylation may play a role in activating transcriptional changes. At the individual protein level this can be further explored by comparing gene expression changes upon introduction of phospho-mimic and phospho-dead variants of these proteins. An increase in SARD1 phosphorylation was detected upon ETI activation (Chapter 3). We aimed to show that this phosphorylation was important for the transcriptional regulation of EDS5 expression. Phospho-mimics of SARD1 increased EDS5 expression, however protoplasts expressing phospho-dead SARD1 and SARD1 wildtype had similar levels of EDS5 expression. Additionally, we were unable to detect differences in EDS5 expression between SARD1 phospho-variants upon ETI or PTI + ETI activation in protoplasts. Based on these results, we cannot conclude that ETI-induced SARD1 phosphorylation is important for transcriptional

regulation. We plan to investigate the role of SARD1 phosphorylation further with transgenic Arabidopsis lines expressing either wildtype, phospho-mimic or phospho-dead variants. Using these lines we can determine if these SARD1 phospho-sites are important for PTI, ETI or PTI + ETI activation *in vivo*. Bacterial growth assays and RT-qPCRs of defence genes e.g. ICS1, would determine if SARD1 phosphorylation is important for bacterial growth restriction and defence gene activation. ChIP-seq with SARD1 phospho-variants would reveal if phosphorylation of SARD1 is directly required for binding to gene promoters and regulating transcription. As mass-spectrometry (MS) data-dependent acquisition (DDA) measures the most abundant peptides, there may be additional phosphorylation sites within SARD1 which were not detected in our large-scale MS analysis. Therefore, immunoprecipitation-MS (IP-MS) of tagged SARD1 would allow us to identify any further phosphorylation changes during PTI, ETI or PTI + ETI activation. These additional experiments would allow us to conclude if SARD1 phosphorylation is important for its function as a transcriptional regulator of immunity-induced transcriptional changes. Additionally, identifying differences in SARD1 phosphorylation between PTI, ETI and PTI + ETI may provide an insight into how transcription is regulated differently between these immunity states.

TPR1 and WRKY18 show a phosphorylation change upon ETI activation (Chapter 3). Additionally, we showed that TPR1 and WRKY18 interact by co-immunoprecipitation (Co-IP) (Chapter 4). However, phospho-mimic and phospho-dead variants of TPR1 or WRKY18 did not change the TPR1-WRKY18 interaction in mock or Pf0-1_XopQ treated samples (Chapter 4). Therefore, these ETI-induced phosphorylation changes are not required for this interaction. This is expected, as we also found that the TPR1-WRKY18 interaction itself does not change upon ETI activation, suggesting ETI does not induce or inhibit the interaction. Therefore, the role of phosphorylation changes of these two proteins remain unknown. As these changes were identified during ETI alone, it would be interesting to investigate if these phosphorylation changes also occur during PTI or PTI + ETI.

No ETI-induced phosphorylation changes were shown to be functionally relevant for SARD1, TPR1 or WRKY18 during ETI activation in the experiments we performed. However, we only focused on SARD1 transcriptional activation of EDS5 and TPR1-WRKY18 interaction. Therefore, there may be other roles and functions for the phosphorylation changes during ETI that we have not tested. For example, phosphorylation of these transcriptional regulators may be important for their interaction with other transcriptional regulators, activating the transcription of other defence genes e.g. ICS1, regulating the transcription of negative regulators of immunity, or controlling their sub-cellular nuclear localisation.

6.3 What kinases or phosphatases are responsible for ETI-induced phosphorylation changes?

TPR1 showed an increase and decrease in phosphorylation at different phosphorylation sites upon ETI activation in our quantitative proteomics study (Chapter 3). Kagale and Rozwadowski (2011) reported that they had unpublished work showing two protein kinases and a phosphatase that interact with TPL (Kagale & Rozwadowski, 2011). However, nothing has since been published on this. Therefore, to help us identify possible kinases or phosphatases that interact with TPR1 and could be responsible for the ETI induced phosphorylation changes of TPR1, we carried out TPR1-TurboID in *N. benthamiana*. Three *N. benthamiana* protein phosphatases were identified as interacting with *At*TPR1 during PTI and PTI + ETI activation (Chapter 4). The protein phosphatase Nbv6.1trA208100 has high protein identity to a SIT4 phosphatase-associated family protein (AT3G45190) in Arabidopsis. The protein phosphatase Nbv6.1trA144181 is orthologous to the Arabidopsis protein phosphatase 2C family protein (AT4G31860). Three SIT4 phosphatase proteins interact with EDS1 (Chapter 4). Therefore, both EDS1 and TPR1 interact with SIT4 protein phosphatases, indicating that SIT4 phosphatases could have an important role in ETI signal transduction. Neither the SIT4 protein phosphatases nor the protein phosphatase 2C family protein have been linked to plant immunity in the current literature. Therefore, these phosphatases need to be further investigated to determine if they are responsible for the decrease in phosphorylation identified at TPR1 T286, T289, and S291. *In-vitro* phosphatase assays would determine if the identified phosphatases could dephosphorylate TPR1. Further phospho-mimic and phospho-dead analysis would reveal if TPR1 phosphorylation changes are important for disease resistance or defence gene activation.

Seventeen protein kinases were identified as TPR1 interactors in our proximity labelling (PL) dataset (Chapter 4). Each of these kinases should be tested to confirm if they are responsible for the TPR1 T395 phosphorylation increases seen during ETI signalling in Chapter 3, e.g. using *in-vitro* kinase assays. Seven protein kinases show phosphorylation changes upon ETI activation (Chapter 3). However, most of these kinases are localised to the plasma membrane, which suggests they are not involved in phosphorylating nuclear proteins. Calcium dependent protein kinase 1 (CPK1) is dephosphorylated upon ETI activation (Chapter 3). CPK1 expression increases 30 minutes after elicitor treatment (Coca & San Segundo, 2010). CPK1 has also been shown to induce RBOHD phosphorylation upon effector recognition (Gao et al., 2013). Over-expression of CPK1 leads to higher SA accumulation and constitutive expression of PR1, ICS1 and PAD4 (Coca & San Segundo, 2010). CPK1 also phosphorylates PHE AMMONIA LYASE 1 (PAL1), an enzyme involved in SA defence signalling (Cheng et al., 2001, Kim & Hwang, 2014). Therefore, CPK1 is an important positive regulator of immunity.

Whether CPK1 is responsible for ETI-induced transcriptional changes should be tested. No calcium-dependent protein kinases were detected in TPR1-TurboID, suggesting TPR1 is phosphorylated by a different class of protein kinases during ETI.

In addition to TPR1, an increase in SARD1 phosphorylation was detected upon ETI activation (Chapter 3). SARD1 is an important transcription factor during ETI activation (Zhang et al., 2010b, Wang et al., 2011a, Sun et al., 2015). Therefore, identifying the kinase responsible for SARD1 phosphorylation would provide insights into ETI signalling and how SARD1 is activated to regulate transcription. To identify the protein kinase that phosphorylates SARD1, we performed SARD1-TurboID in Arabidopsis. However, only one protein kinase was identified as a SARD1 interactor (Chapter 4). MAP KINASE 11 (MPK11) interacts with SARD1 during PTI activation (Chapter 4). MPK11 is activated upon flg22 detection (Bethke et al., 2012). AvrRpt2 from *Pseudomonas syringae* inhibits flg22-induced phosphorylation of MPK11, leading to reduced expression of defence genes (Eschen-Lippold et al., 2016). Therefore, MPK11 is important for plant defence activation. As MPK11 and SARD1 interact, MPK11 could regulate SARD1 activity during PTI activation. However, MPK11 was not identified as a SARD1 interactor during PTI + ETI activation, suggesting MPK11 may not be responsible for the phosphorylation induced upon ETI activation. Additionally, the SARD1 phosphorylation site S75/S76/S77 is not proline directed, suggesting SARD1 is not phosphorylated by a proline-directed MAPK. As no other protein kinases were identified in our PL study, we are unable to comment on which protein kinase is responsible for increases in SARD1 phosphorylation induced upon ETI activation. The protein kinase responsible may be very low abundance and therefore was not able to be detected by mass-spectrometry, or the interaction may be too transient to be detected using PL under the conditions we used. The SARD1 phosphorylation site S77 is within a calcium-dependent protein kinase motif L-X-R-X-X-S (Kawamoto et al., 2015). SARD1 acts redundantly with CBP60g and CBP60g is phosphorylated by the calcium-dependent protein kinase CPK5 (Zhang et al., 2010b, Wang et al., 2011a, Sun et al., 2022). CPK5 was not found to interact with SARD1 with PL (Chapter 4). However, as S77 is a calcium-dependent kinase motif and CPK5 phosphorylates CBP60g, it is important to test if CPK5 phosphorylates SARD1 during PTI or ETI signalling using *in-vitro* kinase assays and *in-vivo* with phos-tag gels and Co-IPs.

To summarise, we have identified ETI-induced phosphorylation sites on multiple proteins including protein kinases, RNA polymerase-associated proteins and transcriptional regulators. We have identified seven protein kinases which interact with TPR1 using PL, providing leads for further analysis to reveal the kinase responsible for ETI-induced TPR1 phosphorylation. Understanding the kinases and phosphatases required for ETI-induced phosphorylation changes will further our

understanding of ETI signal transduction and the molecular mechanisms regulating transcriptional activation.

6.4 Is phosphorylation important for NRG1 activation and oligomerisation?

Upon ETI activation, without PTI, NRG1 forms heterotrimers with EDS1 and SAG101 (Sun et al., 2021, Feehan et al., 2023). However, both PTI and ETI are required for NRG1 oligomerisation and the formation of NRG1-EDS1-SAG101 resistosomes (Feehan et al., 2023). We hypothesise that PTI induces phosphorylation of NRG1 and this PTI-induced phosphorylation is required for NRG1 oligomerisation. We have shown that 4 hours of PTI and PTI + ETI treatment leads to multiple slower migrating NRG1.2 protein bands in Phos-tag gels (Chapter 5). These slower migrating bands disappear after phosphatase treatment, suggesting they are phosphorylated species of NRG1.2. Phosphorylation levels of NRG1.2 at S152 or S433 were similar between mock and 4 hours of PTI, ETI or PTI + ETI -induced samples. Despite this, NRG1 S152 is important for HR activation in *N. benthamiana,* suggesting NRG1 phosphorylation does play a role in HR activation (Chapter 5). The role of S433 phosphorylation is not as clear, as both phospho-mimic and phospho-dead variants of S433 show a reduction in HR. Four hours after PTI or PTI + ETI induction may not be the time point at which phosphorylation increases to induce NRG1 oligomerisation. NRG1 oligomerisation was shown 8 hours after PTI + ETI activation (Feehan et al., 2023). PTI-induced phosphorylation of PTI components has been shown to occur very quickly and transiently (Benschop et al., 2007, Nühse et al., 2007, Lu et al., 2010, Rayapuram et al., 2014, Ngou et al., 2021). However, PTI + ETI leads to prolonged phosphorylation (Tsuda et al., 2013, Ngou et al., 2021, Yu et al., 2021). Therefore, time-course experiments with both early and late time points are needed to determine at what time point phosphorylation of NRG1 is induced and if the phosphorylation is transient or long-lasting. We can see increases in NRG1.2 phosphorylation in Phos-tag gels at four hours after PTI induction but no changes in phosphorylation levels of S152 or S433 during PTI or PTI + ETI compared to mock by MS. Therefore, there may be important changes at additional NRG1 phosphorylation sites at 4 hours, which are responsible for the slower migrating Phos-tag bands and which we have not been able to detect yet by MS. Phos-tag gels with phospho-dead $NRG1^{152A+433A}$ will determine if the slower migrating protein bands are due to increased phosphorylation at S152/S433 or at additional unknown sites.

NRG1.1 and NRG1.2 act redundantly to form heterotrimers with EDS1-SAG101 and activate cell death upon PTI + ETI activation (Castel et al., 2019, Lapin et al., 2019, Wu et al., 2019, Sun et al., 2021). We were not able to detect slower migrating NRG1.1 protein bands in Phos-tag gels four hours after PTI

or PTI + ETI activation (Chapter 5). This suggests there may be some differences in the mechanisms activating NRG1.1 and NRG1.2. Whether NRG1.1 is phosphorylated at earlier or later time points needs to be further investigated with Phos-tag gels, IP-MS and MS quantification of phosphorylation sites. S152 and S433 are both conserved between NRG1.1 and NRG1.2. Therefore, it should be tested if these residues in NRG1.1 are also important for HR activation in *N. benthamiana*. This additional work will reveal any differences between the two NRG1 copies in their signalling mechanisms and if this has any implications for the downstream events e.g. oligomerisation and activation of cell death.

We have generated NRG1.2-TurboID Arabidopsis lines which we aim to use to identify the kinase phosphorylating NRG1.2 during PTI and PTI + ETI activation. NRG1.2 S152 is a proline-directed site suggesting this residue may be phosphorylated by a MAPK. Identification of the kinase responsible for NRG1 phosphorylation will enhance our understanding of PTI and PTI + ETI signalling.

We hypothesis that PTI-induced NRG1 phosphorylation is required for NRG1 oligomerisation, as NRG1 does not oligomerise in the absence of PTI (Feehan et al., 2023). Blue native PAGE gels with phospho-dead mutants of NRG1 will reveal if NRG1 phosphorylation is important for higher-order complex formation. These experiments will provide huge insights into the mechanisms behind helper NLR activation and enhance our understanding of the role of phosphorylation during PTI + ETI signalling.

6.5 Summary

Our study aimed to investigate downstream ETI signalling using several experimental techniques. We used a quantitative phospho-proteomic approach and identified novel ETI-induced phosphorylation sites in proteins involved in transcriptional regulation. Proximity labelling of three key downstream ETI proteins revealed novel protein interactors suggesting a signalling hub for induction of transcriptional changes. Additionally, several proteins were found to be both phosphorylated upon ETI and interact with SARD1, revealing novel ETI signalling proteins involved in transcriptional regulation. We further investigated the interaction between TPR1-WRKY18 and found the WRKY EAR domain to be important for TPR1 nuclear puncta co-localisation. However, several important questions still remain: What is the role of ETI-induced phosphorylation and the role of protein interactions identified in this study? What is the role of WRKY18 in ETI-induced transcriptional regulation? Why is the WRKY18 EAR domain important for TPR1 nuclear puncta co-localisation? To further our understanding of helper NLR biology, we investigated NRG1 phosphorylation during PTI and PTI + ETI activation. We identified two NRG1 phosphorylation sites and showed S152 is important for HR activation. This provides the basis for future work into NRG1 oligomerisation

activation mechanisms. Overall this study provides an insight into the signalling pathways activated for NRG1 activation and the control of transcriptional regulation, both in terms of phosphorylation changes and protein/protein interactions.

References

Adachi H, Contreras MP, Harant A, Wu CH, Derevnina L, Sakai T, Duggan C, Moratto E, Bozkurt TO, Maqbool A, Win J, Kamoun S, 2019a. An N-terminal motif in NLR immune receptors is functionally conserved across distantly related plant species. *Elife* **8**.

Adachi H, Derevnina L, Kamoun S, 2019b. NLR singletons, pairs, and networks: evolution, assembly, and regulation of the intracellular immunoreceptor circuitry of plants. *Curr Opin Plant Biol* **50**, 121-31.

Adachi H, Nakano T, Miyagawa N, Ishihama N, Yoshioka M, Katou Y, Yaeno T, Shirasu K, Yoshioka H, 2015. WRKY Transcription Factors Phosphorylated by MAPK Regulate a Plant Immune NADPH Oxidase in Nicotiana benthamiana. *Plant Cell* **27**, 2645-63.

Agrawal R, Sharma M, Dwivedi N, Maji S, Thakur P, Junaid A, Fajkus J, Laxmi A, Thakur JK, 2022. MEDIATOR SUBUNIT17 integrates jasmonate and auxin signaling pathways to regulate thermomorphogenesis. *Plant Physiol* **189**, 2259-80.

Ahn HK, Lin X, Olave-Achury AC, Derevnina L, Contreras MP, Kourelis J, Wu CH, Kamoun S, Jones JDG, 2023. Effector-dependent activation and oligomerization of plant NRC class helper NLRs by sensor NLR immune receptors Rpi-amr3 and Rpi-amr1. *Embo Journal*.

Alcantara A, Bosch J, Nazari F, Hoffmann G, Gallei M, Uhse S, Darino MA, Olukayode T, Reumann D, Baggaley L, Djamei A, 2019. Systematic Y2H Screening Reveals Extensive Effector-Complex Formation. *Front Plant Sci* **10**, 1437.

An C, Deng L, Zhai H, You Y, Wu F, Zhai Q, Goossens A, Li C, 2022. Regulation of jasmonate signaling by reversible acetylation of TOPLESS in Arabidopsis. *Mol Plant* **15**, 1329-46.

Asai T, Tena G, Plotnikova J, Willmann MR, Chiu WL, Gomez-Gomez L, Boller T, Ausubel FM, Sheen J, 2002. MAP kinase signalling cascade in Arabidopsis innate immunity. *Nature* **415**, 977-83.

Baena G, Xia L, Waghmare S, Karnik R, 2022. SNARE SYP132 mediates divergent traffic of plasma membrane H+-ATPase AHA1 and antimicrobial PR1 during bacterial pathogenesis. *Plant Physiol* **189**, 1639-61.

Baggs EL, Monroe JG, Thanki AS, O'grady R, Schudoma C, Haerty W, Krasileva KV, 2020. Convergent Loss of an EDS1/PAD4 Signaling Pathway in Several Plant Lineages Reveals Coevolved Components of Plant Immunity and Drought Response. *Plant Cell* **32**, 2158-77.

Bardwell L, 2006. Mechanisms of MAPK signalling specificity. *Biochem Soc Trans* **34**, 837-41.

Belakavadi M, Pandey PK, Vijayvargia R, Fondell JD, 2008. MED1 phosphorylation promotes its association with mediator: implications for nuclear receptor signaling. *Mol Cell Biol* **28**, 3932-42.

Benschop JJ, Mohammed S, O'flaherty M, Heck AJR, Slijper M, Menke FLH, 2007. Quantitative Phosphoproteomics of Early Elicitor Signaling in *Arabidopsis*. *Molecular & Cellular Proteomics* **6**, 1198-214.

Bethke G, Pecher P, Eschen-Lippold L, Tsuda K, Katagiri F, Glazebrook J, Scheel D, Lee J, 2012. Activation of the Arabidopsis thaliana mitogen-activated protein kinase MPK11 by the flagellin-derived elicitor peptide, flg22. *Mol Plant Microbe Interact* **25**, 471-80.

Bethke G, Unthan T, Uhrig JF, Poschl Y, Gust AA, Scheel D, Lee J, 2009. Flg22 regulates the release of an ethylene response factor substrate from MAP kinase 6 in Arabidopsis thaliana via ethylene signaling. *Proc Natl Acad Sci U S A* **106**, 8067-72.

Bhandari DD, Lapin D, Kracher B, Von Born P, Bautor J, Niefind K, Parker JE, 2019. An EDS1 heterodimer signalling surface enforces timely reprogramming of immunity genes in Arabidopsis. *Nat Commun* **10**, 772.

Bhattacharjee S, Halane MK, Kim SH, Gassmann W, 2011. Pathogen effectors target Arabidopsis EDS1 and alter its interactions with immune regulators. *Science* **334**, 1405-8.

Bi G, Su M, Li N, Liang Y, Dang S, Xu J, Hu M, Wang J, Zou M, Deng Y, Li Q, Huang S, Li J, Chai J, He K, Chen YH, Zhou JM, 2021. The ZAR1 resistosome is a calcium-permeable channel triggering plant immune signaling. *Cell*.

Bigeard J, Colcombet J, Hirt H, 2015. Signaling mechanisms in pattern-triggered immunity (PTI). *Mol Plant* **8**, 521-39.

Bigeard J, Rayapuram N, Bonhomme L, Hirt H, Pflieger D, 2014. Proteomic and phosphoproteomic analyses of chromatin-associated proteins from Arabidopsis thaliana. *Proteomics* **14**, 2141-55.

Bindics J, Khan M, Uhse S, Kogelmann B, Baggely L, Reumann D, Ingole KD, Stirnberg A, Rybecky A, Darino M, Navarrete F, Doehlemann G, Djamei A, 2022. Many ways to TOPLESS - manipulation of plant auxin signalling by a cluster of fungal effectors. *New Phytol* **236**, 1455-70.

Birkenbihl RP, Kracher B, Roccaro M, Somssich IE, 2017. Induced Genome-Wide Binding of Three Arabidopsis WRKY Transcription Factors during Early MAMP-Triggered Immunity. *Plant Cell* **29**, 20-38.

Bjornson M, Pimprikar P, Nurnberger T, Zipfel C, 2021. The transcriptional landscape of Arabidopsis thaliana pattern-triggered immunity. *Nat Plants* **7**, 579-86.

Bonardi V, Tang S, Stallmann A, Roberts M, Cherkis K, Dangl JL, 2011. Expanded functions for a family of plant intracellular immune receptors beyond specific recognition of pathogen effectors. *Proc Natl Acad Sci U S A* **108**, 16463-8.

Boudsocq M, Willmann MR, Mccormack M, Lee H, Shan L, He P, Bush J, Cheng SH, Sheen J, 2010. Differential innate immune signalling via Ca(2+) sensor protein kinases. *Nature* **464**, 418-22.

Boyes DC, Nam J, Dangl JL, 1998. The Arabidopsis thaliana RPM1 disease resistance gene product is a peripheral plasma membrane protein that is degraded coincident with the hypersensitive response. *Proc Natl Acad Sci U S A* **95**, 15849-54.

Branon TC, Bosch JA, Sanchez AD, Udeshi ND, Svinkina T, Carr SA, Feldman JL, Perrimon N, Ting AY, 2018. Efficient proximity labeling in living cells and organisms with TurboID. *Nat Biotechnol* **36**, 880-7.

Burdett H, Kobe B, Anderson PA, 2019. Animal NLRs continue to inform plant NLR structure and function. *Arch Biochem Biophys* **670**, 58-68.

Castel B, Ngou PM, Cevik V, Redkar A, Kim DS, Yang Y, Ding P, Jones JDG, 2019. Diverse NLR immune receptors activate defence via the RPW8-NLR NRG1. *New Phytol* **222**, 966-80.

Causier B, Ashworth M, Guo W, Davies B, 2012. The TOPLESS interactome: a framework for gene repression in Arabidopsis. *Plant Physiol* **158**, 423-38.

Cesari S, 2018. Multiple strategies for pathogen perception by plant immune receptors. *New Phytologist* **219**, 17-24.

Cesari S, Bernoux M, Moncuquet P, Kroj T, Dodds PN, 2014a. A novel conserved mechanism for plant NLR protein pairs: the "integrated decoy" hypothesis. *Front Plant Sci* **5**, 606.

Cesari S, Kanzaki H, Fujiwara T, Bernoux M, Chalvon V, Kawano Y, Shimamoto K, Dodds P, Terauchi R, Kroj T, 2014b. The NB-LRR proteins RGA4 and RGA5 interact functionally and physically to confer disease resistance. *Embo Journal* **33**, 1941-59.

Cesari S, Thilliez G, Ribot C, Chalvon V, Michel C, Jauneau A, Rivas S, Alaux L, Kanzaki H, Okuyama Y, Morel JB, Fournier E, Tharreau D, Terauchi R, Kroj T, 2013. The rice resistance protein pair RGA4/RGA5 recognizes the Magnaporthe oryzae effectors AVR-Pia and AVR1-CO39 by direct binding. *Plant Cell* **25**, 1463-81.

Chang M, Zhao J, Chen H, Li G, Chen J, Li M, Palmer IA, Song J, Alfano JR, Liu F, Fu ZQ, 2019. PBS3 Protects EDS1 from Proteasome-Mediated Degradation in Plant Immunity. *Mol Plant* **12**, 678-88.

Chapman-Smith A, Mulhern TD, Whelan F, Cronan JE, Wallace JC, 2001. The C-terminal domain of biotin protein ligase from E-coli is required for catalytic activity. *Protein Science* **10**, 2608-17.

Chen C, Chen Z, 2002. Potentiation of developmentally regulated plant defense response by AtWRKY18, a pathogen-induced Arabidopsis transcription factor. *Plant Physiol* **129**, 706-16.

Chen H, Lai Z, Shi J, Xiao Y, Chen Z, Xu X, 2010. Roles of arabidopsis WRKY18, WRKY40 and WRKY60 transcription factors in plant responses to abscisic acid and abiotic stress. *BMC Plant Biol* **10**, 281.

Chen H, Li M, Qi G, Zhao M, Liu L, Zhang J, Chen G, Wang D, Liu F, Fu ZQ, 2021. Two interacting transcriptional coactivators cooperatively control plant immune responses. *Sci Adv* **7**, eabl7173.

Chen J, Mohan R, Zhang Y, Li M, Chen H, Palmer IA, Chang M, Qi G, Spoel SH, Mengiste T, Wang D, Liu F, Fu ZQ, 2019. NPR1 Promotes Its Own and Target Gene Expression in Plant Defense by Recruiting CDK8. *Plant Physiol* **181**, 289-304.

Chen Z, Cheng Q, Hu C, Guo X, Chen Z, Lin Y, Hu T, Bellizzi M, Lu G, Wang GL, Wang Z, Chen S, Wang F, 2017. A Chemical-Induced, Seed-Soaking Activation Procedure for Regulated Gene Expression in Rice. *Front Plant Sci* **8**, 1447.

Cheng SH, Sheen J, Gerrish C, Bolwell GP, 2001. Molecular identification of phenylalanine ammonia-lyase as a substrate of a specific constitutively active Arabidopsis CDPK expressed in maize protoplasts. *FEBS Lett* **503**, 185-8.

Choi SM, Song HR, Han SK, Han M, Kim CY, Park J, Lee YH, Jeon JS, Noh YS, Noh B, 2012. HDA19 is required for the repression of salicylic acid biosynthesis and salicylic acid-mediated defense responses in Arabidopsis. *Plant J* **71**, 135-46.

Clay NK, Adio AM, Denoux C, Jander G, Ausubel FM, 2009. Glucosinolate metabolites required for an Arabidopsis innate immune response. *Science* **323**, 95-101.

Clough SJ, Bent AF, 1998. Floral dip: a simplified method for Agrobacterium-mediated transformation of Arabidopsis thaliana. *Plant J* **16**, 735-43.

Coca M, San Segundo B, 2010. AtCPK1 calcium-dependent protein kinase mediates pathogen resistance in Arabidopsis. *Plant J* **63**, 526-40.

Collier SM, Hamel LP, Moffett P, 2011. Cell death mediated by the N-terminal domains of a unique and highly conserved class of NB-LRR protein. *Mol Plant Microbe Interact* **24**, 918-31.

Collins J, O'grady K, Chen S, Gurley W, 2019. The C-terminal WD40 repeats on the TOPLESS co-repressor function as a protein-protein interaction surface. *Plant Mol Biol* **100**, 47-58.

Conner J, Liu Z, 2000. LEUNIG, a putative transcriptional corepressor that regulates AGAMOUS expression during flower development. *Proc Natl Acad Sci U S A* **97**, 12902-7.

Contreras MP, Pai H, Tumtas Y, Duggan C, Yuen ELH, Cruces AV, Kourelis J, Ahn HK, Lee KT, Wu CH, Bozkurt TO, Derevnina L, Kamoun S, 2022. Sensor NLR immune proteins activate oligomerization of their NRC helpers in response to plant pathogens. *Embo Journal*.

Couto D, Zipfel C, 2016. Regulation of pattern recognition receptor signalling in plants. *Nature Reviews Immunology* **16**, 537-52.

Cramer P, 2019. Organization and regulation of gene transcription. *Nature* **573**, 45-54.

Cramer P, Bushnell DA, Fu J, Gnatt AL, Maier-Davis B, Thompson NE, Burgess RR, Edwards AM, David PR, Kornberg RD, 2000. Architecture of RNA polymerase II and implications for the transcription mechanism. *Science* **288**, 640-9.

Cui H, Qiu J, Zhou Y, Bhandari DD, Zhao C, Bautor J, Parker JE, 2018. Antagonism of Transcription Factor MYC2 by EDS1/PAD4 Complexes Bolsters Salicylic Acid Defense in Arabidopsis Effector-Triggered Immunity. *Mol Plant* **11**, 1053-66.

Cunnac S, Chakravarthy S, Kvitko BH, Russell AB, Martin GB, Collmer A, 2011. Genetic disassembly and combinatorial reassembly identify a minimal functional repertoire of type III effectors in Pseudomonas syringae. *Proc Natl Acad Sci U S A* **108**, 2975-80.

Darino M, Marques J, Chia K-S, Aleksza D, Soto LM, Uhse S, Borg M, Betz R, Bindics J, Zienkiewicz K, Feussner I, Petit-Houdenot Y, Djamei A, 2019. Fungal effector Jsi1 hijacks plant JA/ET signaling through Topless *bioRxiv*.

De La Fuente Van Bentem S, Anrather D, Dohnal I, Roitinger E, Csaszar E, Joore J, Buijnink J, Carreri A, Forzani C, Lorkovic ZJ, Barta A, Lecourieux D, Verhounig A, Jonak C, Hirt H, 2008. Site-specific phosphorylation profiling of Arabidopsis proteins by mass spectrometry and peptide chip analysis. *J Proteome Res* **7**, 2458-70.

De Lorenzo G, Cervone F, 2022. Plant immunity by damage-associated molecular patterns (DAMPs). *Essays Biochem* **66**, 459-69.

De Paolis A, Caretto S, Quarta A, Di Sansebastiano GP, Sbrocca I, Mita G, Frugis G, 2020. Genome-Wide Identification of WRKY Genes in Artemisia annua: Characterization of a Putative Ortholog of AtWRKY40. *Plants (Basel)* **9**.

De Wet JR, Wood KV, Helinski DR, Deluca M, 1985. Cloning of firefly luciferase cDNA and the expression of active luciferase in Escherichia coli. *Proc Natl Acad Sci U S A* **82**, 7870-3.

Deslandes L, Olivier J, Peeters N, Feng DX, Khounlotham M, Boucher C, Somssich I, Genin S, Marco Y, 2003. Physical interaction between RRS1-R, a protein conferring resistance to bacterial wilt, and PopP2, a type III effector targeted to the plant nucleus. *Proc Natl Acad Sci U S A* **100**, 8024-9.

Deslandes L, Olivier J, Theulieres F, Hirsch J, Feng DX, Bittner-Eddy P, Beynon J, Marco Y, 2002. Resistance to Ralstonia solanacearum in Arabidopsis thaliana is conferred by the recessive RRS1-R gene, a member of a novel family of resistance genes. *Proc Natl Acad Sci U S A* **99**, 2404-9.

Ding P, Ngou BPM, Furzer OJ, Sakai T, Shrestha RK, Maclean D, Jones JDG, 2020. High-resolution expression profiling of selected gene sets during plant immune activation. *Plant Biotechnol J*.

Ding P, Sakai T, Krishna Shrestha R, Manosalva Perez N, Guo W, Ngou BPM, He S, Liu C, Feng X, Zhang R, Vandepoele K, Maclean D, Jones JDG, 2021. Chromatin accessibility landscapes activated by cell-surface and intracellular immune receptors. *J Exp Bot* **72**, 7927-41.

Ding Y, Avramova Z, Fromm M, 2011. Two distinct roles of ARABIDOPSIS HOMOLOG OF TRITHORAX1 (ATX1) at promoters and within transcribed regions of ATX1-regulated genes. *Plant Cell* **23**, 350-63.

Ding Y, Sun T, Ao K, Peng Y, Zhang Y, Li X, Zhang Y, 2018. Opposite Roles of Salicylic Acid Receptors NPR1 and NPR3/NPR4 in Transcriptional Regulation of Plant Immunity. *Cell* **173**, 1454-67 e15.

Dongus JA, Bhandari DD, Penner E, Lapin D, Stolze SC, Harzen A, Patel M, Archer L, Dijkgraaf L, Shah J, Nakagami H, Parker JE, 2022. Cavity surface residues of PAD4 and SAG101 contribute to EDS1 dimer signaling specificity in plant immunity. *Plant J* **110**, 1415-32.

Dubiella U, Seybold H, Durian G, Komander E, Lassig R, Witte CP, Schulze WX, Romeis T, 2013. Calcium-dependent protein kinase/NADPH oxidase activation circuit is required for rapid defense signal propagation. *Proc Natl Acad Sci U S A* **110**, 8744-9.

Duggan C, Moratto E, Savage Z, Hamilton E, Adachi H, Wu CH, Leary AY, Tumtas Y, Rothery SM, Maqbool A, Nohut S, Martin TR, Kamoun S, Bozkurt TO, 2021. Dynamic localization of a helper NLR at the plant-pathogen interface underpins pathogen recognition. *Proc Natl Acad Sci U S A* **118**.

Dutta A, Choudhary P, Caruana J, Raina R, 2017. JMJ27, an Arabidopsis H3K9 histone demethylase, modulates defense against Pseudomonas syringae and flowering time. *Plant J* **91**, 1015-28.

Eick D, Geyer M, 2013. The RNA polymerase II carboxy-terminal domain (CTD) code. *Chem Rev* **113**, 8456-90.

Elmore JM, Griffin BD, Walley JW, 2021. Advances in functional proteomics to study interactions. *Current Opinion in Plant Biology* **63**.

Engler C, Gruetzner R, Kandzia R, Marillonnet S, 2009. Golden gate shuffling: a one-pot DNA shuffling method based on type IIs restriction enzymes. *PLoS One* **4**, e5553.

Eschen-Lippold L, Jiang X, Elmore JM, Mackey D, Shan L, Coaker G, Scheel D, Lee J, 2016. Bacterial AvrRpt2-Like Cysteine Proteases Block Activation of the Arabidopsis Mitogen-Activated Protein Kinases, MPK4 and MPK11. *Plant Physiol* **171**, 2223-38.

Eulgem T, Rushton PJ, Robatzek S, Somssich IE, 2000. The WRKY superfamily of plant transcription factors. *Trends Plant Sci* **5**, 199-206.

Falk A, Feys BJ, Frost LN, Jones JD, Daniels MJ, Parker JE, 1999. EDS1, an essential component of R gene-mediated disease resistance in Arabidopsis has homology to eukaryotic lipases. *Proc Natl Acad Sci U S A* **96**, 3292-7.

Fang J, Guo T, Xie Z, Chun Y, Zhao J, Peng L, Zafar SA, Yuan S, Xiao L, Li X, 2021a. The URL1-ROC5-TPL2 transcriptional repressor complex represses the ACL1 gene to modulate leaf rolling in rice. *Plant Physiol* **185**, 1722-44.

Fang X, Meng X, Zhang J, Xia M, Cao S, Tang X, Fan T, 2021b. AtWRKY1 negatively regulates the response of Arabidopsis thaliana to Pst. DC3000. *Plant Physiol Biochem* **166**, 799-806.

Feehan JM, Castel B, Bentham AR, Jones JD, 2020. Plant NLRs get by with a little help from their friends. *Curr Opin Plant Biol* **56**, 99-108.

Feehan JM, Wang J, Sun X, Choi J, Ahn H-K, Ngou BPM, Parker JE, Jones JDG, 2023. Oligomerisation of a plant helper NLR requires cell-surface and intracellular immune receptor activation. *PNAS* **120**, e2210406120.

Felix G, Duran JD, Volko S, Boller T, 1999. Plants have a sensitive perception system for the most conserved domain of bacterial flagellin. *Plant J* **18**, 265-76.

Feys BJ, Moisan LJ, Newman MA, Parker JE, 2001. Direct interaction between the Arabidopsis disease resistance signaling proteins, EDS1 and PAD4. *Embo Journal* **20**, 5400-11.

Feys BJ, Wiermer M, Bhat RA, Moisan LJ, Medina-Escobar N, Neu C, Cabral A, Parker JE, 2005. Arabidopsis SENESCENCE-ASSOCIATED GENE101 stabilizes and signals within an ENHANCED DISEASE SUSCEPTIBILITY1 complex in plant innate immunity. *Plant Cell* **17**, 2601-13.

Forderer A, Li E, Lawson AW, Deng YN, Sun Y, Logemann E, Zhang X, Wen J, Han Z, Chang J, Chen Y, Schulze-Lefert P, Chai J, 2022. A wheat resistosome defines common principles of immune receptor channels. *Nature* **610**, 532-9.

Franks RG, Wang C, Levin JZ, Liu Z, 2002. SEUSS, a member of a novel family of plant regulatory proteins, represses floral homeotic gene expression with LEUNIG. *Development* **129**, 253-63.

Frei Dit Frey N, Mbengue M, Kwaaitaal M, Nitsch L, Altenbach D, Haweker H, Lozano-Duran R, Njo MF, Beeckman T, Huettel B, Borst JW, Panstruga R, Robatzek S, 2012. Plasma membrane calcium ATPases are important components of receptor-mediated signaling in plant immune responses and development. *Plant Physiol* **159**, 798-809.

Galletti R, Ferrari S, De Lorenzo G, 2011. Arabidopsis MPK3 and MPK6 play different roles in basal and oligogalacturonide- or flagellin-induced resistance against Botrytis cinerea. *Plant Physiol* **157**, 804-14.

Gao X, Chen X, Lin W, Chen S, Lu D, Niu Y, Li L, Cheng C, Mccormack M, Sheen J, Shan L, He P, 2013. Bifurcation of Arabidopsis NLR immune signaling via Ca(2)(+)-dependent protein kinases. *PLoS Pathog* **9**, e1003127.

Garcia AV, Blanvillain-Baufume S, Huibers RP, Wiermer M, Li G, Gobbato E, Rietz S, Parker JE, 2010. Balanced nuclear and cytoplasmic activities of EDS1 are required for a complete plant innate immune response. *PLoS Pathog* **6**, e1000970.

Garner CM, Spears BJ, Su J, Cseke LJ, Smith SN, Rogan CJ, Gassmann W, 2021. Opposing functions of the plant TOPLESS gene family during SNC1-mediated autoimmunity. *PLoS Genet* **17**, e1009026.

Gassmann W, Hinsch ME, Staskawicz BJ, 1999. The Arabidopsis RPS4 bacterial-resistance gene is a member of the TIR-NBS-LRR family of disease-resistance genes. *Plant J* **20**, 265-77.

Geilen K, Bohmer M, 2015. Dynamic subnuclear relocalization of WRKY40, a potential new mechanism of ABA-dependent transcription factor regulation. *Plant Signal Behav* **10**, e1106659.

Geu-Flores F, Nour-Eldin HH, Nielsen MT, Halkier BA, 2007. USER fusion: a rapid and efficient method for simultaneous fusion and cloning of multiple PCR products. *Nucleic Acids Res* **35**, e55.

Goker M, Voglmayr H, Blazquez GG, Oberwinkler F, 2009. Species delimitation in downy mildews: the case of Hyaloperonospora in the light of nuclear ribosomal ITS and LSU sequences. *Mycol Res* **113**, 308-25.

Gomez-Gomez L, Boller T, 2000. FLS2: an LRR receptor-like kinase involved in the perception of the bacterial elicitor flagellin in Arabidopsis. *Mol Cell* **5**, 1003-11.

Gomez-Gomez L, Felix G, Boller T, 1999. A single locus determines sensitivity to bacterial flagellin in Arabidopsis thaliana. *Plant J* **18**, 277-84.

Gong BQ, Guo J, Zhang N, Yao X, Wang HB, Li JF, 2019. Cross-Microbial Protection via Priming a Conserved Immune Co-Receptor through Juxtamembrane Phosphorylation in Plants. *Cell Host Microbe* **26**, 810-22 e7.

Gonzalez D, Bowen AJ, Carroll TS, Conlan RS, 2007. The transcription corepressor LEUNIG interacts with the histone deacetylase HDA19 and mediator components MED14 (SWP) and CDK8 (HEN3) to repress transcription. *Mol Cell Biol* **27**, 5306-15.

Griebel T, Lapin D, Kracher B, Concia L, Benhamed M, Parker JE, 2020. Genome-wide chromatin binding of transcriptional corepressor Topless-related 1 in Arabidopsis. *bioRxiv*.

Griebel T, Lapin D, Locci F, Kracher B, Bautor J, Qiu J, Concia L, Benhamed M, Parker JE, 2021. Topless-related 1 mitigates physiological damage and growth penalties of induced immunity. *bioRxiv*, 2021.07.07.451397.

Guerra T, Schilling S, Hake K, Gorzolka K, Sylvester FP, Conrads B, Westermann B, Romeis T, 2020. Calcium-dependent protein kinase 5 links calcium signaling with N-hydroxy-l-pipecolic acid- and SARD1-dependent immune memory in systemic acquired resistance. *New Phytol* **225**, 310-25.

Guo H, Ahn HK, Sklenar J, Huang J, Ma Y, Ding P, Menke FLH, Jones JDG, 2020. Phosphorylation-Regulated Activation of the Arabidopsis RRS1-R/RPS4 Immune Receptor Complex Reveals Two Distinct Effector Recognition Mechanisms. *Cell Host Microbe*.

Guo H, Nolan TM, Song G, Liu S, Xie Z, Chen J, Schnable PS, Walley JW, Yin Y, 2018. FERONIA Receptor Kinase Contributes to Plant Immunity by Suppressing Jasmonic Acid Signaling in Arabidopsis thaliana. *Curr Biol* **28**, 3316-24 e6.

Hamdoun S, Liu Z, Gill M, Yao N, Lu H, 2013. Dynamics of defense responses and cell fate change during Arabidopsis-Pseudomonas syringae interactions. *PLoS One* **8**, e83219.

Hartmann M, Zeier T, Bernsdorff F, Reichel-Deland V, Kim D, Hohmann M, Scholten N, Schuck S, Brautigam A, Holzel T, Ganter C, Zeier J, 2018. Flavin Monooxygenase-Generated N-Hydroxypipecolic Acid Is a Critical Element of Plant Systemic Immunity. *Cell* **173**, 456-69 e16.

Harvey S, Kumari P, Lapin D, Griebel T, Hickman R, Guo W, Zhang R, Parker J, Beynon J, Denby K, Steinbrenner J, 2020. Downy Mildew effector HaRxL21 interacts with the transcriptional repressor TOPLESS to promote pathogen susceptibility. *bioRxiv*.

Heazlewood JL, Verboom RE, Tonti-Filippini J, Small I, Millar AH, 2007. SUBA: the Arabidopsis Subcellular Database. *Nucleic Acids Res* **35**, D213-8.

Heidrich K, Wirthmueller L, Tasset C, Pouzet C, Deslandes L, Parker JE, 2011. Arabidopsis EDS1 Connects Pathogen Effector Recognition to Cell Compartment-Specific Immune Responses. *Science* **334**, 1401-4.

Hinsch M, Staskawicz B, 1996. Identification of a new Arabidopsis disease resistance locus, RPs4, and cloning of the corresponding avirulence gene, avrRps4, from Pseudomonas syringae pv. pisi. *Mol Plant Microbe Interact* **9**, 55-61.

Horsefield S, Burdett H, Zhang X, Manik MK, Shi Y, Chen J, Qi T, Gilley J, Lai JS, Rank MX, Casey LW, Gu W, Ericsson DJ, Foley G, Hughes RO, Bosanac T, Von Itzstein M, Rathjen JP, Nanson JD, Boden M, Dry IB, Williams SJ, Staskawicz BJ, Coleman MP, Ve T, Dodds PN, Kobe B, 2019. NAD(+) cleavage activity by animal and plant TIR domains in cell death pathways. *Science* **365**, 793-9.

Hsu JL, Wang LY, Wang SY, Lin CH, Ho KC, Shi FK, Chang IF, 2009. Functional phosphoproteomic profiling of phosphorylation sites in membrane fractions of salt-stressed Arabidopsis thaliana. *Proteome Sci* **7**, 42.

Hu M, Qi J, Bi G, Zhou JM, 2020. Bacterial Effectors Induce Oligomerization of Immune Receptor ZAR1 In Vivo. *Mol Plant*.

Huang J, Sun Y, Orduna AR, Jetter R, Li X, 2019. The Mediator kinase module serves as a positive regulator of salicylic acid accumulation and systemic acquired resistance. *Plant J* **98**, 842-52.

Huang S, Jia A, Song W, Hessler G, Meng Y, Sun Y, Xu L, Laessle H, Jirschitzka J, Ma S, Xiao Y, Yu D, Hou J, Liu R, Sun H, Liu X, Han Z, Chang J, Parker JE, Chai J, 2022. Identification and receptor mechanism of TIR-catalyzed small molecules in plant immunity. *Science* **377**, eabq3297.

Huang S, Maierhofer T, Hashimoto K, Xu X, Karimi SM, Muller H, Geringer MA, Wang Y, Kudla J, De Smet I, Hedrich R, Geiger D, Roelfsema MRG, 2023. The CIPK23 protein kinase represses SLAC1-type anion channels in Arabidopsis guard cells and stimulates stomatal opening. *New Phytol*.

Huang W, Wu Z, Tian H, Li X, Zhang Y, 2021. Arabidopsis CALMODULIN-BINDING PROTEIN 60b plays dual roles in plant immunity. *Plant Commun* **2**, 100213.

Ishihama N, Yamada R, Yoshioka M, Katou S, Yoshioka H, 2011. Phosphorylation of the Nicotiana benthamiana WRKY8 transcription factor by MAPK functions in the defense response. *Plant Cell* **23**, 1153-70.

Isner JC, Begum A, Nuehse T, Hetherington AM, Maathuis FJM, 2018. KIN7 Kinase Regulates the Vacuolar TPK1 K(+) Channel during Stomatal Closure. *Curr Biol* **28**, 466-72 e4.

Iwata Y, Koizumi N, 2005. An Arabidopsis transcription factor, AtbZIP60, regulates the endoplasmic reticulum stress response in a manner unique to plants. *Proc Natl Acad Sci U S A* **102**, 5280-5.

Jacob P, Kim NH, Wu F, El-Kasmi F, Chi Y, Walton WG, Furzer OJ, Lietzan AD, Sunil S, Kempthorn K, Redinbo MR, Pei ZM, Wan L, Dangl JL, 2021. Plant "helper" immune receptors are Ca(2+)-permeable nonselective cation channels. *Science* **373**, 420-5.

Jayaraman J, Choi S, Prokchorchik M, Choi DS, Spiandore A, Rikkerink EH, Templeton MD, Segonzac C, Sohn KH, 2017. A bacterial acetyltransferase triggers immunity in Arabidopsis thaliana independent of hypersensitive response. *Sci Rep* **7**, 3557.

Jeworutzki E, Roelfsema MR, Anschutz U, Krol E, Elzenga JT, Felix G, Boller T, Hedrich R, Becker D, 2010. Early signaling through the Arabidopsis pattern recognition receptors FLS2 and EFR involves Ca-associated opening of plasma membrane anion channels. *Plant J* **62**, 367-78.

Jia A, Huang S, Song W, Wang J, Meng Y, Sun Y, Xu L, Laessle H, Jirschitzka J, Hou J, Zhang T, Yu W, Hessler G, Li E, Ma S, Yu D, Gebauer J, Baumann U, Liu X, Han Z, Chang J, Parker JE, Chai J, 2022. TIR-catalyzed ADP-ribosylation reactions produce signaling molecules for plant immunity. *Science* **377**, eabq8180.

Jirage D, Tootle TL, Reuber TL, Frost LN, Feys BJ, Parker JE, Ausubel FM, Glazebrook J, 1999. Arabidopsis thaliana PAD4 encodes a lipase-like gene that is important for salicylic acid signaling. *Proc Natl Acad Sci U S A* **96**, 13583-8.

Jones AM, Maclean D, Studholme DJ, Serna-Sanz A, Andreasson E, Rathjen JP, Peck SC, 2009. Phosphoproteomic analysis of nuclei-enriched fractions from Arabidopsis thaliana. *J Proteomics* **72**, 439-51.

Jones JD, Dangl JL, 2006. The plant immune system. *Nature* **444**, 323-9.

Jubic LM, Saile S, Furzer OJ, El Kasmi F, Dangl JL, 2019. Help wanted: helper NLRs and plant immune responses. *Curr Opin Plant Biol* **50**, 82-94.

Kadota Y, Liebrand TWH, Goto Y, Sklenar J, Derbyshire P, Menke FLH, Torres MA, Molina A, Zipfel C, Coaker G, Shirasu K, 2019. Quantitative phosphoproteomic analysis reveals common regulatory mechanisms between effector- and PAMP-triggered immunity in plants. *New Phytol* **221**, 2160-75.

Kadota Y, Sklenar J, Derbyshire P, Stransfeld L, Asai S, Ntoukakis V, Jones JD, Shirasu K, Menke F, Jones A, Zipfel C, 2014. Direct regulation of the NADPH oxidase RBOHD by the PRR-associated kinase BIK1 during plant immunity. *Mol Cell* **54**, 43-55.

Kagale S, Links MG, Rozwadowski K, 2010. Genome-wide analysis of ethylene-responsive element binding factor-associated amphiphilic repression motif-containing transcriptional regulators in Arabidopsis. *Plant Physiol* **152**, 1109-34.

Kang H, Fan T, Wu J, Zhu Y, Shen WH, 2022. Histone modification and chromatin remodeling in plant response to pathogens. *Front Plant Sci* **13**, 986940.

Kawamoto N, Sasabe M, Endo M, Machida Y, Araki T, 2015. Calcium-dependent protein kinases responsible for the phosphorylation of a bZIP transcription factor FD crucial for the florigen complex formation. *Sci Rep* **5**, 8341.

Ke J, Ma H, Gu X, Thelen A, Brunzelle JS, Li J, Xu HE, Melcher K, 2015. Structural basis for recognition of diverse transcriptional repressors by the TOPLESS family of corepressors. *Sci Adv* **1**, e1500107.

Kidokoro S, Yoneda K, Takasaki H, Takahashi F, Shinozaki K, Yamaguchi-Shinozaki K, 2017. Different Cold-Signaling Pathways Function in the Responses to Rapid and Gradual Decreases in Temperature. *Plant Cell* **29**, 760-74.

Kim DS, Hwang BK, 2014. An important role of the pepper phenylalanine ammonia-lyase gene (PAL1) in salicylic acid-dependent signalling of the defence response to microbial pathogens. *J Exp Bot* **65**, 2295-306.

Kim Y, Park S, Gilmour SJ, Thomashow MF, 2013. Roles of CAMTA transcription factors and salicylic acid in configuring the low-temperature transcriptome and freezing tolerance of Arabidopsis. *Plant J* **75**, 364-76.

Kinoshita E, Kinoshita-Kikuta E, Kubota Y, Takekawa M, Koike T, 2016. A Phos-tag SDS-PAGE method that effectively uses phosphoproteomic data for profiling the phosphorylation dynamics of MEK1. *Proteomics* **16**, 1825-36.

Kinoshita E, Kinoshita-Kikuta E, Takiyama K, Koike T, 2006. Phosphate-binding tag, a new tool to visualize phosphorylated proteins. *Mol Cell Proteomics* **5**, 749-57.

Kinoshita E, Takahashi M, Takeda H, Shiro M, Koike T, 2004. Recognition of phosphate monoester dianion by an alkoxide-bridged dinuclear zinc(II) complex. *Dalton Trans*, 1189-93.

Koiwa H, Hausmann S, Bang WY, Ueda A, Kondo N, Hiraguri A, Fukuhara T, Bahk JD, Yun DJ, Bressan RA, Hasegawa PM, Shuman S, 2004. Arabidopsis C-terminal domain phosphatase-like 1 and 2 are essential Ser-5-specific C-terminal domain phosphatases. *Proc Natl Acad Sci U S A* **101**, 14539-44.

Kunkel BN, Bent AF, Dahlbeck D, Innes RW, Staskawicz BJ, 1993. RPS2, an Arabidopsis disease resistance locus specifying recognition of Pseudomonas syringae strains expressing the avirulence gene avrRpt2. *Plant Cell* **5**, 865-75.

Kunze G, Zipfel C, Robatzek S, Niehaus K, Boller T, Felix G, 2004. The N terminus of bacterial elongation factor Tu elicits innate immunity in Arabidopsis plants. *Plant Cell* **16**, 3496-507.

Lang J, Genot B, Bigeard J, Colcombet J, 2022. MPK3 and MPK6 control salicylic acid signaling by up-regulating NLR receptors during pattern- and effector-triggered immunity. *J Exp Bot* **73**, 2190-205.

Lapin D, Kovacova V, Sun X, Dongus JA, Bhandari D, Von Born P, Bautor J, Guarneri N, Rzemieniewski J, Stuttmann J, Beyer A, Parker JE, 2019. A Coevolved EDS1-SAG101-NRG1 Module Mediates Cell Death Signaling by TIR-Domain Immune Receptors. *Plant Cell* **31**, 2430-55.

Le Roux C, Huet G, Jauneau A, Camborde L, Tremousaygue D, Kraut A, Zhou B, Levaillant M, Adachi H, Yoshioka H, Raffaele S, Berthome R, Coute Y, Parker JE, Deslandes L, 2015. A receptor pair with an integrated decoy converts pathogen disabling of transcription factors to immunity. *Cell* **161**, 1074-88.

Lee D, Lal NK, Lin ZD, Ma S, Liu J, Castro B, Toruno T, Dinesh-Kumar SP, Coaker G, 2020. Regulation of reactive oxygen species during plant immunity through phosphorylation and ubiquitination of RBOHD. *Nat Commun* **11**, 1838.

Leydon AR, Wang W, Juarez-Solis S, Zemke JE, Zahler ML, Zheng N, Nemhauser JL, 2020. Structure-function analysis of Arabidopsis TOPLESS reveals conservation of repression mechanisms across eukaryotes.

Li B, Meng X, Shan L, He P, 2016. Transcriptional Regulation of Pattern-Triggered Immunity in Plants. *Cell Host Microbe* **19**, 641-50.

Li F, Cheng C, Cui F, De Oliveira MV, Yu X, Meng X, Intorne AC, Babilonia K, Li M, Li B, Chen S, Ma X, Xiao S, Zheng Y, Fei Z, Metz RP, Johnson CD, Koiwa H, Sun W, Li Z, De Souza Filho GA, Shan L, He P, 2014a. Modulation of RNA polymerase II phosphorylation downstream of pathogen perception orchestrates plant immunity. *Cell Host Microbe* **16**, 748-58.

Li L, Li M, Yu LP, Zhou ZY, Liang XX, Liu ZX, Cai GH, Gao LY, Zhang XJ, Wang YC, Chen S, Zhou JM, 2014b. The FLS2-Associated Kinase BIK1 Directly Phosphorylates the NADPH Oxidase RbohD to Control Plant Immunity. *Cell Host & Microbe* **15**, 329-38.

Li LS, Ying J, Li E, Ma T, Li M, Gong LM, Wei G, Zhang Y, Li S, 2021. Calmodulin-Binding Protein 60b is a central transcriptional activator of immunity. *Plant Physiol*.

Li W, He J, Wang X, Ashline M, Wu Z, Liu F, Fu ZQ, Chang M, 2023. PBS3: a versatile player in and beyond salicylic acid biosynthesis in Arabidopsis. *New Phytol* **237**, 414-22.

Li Y, Lei R, Pu M, Cai Y, Lu C, Li Z, Liang G, 2022a. bHLH11 inhibits bHLH IVc proteins by recruiting the TOPLESS/TOPLESS-RELATED corepressors. *Plant Physiol* **188**, 1335-49.

Li Y, Xue J, Wang FZ, Huang X, Gong BQ, Tao Y, Shen W, Tao K, Yao N, Xiao S, Zhou JM, Li JF, 2022b. Plasma membrane-nucleo-cytoplasmic coordination of a receptor-like cytoplasmic kinase promotes EDS1-dependent plant immunity. *Nat Plants* **8**, 802-16.

Li Z, Takahashi Y, Scavo A, Brandt B, Nguyen D, Rieu P, Schroeder JI, 2018. Abscisic acid-induced degradation of Arabidopsis guanine nucleotide exchange factor requires calcium-dependent protein kinases. *Proc Natl Acad Sci U S A* **115**, E4522-E31.

Lin C, Yeo I, Dufresne CP, Zhao G, Joe S, Chen S, 2022. Identification of MPK4 kinase interactome using TurboID proximity labeling proteomics in Arabidopsis thaliana. *Methods Enzymol* **676**, 369-84.

Lin W, Li B, Lu D, Chen S, Zhu N, He P, Shan L, 2014. Tyrosine phosphorylation of protein kinase complex BAK1/BIK1 mediates Arabidopsis innate immunity. *Proc Natl Acad Sci U S A* **111**, 3632-7.

Liu H, Li Y, Hu Y, Yang Y, Zhang W, He M, Li X, Zhang C, Kong F, Liu X, Hou X, 2021. EDS1-interacting J protein 1 is an essential negative regulator of plant innate immunity in Arabidopsis. *Plant Cell* **33**, 153-71.

Liu J, Elmore JM, Lin ZJ, Coaker G, 2011. A receptor-like cytoplasmic kinase phosphorylates the host target RIN4, leading to the activation of a plant innate immune receptor. *Cell Host Microbe* **9**, 137-46.

Liu L, Sonbol FM, Huot B, Gu Y, Withers J, Mwimba M, Yao J, He SY, Dong X, 2016. Salicylic acid receptors activate jasmonic acid signalling through a non-canonical pathway to promote effector-triggered immunity. *Nat Commun* **7**, 13099.

Liu Q, Axtell MJ, 2015. Quantitating plant microRNA-mediated target repression using a dual-luciferase transient expression system. *Methods Mol Biol* **1284**, 287-303.

Liu Q, Bischof S, Harris CJ, Zhong Z, Zhan L, Nguyen C, Rashoff A, Barshop WD, Sun F, Feng S, Potok M, Gallego-Bartolome J, Zhai J, Wohlschlegel JA, Carey MF, Long JA, Jacobsen SE, 2020. The characterization of Mediator 12 and 13 as conditional positive gene regulators in Arabidopsis. *Nat Commun* **11**, 2798.

Liu Q, Kasuga M, Sakuma Y, Abe H, Miura S, Yamaguchi-Shinozaki K, Shinozaki K, 1998. Two transcription factors, DREB1 and DREB2, with an EREBP/AP2 DNA binding domain separate two cellular signal transduction pathways in drought- and low-temperature-responsive gene expression, respectively, in Arabidopsis. *Plant Cell* **10**, 1391-406.

Liu Y, Zhang S, 2004. Phosphorylation of 1-aminocyclopropane-1-carboxylic acid synthase by MPK6, a stress-responsive mitogen-activated protein kinase, induces ethylene biosynthesis in Arabidopsis. *Plant Cell* **16**, 3386-99.

Liu Z, Karmarkar V, 2008. Groucho/Tup1 family co-repressors in plant development. *Trends Plant Sci* **13**, 137-44.

Lorenz WW, Mccann RO, Longiaru M, Cormier MJ, 1991. Isolation and expression of a cDNA encoding Renilla reniformis luciferase. *Proc Natl Acad Sci U S A* **88**, 4438-42.

Lu D, Wu S, Gao X, Zhang Y, Shan L, He P, 2010. A receptor-like cytoplasmic kinase, BIK1, associates with a flagellin receptor complex to initiate plant innate immunity. *Proc Natl Acad Sci U S A* **107**, 496-501.

Luo X, Wu W, Liang Y, Xu N, Wang Z, Zou H, Liu J, 2020. Tyrosine phosphorylation of the lectin receptor-like kinase LORE regulates plant immunity. *Embo Journal* **39**, e102856.

Lv S, Yang Y, Yu G, Peng L, Zheng S, Singh SK, Vilchez JI, Kaushal R, Zi H, Yi D, Wang Y, Luo S, Wu X, Zuo Z, Huang W, Liu R, Du J, Macho AP, Tang K, Zhang H, 2022. Dysfunction of histone demethylase IBM1 in Arabidopsis causes autoimmunity and reshapes the root microbiome. *ISME J* **16**, 2513-24.

Ma H, Duan J, Ke J, He Y, Gu X, Xu TH, Yu H, Wang Y, Brunzelle JS, Jiang Y, Rothbart SB, Xu HE, Li J, Melcher K, 2017. A D53 repression motif induces oligomerization of TOPLESS corepressors and promotes assembly of a corepressor-nucleosome complex. *Sci Adv* **3**, e1601217.

Ma S, Lapin D, Liu L, Sun Y, Song W, Zhang X, Logemann E, Yu D, Wang J, Jirschitzka J, Han Z, Schulze-Lefert P, Parker JE, Chai J, 2020a. Direct pathogen-induced assembly of an NLR immune receptor complex to form a holoenzyme. *Science* **370**.

Ma X, Claus LaN, Leslie ME, Tao K, Wu Z, Liu J, Yu X, Li B, Zhou J, Savatin DV, Peng J, Tyler BM, Heese A, Russinova E, He P, Shan L, 2020b. Ligand-induced monoubiquitination of BIK1 regulates plant immunity. *Nature* **581**, 199-203.

Ma Y, Guo H, Hu L, Martinez PP, Moschou PN, Cevik V, Ding P, Duxbury Z, Sarris PF, Jones JDG, 2018. Distinct modes of derepression of an Arabidopsis immune receptor complex by two different bacterial effectors. *Proc Natl Acad Sci U S A* **115**, 10218-27.

Mackey D, Holt BF, 3rd, Wiig A, Dangl JL, 2002. RIN4 interacts with Pseudomonas syringae type III effector molecules and is required for RPM1-mediated resistance in Arabidopsis. *Cell* **108**, 743-54.

Maclean D, 2019. Besthr. *Zenodo*.

Mair A, Xu SL, Branon TC, Ting AY, Bergmann DC, 2019. Proximity labeling of protein complexes and cell-type-specific organellar proteomes in Arabidopsis enabled by TurboID. *Elife* **8**.

Mao G, Meng X, Liu Y, Zheng Z, Chen Z, Zhang S, 2011. Phosphorylation of a WRKY transcription factor by two pathogen-responsive MAPKs drives phytoalexin biosynthesis in Arabidopsis. *Plant Cell* **23**, 1639-53.

Martin-Arevalillo R, Nanao MH, Larrieu A, Vinos-Poyo T, Mast D, Galvan-Ampudia C, Brunoud G, Vernoux T, Dumas R, Parcy F, 2017. Structure of the Arabidopsis TOPLESS corepressor provides insight into the evolution of transcriptional repression. *Proc Natl Acad Sci U S A* **114**, 8107-12.

Martin R, Qi T, Zhang H, Liu F, King M, Toth C, Nogales E, Staskawicz BJ, 2020. Structure of the activated ROQ1 resistosome directly recognizing the pathogen effector XopQ. *Science* **370**.

Matiolli CC, Melotto M, 2018. A Comprehensive Arabidopsis Yeast Two-Hybrid Library for Protein-Protein Interaction Studies: A Resource to the Plant Research Community. *Mol Plant Microbe Interact* **31**, 899-902.

Mattei B, Spinelli F, Pontiggia D, De Lorenzo G, 2016. Comprehensive Analysis of the Membrane Phosphoproteome Regulated by Oligogalacturonides in Arabidopsis thaliana. *Front Plant Sci* **7**, 1107.

Melkonian K, Stolze SC, Harzen A, Nakagami H, 2022. miniTurbo-based interactomics of two plasma membrane-localized SNARE proteins in Marchantia polymorpha. *New Phytol* **235**, 786-800.

Mergner J, Frejno M, List M, Papacek M, Chen X, Chaudhary A, Samaras P, Richter S, Shikata H, Messerer M, Lang D, Altmann S, Cyprys P, Zolg DP, Mathieson T, Bantscheff M, Hazarika RR, Schmidt T, Dawid C, Dunkel A, Hofmann T, Sprunck S, Falter-Braun P, Johannes F, Mayer KFX, Jurgens G, Wilhelm M, Baumbach J, Grill E, Schneitz K, Schwechheimer C, Kuster B, 2020. Mass-spectrometry-based draft of the Arabidopsis proteome. *Nature* **579**, 409-14.

Meteignier LV, El Oirdi M, Cohen M, Barff T, Matteau D, Lucier JF, Rodrigue S, Jacques PE, Yoshioka K, Moffett P, 2017. Translatome analysis of an NB-LRR immune response identifies important contributors to plant immunity in Arabidopsis. *J Exp Bot* **68**, 2333-44.

Miller C, Matic I, Maier KC, Schwalb B, Roether S, Strasser K, Tresch A, Mann M, Cramer P, 2012. Mediator phosphorylation prevents stress response transcription during non-stress conditions. *J Biol Chem* **287**, 44017-26.

Mine A, Seyfferth C, Kracher B, Berens ML, Becker D, Tsuda K, 2018. The Defense Phytohormone Signaling Network Enables Rapid, High-Amplitude Transcriptional Reprogramming during Effector-Triggered Immunity. *Plant Cell* **30**, 1199-219.

Mithoe SC, Boersema PJ, Berke L, Snel B, Heck AJ, Menke FL, 2012. Targeted quantitative phosphoproteomics approach for the detection of phospho-tyrosine signaling in plants. *J Proteome Res* **11**, 438-48.

Mithoe SC, Ludwig C, Pel MJ, Cucinotta M, Casartelli A, Mbengue M, Sklenar J, Derbyshire P, Robatzek S, Pieterse CM, Aebersold R, Menke FL, 2016. Attenuation of pattern recognition receptor signaling is mediated by a MAP kinase kinase kinase. *EMBO Rep* **17**, 441-54.

Mukhi N, Brown H, Gorenkin D, Ding P, Bentham AR, Stevenson CEM, Jones JDG, Banfield MJ, 2021. Perception of structurally distinct effectors by the integrated WRKY domain of a plant immune receptor. *Proc Natl Acad Sci U S A* **118**.

Narusaka M, Shirasu K, Noutoshi Y, Kubo Y, Shiraishi T, Iwabuchi M, Narusaka Y, 2009. RRS1 and RPS4 provide a dual Resistance-gene system against fungal and bacterial pathogens. *Plant J* **60**, 218-26.

Navarrete F, Gallei M, Kornienko AE, Saado I, Khan M, Chia KS, Darino MA, Bindics J, Djamei A, 2022. TOPLESS promotes plant immunity by repressing auxin signaling and is targeted by the fungal effector Naked1. *Plant Commun* **3**, 100269.

Navarro L, Zipfel C, Rowland O, Keller I, Robatzek S, Boller T, Jones JD, 2004. The transcriptional innate immune response to flg22. Interplay and overlap with Avr gene-dependent defense responses and bacterial pathogenesis. *Plant Physiol* **135**, 1113-28.

Neubauer M, Serrano I, Rodibaugh N, Bhandari DD, Bautor J, Parker JE, Innes RW, 2020. Arabidopsis EDR1 Protein Kinase Regulates the Association of EDS1 and PAD4 to Inhibit Cell Death. *Mol Plant Microbe Interact* **33**, 693-703.

Ngou BPM, Ahn HK, Ding P, Jones JDG, 2021. Mutual potentiation of plant immunity by cell-surface and intracellular receptors. *Nature* **592**, 110-5.

Ngou BPM, Ahn HK, Ding P, Redkar A, Brown H, Ma Y, Youles M, Tomlinson L, Jones JDG, 2020. Estradiol-inducible AvrRps4 expression reveals distinct properties of TIR-NLR-mediated effector-triggered immunity. *J Exp Bot* **71**, 2186-97.

Niki T, Mitsuhara I, Seo S, Ohtsubo N, Ohashi Y, 1998. Antagonistic effect of salicylic acid and jasmonic acid on the expression of pathogenesis-related (PR) protein genes in wounded mature tobacco leaves. *Plant and Cell Physiology* **39**, 500-7.

Niu, Lin XL, Kong X, Qu GP, Cai B, Lee J, Jin JB, 2019. SIZ1-Mediated SUMOylation of TPR1 Suppresses Plant Immunity in Arabidopsis. *Mol Plant* **12**, 215-28.

Nühse TS, Bottrill AR, Jones AM, Peck SC, 2007. Quantitative phosphoproteomic analysis of plasma membrane proteins reveals regulatory mechanisms of plant innate immune responses. *Plant J* **51**, 931-40.

O'donoghue L, Smolenski A, 2022. Analysis of protein phosphorylation using Phos-tag gels. *J Proteomics* **259**, 104558.

Okawara Y, Hirano H, Kimura A, Sato N, Hayashi Y, Osada M, Kawakami T, Ootake N, Kinoshita E, Fujita K, 2021. Phos-tag diagonal electrophoresis precisely detects the mobility change of phosphoproteins in Phos-tag SDS-PAGE. *J Proteomics* **231**, 104005.

Onodera Y, Nakagawa K, Haag JR, Pikaard D, Mikami T, Ream T, Ito Y, Pikaard CS, 2008. Sex-biased lethality or transmission of defective transcription machinery in Arabidopsis. *Genetics* **180**, 207-18.

Pandey PK, Udayakumar TS, Lin X, Sharma D, Shapiro PS, Fondell JD, 2005. Activation of TRAP/mediator subunit TRAP220/Med1 is regulated by mitogen-activated protein kinase-dependent phosphorylation. *Mol Cell Biol* **25**, 10695-710.

Parker JE, Holub EB, Frost LN, Falk A, Gunn ND, Daniels MJ, 1996. Characterization of eds1, a mutation in Arabidopsis suppressing resistance to Peronospora parasitica specified by several different RPP genes. *Plant Cell* **8**, 2033-46.

Pauwels L, Barbero GF, Geerinck J, Tilleman S, Grunewald W, Perez AC, Chico JM, Bossche RV, Sewell J, Gil E, Garcia-Casado G, Witters E, Inze D, Long JA, De Jaeger G, Solano R, Goossens A, 2010. NINJA connects the co-repressor TOPLESS to jasmonate signalling. *Nature* **464**, 788-91.

Peart JR, Mestre P, Lu R, Malcuit I, Baulcombe DC, 2005. NRG1, a CC-NB-LRR protein, together with N, a TIR-NB-LRR protein, mediates resistance against tobacco mosaic virus. *Curr Biol* **15**, 968-73.

Plant AR, Larrieu A, Causier B, 2021. Repressor for hire! The vital roles of TOPLESS-mediated transcriptional repression in plants. *New Phytol* **231**, 963-73.

Pruitt RN, Locci F, Wanke F, Zhang L, Saile SC, Joe A, Karelina D, Hua C, Frohlich K, Wan WL, Hu M, Rao S, Stolze SC, Harzen A, Gust AA, Harter K, Joosten M, Thomma B, Zhou JM, Dangl JL, Weigel D, Nakagami H, Oecking C, Kasmi FE, Parker JE, Nurnberger T, 2021. The EDS1-PAD4-ADR1 node mediates Arabidopsis pattern-triggered immunity. *Nature* **598**, 495-9.

Qi T, Seong K, Thomazella DPT, Kim JR, Pham J, Seo E, Cho MJ, Schultink A, Staskawicz BJ, 2018. NRG1 functions downstream of EDS1 to regulate TIR-NLR-mediated plant immunity in Nicotiana benthamiana. *Proc Natl Acad Sci U S A* **115**, 10979-87.

Ramirez-Prado JS, Piquerez SJM, Bendahmane A, Hirt H, Raynaud C, Benhamed M, 2018. Modify the Histone to Win the Battle: Chromatin Dynamics in Plant-Pathogen Interactions. *Front Plant Sci* **9**, 355.

Rasmussen MW, Roux M, Petersen M, Mundy J, 2012. MAP Kinase Cascades in Arabidopsis Innate Immunity. *Front Plant Sci* **3**, 169.

Rayapuram N, Bonhomme L, Bigeard J, Haddadou K, Przybylski C, Hirt H, Pflieger D, 2014. Identification of novel PAMP-triggered phosphorylation and dephosphorylation events in Arabidopsis thaliana by quantitative phosphoproteomic analysis. *J Proteome Res* **13**, 2137-51.

Rayapuram N, Jarad M, Alhoraibi HM, Bigeard J, Abulfaraj AA, Volz R, Mariappan KG, Almeida-Trapp M, Schloffel M, Lastrucci E, Bonhomme L, Gust AA, Mithofer A, Arold ST, Pflieger D, Hirt H, 2021. Chromatin phosphoproteomics unravels a function for AT-hook motif nuclear localized protein AHL13 in PAMP-triggered immunity. *Proc Natl Acad Sci U S A* **118**.

Redkar A, Cevik V, Bailey K, Zhao H, Kim DS, Zou Z, Furzer OJ, Fairhead S, Borhan MH, Holub EB, Jones JDG, 2023. The Arabidopsis WRR4A and WRR4B paralogous NLR proteins both confer recognition of multiple Albugo candida effectors. *New Phytol* **237**, 532-47.

Reiland S, Finazzi G, Endler A, Willig A, Baerenfaller K, Grossmann J, Gerrits B, Rutishauser D, Gruissem W, Rochaix JD, Baginsky S, 2011. Comparative phosphoproteome profiling reveals a function of the STN8 kinase in fine-tuning of cyclic electron flow (CEF). *Proc Natl Acad Sci U S A* **108**, 12955-60.

Roux KJ, Kim DI, Raida M, Burke B, 2012. A promiscuous biotin ligase fusion protein identifies proximal and interacting proteins in mammalian cells. *J Cell Biol* **196**, 801-10.

Roux ME, Rasmussen MW, Palma K, Lolle S, Regue AM, Bethke G, Glazebrook J, Zhang W, Sieburth L, Larsen MR, Mundy J, Petersen M, 2015. The mRNA decay factor PAT1 functions in a pathway including MAP kinase 4 and immune receptor SUMM2. *Embo Journal* **34**, 593-608.

Rushton PJ, Macdonald H, Huttly AK, Lazarus CM, Hooley R, 1995. Members of a new family of DNA-binding proteins bind to a conserved cis-element in the promoters of alpha-Amy2 genes. *Plant Mol Biol* **29**, 691-702.

Rushton PJ, Somssich IE, 1998. Transcriptional control of plant genes responsive to pathogens. *Curr Opin Plant Biol* **1**, 311-5.

Saijo Y, Tintor N, Lu X, Rauf P, Pajerowska-Mukhtar K, Haweker H, Dong X, Robatzek S, Schulze-Lefert P, 2009. Receptor quality control in the endoplasmic reticulum for plant innate immunity. *Embo Journal* **28**, 3439-49.

Saile SC, Ackermann FM, Sunil S, Keicher J, Bayless A, Bonardi V, Wan L, Doumane M, Stobbe E, Jaillais Y, Caillaud MC, Dangl JL, Nishimura MT, Oecking C, El Kasmi F, 2021. Arabidopsis ADR1 helper NLR immune receptors localize and function at the plasma membrane in a phospholipid dependent manner. *New Phytol* **232**, 2440-56.

Saile SC, Jacob P, Castel B, Jubic LM, Salas-Gonzales I, Backer M, Jones JDG, Dangl JL, El Kasmi F, 2020. Two unequally redundant "helper" immune receptor families mediate Arabidopsis thaliana intracellular "sensor" immune receptor functions. *PLoS Biol* **18**, e3000783.

Sarris PF, Duxbury Z, Huh SU, Ma Y, Segonzac C, Sklenar J, Derbyshire P, Cevik V, Rallapalli G, Saucet SB, Wirthmueller L, Menke FLH, Sohn KH, Jones JDG, 2015. A Plant Immune Receptor Detects Pathogen Effectors that Target WRKY Transcription Factors. *Cell* **161**, 1089-100.

Saucet SB, Ma Y, Sarris PF, Furzer OJ, Sohn KH, Jones JD, 2015. Two linked pairs of Arabidopsis TNL resistance genes independently confer recognition of bacterial effector AvrRps4. *Nat Commun* **6**, 6338.

Savary S, Willocquet L, Pethybridge SJ, Esker P, Mcroberts N, Nelson A, 2019. The global burden of pathogens and pests on major food crops. *Nat Ecol Evol* **3**, 430-9.

Schlucking K, Edel KH, Koster P, Drerup MM, Eckert C, Steinhorst L, Waadt R, Batistic O, Kudla J, 2013. A new beta-estradiol-inducible vector set that facilitates easy construction and efficient expression of transgenes reveals CBL3-dependent cytoplasm to tonoplast translocation of CIPK5. *Mol Plant* **6**, 1814-29.

Scholthof HB, 2006. The Tombusvirus-encoded P19: from irrelevance to elegance. *Nat Rev Microbiol* **4**, 405-11.

Schon M, Toller A, Diezel C, Roth C, Westphal L, Wiermer M, Somssich IE, 2013. Analyses of wrky18 wrky40 plants reveal critical roles of SA/EDS1 signaling and indole-glucosinolate biosynthesis for Golovinomyces orontii resistance and a loss-of resistance towards Pseudomonas syringae pv. tomato AvrRPS4. *Mol Plant Microbe Interact* **26**, 758-67.

Schreiber KJ, Lewis JD, 2021. Identification of a Putative DNA-Binding Protein in Arabidopsis That Acts as a Susceptibility Hub and Interacts With Multiple Pseudomonas syringae Effectors. *Mol Plant Microbe Interact* **34**, 410-25.

Schultink A, Qi T, Lee A, Steinbrenner AD, Staskawicz B, 2017. Roq1 mediates recognition of the Xanthomonas and Pseudomonas effector proteins XopQ and HopQ1. *Plant J* **92**, 787-95.

Schulze B, Mentzel T, Jehle AK, Mueller K, Beeler S, Boller T, Felix G, Chinchilla D, 2010. Rapid heteromerization and phosphorylation of ligand-activated plant transmembrane receptors and their associated kinase BAK1. *J Biol Chem* **285**, 9444-51.

Segonzac C, Macho AP, Sanmartin M, Ntoukakis V, Sanchez-Serrano JJ, Zipfel C, 2014. Negative control of BAK1 by protein phosphatase 2A during plant innate immunity. *Embo Journal* **33**, 2069-79.

Shao YJ, Zhu QY, Yao ZW, Liu JX, 2021. Phosphoproteomic Analysis of Thermomorphogenic Responses in Arabidopsis. *Front Plant Sci* **12**, 753148.

Shi X, Long Y, He F, Zhang C, Wang R, Zhang T, Wu W, Hao Z, Wang Y, Wang GL, Ning Y, 2018. The fungal pathogen Magnaporthe oryzae suppresses innate immunity by modulating a host potassium channel. *PLoS Pathog* **14**, e1006878.

Shifera AS, Hardin JA, 2010. Factors modulating expression of Renilla luciferase from control plasmids used in luciferase reporter gene assays. *Anal Biochem* **396**, 167-72.

Shimada TL, Shimada T, Hara-Nishimura I, 2010. A rapid and non-destructive screenable marker, FAST, for identifying transformed seeds of Arabidopsis thaliana. *Plant J* **61**, 519-28.

Shioya R, Yamada K, Kido K, Takahashi H, Nozawa A, Kosako H, Sawasaki T, 2022. A simple method for labeling proteins and antibodies with biotin using the proximity biotinylation enzyme TurboID. *Biochem Biophys Res Commun* **592**, 54-9.

Sohn KH, Hughes RK, Piquerez SJ, Jones JD, Banfield MJ, 2012. Distinct regions of the Pseudomonas syringae coiled-coil effector AvrRps4 are required for activation of immunity. *Proc Natl Acad Sci U S A* **109**, 16371-6.

Sohn KH, Zhang Y, Jones JD, 2009. The Pseudomonas syringae effector protein, AvrRPS4, requires in planta processing and the KRVY domain to function. *Plant J* **57**, 1079-91.

Song Z, Zhang C, Jin P, Tetteh C, Dong X, Luo S, Zhang S, Li X, Liu Y, Zhang H, 2022. The cell-type specific role of Arabidopsis bZIP59 transcription factor in plant immunity. *Plant Cell Environ* **45**, 1843-61.

Stakman E, 1915. Relation between Puccinia graminis and plants highly resistant to its attack. *Journal of Agricultural Research* **4**, 193-200.

Stecker KE, Minkoff BB, Sussman MR, 2014. Phosphoproteomic Analyses Reveal Early Signaling Events in the Osmotic Stress Response. *Plant Physiol* **165**, 1171-87.

Sugiyama N, Nakagami H, Mochida K, Daudi A, Tomita M, Shirasu K, Ishihama Y, 2008. Large-scale phosphorylation mapping reveals the extent of tyrosine phosphorylation in Arabidopsis. *Mol Syst Biol* **4**, 193.

Sun L, Qin J, Wu X, Zhang J, Zhang J, 2022. TOUCH 3 and CALMODULIN 1/4/6 cooperate with calcium-dependent protein kinases to trigger calcium-dependent activation of CAM-BINDING PROTEIN 60-LIKE G and regulate fungal resistance in plants. *Plant Cell* **34**, 4088-104.

Sun L, Zhang J, 2020. Regulatory role of receptor-like cytoplasmic kinases in early immune signaling events in plants. *FEMS Microbiol Rev* **44**, 845-56.

Sun T, Zhang Y, Li Y, Zhang Q, Ding Y, Zhang Y, 2015. ChIP-seq reveals broad roles of SARD1 and CBP60g in regulating plant immunity. *Nat Commun* **6**, 10159.

Sun X, Lapin D, Feehan JM, Stolze SC, Kramer K, Dongus JA, Rzemieniewski J, Blanvillain-Baufume S, Harzen A, Bautor J, Derbyshire P, Menke FLH, Finkemeier I, Nakagami H, Jones JDG, Parker JE, 2021. Pathogen effector recognition-dependent association of NRG1 with EDS1 and SAG101 in TNL receptor immunity. *Nat Commun* **12**, 3335.

Szemenyei H, Hannon M, Long JA, 2008. TOPLESS mediates auxin-dependent transcriptional repression during Arabidopsis embryogenesis. *Science* **319**, 1384-6.

Thomas WJ, Thireault CA, Kimbrel JA, Chang JH, 2009. Recombineering and stable integration of the Pseudomonas syringae pv. syringae 61 hrp/hrc cluster into the genome of the soil bacterium Pseudomonas fluorescens Pf0-1. *Plant J* **60**, 919-28.

Thor K, Jiang S, Michard E, George J, Scherzer S, Huang S, Dindas J, Derbyshire P, Leitao N, Defalco TA, Koster P, Hunter K, Kimura S, Gronnier J, Stransfeld L, Kadota Y, Bucherl CA, Charpentier M, Wrzaczek M, Maclean D, Oldroyd GED, Menke FLH, Roelfsema MRG, Hedrich R, Feijo J, Zipfel C, 2020. The calcium-permeable channel OSCA1.3 regulates plant stomatal immunity. *Nature* **585**, 569-73.

Tian H, Wu Z, Chen S, Ao K, Huang W, Yaghmaiean H, Sun T, Xu F, Zhang Y, Wang S, Li X, Zhang Y, 2021. Activation of TIR signalling boosts pattern-triggered immunity. *Nature* **598**, 500-3.

Truman W, Sreekanta S, Lu Y, Bethke G, Tsuda K, Katagiri F, Glazebrook J, 2013. The CALMODULIN-BINDING PROTEIN60 family includes both negative and positive regulators of plant immunity. *Plant Physiol* **163**, 1741-51.

Tsuda K, Katagiri F, 2010. Comparing signaling mechanisms engaged in pattern-triggered and effector-triggered immunity. *Curr Opin Plant Biol* **13**, 459-65.

Tsuda K, Mine A, Bethke G, Igarashi D, Botanga CJ, Tsuda Y, Glazebrook J, Sato M, Katagiri F, 2013. Dual regulation of gene expression mediated by extended MAPK activation and salicylic acid contributes to robust innate immunity in Arabidopsis thaliana. *PLoS Genet* **9**.

Umezawa T, Sugiyama N, Takahashi F, Anderson JC, Ishihama Y, Peck SC, Shinozaki K, 2013. Genetics and phosphoproteomics reveal a protein phosphorylation network in the abscisic acid signaling pathway in Arabidopsis thaliana. *Sci Signal* **6**, rs8.

Van Der Hoorn RA, Kamoun S, 2008. From Guard to Decoy: a new model for perception of plant pathogen effectors. *Plant Cell* **20**, 2009-17.

Vlot AC, Sales JH, Lenk M, Bauer K, Brambilla A, Sommer A, Chen Y, Wenig M, Nayem S, 2021. Systemic propagation of immunity in plants. *New Phytol* **229**, 1234-50.

Wagner S, Stuttmann J, Rietz S, Guerois R, Brunstein E, Bautor J, Niefind K, Parker JE, 2013. Structural Basis for Signaling by Exclusive EDS1 Heteromeric Complexes with SAG101 or PAD4 in Plant Innate Immunity. *Cell Host & Microbe* **14**, 619-30.

Wan L, Essuman K, Anderson RG, Sasaki Y, Monteiro F, Chung EH, Osborne Nishimura E, Diantonio A, Milbrandt J, Dangl JL, Nishimura MT, 2019. TIR domains of plant immune receptors are NAD(+)-cleaving enzymes that promote cell death. *Science* **365**, 799-803.

Wang C, Du X, Mou Z, 2016. The Mediator Complex Subunits MED14, MED15, and MED16 Are Involved in Defense Signaling Crosstalk in Arabidopsis. *Front Plant Sci* **7**, 1947.

Wang G, Roux B, Feng F, Guy E, Li L, Li N, Zhang X, Lautier M, Jardinaud MF, Chabannes M, Arlat M, Chen S, He C, Noel LD, Zhou JM, 2015. The Decoy Substrate of a Pathogen Effector and a Pseudokinase Specify Pathogen-Induced Modified-Self Recognition and Immunity in Plants. *Cell Host Microbe* **18**, 285-95.

Wang J, Hu M, Wang J, Qi J, Han Z, Wang G, Qi Y, Wang HW, Zhou JM, Chai J, 2019a. Reconstitution and structure of a plant NLR resistosome conferring immunity. *Science* **364**.

Wang J, Wang J, Hu M, Wu S, Qi J, Wang G, Han Z, Qi Y, Gao N, Wang HW, Zhou JM, Chai J, 2019b. Ligand-triggered allosteric ADP release primes a plant NLR complex. *Science* **364**.

Wang J, Zhang X, Greene GH, Xu G, Dong X, 2022. PABP/purine-rich motif as an initiation module for cap-independent translation in pattern-triggered immunity. *Cell* **185**, 3186-200 e17.

Wang L, Kim J, Somers DE, 2013. Transcriptional corepressor TOPLESS complexes with pseudoresponse regulator proteins and histone deacetylases to regulate circadian transcription. *Proc Natl Acad Sci U S A* **110**, 761-6.

Wang L, Tsuda K, Truman W, Sato M, Nguyen Le V, Katagiri F, Glazebrook J, 2011a. CBP60g and SARD1 play partially redundant critical roles in salicylic acid signaling. *Plant J* **67**, 1029-41.

Wang Q, Wang M, Zhang X, Hao B, Kaushik SK, Pan Y, 2011b. WRKY gene family evolution in Arabidopsis thaliana. *Genetica* **139**, 973-83.

Wang X, Shen S, Rasam SS, Qu J, 2019c. MS1 ion current-based quantitative proteomics: A promising solution for reliable analysis of large biological cohorts. *Mass Spectrom Rev* **38**, 461-82.

Wang Y, Hu Q, Wu Z, Wang H, Han S, Jin Y, Zhou J, Zhang Z, Jiang J, Shen Y, Shi H, Yang W, 2017. HISTONE DEACETYLASE 6 represses pathogen defence responses in Arabidopsis thaliana. *Plant Cell Environ* **40**, 2972-86.

Wang Z, Liu X, Yu J, Yin S, Cai W-J, Kim NH, Kasmi FE, Dangl JL, Wan L, 2023. Plasma membrane association and resistosome formation of plant helper immune receptors. *bioRxiv*, 2023.01.23.525201.

Wani SH, Anand S, Singh B, Bohra A, Joshi R, 2021. WRKY transcription factors and plant defense responses: latest discoveries and future prospects. *Plant Cell Rep* **40**, 1071-85.

Warren RF, Merritt PM, Holub E, Innes RW, 1999. Identification of three putative signal transduction genes involved in R gene-specified disease resistance in Arabidopsis. *Genetics* **152**, 401-12.

Wu FH, Shen SC, Lee LY, Lee SH, Chan MT, Lin CS, 2009. Tape-Arabidopsis Sandwich - a simpler Arabidopsis protoplast isolation method. *Plant Methods* **5**, 16.

Wu Z, Li M, Dong OX, Xia S, Liang W, Bao Y, Wasteneys G, Li X, 2019. Differential regulation of TNL-mediated immune signaling by redundant helper CNLs. *New Phytol* **222**, 938-53.

Wu Z, Tian L, Liu X, Huang W, Zhang Y, Li X, 2022. The N-terminally truncated helper NLR NRG1C antagonizes immunity mediated by its full-length neighbors NRG1A and NRG1B. *Plant Cell* **34**, 1621-40.

Wu Z, Tian L, Liu X, Zhang Y, Li X, 2021. TIR signal promotes interactions between lipase-like proteins and ADR1-L1 receptor and ADR1-L1 oligomerization. *Plant Physiol* **187**, 681-6.

Xu F, Copeland C, 2012. Nuclear Extraction from Arabidopsis thaliana. *Bio-Protocol* **2**.

Xu F, Jia M, Li X, Tang Y, Jiang K, Bao J, Gu Y, 2021. Exportin-4 coordinates nuclear shuttling of TOPLESS family transcription corepressors to regulate plant immunity. *Plant Cell*.

Xu J, Li HD, Chen LQ, Wang Y, Liu LL, He L, Wu WH, 2006a. A protein kinase, interacting with two calcineurin B-like proteins, regulates K+ transporter AKT1 in Arabidopsis. *Cell* **125**, 1347-60.

Xu N, Luo X, Li W, Wang Z, Liu J, 2017. The Bacterial Effector AvrB-Induced RIN4 Hyperphosphorylation Is Mediated by a Receptor-Like Cytoplasmic Kinase Complex in Arabidopsis. *Mol Plant Microbe Interact* **30**, 502-12.

Xu X, Chen C, Fan B, Chen Z, 2006b. Physical and functional interactions between pathogen-induced Arabidopsis WRKY18, WRKY40, and WRKY60 transcription factors. *Plant Cell* **18**, 1310-26.

Yoo H, Greene GH, Yuan M, Xu G, Burton D, Liu L, Marques J, Dong X, 2020. Translational Regulation of Metabolic Dynamics during Effector-Triggered Immunity. *Mol Plant* **13**, 88-98.

You Y, Zhai Q, An C, Li C, 2019. LEUNIG_HOMOLOG Mediates MYC2-Dependent Transcriptional Activation in Cooperation with the Coactivators HAC1 and MED25. *Plant Cell* **31**, 2187-205.

Yu D, Chen C, Chen Z, 2001. Evidence for an important role of WRKY DNA binding proteins in the regulation of NPR1 gene expression. *Plant Cell* **13**, 1527-40.

Yu J, Gonzalez JM, Dong Z, Shan Q, Tan B, Koh J, Zhang T, Zhu N, Dufresne C, Martin GB, Chen S, 2021. Integrative Proteomic and Phosphoproteomic Analyses of Pattern- and Effector-Triggered Immunity in Tomato. *Front Plant Sci* **12**, 768693.

Yuan M, Jiang Z, Bi G, Nomura K, Liu M, Wang Y, Cai B, Zhou JM, He SY, Xin XF, 2021. Pattern-recognition receptors are required for NLR-mediated plant immunity. *Nature* **592**, 105-9.

Yue X, Guo Z, Shi T, Song L, Cheng Y, 2019. Arabidopsis AGC protein kinases IREH1 and IRE3 control root skewing. *J Genet Genomics* **46**, 259-67.

Zhang H, Zhou H, Berke L, Heck AJ, Mohammed S, Scheres B, Menke FL, 2013. Quantitative phosphoproteomics after auxin-stimulated lateral root induction identifies an SNX1 protein phosphorylation site required for growth. *Mol Cell Proteomics* **12**, 1158-69.

Zhang J, Li W, Xiang T, Liu Z, Laluk K, Ding X, Zou Y, Gao M, Zhang X, Chen S, Mengiste T, Zhang Y, Zhou JM, 2010a. Receptor-like cytoplasmic kinases integrate signaling from multiple plant immune receptors and are targeted by a Pseudomonas syringae effector. *Cell Host Microbe* **7**, 290-301.

Zhang J, Shao F, Li Y, Cui H, Chen L, Li H, Zou Y, Long C, Lan L, Chai J, Chen S, Tang X, Zhou JM, 2007. A Pseudomonas syringae effector inactivates MAPKs to suppress PAMP-induced immunity in plants. *Cell Host Microbe* **1**, 175-85.

Zhang X, Wang C, Zhang Y, Sun Y, Mou Z, 2012. The Arabidopsis mediator complex subunit16 positively regulates salicylate-mediated systemic acquired resistance and jasmonate/ethylene-induced defense pathways. *Plant Cell* **24**, 4294-309.

Zhang Y, Cheng YT, Qu N, Zhao Q, Bi D, Li X, 2006. Negative regulation of defense responses in Arabidopsis by two NPR1 paralogs. *Plant J* **48**, 647-56.

Zhang Y, Goritschnig S, Dong X, Li X, 2003. A gain-of-function mutation in a plant disease resistance gene leads to constitutive activation of downstream signal transduction pathways in suppressor of npr1-1, constitutive 1. *Plant Cell* **15**, 2636-46.

Zhang Y, Song G, Lal NK, Nagalakshmi U, Li Y, Zheng W, Huang PJ, Branon TC, Ting AY, Walley JW, Dinesh-Kumar SP, 2019. TurboID-based proximity labeling reveals that UBR7 is a regulator of N NLR immune receptor-mediated immunity. *Nat Commun* **10**, 3252.

Zhang Y, Xu S, Ding P, Wang D, Cheng YT, He J, Gao M, Xu F, Li Y, Zhu Z, Li X, Zhang Y, 2010b. Control of salicylic acid synthesis and systemic acquired resistance by two members of a plant-specific family of transcription factors. *Proc Natl Acad Sci U S A* **107**, 18220-5.

Zhang ZJ, Peck SC, 2011. Simplified enrichment of plasma membrane proteins for proteomic analyses in Arabidopsis thaliana. *Proteomics* **11**, 1780-8.

Zhang ZM, Ma KW, Gao L, Hu Z, Schwizer S, Ma W, Song J, 2017. Mechanism of host substrate acetylation by a YopJ family effector. *Nat Plants* **3**, 17115.

Zhao YB, Liu MX, Chen TT, Ma X, Li ZK, Zheng Z, Zheng SR, Chen L, Li YZ, Tang LR, Chen Q, Wang P, Ouyang S, 2022. Pathogen effector AvrSr35 triggers Sr35 resistosome assembly via a direct recognition mechanism. *Sci Adv* **8**, eabq5108.

Zhou Z, Wu Y, Yang Y, Du M, Zhang X, Guo Y, Li C, Zhou JM, 2015. An Arabidopsis Plasma Membrane Proton ATPase Modulates JA Signaling and Is Exploited by the Pseudomonas syringae Effector Protein AvrB for Stomatal Invasion. *Plant Cell* **27**, 2032-41.

Zhu Z, Xu F, Zhang Y, Cheng YT, Wiermer M, Li X, Zhang Y, 2010. Arabidopsis resistance protein SNC1 activates immune responses through association with a transcriptional corepressor. *Proc Natl Acad Sci U S A* **107**, 13960-5.

Zipfel C, Kunze G, Chinchilla D, Caniard A, Jones JD, Boller T, Felix G, 2006. Perception of the bacterial PAMP EF-Tu by the receptor EFR restricts Agrobacterium-mediated transformation. *Cell* **125**, 749-60.

Zou L, Yang F, Ma Y, Wu Q, Yi K, Zhang D, 2019. Transcription factor WRKY30 mediates resistance to Cucumber mosaic virus in Arabidopsis. *Biochem Biophys Res Commun* **517**, 118-24.

Appendices

Appendix 1: List of abbreviations

PTI	Pattern triggered immunity
PAMPs	Pathogen-associated molecular patterns
ETI	Effector triggered immunity
DAMPs	Damage-associated-molecular-patterns
SRM	selected reaction monitoring
PRM	Parallel reaction monitoring
Pst	*Pseudomonas syringae pv tomato*
NLR	nucleotide-binding leucine-rich repeat receptor
TIR	Toll/interleukin-1
CC	Coiled-coil
SETI	SUPER-ETI
ICS1	ISOCHORISMATE SYNTHASE1
PR1	PATHOGENESIS RELATED1
SA	Salicylic acid
MS	Mass spectrometry
DDA	Data-dependent acquisition
SM	SETI Mock
KE	SETI_krvy Estradiol
SE	SETI Estradiol
JA	Jasmonic acid
Pol II	RNA POLYMERASE II
SAR	Systemic Acquired Resistance
WT	Wildtype
hpi	Hours post infection
ETS	effector-triggered susceptibility
CTD	C-terminal domain
LRR-RLK	Leucine-rich-repeat receptor-like-kinase
PRRs	Pattern recognition receptors.
ROS	reactive oxygen species
PAMPs	Pathogen-associated molecular patterns
LysM	lysine motifs
HR	hypersensitive response
IP	Immunoprecipitation
ChIP-Seq	Chromatin immunoprecipitation sequencing
GO-terms	Gene Ontology terms
SRM	Selected reaction monitoring
EAR	Ethylene-responsive element binding factor-associated Amphiphilic Repression
EP	EDS1 and PAD4-defined
CHIP	Chromatin Immunoprecipitation
LEA	Late Embryogenesis Abundant
HMA	Heavy Metal Associated
ETS	Effector Triggered Susceptibility
MS	Murashige and Skoog
TPD	TOPLESS Domain
CRA	CT11-RanBPM

LisH	Lissencephaly homology
CTLH	C-terminal to LisH
PL	Proximity labelling

Appendix 2: List of protein names

TPR1	TOPLESS-RELATED 1
RBOHD	RESPIRATORY BURST OXIDASE PROTEIN D
BIK1	BOTRYTIS-INDUCED KINASE1
BAK1	BRI1-ASSOCIATED RECEPTOR KINASE
FLS2	FLAGELLIN-SENSITIVE 2
ACA8	AUTOINHIBITED CA^{2+} -ATPASE
RIPK	RPM1-INDUCED PROTEIN KINASE
ZAR1	HOPZ-ACTIVATED RESISTANCE 1
ROQ1	Recognition of XopQ 1
NRG1	N requirement gene 1
ADR1	ACTIVATED DISEASE RESISTANCE 1
EDS1	ENHANCED DISEASE SUSCEPTIBILITY 1
SAG101	SENESCENCE-ASSOCIATED GENE 101
PAD4	PHYTOALEXIN DEFICIENT 4
RRS1	RESISTANT TO RALSTONIA SOLANACEARUM 1
RPS4	RESISTANT TO P. SYRINGAE 4
PBL19	PBS1-LIKE 19
ICS1	ISOCHORISMATE SYNTHASE1
PR1	PATHOGENESIS RELATED1
SARD1	SAR DEFICIENT 1
CBP60g	CALMODULIN BINDING PROTEIN 60-LIKE G
PUB13	PLANT U-BOX 13
EDS5	ENHANCED DISEASE SUSCEPTIBILITY 5
TPL	TOPLESS
TPR2	Topless-related 2
TPR3	Topless-related 3
SNC1	SUPPRESSOR OF NPR1-1, CONSTITUTIVE 1
LUH	LEUNIG HOMOLOG
DND1	DEFENSE NO DEATH 1
MYC2	MYELOCYTOMATOSIS2
HAC1	HISTONE ACETYLTRANSFERASE OF THE CBP FAMILY 1
NPR3	NPR1-LIKE PROTEIN 3
NPR4	NPR1-LIKE PROTEIN 4
WRKY	WRKY DNA-BINDING PROTEIN
CAMTA2	CALMODULIN-BINDING TRANSCRIPTION ACTIVATOR 2
CAMTA5	CALMODULIN-BINDING TRANSCRIPTION ACTIVATOR 5
DREB1s	Dehydration-responsive element binding proteins
bZIP	Basic-leucine zipper
ANAC019	NAC DOMAIN CONTAINING PROTEIN 19
IBM1	INCREASE IN BONSAI METHYLATION 1
NRPB1	RNA POLYMERASE II LARGE SUBUNIT
CDCK	Cyclin-dependent kinases
MPK	Mitogen activated protein KINASE

CPL3	C-TERMINAL DOMAIN PHOSPHATASE-LIKE 3
MED17	MEDIATOR SUBUNIT 17
MED12	MEDIATOR SUBUNIT 12
IREH1	INCOMPLETE ROOT HAIR ELONGATION 1
KIN7	Receptor kinase 7
TPK1	Two Pore K+ 1
CIPK23	CBL-interacting protein kinase 23
AKT1	K+ TRANSPORTER 1
PAL1	PHE AMMONIA LYASE 1
CPK1	Calcium dependent protein kinase 1
RPP13	RECOGNITION OF PERONOSPORA PARASITICA 13
RPM1	RESISTANCE TO P. SYRINGAE PV MACULICOLA 1,
PEN3	PENETRATION 3
RIN4	RPM1 INTERACTING PROTEIN 4
AHA1	H^+-ATPASE 1
PIP	PLASMA MEMBRANE INTRINSIC PROTEIN
RPS2	RESISTANT TO P. SYRINGAE 2
CPK5	CALCIUM DEPENDENT PROTEIN KINASE 5
FMO1	FLAVIN-DEPENDENT MONOOXYGENASE 1
ALD1	AGD2-LIKE DEFENSE RESPONSE PROTEIN 1
FRK1	FLG22-INDUCED RECEPTOR-LIKE KINASE 1
NHL10	NDR1/HIN1-LIKE 10
FOX1	FAD-LINKED OXIDOREDUCTASE 1
DND1/2	DEFENSE NO DEATH 1/2
LYK5	LysM-domain containing receptor-like kinase 5
CERK1	CHITIN ELICITOR RECEPTOR KINASE 1
CDPK	Calcium-dependent protein kinases
MAPKs	mitogen-activated protein kinases
MKK	MITOGEN-ACTIVATED PROTEIN KINASE KINASE
Ef-Tu	Elongation factor thermo unstable
EFR	EF-Tu Receptor
WRR4A	WHITE RUST RESISTANCE 4A
HDA19	HISTONE DEACETYLASE 19
PBS3	AVRPPHB SUSCEPTIBLE 3
NINJA	Novel Interactor of JAZ
JAZ	jasmonate ZIM-domain
IAA12	INDOLE-3-ACETIC ACID INDUCIBLE 12
D53	DWARF53
REL2	RAMOSA1 ENHANCER LOCUS 2
RAV1	RELATED TO ABI3/VP1 1
VRN5	VERNALIZATION 5
RELK2	REL-like 2
ERF1	ETHYLENE RESPONSE FACTOR 1
FMO1	FLAVIN-DEPENDENT MONOOXYGENASE 1
ALD1	AGD2-LIKE DEFENSE RESPONSE PROTEIN 1
NPR1	NONEXPRESSER OF PR GENES 1
SRFR1	SUPPRESSOR OF RPS4-RLD 1
HDA6	HISTONE DEACETYLASE6
GCN5	General control non-depressible 5
RPW8	RESISTANCE TO POWDERY MILDEW8

EDR1	ENHANCED DISEASE RESISTANCE1
EFR1	ETHYLENE RESPONSE FACTOR 1
PP2A	SERINE/THREONINE PROTEIN PHOSPHATASE 2A
EIJ1	EDS1-INTERACTING J PROTEIN1
PBL1	AVRPPHB SUSCEPTIBLE-LIKE 1

Appendix 3: Protocol for NRG1-HF protein extraction from N. benthamiana

Purification of NLR-FLAG from *Nicotiana benthamiana* leaves by anti-FLAG IP optimised by Dr Joanna Feehan

Buffers required

All buffers should be made fresh before use (maximum 2 days beforehand).

GHMN buffer (750 mL):

10 % Glycerol (75 mL)
100 mM HEPES (pH 7.5) (75mL of 1M)
300 mM NaCl (45 mL of 5M)
5 mM $MgCl_2$ (3.75 mL of 1M)
0.5 % Nonidet-P40 (3.75 mL)

Extraction buffer (100 mL):

GHMN buffer (100 mL)
2 % Polyvinylpolypyrrolidone (PVPP) (2g)
cOmplete™, EDTA-free Protease Inhibitor Cocktail (2 tablets)
10mM DTT (added fresh) (1 mL 1M)
Halt™ Phosphatase Inhibitor Single-Use Cocktail (1ml)

IP buffer:

GHMN buffer

Elution buffer: (80 uL aliquots of 5 mg/mL 3XFLAG peptide)

GHMN buffer
30 uL in 1 mL = 150 ng/µl peptide for 30min
50 uL in 1 mL = 250 ng/µl peptide overnight

Gel Filtration buffer (50 ml):

10 mM HEPES (500 ul of 1M)
150 mM NaCl (1.5ml of 5M)
5 mM $MgCl_2$ (250 ul)
5 % Glycerol (2.5 ml)
1 mM DTT (50 ul of 1M)

PROTEIN ISOLATION

1. Grind ~ 30 g *N. benthamiana* tissue in Liquid Nitrogen; separate into ~25 mL aliquots in 50 mL falcon tubes; add 25 mL extraction buffer.

2. Incubate 15 min rolling in cold room

3. Spin 4000 RPM for 35min at 4°C

4. Filter supernatant through Miracloth and collect into a cold beaker.

5. Split protein solution into 40-mL ultra-centrifuge tubes (compatible ones with A27-8x50 rotor). Centrifuge at 50,000 x g at 4°C for 90 min (LYNX ultracentrifuge, A27-8x50 rotor).

6. Collect supernatant into a cold beaker. Sample 100 ul for input.

ANTI-FLAG IMMUNOPRECIPITATION

Equilibrating the resin

1. Pipette anti-FLAG beads with a 1 mL cut tip into 50 mL falcon tube, add 45 mL of IP buffer and incubate at 4°C with gentle inversion for ~60 minutes (start during lysate centrifugation steps). *(Use 1 mL bead resin total for each sample.)*

2. Centrifuge the falcon tube with resin at 800 x g for 5 minutes at 4°C to pellet beads, and remove the supernatant. Resuspend the beads in IP buffer with the original volume of resin (ie 1 mL resin = 1 mL IP buffer) to produced a 50 % buffer:resin slurry.

Binding of protein to the resin and washing

3. Add 500 µl of the equilibrated resin to each 50 mL tube; add protein solution to resin. Incubate at 4 °C with gentle inversion for 30 minutes. *First binding step 30 minutes, second binding step 1 hour.*

4. Centrifuge at 800 x g for 5 minutes at 4°C. Collect the supernatant in a new 50ml without disturbing the pellet.

5. Gently resuspend the pellets in 1 mL of IP Buffer

6. Top-up the falcon tube to 45 mL with IP buffer and mix by gentle inversion for 5 minutes at 4°C to wash the beads. Centrifuge at 800 x g for 5 minutes at 4°C. Discard wash supernatant without disturbing the pellet, resuspend in 45 mL of IP. Repeat the wash step a further 2 times for a total of 3 washes.

Binding 1	*Binding 2*
Wash 1	*Wash 1*
Wash 2	*Wash 2*
Wash 3	*Wash 3*

7. Add fresh 500 µL FLAG resin to the supernatant and incubate for 1 hour. Repeat steps 3-6 again for 2 total binding incubations. (S*tart during the previous washing steps)*

Elution of protein from the resin

8. Centrifuge falcon tubes containing resin with bound & washed protein at 800 x g for 5 minutes at 4°C. Discard supernatant without disturbing the pellet. Gently resuspend the pellet in 1 mL of IP buffer and transfer to a 1.5 mL eppendorf. (*you can spin again and remove extra supernatant, and top-up to 1 mL mark) (Keep two-rounds of beads separate, combine on the second day before diluting with GF buffer)*

9. Add 30 µL of 5 mg/mL 3XFLAG peptide per mL of resin/IP buffer slurry (final concentration of 150 ng/µL 3XFLAG peptide). Incubate at 4°C 30 min under gentle inversion.

9a. centrifuge at 800 x g at 4°C for 1 min

9b. transfer supernatant (~ 500 uL) to lobind 1.5 mL eppendorf, through chilled spin column (sigmaprep spin column SC1000-1KT); centrifuge at 800 x g at 4°C for 1 min

do not remove beads as another elution step required

9c. Keep supernatant as Elution 1

9d. add fresh IP buffer to beads to 1mL line

10. Add 50 µL of 5 mg/mL 3XFLAG peptide per mL of resin/IP buffer slurry (final concentration of 250 ng/µL 3XFLAG peptide). Incubate at 4°C overnight under gentle inversion.

- NEXT DAY -

11. Centrifuge at 800 x g at 4°C for 1 min

11a. Transfer supernatant (~ 500 uL) to lobind 1.5 mL eppendorf, through chilled spin column; centrifuge at 800 x g at 4°C for 1 min. Use gel-loading tips to remove supernatant from beads.

11b. Keep supernatant as Elution 2.

11c. Boil beads in 1x SDS.

12. Combine eluates into a new 15 mL faclon tube.

CONCENTRATION AND ULTRAFILTRATION OF PROTEIN (50 kDa MWCO)

(Prepared first day)

1. Prepare 4 mL Merck and 0.5 mL sartorious concentrators membranes for overnight incubation at room temperature

11a. Wash the concentrators once with dH_2O, spin the liquid through according to the respective protocol.

11b. Remove residual dH_2O thoroughly by pipetting. (Take care not to damage the membrane with the pipette tip.)

11c. Fill concentrators with dH_2O

11d. Incubate the filled concentrators at room temperature overnight (or for at least 2 hours)

11e. Pour out dH_2O

11f. Rinse the device with dH_2O and finally spin through

- NEXT DAY –

1. Dilute protein solution with GF buffer with 1:5 dilution*. Transfer 4 mL to water-equilibrated 4 mL Merck concentrator. Centrifuge 4000 x g (swing bucket) in 4 minute sessions at 4°C, mixing via pipetting between spins.

1a. Transfer to 0.5 mL concentrator to concentrate down from ~500 uL to ~50 uL with 12,000 x g, 30seconds-4 minute spins.

1b. Transfer protein to a low-bind 1.5 mL eppendorf with gel loading pipette tip.

**This is important because this dilutes ~ 2 mL of eluates at 0.5% NIDP40 to 10 mL at 0.1% NIDP40 which helps maintain protein stability*

2. Phosphotase treatment

2a. Take 5 ul of sample and add 35 ul of GF buffer. Repeat so you have two aliquots for each sample

2b. Add 5 ul of each buffer

2c. Add 1 ul of phopshotase to one aliquot of each sample

2d. Incubate at 30C for 30 minutes, with 300 RPM shaking

3. Boil samples 65C for 5 minutes in 3x SDS

Appendix 4: Primers used for golden gate cloning, domestication and user cloning

SJ1_L0Fw	CGTTATCCCCTGATTCTGTGGATAAC
SJ2_L0Rv	GTCTCATGAGCGGATACATATTTGAATG
SJ3_L1Rv	GAACCCTGTGGTTGGCATGCACATAC
SJ4_L1Fw	CTGGTGGCAGGATATATTGTGGTG
SJ33_L2Fw	GTGGTGTAAACAAATTGACGC
SJ34_L2Rv	GGATAAACCTTTTCACGCCC
SJ5_User_HF_Fw	ACCCTTTCGGTUCCGGAAGAGGATC
SJ6_User_HF_RV	GGTTTAAUTCACTTGTCATCGTCATCCTTG
SJ12_U_GFP_Fw	AGGCTTGGUGAGCAAGGGCGAGGAGC
SJ13_U_GFP_Rv	GGTTTAAUTTACTTGTACAGCTCGTCCATGCCG
SJ18_pSARD1_3	GCTGTCATTTTAAGTTAAGCAGGAG
SJ19_pSARD1_2	GGATTACTCACATCATAGTC
SJ20_pSARD1_1	GTGGTCTCAGGAGAGTGGTCA
SJ31_SARD1_Fw_P1	GGTAACAAACATATGCATG
SJ32_SARD1_fw_P2	GGTGCGAAAGTTGCGAAAG
SJ43_OcsTer_Rv	ACAACGTGCACAACAGAA
SJ47_OCSTer_fw	CGCTTGTCCTGCTTTAAT
SJ55_TPR1_Fw_U	GGCTTAAUATGTCTTCTCTGAGCAGAGA
SJ56_TPR1_Rv_U_HF	AACCTCTCUGAGGCTGGTCAGAGG
SJ57_HF_with_TPR1_U_Fw	AGAGAGGTUCCGGAAGAGGATCGC
SJ58_OCSTer_Rv	ATTAAAGCAGGACAAGCG
SJ59_WRKY18_FW_User	GGCTTAAUATGGACGGTTCTTCGTTTCTCGACATC
SJ60_WRKY18_Rv_User	ACTGTTCUAGATTGCTCCATTAACCTCCC
SJ61_GFP wt_WRKY18_Fw_U	AGAACAGUGAGCAAGGGCGAG
SJ62_TPR1AAAF2_FW	CTCCTCCTGCTAATGCCGCTGTAGA
SJ63_TPR1AAA_F1_Rv	ATTAGCAGGAGGAGCTCTCGGGTG
SJ73_TPR1DDDF2_FW	CCGAGAGATCCTCCTGATAATGACGCTG
SJ74_TPR1DDDF2_Rv	AGGAGGATCTCTCGGGTGTTT
SJ84_GFP_M_Fw	GCATCGACTTCAAGGAGGA
SJ86_WRKY18_Fw	GTTACGAGAGGAGCTAAACAGAG
SJ87_WRKY18Rv	CATTAACCAGATCCAAAGTCACTG
SJ88_gTPR1_fw	ATCAATCATGUCTTCTCTGAGCAGA
SJ89_ocsTerUser_Rv	GGTTTAAUGTCCTGCTGAGCCTCGAC
SJ90_pTPR1_Rv	ACATGATTGAUTTTGCCACTCAGTCC
SJ91_pTPR1_fw	GGCTTAAUGCTCACATCACATTATGCG
SJ95_EDS1_Fw	ATGGCGTTTGAAGCTCTTACC
SJ96_EDS1_Rv	CCGGTATCTGTTATTTCATCC
SJ103_OcsTer_Fw	ACCTAAGCTTGUCCTGCTTTAATGAG
SJ104_WRKY18_f2_fw	gaattcGAAGACAAGGCTTCTACTCACTTAAAGAG
SJ105_WRKY18_F2_rv	gaattcGAAGACAACGAACCTGTTCTAGATTGCTCCA
SJ106_WRKY18_f1_fw	gaattcGAAGACAAAATGGACGGTTCTTCGTTTC
SJ107_WRKY18_f1_rv	gaattcGAAGACAAAGCCAAAACTGAGACTTCCTTCTTC
SJ109_SARD1_Rv	CGTGAAGAGCAACGATGTCTAG
SJ110_pTPR1_fw	GCTCACATCACATTATGCG

SJ111_pTPR1_rv	GATTGATTTTGCCACTCAGTCC
SJ112_gTPR1_fw	ATGTCTTCTCTGAGCAGAG
SJ113_gTPR1_rv	TCTCTGAGGCTGGTCAGA
SJ116_pWRKY18_Fw	tacataaggaataatatgtctggct
SJ117_pWRKY18_rv	aaaagaaacctttatcttaagatacaaaccaaagg
SJ120_WRKY18AA_F1fw	aattcGAAGACAAAatggacggttcttcgt
SJ121_WRKY18AA_F1rv	gaattcGAAGACAAtggcgagcctgaagc
SJ122_WRKY18AA_F2fw	gaattcGAAGACAAgccaggcccctgaaatc
SJ123_WRKY18AA_F2rv	gaattcGAAGACAACGAACCtgttctagattgc
SJ124_WRKY18DD_F1fw	aattcGAAGACAAATGGACGGTTCTTCGt
SJ125_WRKY18DD_F1rv	gaattcGAAGACAATGGCGATCCTGAAGCTT
SJ126_WRKY18DD_F2fw	aattcGAAGACAAGCCAGGACCCTGAAATC
SJ127_WRKY18DD_F2rv	gaattcGAAGACAACGAACCTGTTCTAGATTGC
SJ128_WRKY18_rv	GATGATGATCTTCGTTGCTGG
SJ129_pWRKY18_UserFw	GGCTTAAUTACATAAGGAATAATATGTCTGGC
SJ130_pWRKY18_Userrv	ATAAAAGAAACCUTTATCTTAAGATACAAACC
SJ131_gWRKY18_Userfw	AGGTTTCTTTTAUGGACGGTTCTTCG
SJ133_HF_OcsTer_URv	ACAAGCTCACUTGTCATCGTCATCCTTG
SJ134_OCsTer_User	AGTGAGCTTGUCCTGCTTTAATGAGA
SJ136_GFP_User_forwrky	ACAAGCTTACUTGTACAGCTCGTCC
SJ137_OcsTer_wGFP_user	AGTAAGCTTGUCCTGCTTTAATGAGATATG
SJ141_TPR1- Fw1	GAACTTCACGCCTCAGGACTC
SJ142_TPR1- Fw2	AAAGCGAACCAGACCTATG
SJ143_TPR1- Fw3	TATACTCTTATCACGGTGG
SJ144_TPR1- Fw4	GATTCCACAAGCGTTCCCTTG
SJ145_TPR1- Fw5	GCAATTTTGGCATTGGCATCAAATG
SJ148_WRKY18_Rv	CGGTATATCGGTCTGCTCG
SJ152_pSARD1_Fw	GGAAACCGATGTAAACCG
SJ153_gSARD1_Fw	ATGGCAGGGAAGAGGTTATTTC
SJ154_WRKY18_GABI_fw	TAAAGCCATTTTGCTCCGAGGAAC
SJ155_WRKY18_GABI_rv	CTAAAGTAAGCTCTAGGTGACGGG
SJ158_WRKY18_GT_Fw	CGGATTTCGTCTGATCCATT
SJ159_WRKY18_GT_Rv	ATCTTCGTTGCTGGAGCTGT
SJ160_WRKY40_GT_Fw	AGCTTACGGGAACTTCCACA
SJ161_WRKY40_GT_Rv	AGGGCTGATTTGATCCCTCT
SJ173_pWRKY18_Rv	GCTTGGTAATTAGTGTACGAAAC
SJ174_pWRKY18_fw	CAAACTTCTAGTGATGAGAA
SJ175_pWRKY18_fw2	GGAATAGTGGTTAGCATTTGTATC
SJ176_TPR1_rv	CGAATTTCAACTTGTACTTAGC
SJ177_TPR1_Fw	ATGTCTTCTCTGAGCAGAGAGCTCG
SJ178_TPR1_Rv	TCTCTGAGGCTGGTCAGAGGC
SJ179_pWRKY18_Rv	GTCGAGATACATTGTGAAAACGAAC
SJ180_TPR2_P2ARV	CTTCTGGACTAGACGTTCTCGAG
SJ181_TPR1_P2AFw	CGTCTAGTCCAGAAGGCTTTCAAAGTTTGG
SJ182_TPR1_P2DRv	CTTCTGGACTAGACGTTCTCGAG
SJ183_TPR1_P2Dfw	CGTCTAGTCCAGAAGGATTTCAAAGTTTGG

SJ200_pWRKY18	CTTGTCTCTGTCTTTGTAGTTTTAG
SJ201_TPR1_AAA	CACCCGAGAGCTCCTCCTGCTAATG
SJ202_pTPR1_F1Fw	AATTCGAAGACAAGGAGGCTCACATCACATTAT
SJ203_pTPR1_F1rv	AATTCGAAGACAATCGATCGATTTCAGAAACA
SJ204_pTPR1F2fw	AATTCGAAGACAATCGACTTCTTCTTCTTCATG
SJ205_pTPR1_F2rv	AATTCGAAGACAAACCTAGTATTATTATTGTCC
SJ206_pTPR1_F3fw	AATTCGAAGACAAAGGTAGACCTAATTTTTGTG
SJ207_pTPR1_F3rv	AATTCGAAGACAACATTGATTGATTTTGCCAC
SJ208_TPR1_DDD_Rv	AGGAGGATCTCTCGGGTGTTTCAAGGCT
SJ209_TPR1_DDD_Fw	GATAATGACGCTGTAGACTATCCATCAG
SJ210_TPR1_AAA_Fw	TGCTAATGCCGCTGTAGACTATCCATC
SJ211_TPR1_AAA_rv	GGAGGAGCTCTCGGGTGTTTCAAGGC
SJ216_TPR1_P2Rv	TTCTCGAGAACCGACTTCCCAGAGCC
SJ220_TDNAinsertiondspm5	CGGGATCCGACACTCTTTAATTAACTGACACTC
SJ221_GABI_genotyping	ATATTGACCATCATACTCATTGC
SJ222_mCherry-NLS-Fw	GGTCTCAAATGGTGAGCAAGGGC
SJ223_mCherry-NLS_Rv	GGTCTCACGAACCCACCTTCCTCTTC
SJ224_mCherry-NLS-Fw	ATGGTGAGCAAGGGCGAG
SJ225_pTPR1_mid	GGCCTCTTTCAATATCAGGAG
SJ226_TPR1	CAGCAACTCGAATGTCCATCC
SJ229_pTPR1_midRV	CATTTCCCTCATAACACGACAAAGC
SJ238_TPR1_P2A_Fw	AGTCCAGAAGGCTTTCAAAGTTTG
SJ239_TPR1_P2A_Rv	AGACGTTCTCGAGAACCG
SJ240_TPR1_P2D_Fw	AGTCCAGAAGGATTTCAAAGTTTGGGAC
SJ241_TPR1_P2D_Rv	AGACGTTCTCGAGAACCG
SJ242_TPR1_P2A_rv	AGACGTTCTCGAGAACCGACTTC
SJ243_TPR1_AAArv	AGGAGGAGCTCTCGGGTGTTTCA
SJ244_TPR1_AAAfw	GCTAATGCCGCTGTAGACTATCCATC
SJ245_TPR1_AAAfw	GCCGCTGTAGACTATCCATCAGGTG
SJ256_TPR1_DDDfw	GATCCTCCTGATAATGACGCTGTAGACTATCCATC
SJ257_TPR1_DDDrv	TCTCGGGTGTTTCAAGGCTGCTAAGAAC
SJ249_TPR1_AAA_Rv	CTCTCGGGTGTTTCAAGGCTGC
SJ250_TPR1	AGCTGTGTGGAACTATAGTCTTAAAT
SJ251_TPR1	CATGTTCACACCTAGACTCACC
SJ252_TPR1Rv	CACTGCTGAGGAGGTAAAGAAGC
SJ253_TPR1_F1RV_U	AGGAGCTCUCGGGTGTTTCAAGG
SJ254_TPR1_F2_Fw_U	AGAGCTCCUCCTGCTAATGCCG
SJ255_TPR1_DDD_Rv_UF1	AGGATCTCUCGGGTGTTTCAAGGCTG
SJ258_TPR1_DDD_F2U	AGAGATCCUCCTGATAATGACGCTGTAGAC
SJ259_TPR1_P2A_fwU	ACGTCTAGUCCAGAAGGCTTTCAAAGTTTGG
SJ260_TPR1_P2A_RvU	ACTAGACGUTCTCGAGAACCGACTTCC
SJ271_TPR1_fwTID	AGCCATTCUCTGAGGCTGGTCAGAG
SJ272_Turbo_fwTPR1	AGAATGGCUCGGGATCCACCG
SJ281_TPR1 fwTID	ATCAATCATGUCTTCTCTGAGCAGAGAGC
SJ282_TIDfor35s	GGTTTAAUTTAGGTGCTGTCCAGGCCCA
SJ283_TPR1_P2D_F2	ACGTCTAGUCCAGAAGGATTTCAAAGTTTGG

SJ288_pSARD1_fw	CATCGCCGTATAAGATTATGTC
SJ295_WRKY18_end	GGTCCAAATGCTTCTGAAGG
SJ296_WRKYFw	GAAACATCGGACACAAGCTTGG
SJ299_WRKY18_TerRV	CGAAAACGAAGAATCATTC
SJ300_WRKY18_Fw	GTTTCTCGACATCTCTCTCG
SJ338_TurboID	GACAATACTGTGCCTCTGAAGC
SJ342_TurboIDMid	ATCAGGGCTGGATCACACTG
SJ344_OcsTerWTurbo_U	AGCTTGTCCUGCTTTAATGAGATATGCG
SJ343_TurbowOcsTer_U	AGGACAAGCUTAGGTGCTGTCCAGG
SJ353_Turbo_Rv	AGCCAGGAGAGCGATCAG
SJ354_EARmotif_F1Fw	aattcGAAGACAAAaTGGACGGTTCTTCGT
SJ355_EARmotif_F1Rv	gaattcGAAGACAAAGCAGCGAGAGAGATGTCGA
SJ356_EARmotif_F2Fw	gaattcGAAGACAATGCTGCTACCAATCCTTTCTCCG
SJ357_EARmotif_F2Rv	gaattcGAAGACAACCTGTTCTAGATTGCTCC
SJ363_WRKY18_Fw	ATGGACGGTTCTTCGTTTC
SJ364_WRK18_OCsTer_Rv	GTCCTGCTGAGCCTCGAC
SJ365_WRKY18_rv	GTTCATAGAAATTGAAGGGATAC
SJ371_TPR1_Rv_mCherry_U	ATTCTCUGAGGCTGGTCAGAGGCAG
SJ372_mCherry_Fw_User	AGAGAAUGGTGAGCAAGGGCGAGG
SJ373_mCherry_rv_User	GGTTTAAUTCACTTGTACAGCTCGTCCA
SJ374_mCherry_Fw	ATGGTGAGCAAGGGCGAGG
SJ375_mCherry_Rv	TCACTTGTACAGCTCGTCCA
SJ378_TPR1_Fw	GGCTTAATATGTCTTCTCTGAGCAGAGA
SJ380_TPR1_mCherry_RV	ATTCTCTGAGGCTGGTCAGAGGCAG
SJ381_mCherry_Fw	AGAGAATGGTGAGCAAGGGCGAGG
SJ382_mCherry_Rv	GGTTTAATTCACTTGTACAGCTCGTCCA
SJ383_NosterFw	GATAGAAAACAAAATATAGCGC
SJ419_NRG1B_AA_F2fw	aattcGAAGACAACGTTTGGCTGGTGCTCC
SJ390_NRG1B_F2_Rv	gaattcGAAGACAACGAACCAAACGTTAGAAG
SJ418_NRG1_F1Rv	gaattcGAAGACAAAACGGTCGAGCTTCTTAT
SJ392_NRG1B_F1_Fw	aattcGAAGACAAAATGGTCGTGGTCGATTG
SJ420_NRG1B_DD_F2fw	aattcGAAGACAACGTTTGGATGGTGATCCTG
SJ421_NRG1B_D2_F2fw	aattcGAAGACAACGTTTGAGTGGTGATCCTG
SJ395_NRG1B_A2F2_Fw	aattcGAAGACAATTTGAGTGGTGCTCCTGCT
SJ396_NRG1B_A1F2_Fw	aattcGAAGACAATTTGGCTGGTTCTCCTGCT
SJ397_NRG1B_D1F2_Fw	aattcGAAGACAATTTGGATGGTTCTCCTGCT
SJ398_NRG1B_479_F1_Rv	gaattcGAAGACAAAGCACGTATCTTTTGGTC
SJ399_NRG1B_479A_F2_fw	aattcGAAGACAATGCTGCGCTTATAATTGAC
SJ400_NRG1B_479D_F2_FW	aattcGAAGACAATGCTGACCTTATAATTGAC
SJ401_NRG1A_Fw	aattcGAAGACAAAATGCAATTCGTCTCCTTC
SJ408_NRG1B_Fw1	GAGAAGTGTTCACATGTCGAG
SJ409_NRG1B_Fw2	GGTACCTTTGAAATATGAATATGC
SJ410_NRG1B_Fw3	GAGTGTTTAAATCAACCTATTAATGCTC
SJ411_NRG1B_Fw4	GCGAGTTGCCGGATTCAGTG
SJ412_NRG1B_Rv	GTCTCATGAGCGGATACATATTTGAATG
SJ414_WRKY18_EARdel_FW	aattcGAAGACAAAaTGTTCTCCGCAAAACTTCC

SJ415_WKRY18_Rv	gaattcGAAGACAACGAACCTGTTCTAGATTGCTC
SJ416_WRKY18_EARdelFW	TTCTCCGCAAAACTTCCG
SJ417_WKRY18_Rv	TGTTCTAGATTGCTCCATTAACC

Appendix 5. Constructs cloned and used for transient assays or transformed into Arabidopsis

Name	**Details**	**Method of cloning**
SJJJ32	p35S:WRKY18-GFP:OcsTer	Golden gate
SJJJ34	p35S:WRKY18^{DD}-GFP:OcsTer	Golden gate
SJJJ35	p35S:WRKY18^{AA}-GFP:OcsTer	Golden gate
SJJJ72	p35S:TPR1-HF:OcsTer	User cloning
SJJJ74	p35S:TPR1$^{286A+289A+291A}$-HF:OcsTer	User cloning
SJJJ75	p35S:TPR1$^{286D+289D+291D}$-HF:OcsTer	User cloning
SJJJ72	p35S:TPR1-HF:OcsTer	User cloning
SJJJ76	p35S:TPR1^{395A}-HF:OcsTer	User cloning
SJJJ77	p35S:TPR1^{395D}-HF:OcsTer	User cloning
SJJJ98	p35S:GFP	Provided by Xiao Lin
SJJJ40	p35S:SARD1-HF:OcsTer	User cloning
SJJJ96	p35S:WRKY_EarDeletion-GFP:OcsTer	Golden gate
SJJJ97	p35S:TPR1-mCherry:OcsTer	User cloning
SJJJ100	p35S-WRKY^{DLN_AAA}-GFP:OcsTer	Golden gate
SJJJ99	p35S-mCherry	Provided by Hee-Kyung Ahn
SJJJ92	35S-NRG1B-152A-HF:OcsTer	Golden gate
SJJJ93	35S-NRG1B-152A_433A-HF:OcsTer	Golden gate
SJJJ94	35S-NRG1B-433A-HF:OcsTer	Golden gate
SJJJ95	35S-NRG1B-433D-HF:OcsTer	Golden gate
SJJJ101	35S:NRG1B-HF:OcsTer	Provided by Joanna Feehan
SJJJ102	35S:EDS1-V5	Provided by Joanna Feehan
SJJJ103	35S-SAG101-Myc	Provided by Joanna Feehan
SJJJ104	35S:NRG1B-E21A-E29A-HF	Provided by Joanna Feehan
SJJJ111	35S:WRR4A-Flag	Provided by He Zhao
SJJJ112	35S:CCG28-Myc-E9	Provided by He Zhao
SJJJ113	35S:Strep-XopQ	Provided by Hee-Kyung Ahn

SJJJ79	35S:TPR1-TurboID:OcsTer	User cloning
SJJJ116	35s:NLS-GFP-TurboID	Provided by Jianhua Huang
SJJJ9	BASTA::pEDS1:gEDS1-TurboID-V5:NosTer	Golden gate
SJJJ10	BASTA::pSARD1:gSARD1-TurboID-V5:NosTer	Golden gate
SJJJ25	pEDS5:ff Luciferase-V5:OcsTer::pUbi10:SARD1_S77D-HF:35STer::p35S:Renilla Luciferase-6xHA:NosTer	Created by Mark Youles-Golden gate
SJJJ26	pEDS5:ff Luciferase-V5:OcsTer::pUbi10:SARD1_S75D-HF:35STer::p35S:Renilla Luciferase-6xHA:NosTer	Created by Mark Youles-Golden gate
SJJJ27	pEDS5:ff Luciferase-V5:OcsTer::pUbi10:SARD1_S75D_77D-HF:35STer::p35S:Renilla Luciferase-6xHA:NosTer	Created by Mark Youles-Golden gate
SJJJ28	pEDS5:ff Luciferase-V5:OcsTer::pUbi10:SARD1_S75D_76D_77D-HF:35STer::p35S:Renilla Luciferase-6xHA:NosTer	Created by Mark Youles-Golden gate
SJJJ1	pEDS5:ff Luciferase-V5:OcsTer::pUbi10:SARD1-HF:35STer::p35S:Renilla Luciferase-6xHA:NosTer	Created by Mark Youles-Golden gate
SJJJ2	pEDS5:ff Luciferase-V5:OcsTer::pUbi10:SARD1_S77A-HF:35STer::p35S:Renilla Luciferase-6xHA:NosTer	Created by Mark Youles-Golden gate
SJJJ3	pEDS5:ff Luciferase-V5:OcsTer::pUbi10:SARD1_S75A-HF:35STer::p35S:Renilla Luciferase-6xHA:NosTer	Created by Mark Youles-Golden gate
SJJJ4	pEDS5:ff Luciferase-V5:OcsTer::pUbi10:SARD1_S75A_77A-HF:35STer::p35S:Renilla Luciferase-6xHA:NosTer	Created by Mark Youles-Golden gate
SJJJ5	pEDS5:ff Luciferase-V5:OcsTer::pUbi10:SARD1_S75A_76A_77A-HF:35STer::p35S:Renilla Luciferase-6xHA:NosTer	Created by Mark Youles-Golden gate
SJJJ6	pEDS5:ff Luciferase-V5:OcsTer::Ubi10:mCherry-NLS-HF:35STer::p35S:Renilla Luciferase:6xHA:NosTer	Created by Mark Youles-Golden gate